The transition from Calc-alkaline to Potassic Volcanism in the Aeolian Islands, Southern Italy

Thesis

The Transition from Calc-alkaline to Potassic Volcanism in the Aeolian Islands, Southern Italy

A thesis presented for the degree of Doctor of Philosophy

Robert Mark Ellam B.Sc. A.R.S.M.

Department of Earth Sciences,
The Open University,
Walton Hall,
Milton Keynes.
MK7 6AA

December 1986

DATE OF SUBMISSION - - - 03-12-86
DATE OF AWARD - - - - - - 09-06-87

"The great tragedy of science - the slaying of a beautiful hypothesis by an ugly fact."

T.H. Huxley (1825 - 1895) *Biogenesis and Abiogenesis*

ABSTRACT

The geochemical and petrological variations of a range of lavas from the Aeolian Islands volcanic arc, southern Italy are investigated and compared with potassic and ultra-potassic volcanism in the Roman region, and with subduction related basalts from throughout the world.

Aeolian Islands lavas range from calc-alkaline basalts and andesites, typified by lavas from the island of Salina, to potassium rich shoshonites and tephrites found at Stromboli and Vulcano. Variations within individual lava series may be largely explained by fractional crystallisation, however the differences between the series are not due to this process and the various series are thought to originate from a range of parental magmas with quite different K_2O content.

Potassic lavas from Vulcano are characterised by incompatible element ratios typical of subduction related volcanism, and by relatively low $^{87}Sr/^{86}Sr$ ratios (0.70432-0.70494) similar to those of calc-alkaline lavas from Salina (0.70411-0.70466). In contrast at Stromboli, potassic lavas have relatively high Nb and Ta contents and elevated $^{87}Sr/^{86}Sr$ (0.7050-0.7075)

A three component mixing model is proposed to explain the geochemistry of the Aeolian Islands lavas, this involves mantle wedge, a subduction related component thought to originate by dehydration of the subducting lithosphere, and a component derived from subducted sedimentary material. In addition some heterogeneity of the mantle wedge is indicated by within-plate style trace element enrichment in Stromboli lavas. A similar mixing model is applicable to Roman province lavas and also to subduction related basalts throughout the world.

Evidence is presented to suggest that variations in certain incompatible element ratios may result from the involvement of small degree partial melting in the genesis of island arc basalts. However it is clear that such a process is not solely responsible for the anomalous trace element geochemistry of subduction related magmatism.

CONTENTS

List of Figures

LIST OF TABLES

ACKNOWLEDGEMENTS

I would like to express my gratitude to the following for their help during the course of this work.

Chris Hawkesworth for support and guidance throughout this project and especially for the "red pen jobs" on earlier versions of this thesis.

Martin Menzies for supervision and assistance both in the lab and the field, for comments on earlier versions of the thesis and for introducing me to *Vera Pizza*.

N.A.T.O. collaborative research grant 776/83 supported fieldwork.

Nick Rogers for many detailed discussions of Italian volcanism, performing the INAA counting, enduring Naples and fighting off the volleyball team.

Everyone in the isotope lab, particularly Peter van Calsteren, Andy Gledhill and Zen Palacz for their efforts in keeping things running smoothly. Thanks especially to Peter for patiently answering my early morning cries for help.

Giancarlo Serri and Mauro Rosi for assistance in Italy and for providing a number of the samples used in this study.

Prof. J. Keller for providing some of the crustal xenoliths studied.

John Watson (XRF), Andy Tindle ('probe & Macs), Ian Chaplin (thin sections) and John Taylor (cartography) for assistance in their fields.

Tim Brewer, P.K. Harvey and B.P. Atkin for XRF analyses at Nottingham University.

Bill Leeman for assistance in the lab and in the field.

The staff of the British Consulate in Naples (especially Lesley) for help in getting the rocks home, and for the best cup of instant coffee ever.

Massimo Cortini for logistical support in Naples.

Mike Rhodes for helping me understand CMAS.

Dave Wright for use of computer programs, especially SUPERMIX.

Graeme Rogers and Mike Norry for helpful discussions during the course of the project.

Rowena for continual encouragement and for collecting crustal xenoliths where I'd previously failed. ("Just look for the white bits.")

Pete Hopwood for kindling my initial interest in geology.

My parents for their generous help and support throughout my education.

CHAPTER ONE

Introduction to the Aeolian Islands

1.1 Geography and Physiology.

1.1.1 Introduction.

The Aeolian or Lipari islands are situated in the southern Tyrrhenian area of the Mediterranean Sea between 30 and 80 km from the northern coast of Sicily. There are seven main islands and several small islets which may be related to the larger volcanic structures. The total surface area of the islands is around 117 km^2 but this represents only the exposed summits of much larger volcanoes, in places the sea-floor reaches depths of around 2000 m so that, the Stromboli volcano for example, is similar in height to Mount Etna. Above Sea-level, maximum elevations of over 900 m are reached by Salina and Stromboli. Figure1.1 shows the location of the islands within the archipelago which extends around 100 Km in a roughly east - west direction. The islands have a mild Mediterranean climate, rainfall is low and mostly restricted to autumn and winter, mean annual temperature is around 15°C but maximum temperatures up to 35°C are not unknown. As their name suggests, strong winds are quite common in the islands particularly in the winter months. This climate is condusive to viniculture although all agriculture is on a relatively small scale. Other crops include olives, capers and figs. This can be obstructive both to exposure and access.

1.1.2 Lipari

This is the principal island of the archipelago, and with a surface area of 37.6 Km^2 it is also the largest. Its population of around 10,000 accounts for over 80% of that of all the Aeolian Islands. Lipari consists of a complex association of several volcanic structures ranging in age from around 100,000 years B.P. to a little more than 1,000 years B.P. (Pichler, 1980). During Neolithic times the obsidians of Lipari were much in demand for tools and weapons, but today the associated pumices are exploited. Pumice is used as an industrial filler and as a mild abrasive and polishing agent.

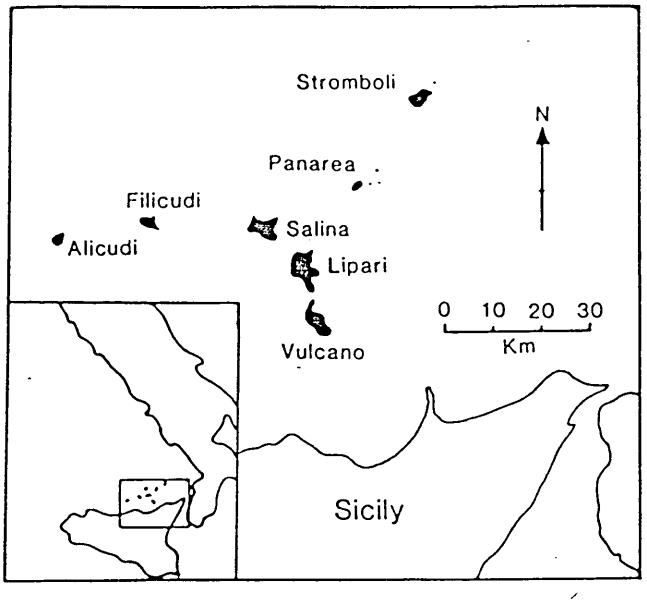

Fig. 1.1 Map showing the location of the Aeolian Islands.

1.1.3 Salina

Within it's 26.75 Km^2, Salina preserves evidence of six volcanic episodes. These range in age from around 450,000 years B.P. (Gillot & Villari, 1980) to 13,000 years B.P. (Keller, 1967). The twin volcanic cones of Fossa delle Felci, (962 m) and M. dei Porri (860 m) exhibit youthful morphology and are amongst the highest peaks in the archipelago. Salina derives it's name from the salt extraction which took place at Lingua in the south - east of the island, which has since been abandoned.

1.1.4 Vulcano

The southern half of Vulcano is dominated by a partial caldera structure which has been largely infilled by dominantly pyroclastic material. To the north the small cone of Fossa di Vulcano (391 m) was last active in 1890 and remains in a state of intense fumarolic activity. To the west of this cone are the Lentia hills which consist of rhyolite domes and flows. To the north of Vulcano, a recently accumulated sand bar links Vulcano to Vulcanello which is composed of a platform of lavas. A group of small craters reach a maximum elevation of 123 m a.s.l.

1.1.5 Stromboli

The Stromboli volcano has been in persistant activity throughout historical time. The island has a surface area of 12.5 Km^2 and reaches a height of 918 m a.s.l. However this represents only the exposed top one third of a large stratovolcano. The current activity is restricted to the north - west side of the island and all the recent volcanic products have been deposited on the Sciara del Fuoco (Pit of Fire). The present active crater is offset

towards the western side of the volcano's summit allowing a spectacular view into the crater area. The crater itself is quite complex, consisting of at least four individual eruptive centres or bocca. During periods of normal strombolian fire-fountaining activity, these bocca expel incandescent lava bombs and fine ash along with large quantities of volcanic gases. These eruptions occur approximately every 10-15 minutes. In addition to this minor activity, small lava flows are erupted every few years, the most recent of these being that of December 6th 1985.

1.1.6 Filicudi

The island of Filicudi, to the west of Salina, has a surface area of only 9.5 Km^2 and the summit of an extinct stratovolcano stands at 774 m. This structure dominates the island, but other eruptive centres have been recognised, (Villari, 1980a) and particularly outstanding are the endogenous domes of Capo Graziano and M. Montagnola. The Filicudi volcanic structure extends widely below sea-level to a depth of around 1100 m, where the elliptical base of the volcano has a major axis of around 18 Km.

1.1.7 Alicudi

This is the western-most Aeolian Island. It has an area of 5.2 Km^2,reaches a height of 675 m a.s.l. and has a relatively simple structure as the top of a large, roughly conical stratovolcano, extending below sea-level to a depth of around 1100 m.

1.1.8 Panarea

This, the smallest of the inhabited Aeolian Islands , is located between Lipari and Stromboli. Its area is only 3.4 Km^2, and its highest point is only 421 m a.s.l. Panarea displays some of the oldest Aeolian Islands rocks (~0.5 Ma) and consistent with this old age, the island has an eroded morphology preserving little of its original volcanic structure.

1.2 Previous Work in the Aeolian Islands

1.2.1 Classical References to Volcanic Activity

Probably the earliest record of volcanic activity in the Aeolian Islands is to be found in Homer's *"Odyssey."* This is thought to date back to the 8th century B.C. However Homer was most likely applying his contemporary knowledge of the newly colonised Sicily to the mythical voyages of Odysseus, traditionally dated as 13th century B.C. (Stothers & Rampino, 1983). Classical references abound (Stothers & Rampino *op. cit.*) but the first explicit descriptions were made in the 1st century B.C. (*e.g.* Vergil's *"Aeneid "*). Eruptions were further described in the 1st century A.D. by Pliny the Elder.

1.2.2 Modern Field Studies

The Aeolian Islands played a major role in the early stages of development of modern volcanology. The terms strombolian and vulcanian remain in use as part of a descriptive classification of eruptive phenomena. Important in these early developments were workers such as Mercalli & Silvestri (1891), who studied the 1888-1890 eruption of Vulcano, Bergeat (1899) who described the geology of all the islands and a number of volcanologists *e.g.* Cortese & Sabatini (1892), and De Fiore (1922) who studied the volcanic morphology of Vulcano.

More recent work of the past twenty-five years or so has been summarised in a series of papers first published in *Rendiconti Societa Italiana di Mineralogia e Petrologia* 36(1) and reprinted along with 1:10,000 scale geological maps in a guidebook to the geology of the islands (Villari Ed. 1980). This includes reviews and maps of six Aeolian Islands whilst these are available for the seventh, Panarea, in Romano (1973). The volcanic activity of the Aeolian Islands has been divided into two temporal groups by many workers, *eg* Keller (1967), Pichler (1968), Romano (1973), Villari (1972). These two groups are divided by a phase of marine erosion which produced marine terraces and raised beach deposits on the islands of Salina, Lipari, Panarea and Filicudi. This erosional phase produced a sequence of terraces corresponding to former sea-levels during a period of glacioeustatic regression attributed by Keller (1980a) to the interstadial period which preceeded the last (Würm) glaciation. The older group of volcanic rocks has been dated as extending back to 0.4 - 0.5 Ma on Salina and Panarea, but older lavas have been discovered by dredging of seamounts to the west of the Aeolian Islands. These yield dates as old as 1.3 Ma (Beccaluva *et al.* 1982). Figure 1.2 shows the available geochronological data on the Aeolian Islands. This has been compiled from radiometric determinations (K - Ar, ^{14}C and fission track), tephrostratigraphic correlations and field observations. This figure may be used as an age reference during the following discussion of the evolution of each island, which are dealt with where appropriate in order of decreasing age.

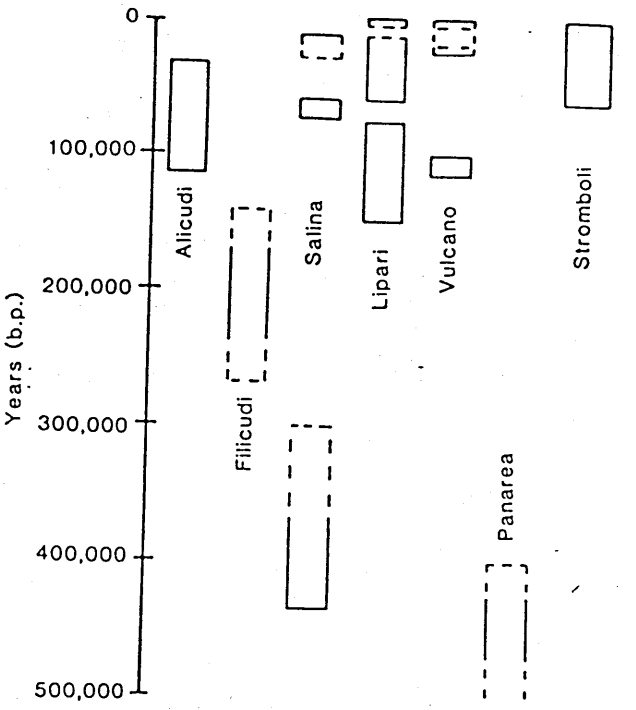

Fig. 1.2 Temporal distribution of Aeolian Islands Volcanism. Data sources Gillot & Villari (1980), Villari (Ed.1980).

1.2.2 a Panarea

Apparently the oldest of the exposed Aeolian products, the lavas of Panarea are dominated by highly evolved silicic flows and domes. No basic lavas have been found, however this does not preclude there having been basaltic activity as only fragments of the original volcanic structure remain.

1.2.2 b Salina

The oldest rocks on Salina are found in the eroded remnants of three volcanic centres (Capo, Corvo and Rivi). The remains of these volcanoes are composed of basic dykes and lava flows which are locally highly weathered. Rivi and Capo centres also preserve pyroclastic material. The early centres were anteceded by the stratocone of M. Fossa delle Felci which remains largely intact and dominates the east of Salina. The cone is composed of andesitic lava flows, tuffs and scoria. A hiatus in activity was followed by the activity which built the M. Porri volcanic cone. This is composed of intercalated basaltic andesite lava flows, scoria and minor tuffs, perhaps suggesting strombolian type activity. The final volcanic episode on Salina is represented by the explosion crater and extensive rhyodacite pumice of Pollara. Only minor high SiO_2 andesite lava flows are associated with this crater which is around 225 m deep with a diameter of around 700 m at its base. The pyroclastic units of the Pollara and Porri phases contain quite abundant, albeit small (<10 cm diameter) xenoliths of crustal basement which will be discussed in a later section.

1.2.2 c Lipari

The island of Lipari has been mapped in detail by Pichler (1980). The only basic lavas found on Lipari are the oldest exposed products which are found around much of the western coastline of the island. The bulk of Lipari however is composed of intermediate and acidic rocks with the former being succeeded by the latter about 40,000 years B.P. The intermediate lavas include a group which contain abundant xenocrysts of crustal origin. These include cordierite, sillimanite and garnet. The M. Guardia endogenous rhyolite domes are the only area of Lipari where lavas rival pyroclastics in abundance, although even here the rocks tend to be an admixture of glassy rhyolitic lava and pumiceous material. The most recent products of Lipari dominate the north-east of the island. These are three main flows of highly vitreous obsidian and associated with the most recent of these a vast extent of rhyolitic pumice which covers an area of at least 10 Km^2.

1.2.2 d Filicudi

Villari (1980a) recognised six phases of volcanism on Filicudi. The first four of these were stratocones which survive in varying degrees of preservation and were composed of basaltic andesite to andesite lavas and pyroclastic units in variable proportions. The two most recent volcanic structures are the endogenous domes of evolved latite lava found at M.Montagnola and Capo Graziano.

1.2.2 e Alicudi

A single central eruptive site appears responsible for all the volcanic products of Alicudi which were erupted in four cycles of volcanism (Villari, 1980b). The first phase of volcanism was followed by caldera formation prior to the second cycle, which filled the caldera and overflowed its rim. A crater formed during this second cycle was later partially filled by the third cycle lavas, some of which also overflowed to the south-east of the island. The final cycle of activity was accompanied by collapse of the summit dome causing outpourings of viscous andesite and forming small tongues of lava. Only minor pyroclastics (agglomerates and breccias) are found on Alicudi and the most common lavas are basalts and basaltic andesites. More evolved intermediate rocks are restricted to the late stages of activity.

1.2.2 f Vulcano

The island of Vulcano consists of the products of at least five phases of activity,

(Keller, 1980 b). The oldest rocks form the southern coastline and represent a partially complete caldera structure developed within an old volcanic cone. This cone is dominated by lava flows with only minor pyroclastics. Caldera collapse was followed by infilling of the caldera by pyroclastics, scoria and minor lava flows. The cones of Vulcanello and Fossa di Vulcano have evolved coevally; a third highly altered and eroded structure, il Faraglione may also have been contemporary. Vulcanello is dominated by a series of platform lavas and a single trachyte flow with only minor pyroclastics, in contrast Fossa di Vulcano has erupted much pyroclastic material with only minor lavas which are evolved trachytes and rhyolitic obsidians. The last eruption of Fossa di Vulcano (1888 - 1890) erupted no lava flow but the summit area is littered with vast quantities of breadcrust bombs, some over $1m^3$ in size. Erupted during this final phase, these typify the eruption style known as vulcanian. The Lentia hills area of Vulcano in the north-western corner is composed of acid domes and flows with minor intermediate lavas. The age and origin of these lavas are controversial. Keller, (1980b) believed them to be part of the volcanic structure of Vulcano, based on the dips of flows away from Vulcano (*i.e.* west). In Keller's stratigraphy these lavas are contemporary with the period of caldera infill. The present study however emphasises the lack of exposure and highly altered nature of the rocks at the margin of the Lentia formation. No unequivocal contact relationship was found to support Keller's interpretation. Furthermore the Lentia rhyolites appear very similar to the M. Guardia lavas on Lipari from which they are separated by only a relatively narrow stretch of fairly shallow sea. It is quite conceivable that the Lentia formation is related to the M. Guardia structure *not* the Vulcano structure. In this case the westerly dips of lava flows may represent "piling up" of viscous lava against the topography of Vulcano.

1.2.2 g Stromboli

This island may be divided into two halves, (Rosi, 1980). The eastern half of Stromboli consists of the older products which are intercalated lavas and tuffs. The lavas range in composition from basic to intermediate. The western half of the island is dominated by lavas and interbedded welded scoria. It is apparent that these types of succesion are likely to represent the products of strombolian activity in which a period of fire-fountaining produces an horizon of welded scoria which is eventually overlain by a thin lava flow to complete one cycle of activity. Several cycles of this type gave rise to the deposits seen throughout the western side of Stromboli and are similar to those being formed at the

present time on the Sciara del Fuoco. This younger phase of volcanism at Stromboli is characterised by a prevalence of basic lavas.

1.2.3 Tectonic Studies

The tectonic setting of the Aeolian arc is of central importance to an understanding of the genesis of its volcanic rocks. The whole Mediterranean area is tectonically complex; for while on a large scale the area may be viewed in terms of the northward drift of Africa and its impingement on Europe, the details of this collision are complicated and can only be fully understood by reference to much smaller scale processes and complex interactions between microplates. The Aeolian Islands lie close to the suture between Europe and Africa. The exact position of this suture is unclear, although palaeomagnetic data (Barberi *et al.*, 1974) indicate that south-east Sicily has been part of the African plate since at least the Upper Cretaceous (see fig. 1.3). Caputo *et al.* (1972) established that a Benioff zone is present beneath the Aeolian Islands. Earthquake foci occur at a depth of around 200 km beneath the islands and the Benioff zone dips towards the north-west at an angle of around 60°. Extrapolation of the Benioff zone suggests that the suture passes through central Sicily as shown in figure 1.3. Although to the south of that proposed by Barberi *et.al.* (1974), this position is consistent with palaeomagnetic data.

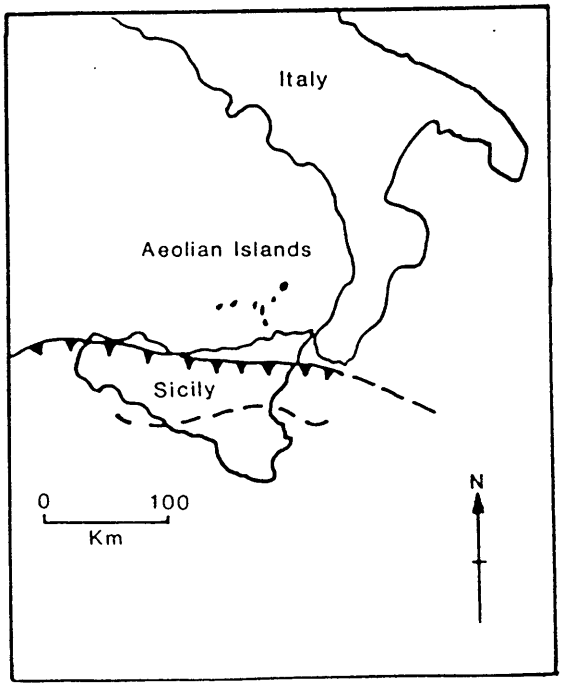

Fig. 1.3 Location of the Africa - Europe plate boundary. Arrowed line is the suture proposed by Barberi *et.al.* (1974), dashed line is an approximate projection of the Benioff zone to the surface, after Caputo *et al.* (1972).

The absence of oceanic crust between the African and European continental plates in this area has been taken to indicate that the subduction zone is in a senile stage of its evolution (Barberi *et al.*,1974). The volcanic arc sits on continental crust which is thinned to around 16-18 km beneath the arc, but thickens to around 40 km beneath central Sicily (Schutte *et al.*, 1978). A complex range of crustal lithologies has been recognised as xenoliths in the pyroclastic deposits of Salina (Keller, 1980a, Appendix A). These include granites, gneisses, metapelites, metabasites, metamorphosed calc-silicates and sandstones. Such a range is similar to the exposed crust of Calabria, (Schenk, 1984) and by analogy with Calabria one may infer a maximum age for the crust of Palaeozoic, with no evidence for Precambrian rocks in this region. Metamorphism is likely to have occured during both the Hercynian and Alpine orogenies and it seems likely that the Aeolian arc crust contains significant quantities of both Hercynian and Alpine granitoids. To the north of the Aeolian islands, site 373 of the Deep Sea Drilling Project (D.S.D.P.) discovered tholeiitic basalts which are taken to indicate the growth of oceanic crust in a back-arc basin environment (Beccaluva *et al.*, 1982).

Barberi *et al.* (1974) suggested that the subducted slab present beneath the Aeolian Islands consists of oceanic crust, now fully consumed, which was formed during a period of extensional tectonics caused by south-easterly drifting of Africa. Alternatively, Scandone (1979) argued that the slab is made of continental lithospheric material, perhaps a mixture of lower crust and upper mantle, which was subducted following separation from the upper crust by a process akin to "flake tectonics" (Oxburgh, 1972). Keller (1974) has interpreted an apparent gap in seismicity between 35 km and 200 km depth as indicative of a detatched lithospheric slab sinking rapidly into the mantle. Recent data however, (Gasparini *et al.*,1982) appear to support a more complete Benioff zone than that previously recognised.

1.2.4 Geochemical Studies

A number of geochemical studies have been carried out in the Aeolian Islands although in general these have included relatively few data from samples scattered throughout the arc. However some important basic points have been established. Barberi *et al.* (1974) have recognised the subduction related nature of the Aeolian volcanics and also noticed a large range in K_2O content of the basic lavas on the basis of

which they distinguished four series, namely calc-alkaline, high-K andesite, shoshonitic and leucite tephrite. Calc-alkaline lavas occur on Salina Filicudi, Alicudi, Panarea and in the older lavas of Stromboli. High-K calc-alkaline lavas occur on Lipari and in the Stromboli older series, with shoshonitic and leucite tephritic volcanism restricted to Vulcano and the younger lavas of Stromboli. Barberi *et al.* (1974) further suggested a relationship between potassium content (K) and depth of earthquake foci (h) within the Aeolian Islands, similar to that seen by Hatherton & Dickinson (1969) in circum-Pacific island arcs. However, Keller (1974) used an apparent lack of any K-h relationship to infer a vertically dipping subduction zone beneath the Aeolian region, a hypothesis which is clearly at odds with the seismic data of Gasparini *et al.* (1982). Furthermore, Barberi *et.al.* (1974) recognised a general increase in K_2O content with time which will be further discussed in a later section. These authors considered potassic volcanism to be due to melting deeper parts of the mantle.

In a study of the trace element geochemistry of Stromboli, Dupuy *et al.* (1981) reported a systematic increase in K and related element concentrations with decreasing age of the lavas. In addition they recognised decreases in K/Rb, K/Ba, Zr/Ce and Zr/Nb ratios and an increase in La/Yb with time. These variations were explained as reflecting the length of time during which subduction derived fluids remained in contact with the upper mantle source.

Barberi *et al.* (1974) reported a range in $^{87}Sr/^{86}Sr$ from 0.7030 - 0.7064 with the more radiogenic values being from the Stromboli shoshonites. This was suggested to be due to wall-rock reaction although Klerkx *et al.* (1974) considered the elevated Sr isotope ratios to be due to crustal contamination of the Stromboli lavas. Pb isotope determinations (Cortini, 1981) further suggest that the source of Stromboli lavas was distinct from that of the other Aeolian Islands, and recent work (Cortini & van Calsteren,1985) has shown that mineral phenocrysts and whole rocks from Stromboli display disequilibrium suggesting the action of a process responsible for changing Pb isotope ratios during the fractional crystallisation of these lavas. Significantly these authors and Vollmer *et al.* (1981) have demonstrated Sr isotope equilibrium between phenocrysts and whole rocks from Stromboli.

1.3 Thesis Aims

Given the basic geochemical information available for the Aeolian Islands, it was

possible at an early stage to identify many of the problems to be addressed in this work. Accordingly the aims of this thesis are:-

1. To study the geochemical variations which accompany the transition from calc-alkaline to potassic volcanism.

2. To compare and contrast suites of K_2O-rich lavas from different volcanic centres.

3. To consider and develop tests to ascertain the sources and processes of K_2O (and trace element) enrichment in the various suites of lavas and to discuss to what extent various potential sources of potassium (*e.g.* continental crust, lithospheric mantle) have contributed to the trace element budget of these lavas.

4. To compare potassic lavas from the Aeolian Islands which are demonstrably related to subduction with potassic and ultra-potassic Roman province lavas whose tectonic setting is less clear but which show many similarities to subduction related rocks (Rogers *et al.* ,1985).

5. To examine whether the Aeolian and Roman lavas may be explained by reference to the same or similar trace element components

6. To consider the implications which Aeolian lava geochemistry may have for the source of and processes active during the genesis of subduction related lavas worldwide.

1.4 Methodology

At an early stage of this study a decision was made to concentrate on the islands of Salina, Stromboli and Vulcano. These represent the exposed temporal range of the archipelago and are believed to be representative of the full range of lava types. Salina shows a wide age range of wholely calc-alkaline volcanism. Stromboli lavas range from calc-alkaline to shoshonitic with an apparently rapid transition, and Vulcano is composed exclusively of potassic rocks amongst which are the most K_2O-rich lavas of the Aeolian arc.

This study has evolved in response to growing evidence of the ambiguity of isotope ratios in igneous rocks. The discovery of enriched isotopic signatures in mantle xenoliths (*e.g.* Menzies & Murthy, 1980) shows conclusively that isotopes cannot be used to effectively distinguish mantle derived rocks from those which have interacted with the continental crust. However by introducing trace elements it is possible to study the elemental changes which accompany isotopic variations.

Coupled isotope and trace element studies also allow some assessment of the importance of complex regimes of melting (O'Hara, 1985) and fractional crystallisation

(O'Hara, 1977, O'Hara & Matthews, 1981). Whilst it is clear that these processes may cause fractionation of incompatible trace element ratios, it is unlikely that they would produce isotopic variations, for two reasons:-

1. During analysis, radiogenic Sr and Nd isotope ratios are normalised to non-radiogenic reference ratios ($^{86}Sr/^{88}Sr$, $^{146}Nd/^{144}Nd$) in order to eliminate mass dependant fractionations within the mass spectrometer. This correction will also eliminate such fractionations due to petrogenetic processes.

2. Fractionation of isotope ratios in igneous systems is unlikely to be significant. Partition coefficients are dependant on ionic radius and ionic charge, whilst the former will of course vary with atomic mass, the latter will not. It is therefore likely that the differences in atomic radii of different isotopes are insignificant compared with the effects of ionic charge. This is particularly true of the heavy radiogenic isotopes whose mass difference relative to their atomic mass is very small. Therefore, by consideration of elemental variations which are not accompanied by isotopic changes, one may quite confidently assess the role of melting and crystallisation.

A useful point which does emerge from consideration of complex regimes of open system melting and crystallisation, is that the calculated degrees of melting and crystallisation (F) derived from trace element modelling are meaningful only within the chosen model. This has important consequences within igneous petrology where calculation of these parameters has been a major goal. In this study this model dependance is recognised and is implied where values of F are quoted. Perhaps a more meaningful goal is calculation of the bulk partition coefficient (Kd) of a trace element during a magmatic process. This is *not* model dependant and has important implications for the stable mineral assemblage during the process and hence the physical environment (*e.g.* pressure and temperature) in which the process took place. It is this type of approach to modelling which is favoured in this work.

Also of importance to the methodology of this work is the observation that different styles of trace element enrichment are found in different tectonic environments (*e.g.* Pearce, 1983), and that different elemental enrichment styles accompany isotopic enrichment (Hawkesworth *et al.* 1984). Characteristics of these enrichment styles may be taken as end members in mixing models and may be used to infer the source of the enrichment.

CHAPTER TWO

Petrography and Major Element Geochemistry

2.1 Introduction

The aim of this chapter is to describe the petrography and major element geochemistry of those islands which have been studied in detail. These will be used to classify the lavas and begin to investigate the petrogenesis of the lava series. In particular the effects of fractional crystallisation on the major elements will be considered in order to distinguish the effects of crystallisation from those of other petrogenetic processes.

2.2 Petrography

2.2.1 Salina

Sample localities on Salina are shown in figure 2.1 and represent lavas from all the volcanic episodes discussed in the previous chapter. Lavas range from basalt to andesite. The basaltic rocks are rich in clinopyroxene, with orthopyroxene and olivine also present as phenocrysts. Olivine crystals commonly have dark rims and also show alteration to serpentine minerals along intra-crystalline fractures and around their edges. Although these phenomena are not extensively developed and may represent late stage hydrothermal or even sub-aerial alteration effects, they may alternatively suggest that the olivine crystals did not crystallise from the lava in which they now reside. Plagioclase phenocrysts follow clinopyroxene in order of decreasing modal abundance. An opaque spinel (titaniferous magnetite) is a common accessory phase.

More evolved lavas are still quite similar to the basaltic rocks in their petrography; olivine is less common, feldspars are modally dominant and alkali feldspar occurs. The andesite lava of the Pollara centre (ESAL 19) is unique in containing phenocrysts of hornblende. The only other hydrous phases present in Salina lavas are small, corroded, greenish micas whose habit suggests that they are likely to be xenocrystal in origin.

Common within the lavas of Salina are numerous glomeroporphyritic clusters of gabbroic mineralogy (pyroxene + plagioclase ± olivine ± opaque) which are interpreted as xenolithic inclusions of the fractionating phenocryst phases. Textural evidence of magma mixing is displayed by one flow unit within the Favarolo series of Keller (1980a), which

Fig. 2.1 Salina sample localities, numeric labels are prefaced by "ESAL" elsewhere. Geology after Keller (1980a).

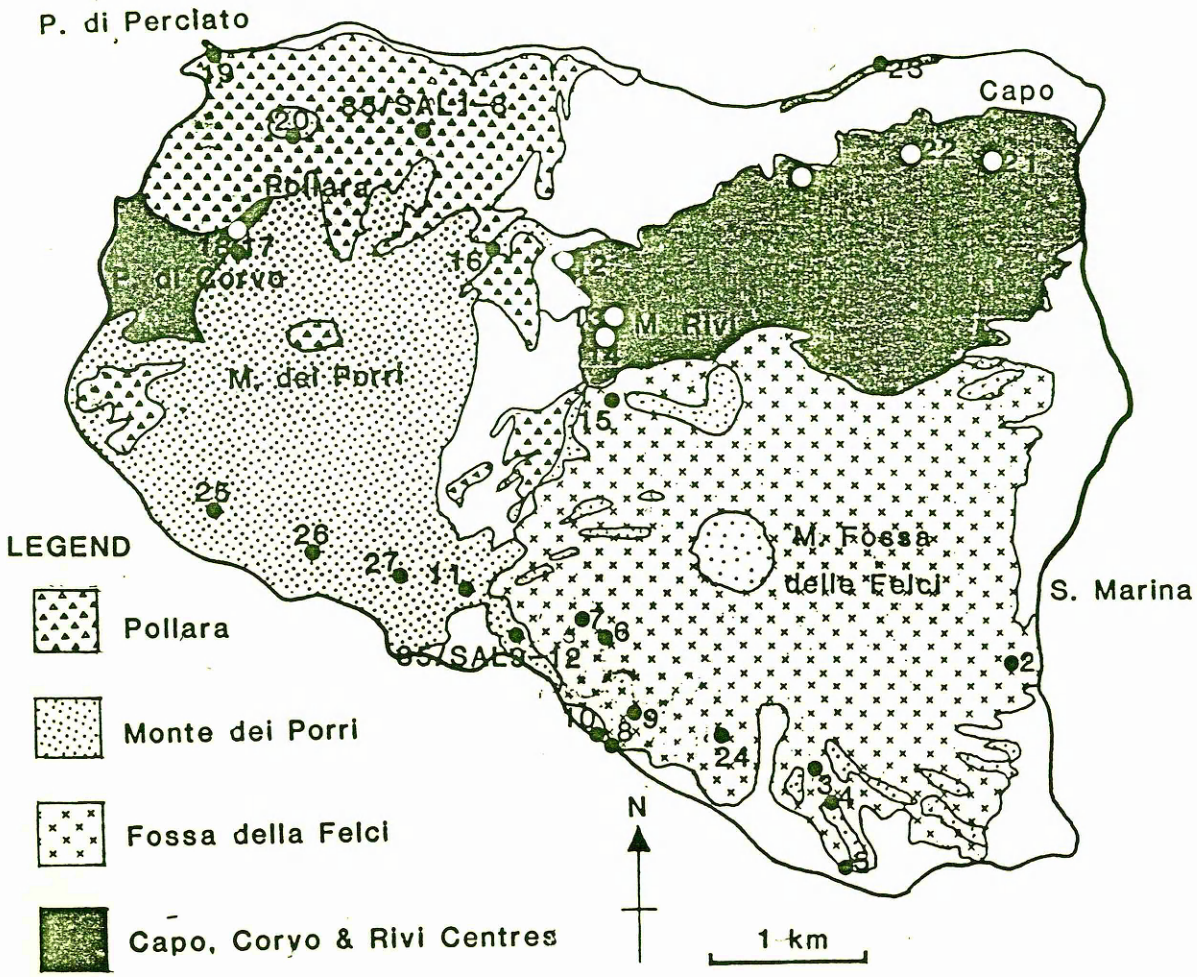

emanated from the Fossa delle Felci centre. Two distinct textures are recognisable and are intimately mixed down to a scale of a few centimetres. One of these textures is fine grained with a vitreous matrix and contains clinopyroxene, orthopyroxene, plagioclase, microperthite, spinel and occasional olivine. the second texture is much coarser grained with a similar mineralogy, but with higher modal abundance of pyroxene, particularly the orthorhombic form, and feldspar. The contact between the two textures is rather diffuse, no obvious chilling of either component is apparent which may suggest a liquid - liquid contact, but the boundary does not display the cuspate morphology often typical of liquid - liquid contacts.

2.2.2 Petrography of Stromboli

The sample locality map (fig. 2.2) shows the division between the older series lavas to the south and east of the island and the younger series lavas. Recent activity is restricted to the Sciara del Fuoco. The older series lavas contain phenocrysts of clinopyroxene and plagioclase in all samples with alkali feldspar present in more evolved samples. Orthopyroxene, olivine and an opaque spinel are also present in many lavas. In evolved rocks the feldspars are modally dominant over ferromagnesian phases, but in all cases plagioclase is in modal excess of alkali feldspar. Occasional biotite occurs but this is always highly altered and partially resorbed, suggesting a xenocrystal origin. Hornblende is also occasionally present and may have a similar origin. Cumulate xenoliths of largely gabbroic mineralogy, (clinopyroxene + plagioclase ± spinel ± olivine, often partially serpentinised ± orthopyroxene), similar to those described from Salina also occur in these Stromboli lavas.

Ubiquitous in the younger series is the phenocryst assemblage clinopyroxene, olivine, plagioclase and minor alkali feldspar. A few lavas also contain small euhedral pseudomorphs after leucite which are composed of optically isotropic analcite. There is no co-existance of leucite and alkali feldspar, the presence of the feldspathoid illustrates the potassium - rich, silica undersaturated nature of these lavas. The absence of orthopyroxene is also an effect of SiO_2 undersaturation, as the crystallisation of the SiO_2 rich orthopyroxenes is unlikely to be accomplished in SiO_2 undersaturated liquids.

Fig. 2.2 Stromboli sample localities, alphanumeric sample labels are prefaced by "St" and solely numeric labels by "ESTR" elsewhere. Geology after Rosi (1980).

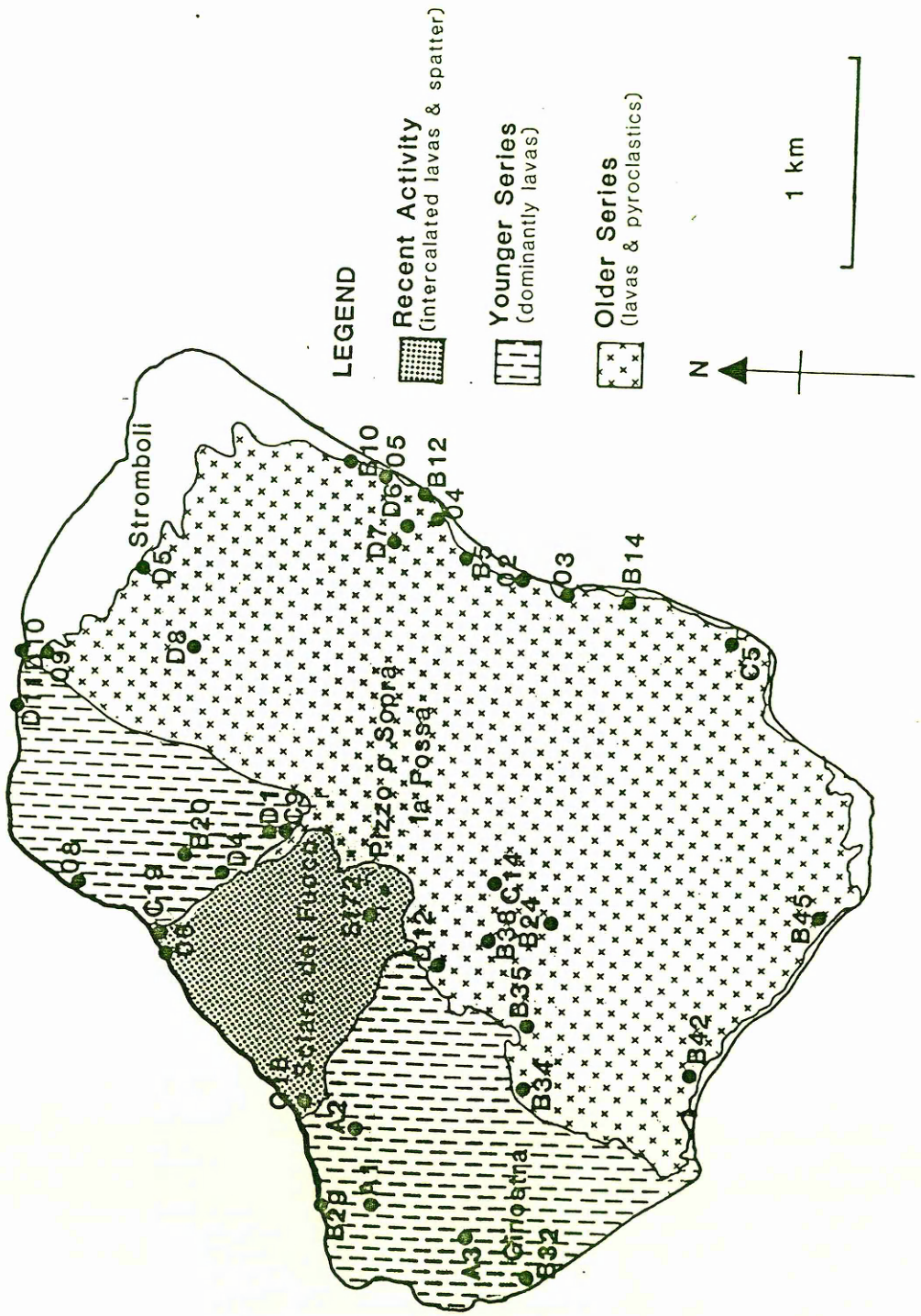

2.2.3 Petrography of Vulcano

Following Keller (1980b) the lavas of Vulcano are sub-divided into five spatially and temporally distinct groups, which are shown along with sample localities in figure 2.3

(a) Vulcano Primordiale — Oldest
(b) Caldera del Piano
(c) Lentia Hills
(d) Vulcanello
(e) Fossa di Vulcano — Youngest

2.2.3 a Vulcano Primordiale

These form a petrographically uniform suite of lavas containing phenocrysts of pale green clinopyroxene, olivine, plagioclase and opaque spinel in a fine grained matrix of these phases and glass. The spinel often occurs as inclusions within the pyroxene phenocrysts, but does not appear to display such a relationship with plagioclase.

2.2.3 b Caldera del Piano

This infilled caldera is dominated by pyroclastic units with only a few lava flows. These contain phenocrysts of clinopyroxene, olivine and plagioclase. Keller (1980b) described some of these lavas as leucite tephrites,however leucite does not occur as a phenocryst phase in any of the samples from Caldera del Piano studied here. However, isotropic pseudomorphs of analcite after leucite do occur in the groundmass. Some of the lavas show quite extensive alteration, particularly of the groundmass and olivine phenocrysts.

2.2.3 c Lentia Hills

These are evolved rocks which have clinopyroxene as their only ferromagnesian phase; these are often rounded and resorbed suggesting that they are not in equilibrium with the acid matrix in which they now occur. Alkali feldspar is modally dominant over plagioclase and opaque spinel occurs as an accessory phase in a groundmass which ranges from vitreous to fine grained holocrystalline.

2.2.3 d Vulcanello

The most abundant lavas on Vulcanello contain clinopyroxene, olivine, leucite and plagioclase phenocrysts in a matrix of acicular plagioclase,analcite pseudomorphs after

Fig. 2.3 Vulcano sample localities, numeric labels are prefaced by "EVUL" elsewhere. Geology after Keller (1980b).

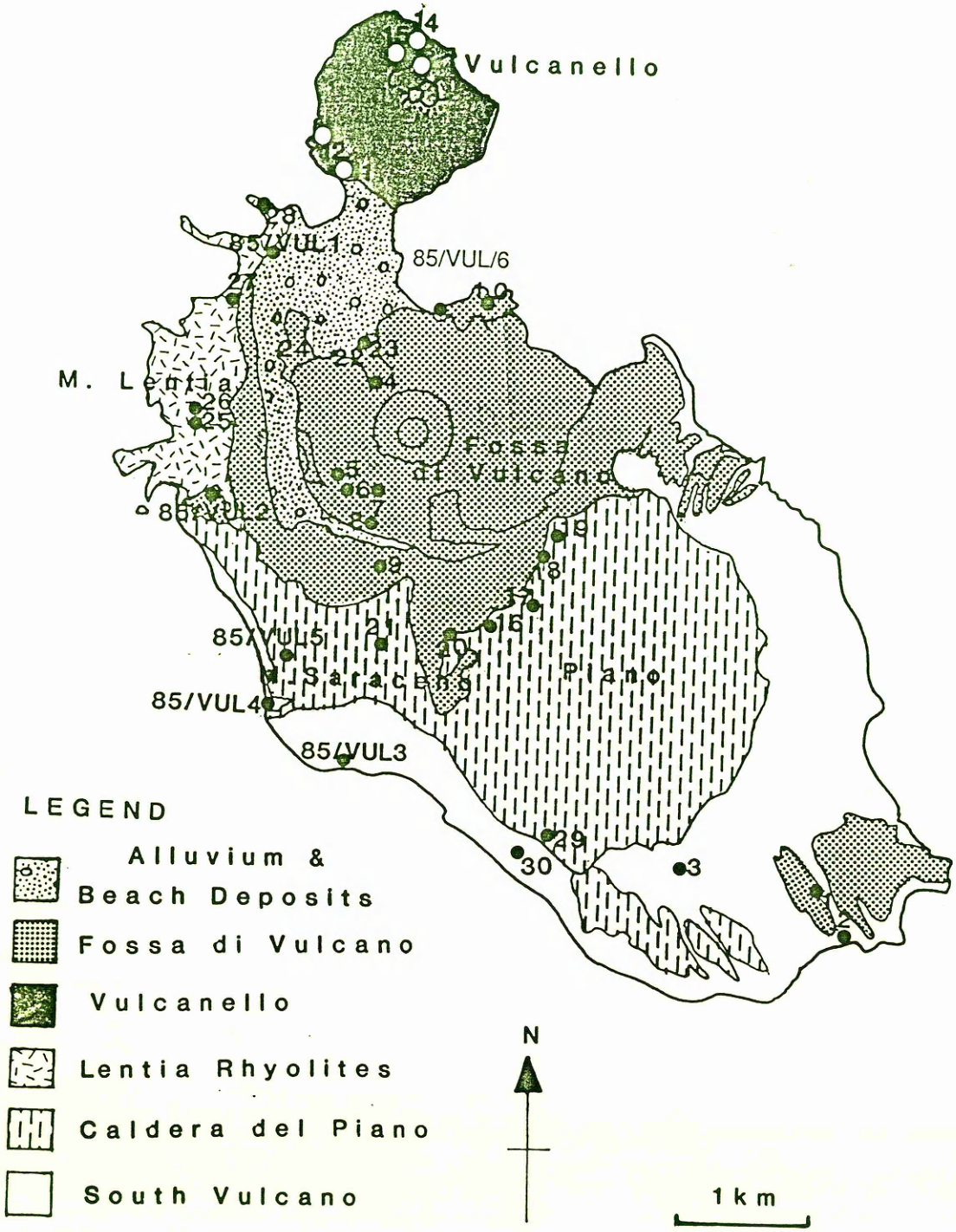

leucite, and spinel. Keller (1980b) classified these lavas as leucite tephrites; on strictly petrographic grounds this term is incorrect, tephrites do not contain olivine. However the term tephrite is retained here to remain consistent with previous workers and for geochemical reasons which are outlined below. A single trachyte flow outcrops on Vulcanello which contains clinopyroxene, plagioclase, alkali feldspar and spinel phenocrysts in a matrix of similar mineralogy.

2.2.3 e Fossa di Vulcano

Fossa lavas range from trachyte to rhyolitic obsidian. The trachytes contain clinopyroxene and occasional tiny olivine crystals. Feldspar phenocrysts dominate, with alkali feldspar in greater modal abundance than plagioclase. Sanidine, anorthoclase and untwinned alkali feldspar all occur in the trachytes and an opaque spinel phase is also present. Fossa obsidians are highly vitreous, however phenocrysts of clinopyroxene and plagioclase do occur, but may actually be entrained xenocrysts. In addition sample EVUL 22 contains very large haloes of radiation damage in the glass matrix perhaps due to the presence of small crystals of a minor phase rich in radioactive elements, *e.g.* monazite.

2.3 Comparison of Lava Petrography

Descriptions of the samples studied petrographically are given in appendix A. It is clear that the groups of lavas discussed above reflect a range of rock types. Many groups include both basic lavas and associated differentiated andesites, trachytes and rhyolites with the evolved lavas rich in feldspar. Also evident, is the variation in the basic lavas from pyroxene, olivine, plagioclase assemblages to feldspathoid or alkali feldspar bearing lavas. The presence of these K_2O-rich phases reflects the potassic nature of the Stromboli younger series lavas and all the Vulcano lavas. The occurrence of leucite along with the absence of SiO_2 - rich orthopyroxene is a petrographic response to increasing SiO_2 undersaturation towards the leucite bearing lavas.

2.4 Major Element Classification

The classification of Peccerillo & Taylor (1976), based upon the K_2O v. SiO_2 diagram

(fig. 2.4) is often used to classify lavas from the convergent plate margin environment. Barberi *et.al.* (1974) have established average trends for four lava series recognised from the Aeolian Islands and shown in figure 2.4. these are:-

(a) Calc-alkaline

(b) High K Andesite

(c) Shoshonitic

(d) Leucite Tephrite

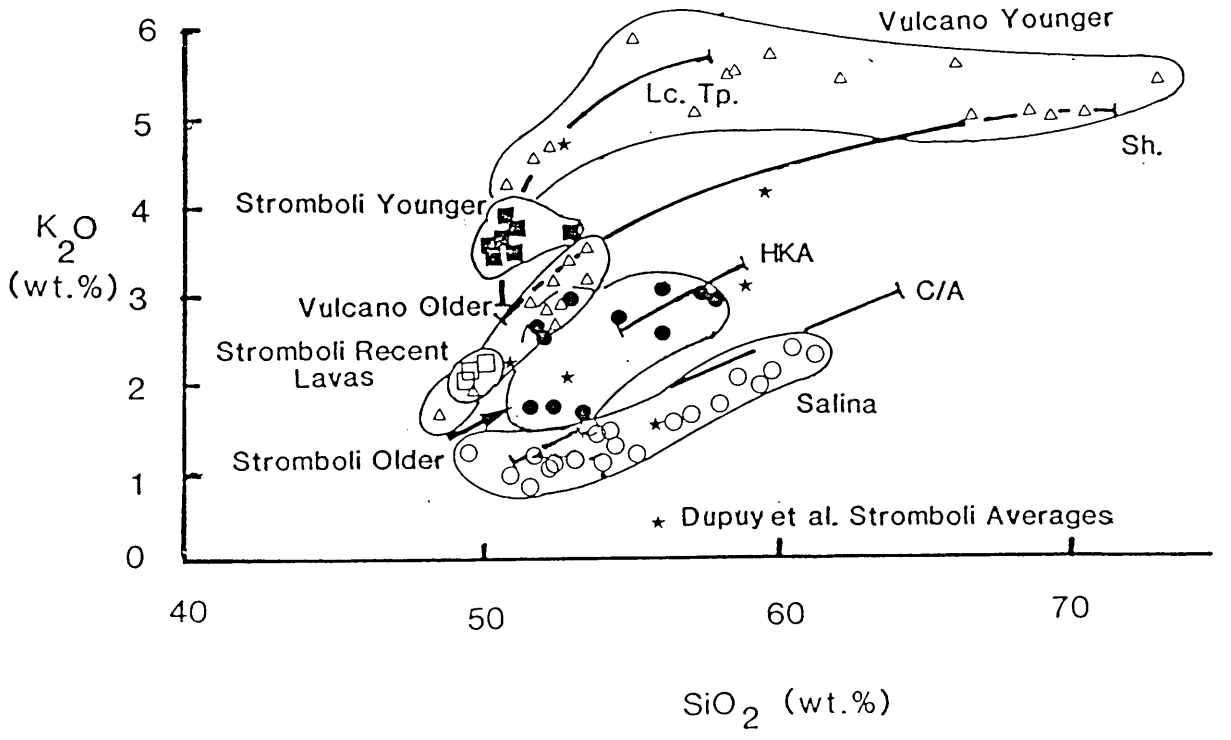

Fig. 2.4 K_2O v. SiO_2 for Aeolian lavas (this study). Solid lines are average trends of Barberi *et al* (1974) Key lc tp is leucite tephrite series, Sh is shoshonitic series, HKA is high k andesite series and C/A is calc alkaline series. Average Stromboli analyses (Dupuy *et al* 1981) are included for comparison

2.4.1 Salina

New analyses of Salina lavas agree well with the calc-alkaline trend of Barberi *et.al.* (1974). Lavas range from basalt to SiO_2 - rich andesite. Evidently lavas from Salina are representative of the Aeolian Islands calc-alkaline lavas which also occur on Filicudi and Alicudi.

2.4.2 Stromboli

Previous work by Rosi (1980) subdivided the Stromboli lavas into three groups, namely:-

(a) Calc-alkaline

(b) High K andesite

(c) Shoshonitic

which were thought to correspond to the whole arc trends of Barberi *et al.* (1974). These groups contained basic and intermediate end members which could be related by fractional crystallisation from three distinct parental magmas. The present study is principally concerned with the differences between the three groups and a number of the more basic lavas of Rosi's collection have been re - analysed. New data do not support the division into three series but agree with the classification of Dupuy *et al.* (1981) into four series, consistent with the original four trends of Barberi *et.al.* (1974). Average analyses from Dupuy *et al.* (1981) are included in figure 2.4. Along with the new data, these allow extension of thr high K andesite trend to more basic compositions.

Many workers *e.g.* Rosi (1980),Barberi *et al.* (1974) have noted a relationship between K_2O content and age, in the lavas of Stromboli. New data however, reveal that there is no detailed correlation between age and K_2O content. In fact within individual time intervals the K_2O content of lavas at a given SiO_2 content is quite variable. Whilst lavas with the highest K_2O content are indeed restricted to the younger series, it is also clear that the most recent lavas of the current activity are not the most potassic. A simple increase in K_2O content with time may not be implied.

2.4.3 Vulcano

The five stratigraphic groups recognised by Keller (1980b) and used in the discussion above may be considered in just two geochemical groups:-

GEOCHEMICAL GROUP	STRATIGRAPHIC GROUP
Older Series	VulcanoPrimordiale
	Caldera del Piano
Younger Series	Lentia Hills
	Vulcanello
	Fossa di Vulcano

The Lentia group of rhyolites are included in the Younger Series although it is unclear whether they are truely related to the other lavas of this group. Indeed as can be seen (fig. 2.4) the leucite tephrite (younger series) and shoshonitic (older series) trends tend to converge if the latter is extrapolated to SiO_2 - rich compositions. The older series lavas range from compositions close to the basalt - absarokite boundary to compositions which lie close to the shoshonitic trend of Barberi *et al.* (1974). The younger series lavas correspond quite closely to the leucite tephritic trend, but appear to extend the trend to higher SiO_2 values. As noted above the basic lavas of this group are not leucite tephrites in the strictest petrographic sense, however their major element geochemistry favours such a name rather than the term leucite basanite which better describes their petrography but generally refers to somewhat more mafic lavas.

2.5 CIPW Normative Compositions

2.5.1 Introduction

The classification of Peccerillo & Taylor (1976) utilised above, works well for subduction related lavas as shown. However, it considers only two of the major elements. The CIPW norm may be used to represent the whole major element analysis of a rock in terms of normative mineral phases. In a number of diagrams (figs. 2.5,2.6,2.7) normative data, which have been calculated assuming that 85% of the total iron is ferrous, are presented on a projection from plagioclase of the normative basalt tetrahedron (Yoder & Tilley,1962), generalised to include iron bearing end members of olivine and pyroxene. In this diagram the join diopside - olivine represents the critical plane of silica undersaturation (CPSU) whilst the join diopside - hypersthene is the critical plane of silica

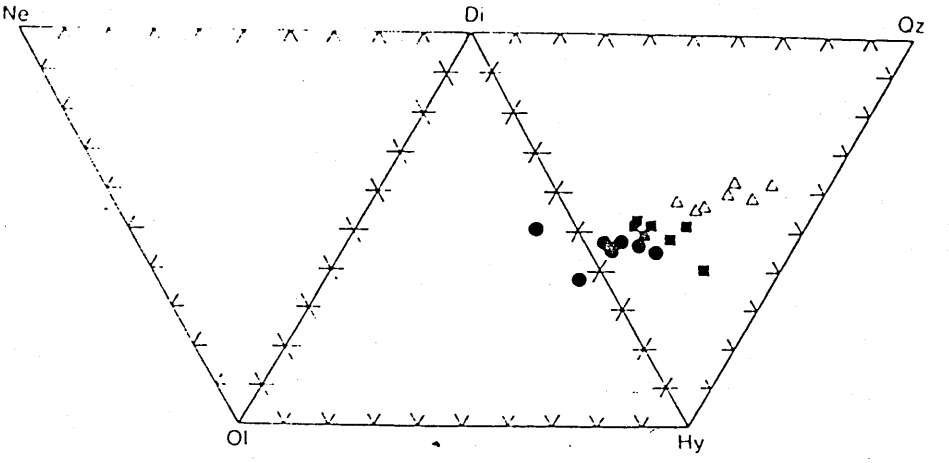

Fig. 2.5 Projection of the normative basalt tetrahedron for Salina lavas. Dots, SiO_2<53%, squares SiO_2=53 - 57% , triangles SiO_2>57%.

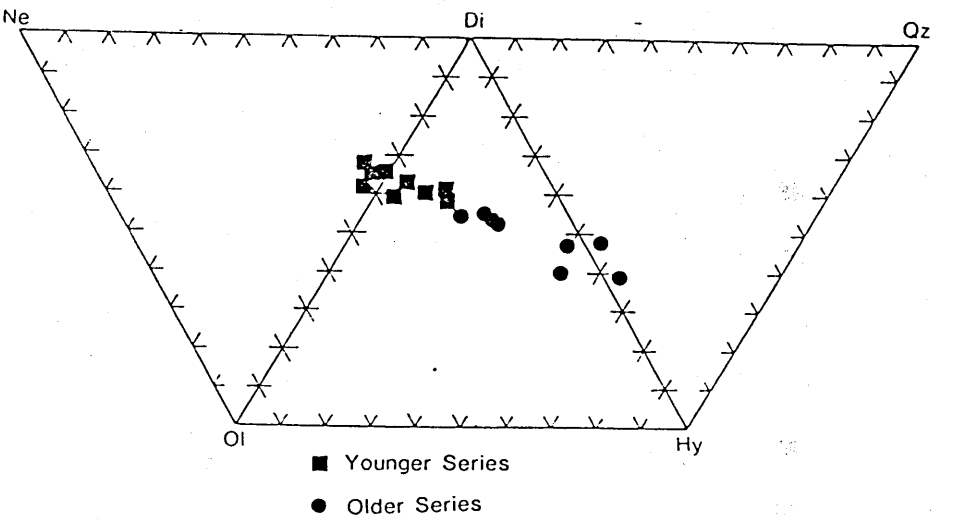

Fig. 2.6 Projection of the normative basalt tetrahedron for Stromboli basalts

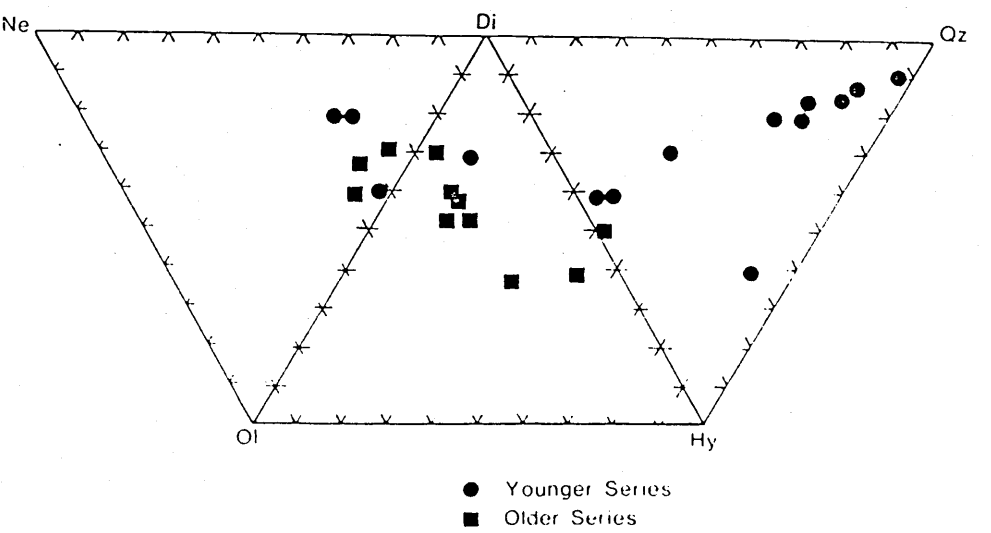

Fig. 2.7 Projection of the normative basalt tetrahedron for Vulcano lavas

saturation (CPSS). Though strictly applicable only to basalts, the evolved samples are plotted for Salina and Vulcano to illustrate possible fractionation effects.

2.5.2 Salina

Lavas from Salina (fig 2.5) straddle the CPSS. Only the most mafic lavas are olivine normative with more evolved compositions being quartz normative. It is clear that parental magmas to the Salina basalts were olivine, hypersthene normative *ie.* olivine tholeiites.

2.5.3 Stromboli

Basic lavas range from mildly nepheline normative to slightly quartz normative (fig 2.6). This variation is apparently not due to fractional crystallisation as the lavas plotted (fig.2.6) are all basaltic (SiO_2<53%) and furthermore no relationship between degree of silica saturation and degree of differentiation exists. This suggest that a range of parental magmas with variable SiO_2 saturation gave rise to the Stromboli lavas.

2.5.4 Vulcano

Vulcano older series lavas show a range from mildly nepheline normative to slightly quartz normative. The range of young series lavas is even wider with the rhyolites being highly quartz normative whilst basic tephrites are significantly nepheline normative (fig. 2.7). Notable in the Vulcano data is the fact that they, and indeed the Stromboli lavas straddle the CPSU. In low potassium systems the CPSU is a thermal divide which cannot be crossed by fractionation. Normally, nepheline normative basalts fractionate towards highly undersaturated phonolites. However, in K_2O - rich systems such as those under consideration here the role of potassium bearing mineral phases must be considered. At low pressure (<~2.5 Kb) leucite is the stable product of incongruent melting of alkali feldspar (Deer *et al.* 1966),hence during crystallisation leucite will precipitate on the liquidus before alkali feldspar. The effect of leucite fractionation from mildly undersaturated liquids is to push the liquid towards SiO_2 in the system Mg_2SiO_4 - $KAlSiO_4$ - SiO_2 (Luth, 1967). Therefore where lava series do span the CPSU this is indicative of relatively low pressure fractionation with leucite as an important phenocryst phase.

2.5.5 Summary of Normative Compositions

A range of normative composition exist , even within the basic lavas. Also these lavas show a wide range in K_2O content. Is it likely that these two features are in some way related ? Figure 2.8 shows a plot of K_2O against degree of SiO_2 saturation, expressed as the percentage nepheline or hypersthene in the norm. These two minerals are mutually

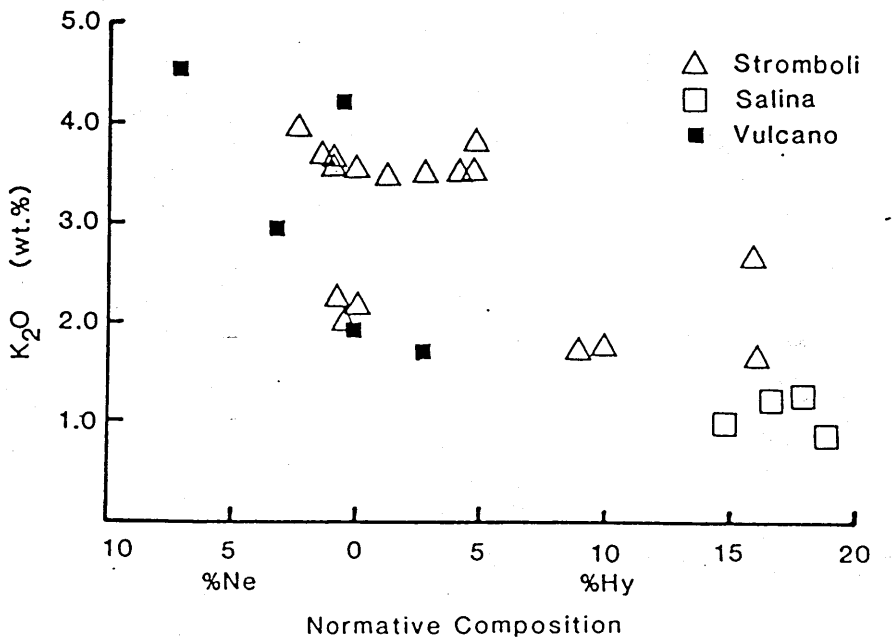

Fig. 2.8 K_2O v. SiO_2 saturation index for basaltic lavas (<52% SiO_2)

exclusive in the norm and give a measure of SiO_2 saturation. Only lavas with less than 52% SiO_2 are included in an effort to minimise the effects of fractional crystallisation. The diagram shows a negative correlation which implies that the K_2O content and SiO_2

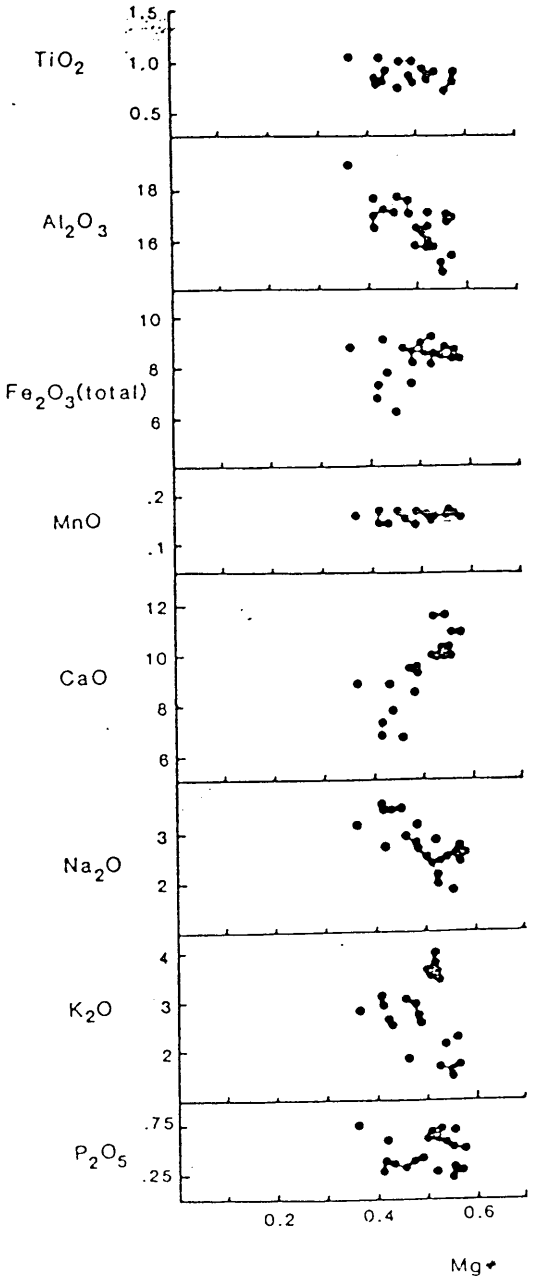

Fig. 2.9a Stromboli major element variation diagrams against Mg number assuming FeO = 0.85 total Fe.

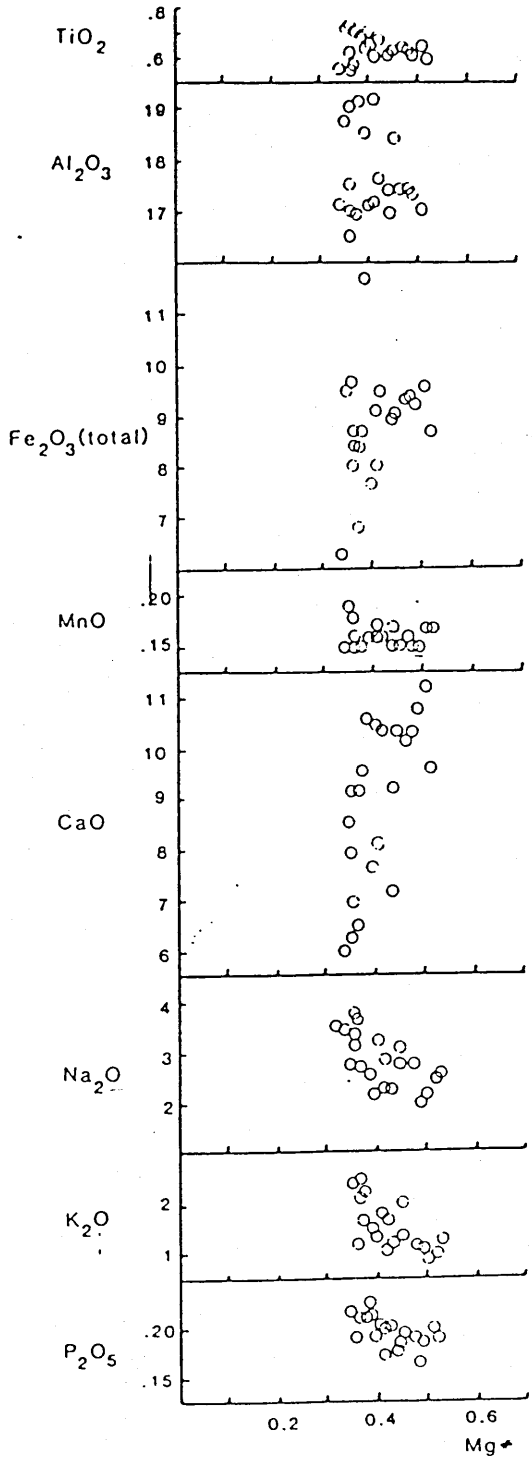

Fig. 2.9b Salina major element variation diagrams against Mg number assuming FeO = 85% total Fe.

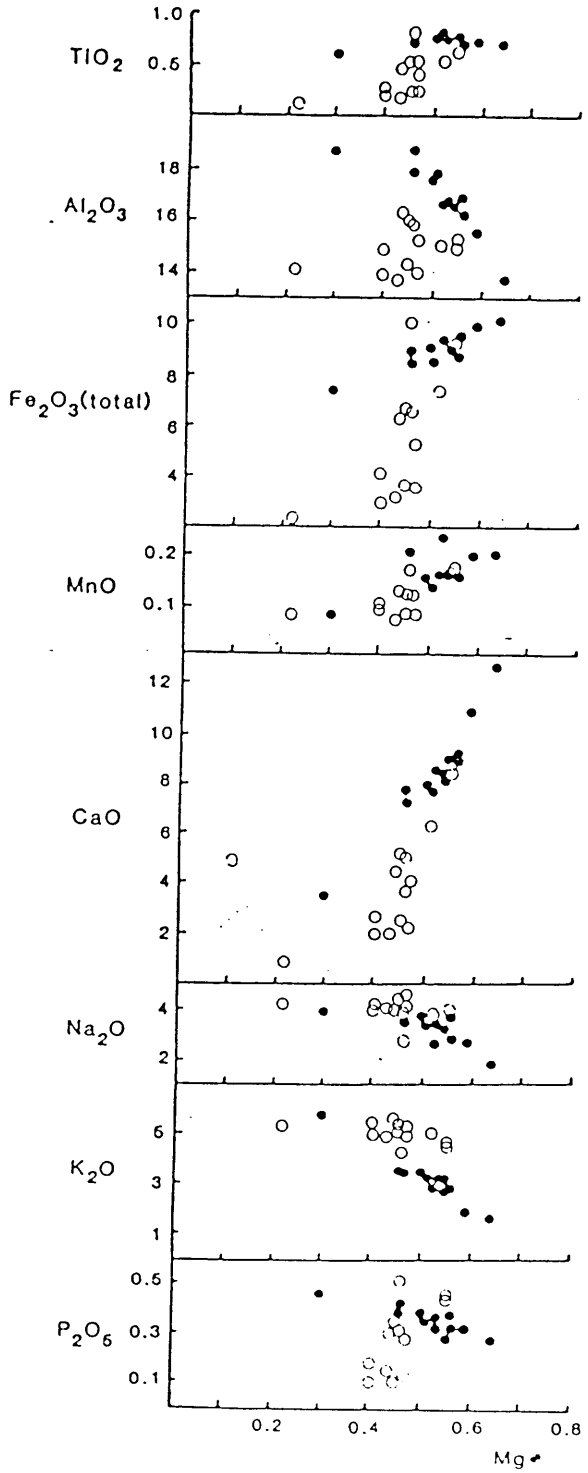

Fig. 2.9c Vulcano major element variation diagrams against Mg number assuming FeO = 85% total Fe. Open circles are younger series, closed circles are older series.

saturation state are linked. It should be noted that fractional crystallisation is likely to produce the opposite effect *ie.* increasing silica saturation (normative hypersthene) with increasing K_2O content.

The effect of increased K_2O in a lava on the norm will be to raise the amount of orthoclase produced. This in turn depletes the SiO_2 available for hypersthene and eventually nepheline must be produced to counter this SiO_2 deficiency, whilst the FeO and MgO in hypersthene are redistributed between olivine and diopside.

Given that K_2O plays a very important role in controlling the normative composition of these lavas, it is of interest to examine if the lavas analysed show significant variation in elements other than K_2O. In figure 2.9 a,b,c variation diagrams for the major elements against Mg number ($Mg/Mg+Fe^{2+}$) are plotted. These diagrams show very similar trends for most elements. Further investigation of the major element variations is required. This involves comparison of the major oxides recalculated on an anhydrous, K_2O - free basis, if K_2O is the only major oxide which shows significant variation then K_2O - free analyses should be similar for rocks of different K_2O content. In reality this is complicated by the effects of fractionation, but it is clear that if variations due to K_2O content are removed the trends for fractionation should be tightly constrained on major element variation diagrams. Selected K_2O - free, anhydrous analyses are plotted (fig.2.10) for rocks from Salina, Stromboli and Vulcano. The trends for Na_2O, CaO and MgO are extremely convincing, those for Fe_2O_3 and Al_2O_3 slightly less so. However it may be argued that these elements are reflecting variations in the fractionating assemblage rather than between parental magmas. This is especially pertinant given the relatively high recalculated SiO_2 values of the outlying Vulcano lavas.

2.6 Fractional Crystallisation Effects

2.6.1 Introduction

It was demonstrated in an earlier section that at least four distinct series of lavas can be recognised within the Aeolian Islands. Previous workers have assumed that these series represent fractional crystallisation trends. It is important to test such a hypothesis

particularly in order to ascertain that the large variation in K_2O between the series is not a

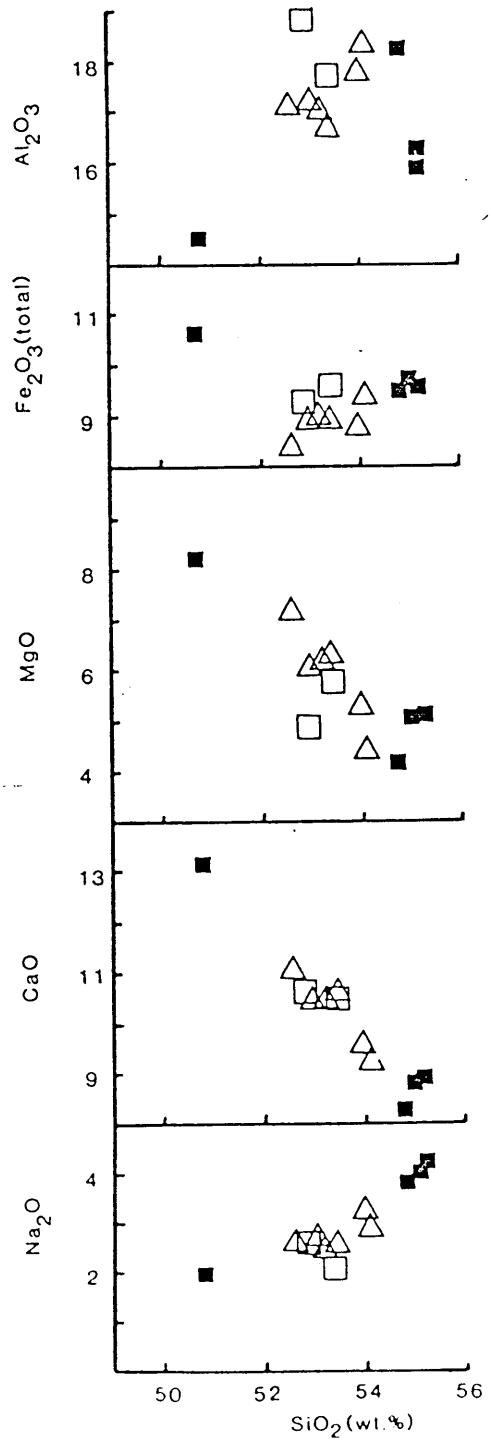

Fig. 2.10 Anhydrous, K_2O - free analyses of Aeolian lavas selected to span a wide range of K_2O contents. Filled squares are Vulcano, open squares are Salina and triangles are Stromboli.

result of fractional crystallisation. The calc-alkaline series of Salina was chosen for modelling as this shows a wide range of composition with continuous variation from basalt to andesite. It is believed that a model of this series is likely to be applicable to the high K andesite and shoshonitic trends as rocks from these groups have similar phenocryst assemblages to the Salina lavas. The Salina model is unlikely to accurately represent the leucite tephrite series whose lavas have significantly different mineralogy, with the occurrence of leucite and the lack of orthopyroxene. The leucite tephrite - rhyolite sequence of the Vulcano younger series will be modelled in the following chapter as it involves closer links with the trace element data.

2.6.2 Salina Variation Diagrams

As fractional crystallisation of basalt involves the removal of Ca , Al and Mg bearing phases, then bi-variate diagrams involving these three elements in various combinations may be used to infer the fractionating phases. In figures 2.11 and 2.12 a sympathetic relationship is established between CaO, Al_2O_3 and MgO which implies removal of phases rich in all three of these oxides. Suitable minerals which are found as phenocryst phases include clinopyroxene, orthopyroxene, olivine and plagioclase. A unique solution cannot however be obtained from these diagrams, therefore more detailed modelling is required.

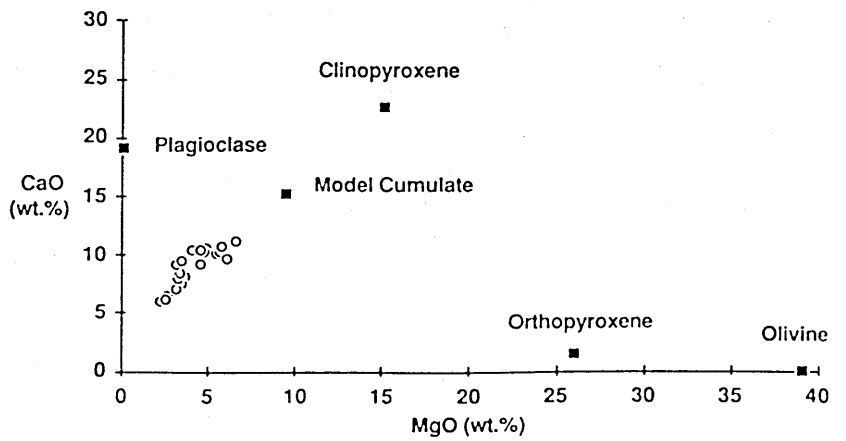

Fig. 2.11 CaO v. MgO of Salina lavas and mineral compositions used in least squares modelling

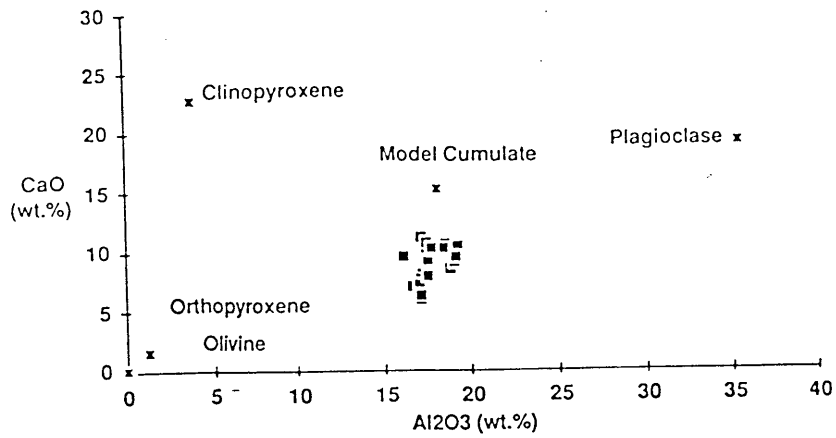

Fig. 2.12 CaO v.Al_2O_3 of Salina lavas and mineral compositions used in least squares modelling

2.6.3 Salina Least Squares Modelling

Fractional crystallisation can be modelled using the linear programming and least squares analysis method of Wright & Doherty (1970). In this approach the compositions of fractionating phases are added to the composition of an evolved liquid in an attempt to reproduce the composition of the parental liquid. The proportions of the various component phases are varied in order to achieve a best estimate by minimising the deviation between the modelled parent and the inferred parental lava. For each element a difference between the real rock and the modelled parent is produced (the residual). The sum of squares of all the residuals is an indication of the suitability of the model.

Table 2.2 shows the results of two least squares models for the lavas of Salina. These attempt to relate basalt ESAL 14 to andesite ESAL 24 by fractional crystallisation of observed phenocryst phases, using mineral analyses from a gabbroic cumulate xenolith from Pollara, NW Salina which contains olivine, orthopyroxene, clinopyroxene,plagioclase and titaniferous magnetite (Keller,1980a). These phases are plotted in the variation diagrams (figs. 2.11, 2.12).

Model One

	Opx	Ol	Cpx	Plag	Ore	ESAL24	ESAL14	Prod.
SiO_2	53.57	37.90	50.80	44.10		60.56	52.54	52.54
TiO_2	0.18		0.35		4.50	0.55	0.63	0.52
Al_2O_3	1.30		3.90	35.50	8.05	17.09	17.43	17.43
FeO	16.27	22.60	6.90		82.24	6.04	8.51	8.52
MnO	0.53	0.38			0.21	0.15	0.15	0.14
MgO	26.01	39.00	15.20		4.43	2.49	5.67	5.67
CaO	1.48	0.07	22.65	19.10		6.25	10.33	10.33
Na_2O	0.02			0.60		3.33	1.99	1.86
K_2O						2.43	1.10	1.26
% of	22	-2	26	46	8	F=0.52		
Cumulate				Sum of Squares of Residuals = 0.057				

Model Two

	Opx	Cpx	Plag	Ore	ESAL 24	ESAL 14	Product
SiO_2	53.57	50.80	44.10		60.56	52.54	52.54
TiO_2	0.18	0.35		4.50	0.55	0.63	0.52
Al_2O_3	1.30	3.90	35.5	8.05	17.09	17.43	17.43
FeO	16.27	6.9		82.24	6.04	8.51	8.52
MnO	0.53			0.21	0.15	0.15	0.13
MgO	26.01	15.20		4.43	2.49	5.67	5.68
CaO	1.48	22.65	19.10		6.25	10.33	10.33
Na_2O	0.02		0.60		3.33	1.99	1.90
K_2O					2.43	1.10	1.29
% of	19	28	46	7	F= 0.53		
cumulate				Sum of Squares of Residuals = 0.058			

Table 2.1 Salina least squares fractional Crystallisation models

Model one produces a good fit to the data, however a negative contribution from olivine is required. This may be geologically unreasonable or alternatively it may represent addition of olivine to the liquid along a reaction curve. In model two olivine is omitted and again the fit is good, albeit slightly worse than model one. Notably both models yield similar results involving an extract assemblage of:-

~20% Orthopyroxene

~27% Clinopyroxene

~45% Plagioclase

~ 8% Titaniferous Magnetite

with the degree of crystallisation around 47%.

The bulk composition of the model two cumulate is plotted in the variation diagrams (figs.2.11 , 2.12) and agrees well with the observed fractionation trends, emphasising the value of the least squares technique. It appears then that olivine is unlikely to be a fractionating phase during the evolution from basalt to andesite. The trace element implications of this observation will be discussed in the following chapter. The absence of olivine in the fractionating assemblage may explain the apparent disequilibrium textures of the olivine phenocryst in Salina lavas (as described above). These perhaps suggest a xenocrystal origin for the olivine crystals.

2.6.4 Implications of the Major Element Modelling

The results of major element modelling may be compared with experimental petrology to evaluate the model and help constrain some of the physical conditions which existed during magma evolution. Many experimental studies on calc-alkaline rocks have focussed on the nature of andesite genesis, and the likelihood of generating andesites as primary melts (*e.g.* Eggler & Burnham, 1973). Modelling predicts that the andesites of Salina are not primary but are differentiates of already quite evolved basalts. Many experimental studies are therefore not pertinant to discussion of Aeolian Island lavas.

Grove & Baker (1984) studied the evolution of tholeiitic and calc-alkaline lava series in terms of the system clinopyroxene - olivine - quartz - plagioclase. Lavas from Salina are plotted in the plagioclase saturated pseudoternary projection of this system (fig. 2.13). Many of the lavas lie within the primary phase field of olivine which is inconsistent with the absence of olivine as fractionating phase in the least squares modelling. However at elevated pressure in the system forsterite - diopside - silica (Kushiro, 1969) and in natural basalts (Kushiro, 1974, Bender *et al.*, 1978) the primary phase volume of olivine contracts whilst that of orthopyroxene grows, such that at a pressure of 5 kb the modelled parental

magma lies within the orthopyroxene stability field, and orthopyroxene, clinopyroxene and plagioclase are the liquidus phases as required by the least squares model.

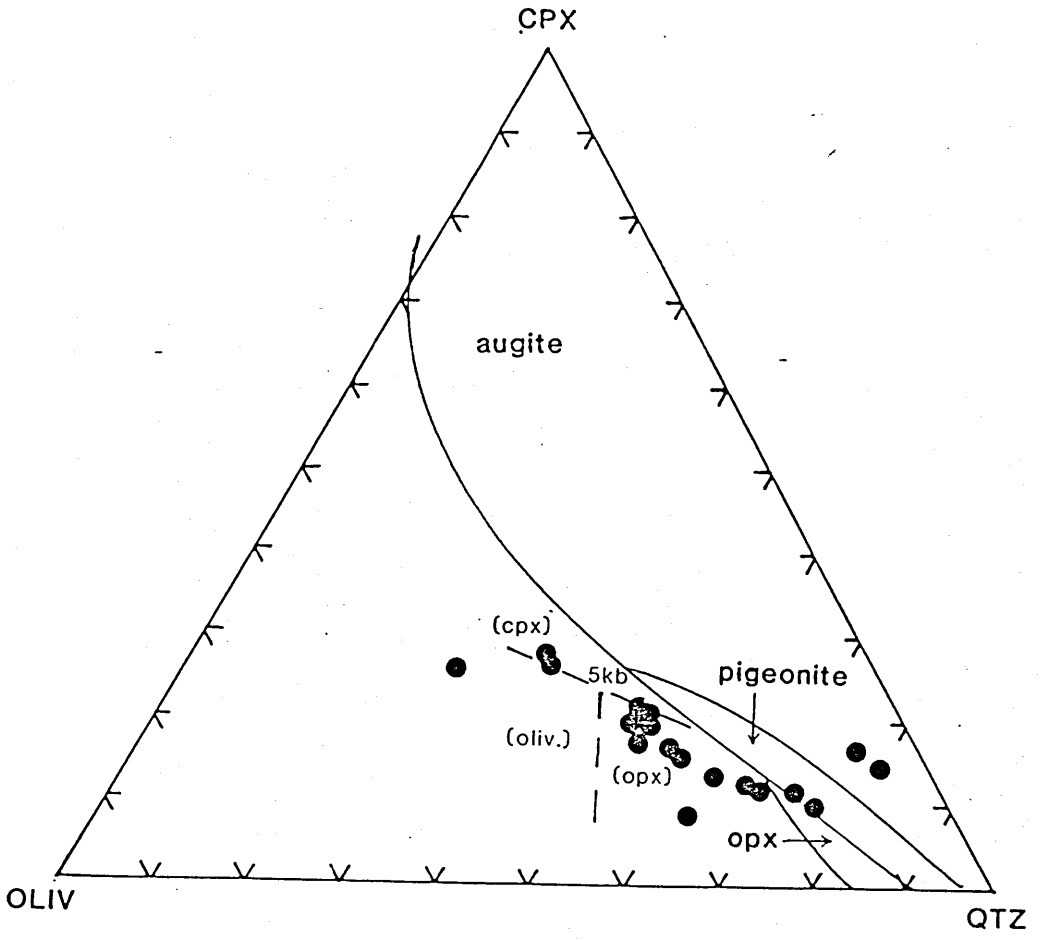

Fig. 2.13 Plagioclase saturated pseudoternary after Grove & Baker, (1984). Solid phase boundaries are 1 atm. Dashed phase boundaries correspond to 5 Kb. Dots are Salina lavas

Although high pressure investigations of this system have not been widely carried out, and conclusions rely on a small number of data it appears that an important constraint has been placed on the depth of fractionation. A pressure of around 5 Kb is required. It is perhaps significant that this estimate is close to that predicted at the base of the crust in

this region (~18 km). Further information may be obtained from the presence of plagioclase in the fractionating assemblage. In H_2O undersaturated systems, plagioclase may persist to pressures around 20 Kb (Baker & Eggler, 1982) but it is rapidly destabilised by increasing H_2O saturation (Yoder & Tilley, 1962, Eggler, 1972). Plagioclase presence does not therefore rule out fractionation at 5Kb. Evolution of magmas from the primary parental magma to basalt requires the use of trace elements in its assessment and will therefore be discussed in the following chapter.

2.6.5 Relevance of the Salina Model to Other Islands

As shown above four trends have been recognised on a K_2O v. SiO_2 diagram. One of these, the calc-alkaline trend has been successfully modelled in terms of fractional crystallisation. Two other trends, high K andesite and shoshonitic lie roughly parallel to the calc-alkaline trend, which suggests that they may be explained by similar models. Notably however, the leucite tephrite trend does not lie parallel to the others and cannot therefore be explained with a similar model. This is entirely as expected given that the leucite tephrite series lavas show distinctly different mineralogy to the less potassic lavas.

A dominant characteristic of the Aeolian Islands lavas is the wide range of K_2O observed within lavas of similar SiO_2 content. It is necessary to examine whether this variation may be produced by fractional crystallisation. Combinations of minerals may be inferred which will produce K_2O enrichment with only minor variations in SiO_2 (*eg.* pyroxene). However a minimum estimate of the amount of fractionation required to generate an absarokite (K_2O = 3.5%, SiO_2 = 51%) from a basalt of calc-alkaline affinity (K_2O = 1%, SiO_2 = 51%) may be obtained by treating K as a totally incompatible element (Kd = 0). In this case 72% crystallisation is required to produce the observed variation. Furthermore a lack of depletion in the compatible elements (Ba, Sr, Cr, Ni) in the potassic lavas implies that alkali feldspar, plagioclase, pyroxene and olivine cannot be included in the fractionating assemblage. Clearly the range of K_2O in these lavas is highly unlikely to be due to fractional crystallisation.

2.7 Summary of Major Element Data

Petrography and major element geochemistry have allowed the recognition of several distinguishable series of lavas within the Aeolian Islands. One of these has been successfully modelled and shown to be consistent with fractional crystallisation of observed phenocryst phases at pressures of 5 kb or greater. It is proposed that trends parallel to the modelled calc-alkaline trend may be explained by similar processes acting on different parental magmas. The high K_2O leucite tephrite trend may not be explained in this manner and will be further studied in the following chapter. It is therefore evident that the range of basic magmas is not likely to be the result of fractional crystallisation. It appears that the lava series recognised show great similarity in their major element compositions for all elements except potassium, this implies that the lava series originated from parental magmas which were similar in many characteristics but which displayed variable enrichment in K_2O.

CHAPTER THREE

Trace Element Geochemistry and an Introduction to Sr Isotope Geochemistry

3.1 Introduction

3.1.1 Aims of This Chapter

The aim of this chapter is to describe the trace element variations found in the lavas of Salina, Stromboli and Vulcano. These will be used to examine and extend hypotheses developed in the previous chapters, and to develop models based upon trace element and isotope data. In many cases the combined use of trace element and isotope data is important in interpretation and to this end Sr isotope data will be introduced, although the detailed relationships between different isotope systems and important element abundances and ratios will be discussed in more detail in chapter four.

3.1.2 MORB - Normalised Trace Element Patterns

The trace element compositions of rocks may be usefully presented on normalised abundance patterns. In figure 3.1 the compositions of representative Aeolian Islands basic lavas are shown normalised to the average mid ocean ridge basalt (MORB) of Pearce *et al.* (1981). In so far as these trace element patterns reflect the operation of various petrogenetic processes, they may be used to discriminate between lavas erupted in different tectonic environments. To illustrate this point, a subduction related lava from Grenada (6104, Thirlwall & Graham, 1984) and a lava from an intraplate environment , Bufumbira, Uganda (4342, Thompson *et al.*, 1984) are included for comparison with the Aeolian lavas (fig.3.1). The Grenada lava has a trace element pattern often recognised as typical of subduction related lavas; the large ion lithophile elements (LILE) *e.g.* Sr, Rb Ba, Th, K are highly enriched relative to the high field strength elements (HFSE) *e.g.* Nb, Ta, Zr, Hf which have abundances similar to average MORB. In contrast the intraplate lava is enriched in both the LILE and HFSE with Nb and Ta amongst the most enriched elements, relative to MORB.

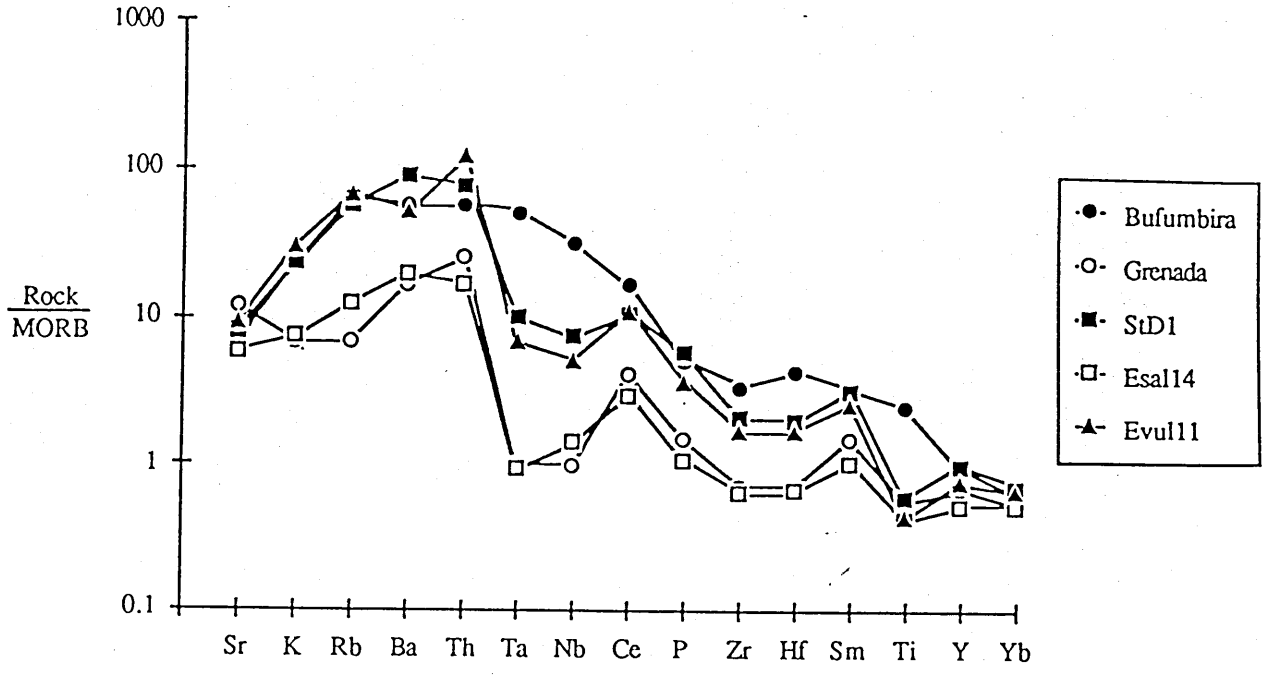

Fig. 3.1 MORB normalised trace element abundance patterns of Aeolian lavas, a subduction related lava from Grenada (Thirwall & Graham, 1984) and an intraplate lava from Bufumbira, Uganda (Thompson *et al.*, 1984) MORB normalising factors are from Pearce *et al.* (1981)

Lavas from the Aeolian Islands all display the negative anomalies for the HFSE which characterise subduction related lavas. The Salina lava (ESAL 14) is in fact very similar to the Grenada lava, emphasising its subduction related origin. Lavas from Stromboli on the other hand, whilst maintaining the characteristic pattern of subduction related lavas, have HFSE *abundances* considerably higher than those in average MORB. In a somewhat qualitative assessment it appears that Stromboli and Vulcano lavas display features of both subduction related and intraplate lavas, maintaining the characteristic shape of trace element pattern of the former whilst having HFSE abundances which approach those of the latter.

3.1.3 LILE - HFSE Relationships

To investigate the relationship between the LILE and the HFSE in the Aeolian lavas, they are plotted on a diagram of Rb/Y v. Nb/Y (fig. 3.2). Fields for Grenada (Thirwall & Graham, 1984) and the Italian Roman Province (Civetta *et.al.* , 1981, Rogers *et al.* 1985) define a vertical trend which is thought to be characteristic of subduction related trace element enrichment. Data from the Caroline Islands (Mattey, 1982) define an intraplate

enrichment style with a gradient close to unity.

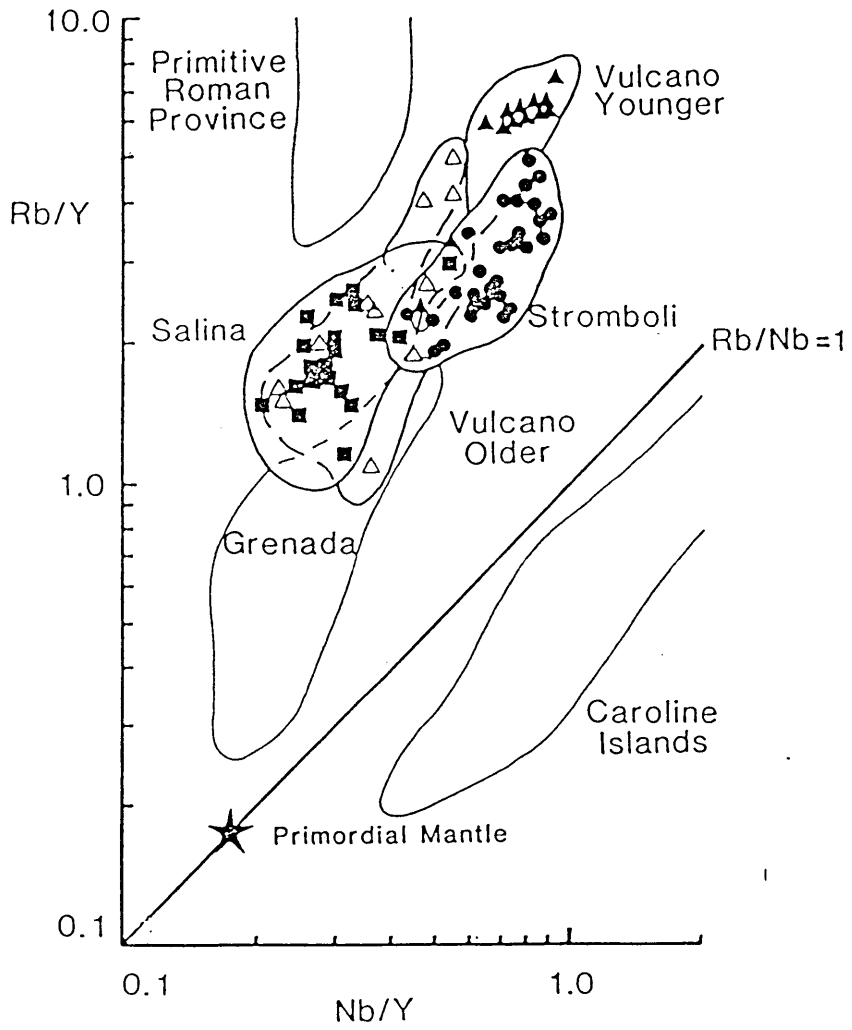

Fig. 3.2 Rb/Y v Nb/Y of Aeolian Islands lavas and comparison with basic Roman province lavas (Civetta *et al.*, 1981, Rogers *et al.*, 1985), Grenada lavas (Thirlwall & Graham, 1984), and Caroline Islands lavas (Mattey, 1982).

Clearly the Aeolian Islands show a component of subduction related enrichment, having elevated Rb/Nb relative to the primitive mantle value. However within the Aeolian data a significant component of HFSE enrichment is represented by elevated Nb/Y in the Stromboli and Vulcano lavas. Such an enrichment in the HFSE is inconsistent with the generally accepted view of the subduction related style of enrichment (*eg.* Pearce, 1983).

3.1.4 HFSE Variations

Given the conventional view that HFSE are not enriched by subduction processes, it is possible to explore the variations between lavas that are not due to subduction by considering only the HFSE. In a diagram of Zr/Nb v. Y/Nb (fig. 3.3) the Aeolian Islands display a range similar to that seen in a variety of oceanic basalts (Le Roex *et al.*, 1985). Lavas from Salina plot within the fields of normal (N - type) and transitional (T -type) MORB whilst Stromboli and some Vulcano lavas resemble "enriched" P - type (plume) MORB. This observation implies that a process other than subduction played a role in the genesis of the Aeolian arc lavas.

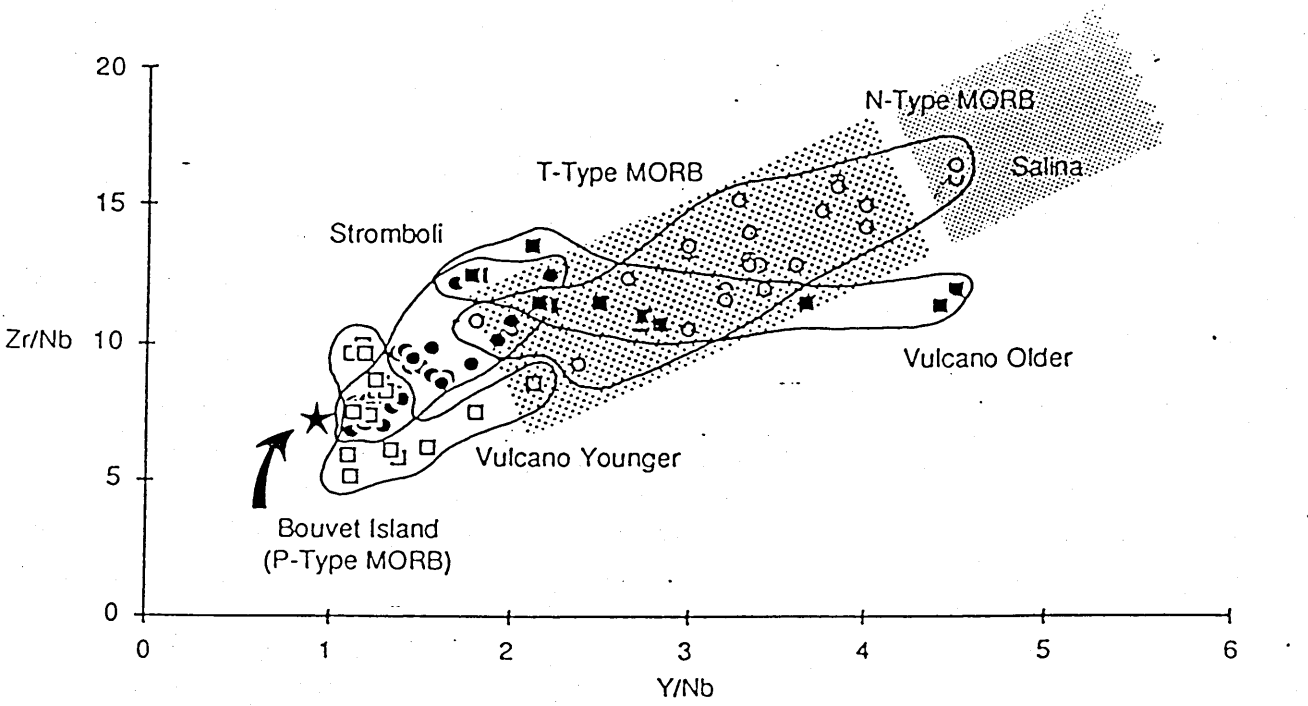

Fig. 3.3 Zr/Nb v. Y/Nb of Aeolian Island lavas. MORB and Bouvet fields from Le Roex *et al.* (1983).

3.2 Salina

3.2.1 Closed System Fractional Crystallisation

In order to verify the model of fractional crystallisation developed from major element data in chapter two, it is necessary to test its applicability to trace element data. Fractional crystallisation is modelled using the Rayleigh fractionation equation:

$$C_L = C_O \cdot F^{D-1}$$

where C_L is the composition of an element in the fractionated liquid,

C_O is the compostion of an element in the original liquid,

F is the fraction of liquid remaining,

and D is the bulk solid - liquid partition coefficient.

The form of the equation is such that for elements whose D is lower than around 0.1 it is possible to assume that D=0 without introducing significant errors, as the F^{D-1} term will not be greatly affected by such an assumption. In table 3.1 this assumption is made for a number of highly incompatible elements and the modelled fractionate from basalt ESAL 14 is compared with andesite ESAL 24. In the model F is set to 0.53, the value derived from major element modelling.

Element	C_L	$C_{ESAL\ 24}$
Rb	47	62
Th	6.32	5.87
Ta	0.32	0.36
Nb	9.4	8
Zr	109	108

Table 3.1 Model incompatible element abundances compared with those in andesite ESAL 24, for fractional crystallisation from basalt ESAL 14. D for all elements is 0 and F is set to 0.53

With the exception of Rb a good agreement between modelled and observed fractionate is obtained. Realistic assessment of analytical error requires reference to appendix C, however in short, it is believed that,with the possible exception of Rb, the incompatible elements are consistent with a closed system fractionation model in which 47% of crystallisation is required to produce the andesite from the basalt. The model is supported by the observation that there is no consistency in the errors of the calculated fractionate, for Rb and Ta the calculated abundances are lower than those required, whilst Th, Nb and Zr are all slightly in excess of their target values. If the discrepancies in the model were the result of a more complex open system process, then those discrepancies should at least all be in the same sense.

Incompatible elements suggest that the degree of crystallisation implied by major element modelling is indeed correct; however to assess the suitability of the modelled assemblage to the trace element data, it is necessary to examine the data for compatible elements. Table 3.2 shows a list of the elements which are used along with the phases into which they partition strongly, and the likely ranges of partition coefficient in those phases (Henderson, 1982).

Ni	Olivine (8 - 19), Clinopyroxene (1.4 - 4.4) Magnetite , Orthopyroxene (5)
Cr	Clinopyroxene (4.7 - 20), Orthopyroxene (10) Magnetite, Olivine (1.1 - 3.1)
Sr	Plagioclase (1.3 - 2.9)
V	Clinopyroxene, Magnetite
Sc	Orthopyroxene, Clinopyroxene, Magnetite

Table 3.2 A list of elements which are compatible during the fractionation of the Salina lavas and the phases into which they are strongly partitioned. Figures in parentheses are likely partition coefficients in basic magmas.

The elements shown in table 3.2 all behave compatibly during the evolution of Salina lavas from basalt to andesite, having lower concentrations in ESAL 24 than in ESAL 14. Of these elements the widest selection of distribution coefficient data is available for Ni, Cr and Sr, although even these are not well constrained for all the relevant mineral phases. However these three elements do provide a suitable test for the mineral assemblage implied by major element modelling.

The results of Rayleigh fractionation modelling of these compatible elements by 47% fractionation from ESAL 14 are shown in table 3.3 along with the partition coefficients which were utilised. The calculated values of Ni, Cr and Sr agree well with those analysed in andesite ESAL 24, emphasising the suitability of the fractional crystallisation model.

Trace element modelling of both incompatible and compatible elements reveals that the simple closed system fractionation model, developed to explain major element variations is quite adequate to explain many of the trace element variations observed in the lavas of Salina.

	Proportion of fractionating assemblage				
	.27	.19	.45	.08	
ELEMENT	D_{cpx}	D_{opx}	D_{plag}	D_{mt}	Kd
Ni	4.4	5.0	0.01*	15.0*	3.3
Cr	4.7	10.0	0.01*	5.0	3.6
Sr	0.14	0.02	2.3	0.01*	1.1

(* indicates estimated D)

	C_O (ESAL 14)	C_L (MODEL)	ESAL 24
Ni	21	5	3
Cr	64	13	16
Sr	698	655	660

Table 3.3 Salina compatible element fractionation model

3.2.2 Volcanological Implications of the Fractional Crystallisation Model

Although the model developed above adequately explains the variation from basalt ESAL 14 to andesite ESAL 24 it is by no means clear that such a process actually occurred to directly relate these two lavas. In a truly closed system one may expect the most evolved lavas to be erupted last and a relationship between increasing degree of evolution and time to exist. No such relationship exists on Salina (fig. 3.4). However it must be remembered that volcanism on Salina spans a time period of almost 0.5 Ma and occurred in at least six distinct episodes with, no doubt, periods of inactivity between them. Consideration of individual volcanic centres allows recognition of several trends of increasing SiO_2 with time (fig. 3.4). Perhaps these individual trends represent closed system fractionation of the magma bodies associated with individual active centres. The model developed above simply illustrates a hypothetical fractionation scheme which appears to have been followed by several magma batches of similar composition, fractionation having proceeded to different extents for different magma chambers.

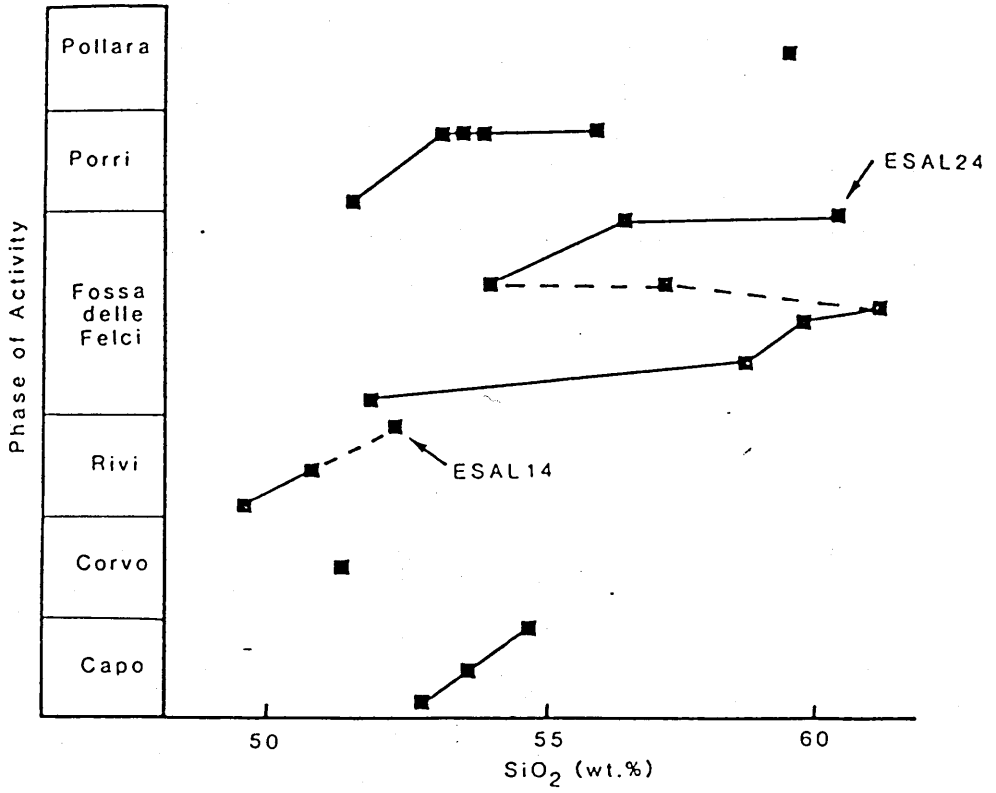

Fig. 3.4 Range in SiO_2 for the various phases of activity on Salina

In only one case does a single volcanic centre divert from a single trend in figure 3.4. The Fossa delle Felci centre shows a sharp decrease in SiO_2 associated with the eruption of the Favarolo series (Keller, 1980a) of lavas and pyroclastics. Such a variation may reflect an influx of primitive magma into the evolved magma chamber. In chapter two the hybrid nature of the Favarolo lavas was noted petrographically, perhaps then these lavas represent admixtures of fresh basic magma replenishing the magma chamber, with fractionated dacitic magma left within the chamber, itself a product of similar primitive magma to that replenishing the system. In such a case mixing would cause displacements parallel to the fractionation trends making its detection difficult.

Support for the above hypothesis is found in the observations of Keller (1980a) who described the Favarolo series as displaying a decrease in SiO_2 from base to top, ranging from dacitic pumice to low SiO_2 andesite. Such a variation is consistent with the Favarolo series representing the frozen relic of magma chamber replenishment, erupted prior to homogenisation of the magma body.

3.2.2 The Effects of Fractional Crystallisation on Trace Element Ratios

In an earlier section the trace element ratio Nb/Y was used to illustrate the enrichment style characteristic of intraplate volcanoes. Given the wealth of evidence in support of fractional crystallisation in lavas from Salina, the effects of this process on trace element ratios must be explored before inferences may be made about processes which occur prior to or during magma genesis. In the discussion which follows Nb and Y are replaced by Ta and Yb respectively, these elements have similar chemical properties and hence geological affinities, but they are analysed at higher precision by Instrumental neutron activation analysis (INAA).

In table 3.4 the effects of the Salina fractionation model are calculated for Ta and Yb. The evolved compositions which are calculated agree well with those of andesite ESAL 24 and illustate that fractional crystallisation of a pyroxene bearing assemblage is capable of raising Ta/Yb quite significantly. The variation is achieved because $D_{Yb} > D_{Ta}$ for clinopyroxene *ie.* Ta is more incompatible than Yb, and as such the Ta concentration is increased more rapidly than that of Yb during fractional crystallisation involving pyroxene.

	Proportion of Fractionating Assemblage				
	Opx	Cpx	Plag	Mt	Kd
D_{Yb}	0.5	1.2	0.07	0.01	0.46
D_{Ta}	all assumed to be equal to 0.001				0.001
ESAL 14	C_O	Ta = 0.17, Yb = 1.77, Ta/Yb =0.096			
MODEL	C_L	Ta =0.32, Yb = 2.49, Ta/Yb = 0.129			
ESAL 24		Ta =0.36, Yb = 2.44, Ta/Yb = 0.148			

Table 3.4 Salina fractional crystallisation model for Ta and Yb. Partition coefficient data are from Henderson (1982). N.B. D_{Ta} in magnetite may be considerably higher than 0.001. Data are scarce but Ewart (1982) suggests a value in excess of 10 for D_{Nb} in magnetite which is likely to be similar to D_{Ta}.

It would appear then that the range of Ta/Yb values in the Salina lavas is the result of fractional crystallisation, not a reflection of within plate enrichment processes.

Sample ESAL 19, an evolved andesite has Ta/Yb greater than ESAL 24 (0.23). Hornblende phenocrysts were reported from this lava in chapter two. As amphibole has a

high D_{Yb} (≈1) (Henderson, 1982) it is likely that amphibole fractionation has led to elevated Ta/Yb. Fractionation of amphibole will not only alter Ta/Yb ratios but will also affect the shape of the rare earth element (REE) patterns. Introducing amphibole into the fractionating assemblage is likely to increase REE D values particularly those of the middle REE. Figure 3.5 illustrates the effect of replacing pyroxene with amphibole in a fractionation model similar to that implied for Salina. Lavas which fractionate amphibole are likely to have lower abundances of the MREE than those which do not. This is indeed the case for ESAL 19 whose REE pattern is similar to those of amphibole - free Salina lavas except for lower Tb (and Gd) values (fig. 3.6).

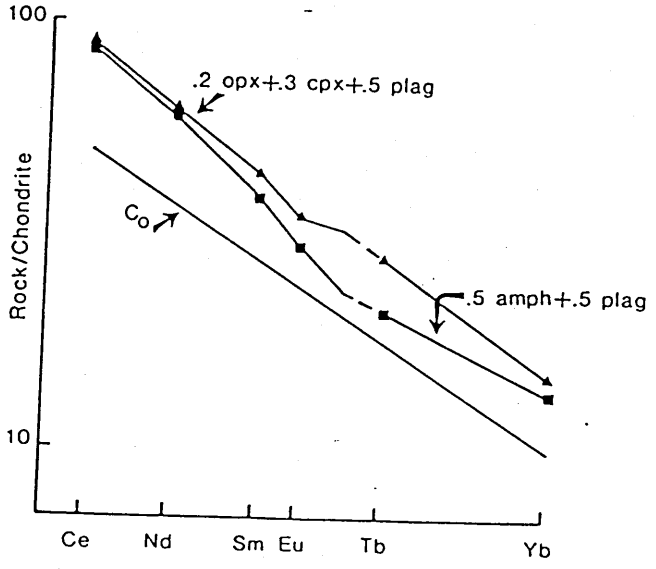

	D_{Opx}	D_{Cpx}	D_{Plag}	D_{Amph}
Ce	.02	.34	.14	.34
Nd	.04	.60	.08	.60
Sm	.05	.90	.08	.91
Eu	.06	.90	.32	1.01
Tb	.05	1.0	.10	1.40
Yb	.34	1.0	.07	.97

Fig 3.5 Model to contrast the effect of pyroxene and amphibole on the REE. Partition coefficients are given in the table.

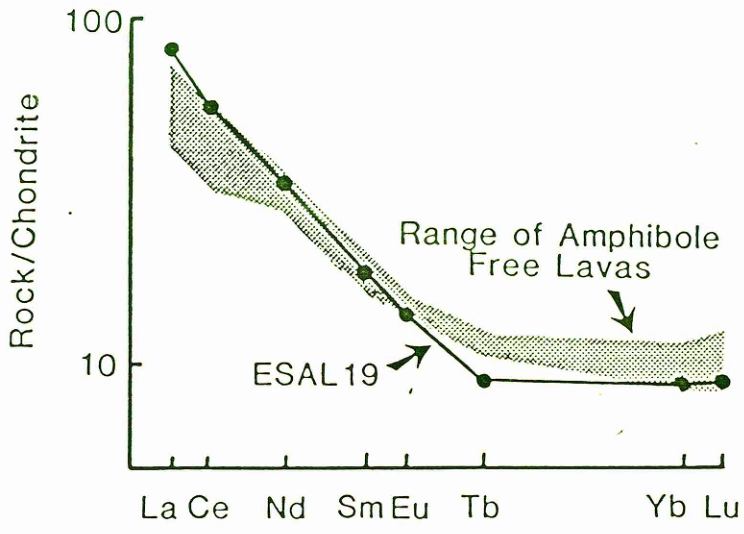

Fig 3.6 Effect of amphibole fractionation on ESAL 19 in contrast with amphibole free lavas.

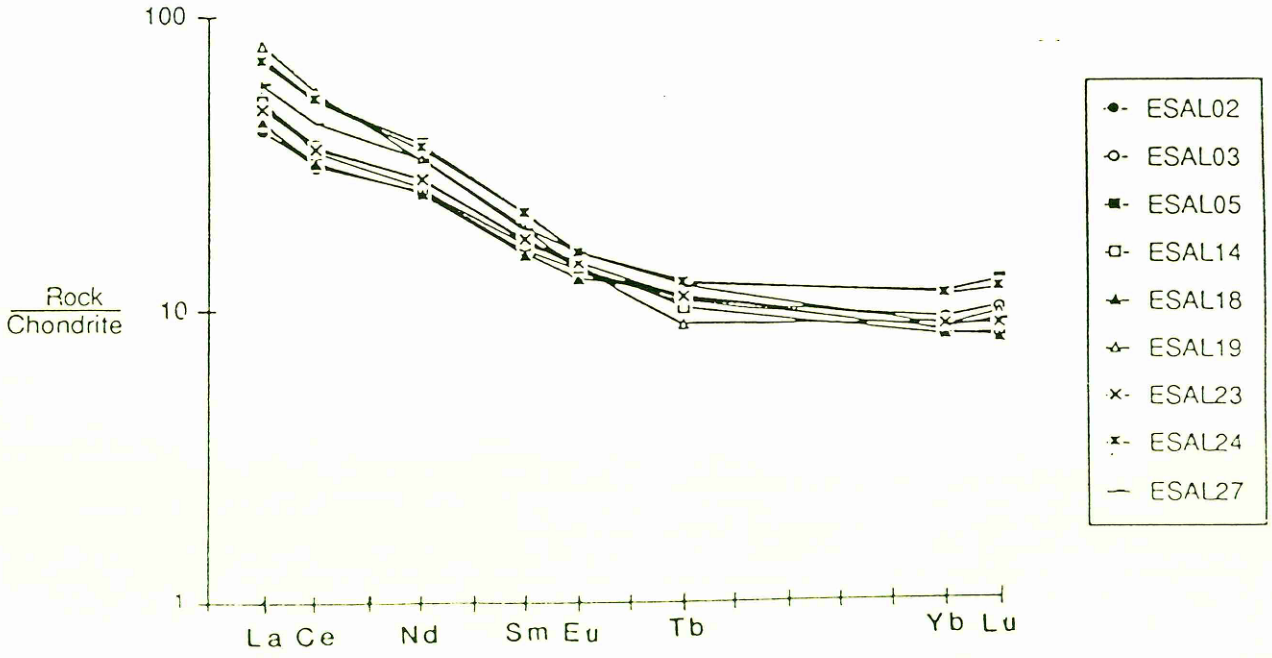

Fig 3.7 REE patterns of Salina lavas

Another point of interest in these REE fractional crystallisation models (fig. 3.5), is the absence of a significant Eu anomaly in either model despite the presence of 50% plagioclase in the fractionating assemblage. Such a situation is consistent with the lavas of Salina (fig.3.7). Conventionally Eu anomalies are thought to arise in response to the preferential incorporation of divalent Eu into the plagioclase structure relative to the other trivalent REE cations which cannot enter the Ca^{2+} site. Clearly the partitioning of Eu into plagioclase will be strongly dependant on the redox conditions of the magma. High fO_2 will oxidise Eu and discourage the formation of Eu anomalies. Such an explanation *may* be used to reconcile the lack of Eu anomalies in the Salina lavas. However, an alternative, preferable explanation is available. The partition coefficient of Eu in plagioclase is strongly temperature dependant, an inverse relationship exists between D_{Eu} and temperature (Drake & Weill, 1975). In hot basaltic liquids D_{Eu} is around 0.32 (Henderson, 1982), if pyroxene (particularly clinopyroxene) is also present in the fractionating assemblage its relatively high partition coefficients tend to dominate the bulk partition coefficients of the REE to such an extent that $Kd_{Sm} \approx Kd_{Eu} \approx Kd_{Gd}$ and hence only small Eu anomalies are produced.

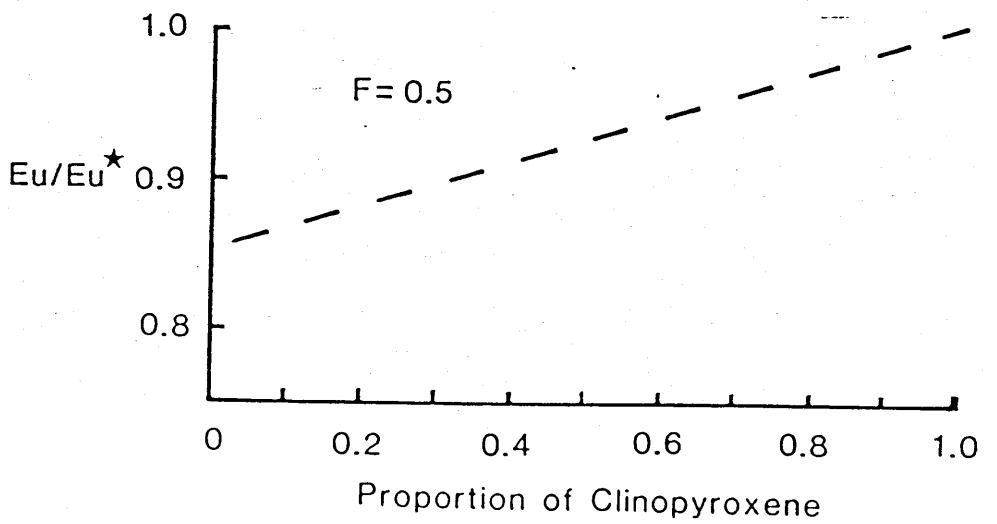

Fig 3.8 Model to illustrate the effect of changing the clinopyroxene to plagioclase ratio of the cumulate in fractional crystallisation of these two minerals, for a given degree of crystallisation (F=0.5). D_{Sm}(Plag.)=0.08, D_{Sm}(Cpx)=0.9, D_{EU} (Plag.) =0.32, D_{Eu}(Cpx)=0.9 D_{Gd}(Plag.)=0.1, D_{Gd}(Cpx)=0.9.

Figure 3.8 illustrates the size of Eu anomaly produced by 50% crystallisation of assemblages which vary from pure plagioclase to pure clinopyroxene, even in the former case only a relatively small Eu anomaly is produced ($Eu/Eu^* \approx 0.85$). Clearly the presence or absence of pyroxene in the fractionating assemblage plays an important role in controlling the development of Eu anomalies. This mineralogical constraint must be borne in mind before any assessment of redox conditions based upon REE distribution may be made. Further discussion of the temperature dependance of D_{Eu} in plagioclase will be carried out in a later section dealing with intermediate and acidic lavas from Vulcano.

It has been shown then that the absence of negative Eu anomalies in the REE pattern of the Salina lavas is consistent with the preferred fractional crystallisation model. The phase diagram modelling of this fractionation sequence implied that the early stages of evolution from primary melt to basalt should be accomplished by removal of olivine + plagioclase. Olivine has very low D values for REE and would not dominate the bulk Kd in the manner implied for pyroxene. Negative Eu anomalies would arise in response to crystallisation of olivine + plagioclase, although these would be relatively small ($Eu/Eu^* > 0.85$). Salina basalts do not show even small negative Eu anomalies implying that olivine + plagioclase was not the stable assemblage during early fractionation. Perhaps more significant are the low abundances of Ni and Cr in all Salina lavas which implies removal of olivine and pyroxene rather than olivine and plagioclase.

Despite the lack of primitive samples from Salina a simple model to represent the evolution from primitive parental magma to the basaltic lavas erupted may be constructed. The highest Ni and Cr contents of any Salina lava are 38 ppm and 140 ppm respectively (ESAL 13). An estimate of the composition of a primary melt is Ni = 250 ppm, Cr = 800 ppm, these values are similar to the most likely candidates for primary magmas in the Roman province, the Vulsini leucite basanites (Rogers *et al.*, 1985). As such this estimate probably represents a minimum value. If an assemblage with equal quantities of orthopyroxene and olivine is assumed, then the transition from parental magma to basalt is found to require around 25% crystallisation. Furthermore if the compositions of olivine (Fo_{85}) and pyroxene (En_{85}) are assumed an estimate of the primary magma composition may be calculated (table 3.5)

SiO_2	50.69
TiO_2	0.50
Al_2O_3	12.92
Fe_2O_3*	1.07
FeO	8.67
MnO	0.13
MgO	14.75
CaO	8.50
Na_2O	1.88
K_2O	0.76
P_2O_5	0.15

* FeO = 0.85 total Fe

Table 3.5 Calculated composition of Salina primary magma

The replacement of plagioclase with orthopyroxene may be reconciled with the results of experimental petrology. In dry systems plagioclase may persist to pressures of around 20 Kb. However, Eggler (1972) has shown the rapid destabilisation of plagioclase in systems which approach H_2O saturation. In 10 kb experiments orthopyroxene replaced plagioclase as a liquidus phase in H_2O saturated conditions (H_2O > 2.5%). The assemblage required by the basalt to andesite fractionation already suggests elevated pressures (>5 kb). The presence of orthopyroxene during the earliest stages of fractionation emphasises the high pressure (>10 Kb) fractionation process which was active beneath Salina and the likely polybaric nature of fractional crystallisation beneath Salina.

A model of fractional crystallisation has been developed for the lavas of Salina which explains the range of rocks as products of relatively high pressure (5 - 10 kb) closed system fractionation of primary magmas rich in MgO. The model is consistent with both major and trace element distributions within the lavas and its dominantly closed system is consistent with the relatively restricted variations in $^{87}Sr/^{86}Sr$ (0.7041 - 0.7047),changes in which are indicative of open system behaviour.

3.2.4 Trace Element Component Recognition

Pearce (1983) established an approach based upon MORB normalised trace element patterns which aims to divide the trace element composition of a lava into three components whose relative contribution may be assessed. These components are:-

(a) Depleted Mantle

(b) Within - plate (enriched) mantle

(c) Subduction zone component

This approach has not been extensively tested and very rarely linked to isotopic work. In the discussion which follows the model will be used as an investigative tool and its findings tested for compatibility with isotopic data.

Peculiarities of the trace element pattern of Aeolian Islands lavas have required some minor adjustments to the method of trace element component recognition proposed by Pearce (1983). Details of the construction used here are given in appendix D. In essence the model depends on a number of simple assumptions derived from investigation of the trace element pattern of lavas worldwide.

(a) Yb is not enriched by either subduction or within - plate processes. Its normalised abundance is therefore representative of the depleted mantle component.

(b) HFSE are not enriched by subduction related processes, hence their normalised abundance represents the within - plate plus depleted mantle components.

(c) The remaining area of the trace element pattern represents the subduction related component.

A temptation of the method is to ascribe the three components to distinct sources, this may have dangerous consequences. The trace element composition of a source is controlled by the processes that have occured within that reservoir. It is a function of the partition coefficients pertaining during any transport of material into, out of or through the reservoir. For example, the ratio Ta/Yb is a direct measure of the importance of the within - plate component. It was shown above that fractional crystallisation of pyroxene may increase Ta/Yb giving rise to a larger within - plate component. In a similar manner, small volume partial melts of the mantle may have elevated Ta/Yb compared with their source leading to over estimation of the importance of enriched mantle in their genesis. Only when isotopic evidence of an *ancient* trace element fractionation event is available is it safe to assume that the within - plate component represents an enriched mantle source.

The approach developed by Pearce (1983) is strong in the distinction of enrichment associated with subduction related processes, from those mantle enrichment processes not related to subduction. With the exception of Sr, the MORB normalised diagram displays the elements in order of increasing (left to right) bulk partition coefficient (Kd) in a

lherzolite mantle. Hence, any process, however complex, which involves melt production or migration within the mantle will not produce anomalous peaks or troughs in the resultant trace element pattern. However, it was shown above that the HFSE show negative anomalies in subduction related lavas. A subduction component may therefore be distinguished from the mantle - derived component, where the former is the source of HFSE anomalies caused because the subduction component evolved in an environment with radically different Kds to the lherzolite mantle. The nature of this environment is controversial, but hypotheses include:-

(a) The subducting slab in eclogite facies P-T conditions with a stable minor phase rich in HFSE (*eg.* Green, 1981).

(b) The mantle wedge above the subducting slab with a stable minor phase (*eg.* Morris & Hart, 1983).

(c) An aqueous environment derived by dehydration of the subducting slab where element abundances are controlled by H_2O-rock partition coefficients. (*e.g.* Hawkesworth *et al.* 1977).

The MORB normalised trace element pattern of a Salina basalt (ESAL 14) is trisected into its constituent components (fig 3.9). The LILE are dominantly subduction derived, including for example around 90% of the potassium. The low HFSE abundances imply only minor LILE contribution from the mantle components. Notably around 85% of the Sr in ESAL 14 is subduction derived, this is in fact a minimum value as removal of Sr during fractional crystallisation of plagioclase would tend to reduce the calculated subduction zone contribution. The $^{87}Sr/^{86}Sr$ ratios of Salina lavas fall within a narrow range (0.7041 - 0.7047), if the above hypothesis is correct then ~85% of this Sr is subduction derived, implying an isotopic composition of the subduction component close to that of the lavas. Such a low $^{87}Sr/^{86}Sr$ precludes a dominant contribution of radiogenic Sr in the subduction component from subducted crustal material, as suggested elsewhere in subduction/ continental collision zones (Rogers *et al.* , 1985, Whitford *et al.* , 1981).

Another feature of interest in the trace element patterns of Salina and indeed all the Aeolian Islands lavas is the ubiquitous negative Ti anomaly, with the Ti abundance always below that required to form the depleted mantle component ($Ti_n < Yb_n$). Such an anomaly may be explained by fractionation of a titaniferous phase*eg.* magnetite, but the occurrence of an anomaly even in the basalts requires very early involvement of this phase.

Alternatively the anomaly may reflect the presence of a titaniferous minor phase within the mantle wedge.

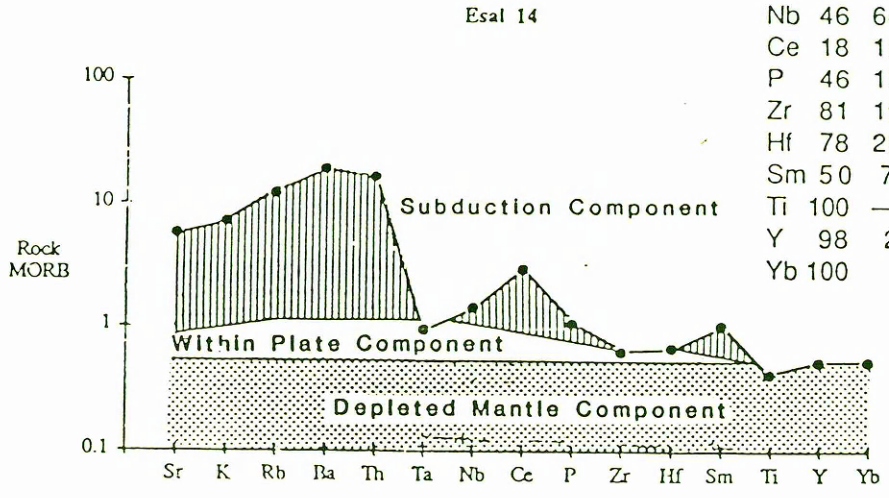

	DM	WP	SZ
Sr	9	9	85
K	7	4	89
Rb	4	6	90
Ba	2	4	94
Th	3	4	93
Ta	53	47	—
Nb	46	64	—
Ce	18	12	70
P	46	16	38
Zr	81	19	—
Hf	78	22	—
Sm	50	7	43
Ti	100	—	—
Y	98	2	—
Yb	100		

Fig 3.9 MORB normalised trace element abundance pattern of Salina lava ESAL 14, showing trace element components, after Pearce, (1983). Table gives percentage contribution of the components. DM depleted mantle, WP within plate, SZ subduction zone

3.3 Stromboli

3.3.1 Introduction

In chapter two it was shown that the island of Stromboli has erupted lavas with a large range of K_2O contents; representatives of all four Aeolian Islands lava series are found on Stromboli and it has been emphasised that the variations between these series are unlikely to be the result of fractional crystallisation. Also recognised above was the relatively high HFSE abundances of the Stromboli lavas compared with other subduction related lavas. It was shown above that fractionation of pyroxene can alter Ta/Yb but it is clear that this has had little effect on Stromboli lavas as no correlation exists between Ta/Yb and Mg number (fig. 3.10). Furthermore the lavas which have the highest Ta/Yb are amongst the least evolved products of the volcano. It appears likely that the Stromboli range in Ta/Yb reflects variation between different parental magmas. A positive correlation (fig 3.11) between K_2O and Ta/Yb implies that this within - plate style of (HFSE) enrichment

accompanied the transition from calc-alkaline to potassic magmatism.

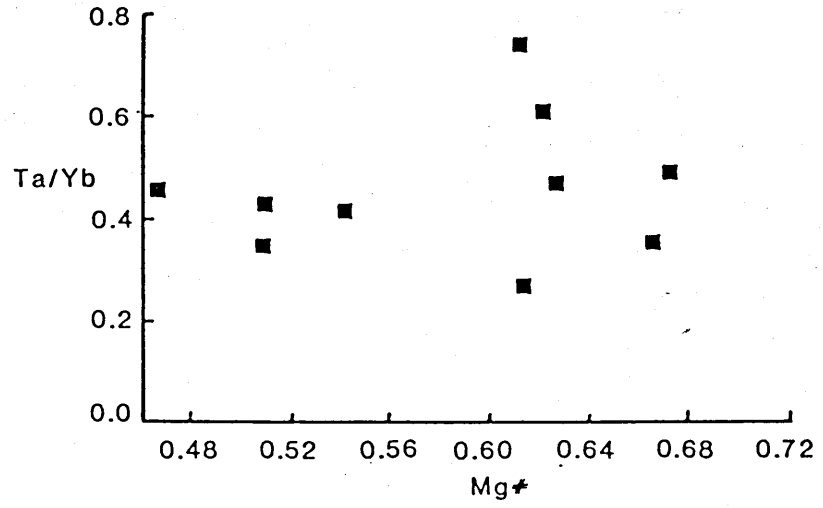

Fig. 3.10 Ta/Yb v. Mg Number for Stromboli lavas

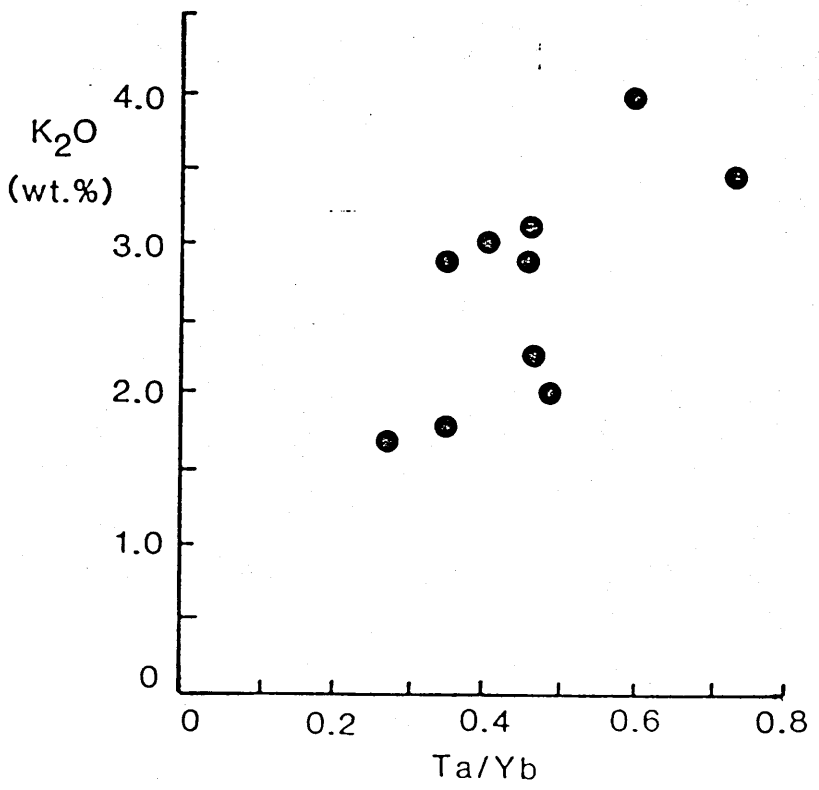

Fig 3.11 K_2O v. Ta/Yb for Stromboli lavas

3.3.2 Relationship Between the LILE and HFSE

The relationship between the LILE and HFSE was introduced above in figure 3.2 which is geochemically analogous to figure 3.12 This was used by Pearce (1983) to

distinguish subduction related LILE (Th) enrichment from within - plate enrichment in which both the LILE (Th) and the HFSE (Ta) are equally enriched. Stromboli data plotted on such a diagram (fig. 3.12) fall on a rather ill-defined trend towards higher Th/Yb and Ta/Yb. However it is unclear whether the data are more consistent with a trend parallel to the within - plate array or with a trend which converges upon that array. However a fairly good inverse correlation between Th/Ta and Ta/Yb (fig. 3.12 inset) reveals that a trend convergent upon the within - plate array is favoured.

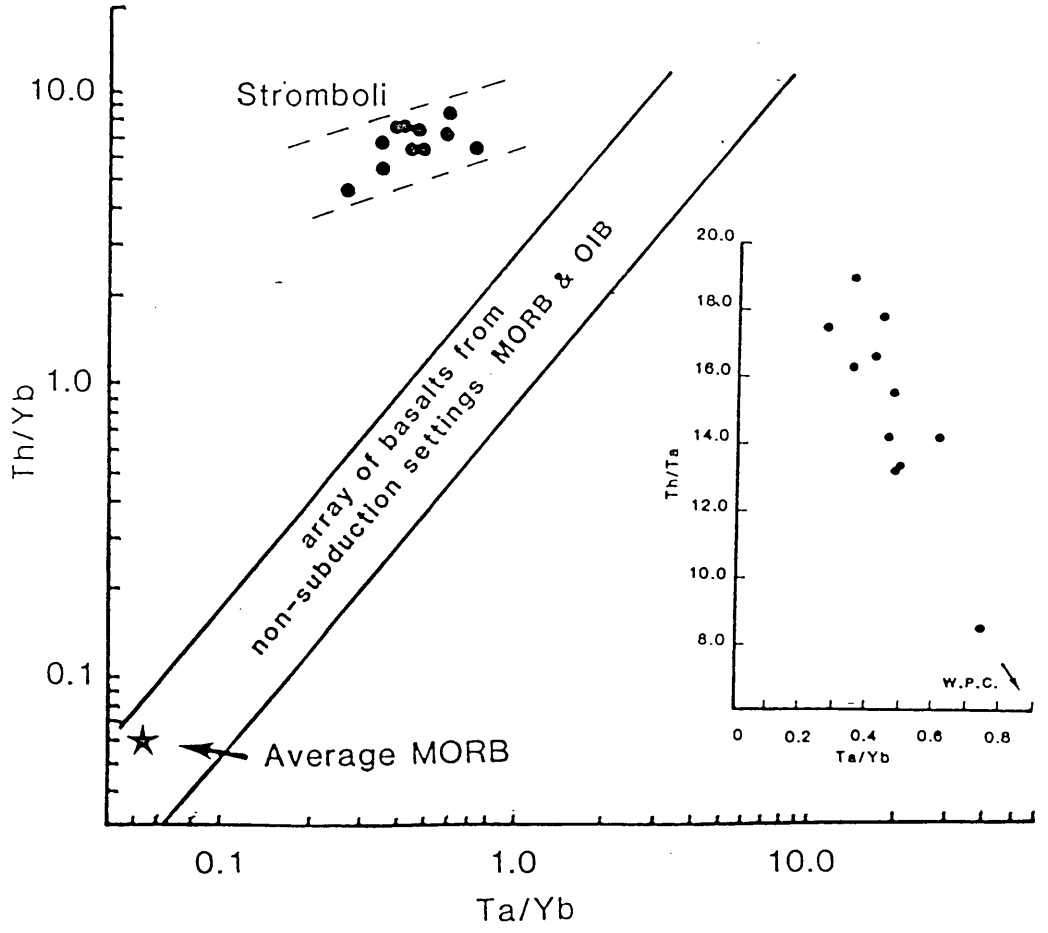

Fig. 3.12 Th/Yb v. Ta/Yb after Pearce (1983), showing Stromboli lavas convergent on the within-plate array. Inset Th/Ta v. Ta/Yb enforces this conclusion, WPC indicates within plate component.

Modelling has shown that the above observation is critical to the interpretation of the Stromboli data. The observed variations may imply simple mixing of a subduction related component with a within plate enriched mantle source, or the data may reflect extraction of magma from a source enriched (in Th/Yb) by subduction by a process capable of enriching Ta/Yb *e.g.* small degree partial melting, zone melting. The difference between these two types of process is subtle yet important; did HFSE enrichment precede or follow subduction related enrichment ?

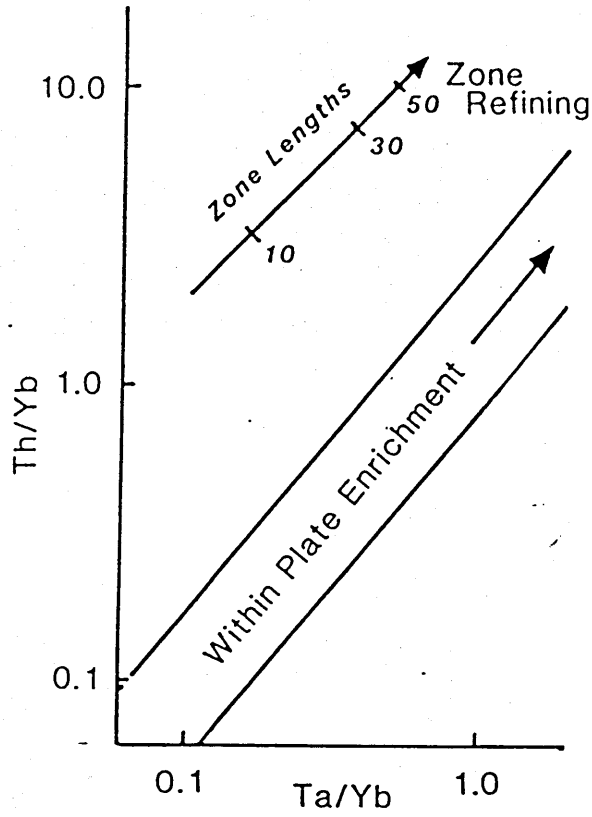

Fig. 3.13a Th/Yb v. Ta/Yb Zone melting model.

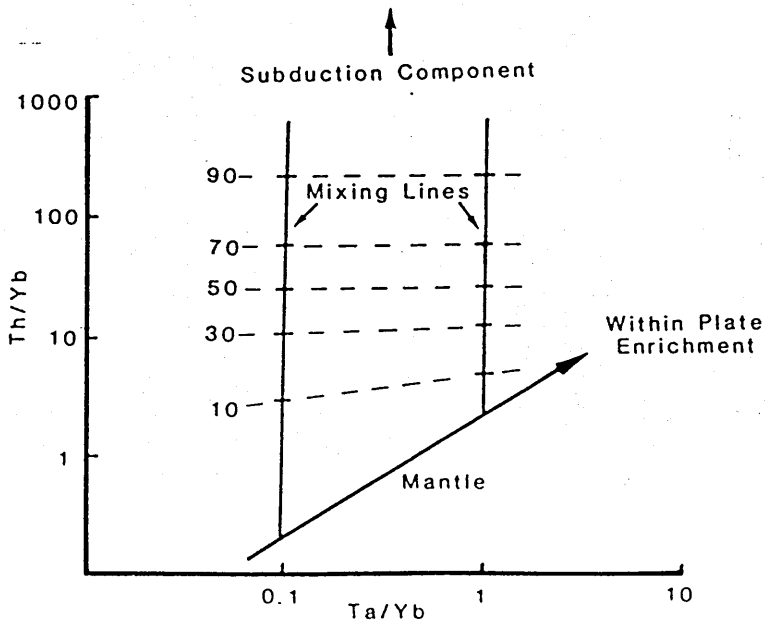

Fig. 3.13b Th/Yb v. Ta/Yb Mixing model between variably enriched within-plate mantle and very high Th/Yb subduction component. Dashed lines represent tie-lines of equal percentage contribution of the subduction component (as indicated by numbers) to the mixture

Zone melting (Harris,1957) is a suitable method of increasing Ta/Yb during magma formation (fig. 3.13a). Th/Yb and Ta/Yb will increase during zone melting as D_{Th} and D_{Ta} are much lower than D_{Yb} in a clinopyroxene and garnet bearing mantle lherzolite assemblage. However as $D_{Th} \approx D_{Ta}$ it is unlikely that Th/Ta ratios will change during extraction of magma. Only if anomalously high D_{Ta} is assumed implying stabilisation of a residual Ta bearing phase in the mantle during melting may a trend convergent on the within - plate array be modelled.

Addition of a uniform subduction zone component rich in Th but very poor in Ta and Yb to a heterogeneous mantle lying along the within - plate trend has been modelled (fig. 3.13b). In this case tie - lines representing a constant subduction component to mantle component ratio converge on the within - plate array. This property is simply a reflection of the diminishing effect of adding a subduction zone component with constant Th content into a mantle wedge whose Th content is increasing with increasing Ta/Yb. At some point the Th composition of the enriched mantle wedge is identical to that of the subduction component , the effect of the subduction component is nullified and the two trends meet. A secondary effect of this mixing model is to encourage the development of highly diffuse fields of data similar to that seen for Stromboli (fig. 3.12). Any single batch of magma is likely to sample mantle whose subduction component to mantle component ratio is unique, hence mixing occurs along a multitude of tie - lines (fig. 3.13b) and a diffuse trend is produced.

Diagrams of Sr/Yb v.Ta/Yb and Nd/Yb v. Ta/Yb (fig.3.14a,b) show data arrays which are consistent with the hypothesis developed above. In both cases fields of data may be adequately enclosed by trends convergent on the within - plate enrichment vector, although it must be conceded that in neither case is the data unequivocal.

3.3.3 Rare Earth Element Geochemistry

REE patterns of the Stromboli lavas (fig. 3.15 a,b) are unremarkable. All the lavas are LREE enriched as is often typical of subduction related lavas. The HREE show a restricted range which may well imply the presence of garnet in their source. Moreover the restricted range of Yb emphasises the dependance of Ta/Yb on Ta enrichment rather than Yb depletion. Eu anomalies are small but perhaps significant and as shown above this does not preclude the occurence of plagioclase as a fractionating phase.

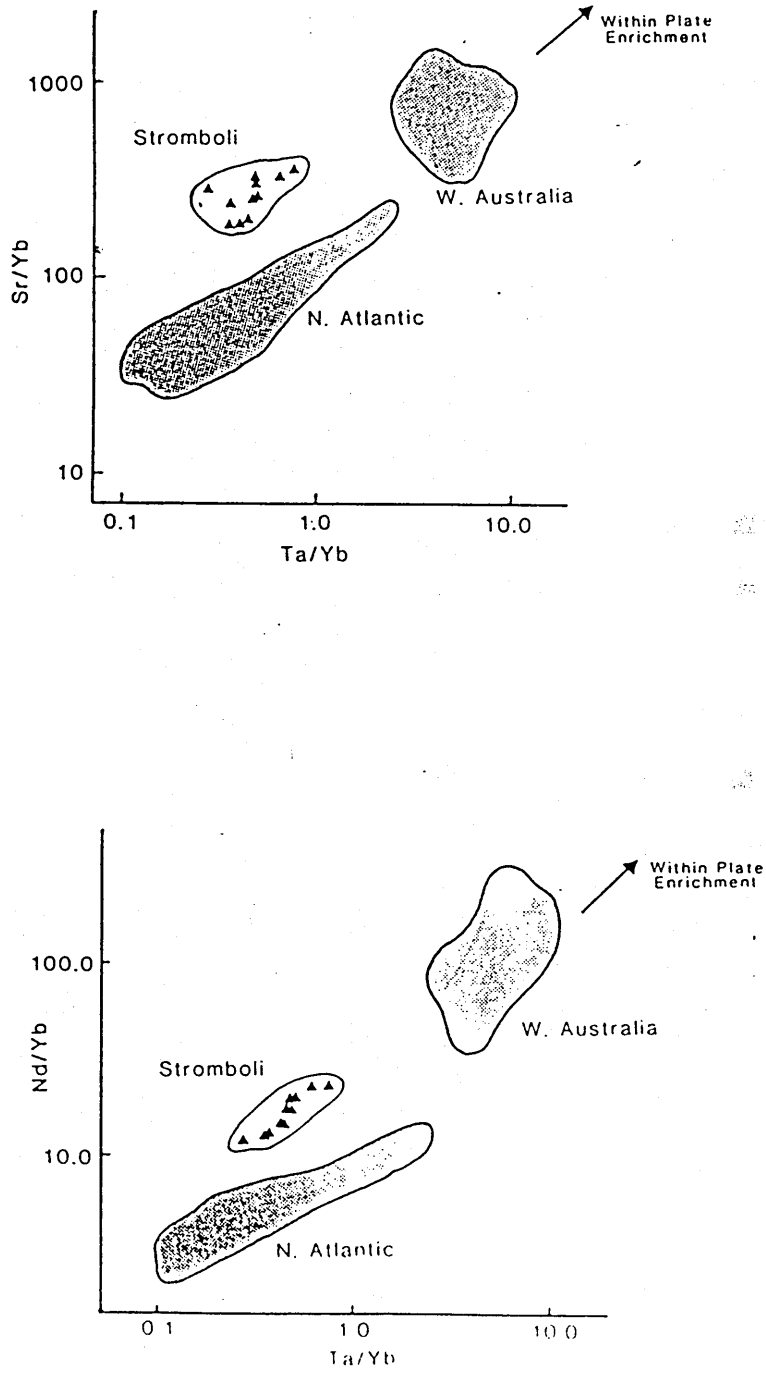

Fig. 3.14 Sr/Yb (a) and Nd/Yb (b) v. Ta/Yb. Within-plate enrichment vectors are based upon N Atlantic (Wood *et al* 1979) and W. Australian lamproites (Fraser *et al.* 1985)

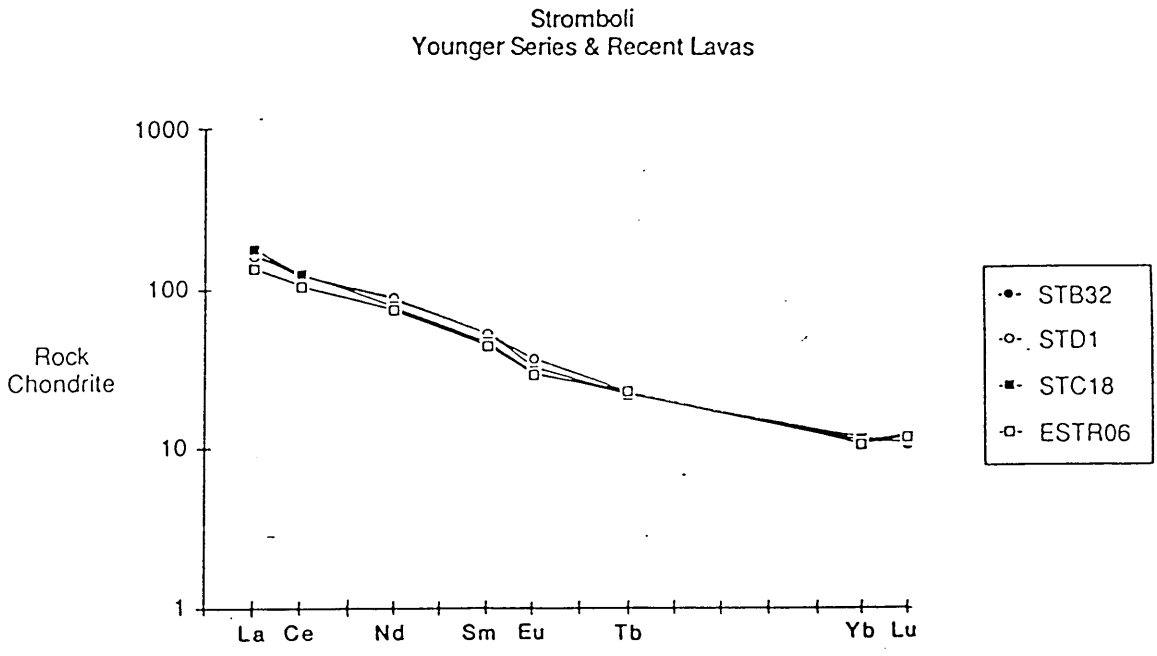

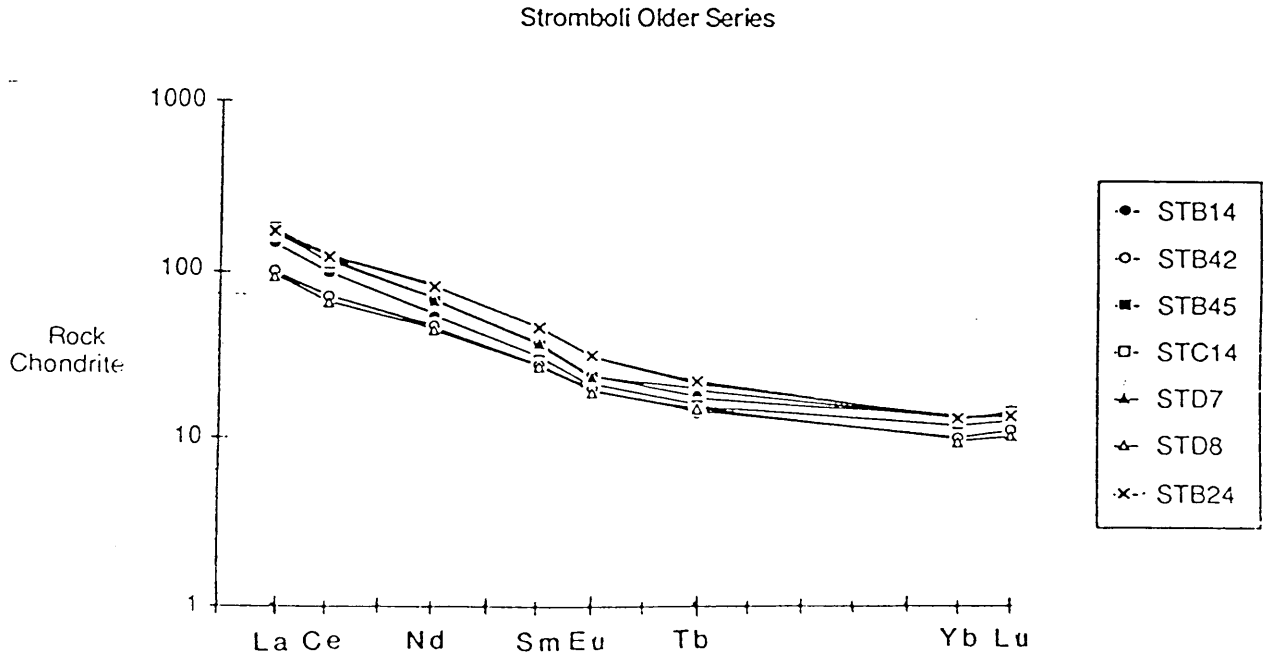

Fig 3.15 REE patterns of Stromboli lavas.

	DM	WP	SZ
Sr	12	26	62
K	5	13	82
Rb	2	13	85
Ba	2	8	90
Th	13	5	82
Ta	20	80	—
Nb	19	81	—
Ce	11	22	67
P	30	30	40
Zr	50	50	—
Hf	56	44	—
Sm	39	15	46
Ti	100	—	—
Y	87	13	—
Yb	100	—	—

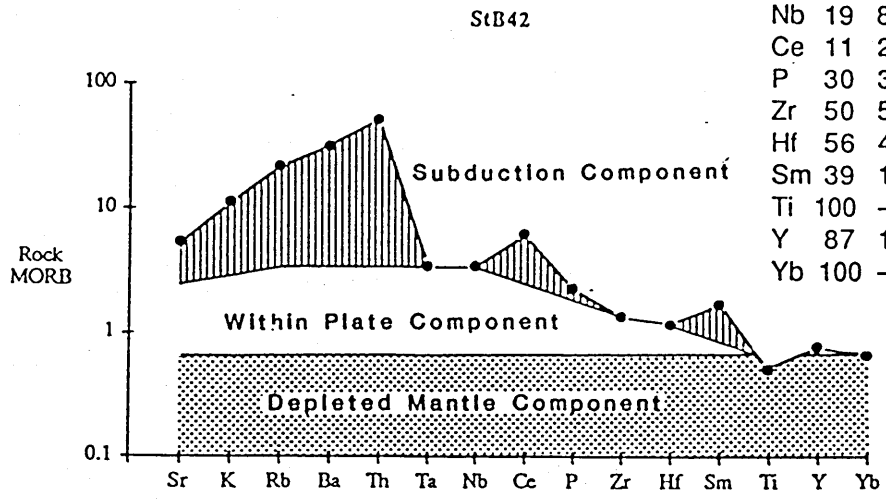

	DM	WP	SZ
Sr	10	63	27
K	3	15	78
Rb	1	14	85
Ba	1	9	90
Th	1	10	89
Ta	7	93	—
Nb	10	90	—
Ce	7	42	51
P	13	38	49
Zr	35	65	—
Hf	36	64	—
Sm	22	19	59
Ti	100	—	—
Y	71	29	—
Yb	100	—	—

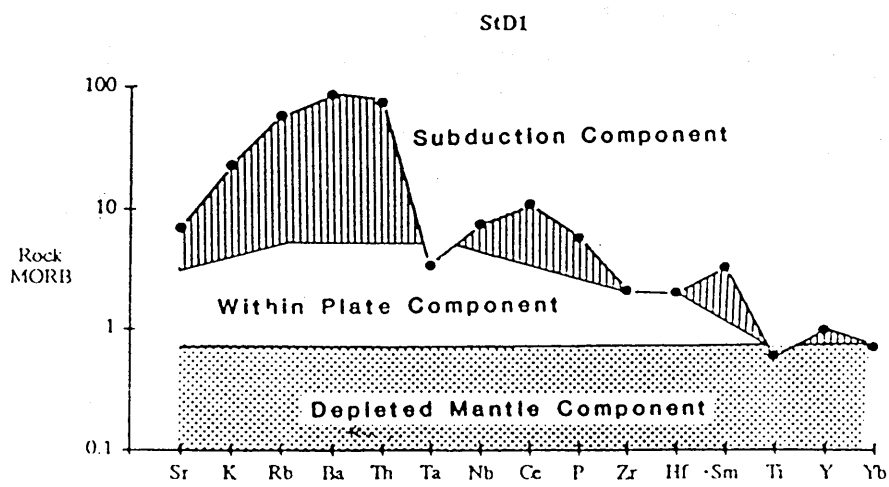

Fig. 3.16 MORB normalised trace element abundance patterns of Stromboli calc-alkaline basalt StB42 (a) and shoshonite (b) showing trace element components after Pearce (1983). Table shows percentage contribution of the components, DM depleted mantle, WP within plate & SZ subduction zone.

3.3.4 Trace Element Component Recognition

Using the method of Pearce (1983) which was described above, the trace element patterns of the Stromboli lavas may be divided into their constituent components. Samples with the highest (StD1) and lowest (StB42) Ta/Yb are compared in figure 3.16. As implied by its high Ta/Yb, sample StD1 contains a larger relative contribution from the within - plate component than StB42. Whilst both lavas contain similar relative contributions of Ba, Rb and Th from the subduction zone it is clear that StD1 contains a larger percentage of Sr and K from the within - plate component than StB42. As the Stromboli lavas are plagioclase phyric it is possible that their Sr content has been reduced by plagioclase fractionation. However, to maintain the mantle:subduction zone relationship observed in StB42 would require StD1 to have undergone around 50% crystallisation of a pure plagioclase extract. Clearly this is unlikely, particularly as both lavas have similar CaO and Al_2O_3 contents. More likely the effect of Sr and K addition in the subduction component on the source of StD1 was diminished by the large contribution of these elements from the within - plate component.

3.3.5 Introduction to Sr Isotope Geochemistry

The large variation in $^{87}Sr/^{86}Sr$ observed in the Stromboli lavas (0.7050 - 0.7075) is evidence of open system processes, in contrast to the closed system model developed for Salina. The association of radiogenic Sr isotopes with a large relative Sr contribution from the within - plate component implies that this component has elevated $^{87}Sr/^{86}Sr$ in contrast with the low $^{87}Sr/^{86}Sr$ subduction component. This is possibly evidence to link the within - plate component with an enriched mantle source, a possibility that will be considered in the following chapter.

3.4 Vulcano

3.4.1 Introduction

The division of the Vulcano lavas into two groups; the older and younger series as established in the previous chapter is maintained here. Lavas of the younger series are the most potassic of the Aeolian Islands. Older series lavas are also potassic but less so than the younger series

3.4.2 Older Series: The Role of Fractional Crystallisation

As shown in chapter two, many of these lavas display similar major element

compositions. Only two samples are considerably less evolved than the majority.

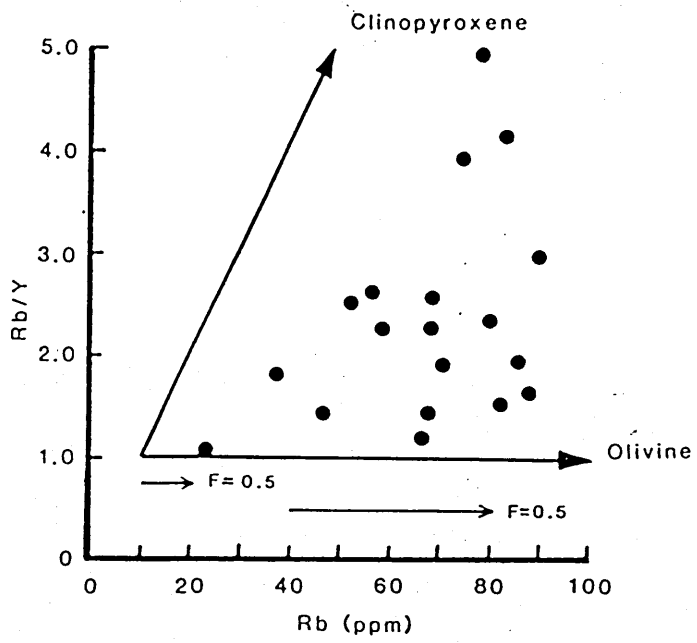

Fig. 3.17 Rb/Y v. Rb for Vulcano older series lavas. Large vectors are for clinopyroxene and olivine fractional crystallisation . Small vectors indicate the amount of enrichment produced by 50 % fractional crystallisation of a phase with $D_{Rb}=D_{Yb}=0$, for different original compositions.

It is clear from the compatible element compositions of these lavas that they have all undergone significant fractionation (≥ 20 %) of olivine and pyroxene. However the lack of coherent trends for the incompatible trace elements (fig. 3.17) indicates that these lavas may not be simply related by fractional crystallisation of a single parental magma. More likely, the wide scatter of data reflects variations in the olivine: pyroxene ratio during melting and/or fractional crystallisation, resulting in evolution lines (fig. 3.17) between those shown for olivine and clinopyroxene. The diminishing effect of fractional crystallisation (fig. 3.17) with decreasing Rb and Y composition of the original liquid should also be noted.

3.4.3 Older Series: REE Geochemistry

Important information about the genesis of the older series lavas may be obtained from their chondrite normalised REE patterns. (fig.3.18 a,b). These are unusual in that they show a wide range of HREE compositions but a narrower range of the LREE. This observation is supported by a wide range in Y content (16 -54 ppm) In order to attribute

such a variation to fractional crystallisation, would require crystallisation of a phase rich in LREE but relatively poor in HREE *ie.* $D_{LREE} > D_{HREE}$. However the common basaltic minerals and certainly those observed as phenocrysts in these lavas tend to have $D_{LREE} < D_{HREE}$ (Henderson, 1982). Fractional crystallisation trends therefore produce increased Ce/Yb with fractionation resulting in positive correlations in figure 3.19 compared with the broad negative trend observed.

If fractional crystallisation is unlikely to produce the observed variations in the older series lavas, the inferred variation in olivine : clinopyroxene (fig. 3.17) must be incorporated into the melting regime. It is unlikely that these lavas originated from a garnet bearing source as any such source is likely to have Kd_{Yb} close to unity which would buffer the REE during melting, such that the large range in Yb would require an external addition of the HREE, which seems unlikely. However if a garnet - free, clinopyroxene bearing source is inferred then, as $D^{cpx} < D^{gt}$ for the HREE the Kd of Yb may be significantly less than one. During melting Yb would behave incompatibly and as a result, successive batches of relatively small degree partial melts (<5% ?) of the same source will contain successively lower concentrations of Yb. If melting is coupled with LREE enrichment between (or during) individual batches of melting, it may be possible to buffer the LREE at fairly constant compositions whilst progressively depleting the HREE.

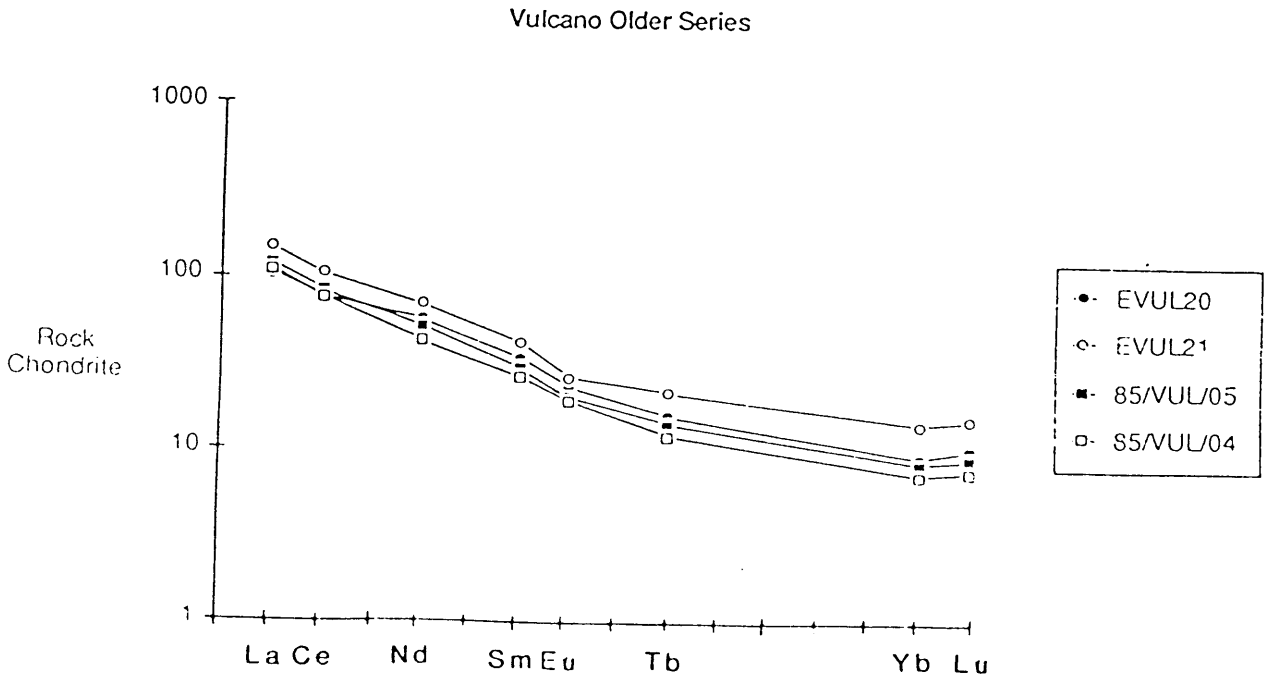

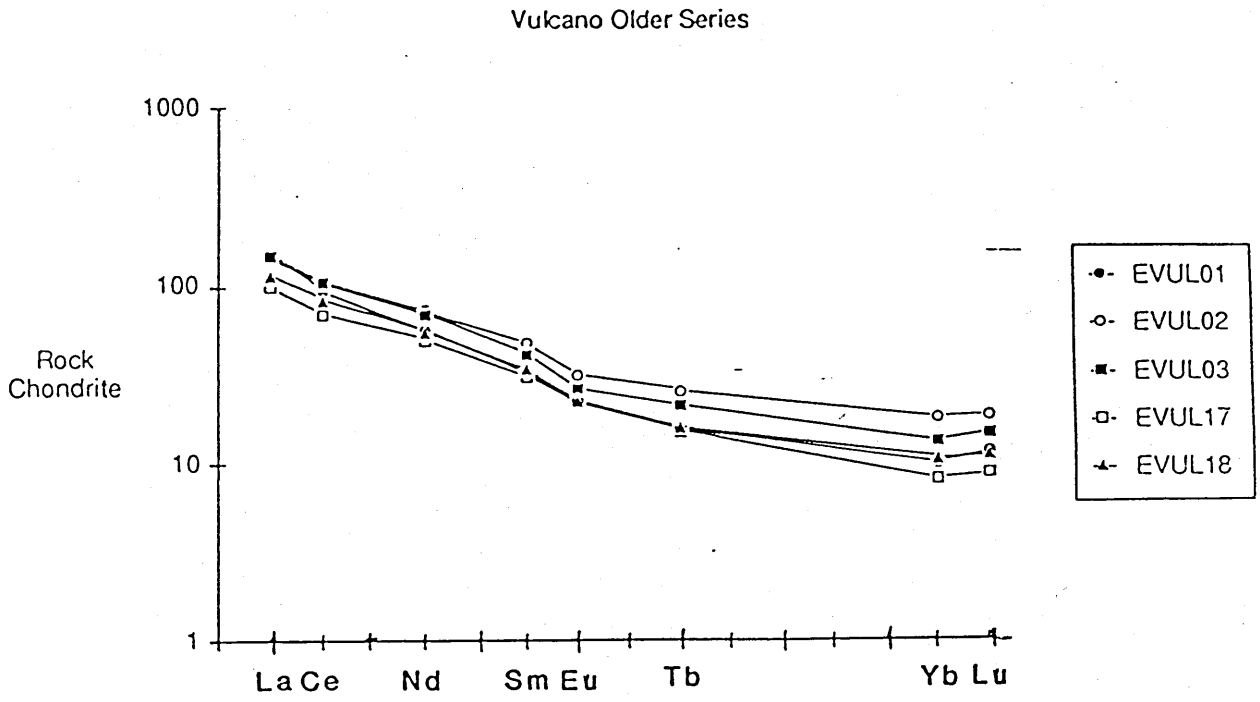

Fig. 3.18 REE patterns of Vulcano older series lavas.

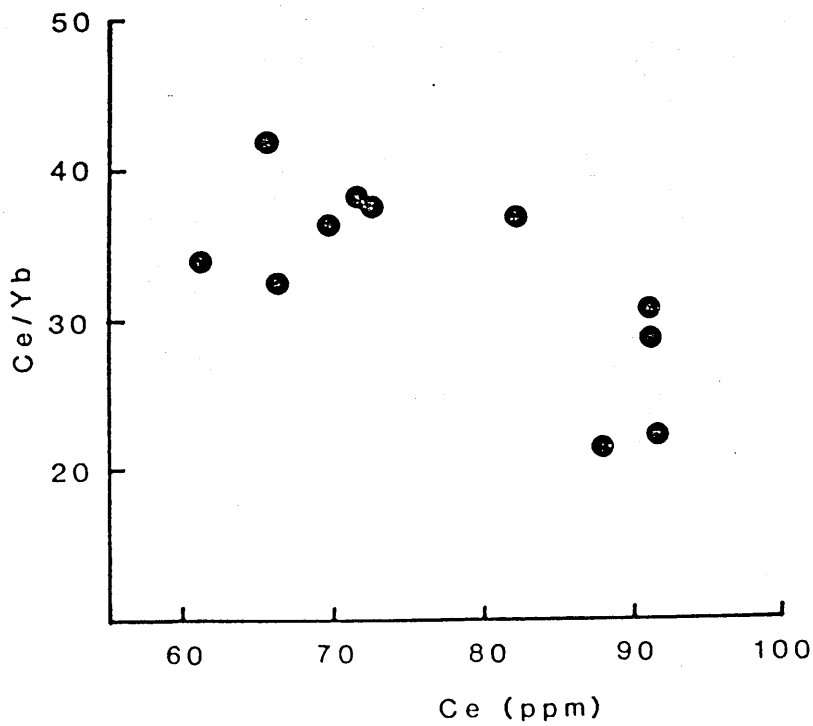

Fig. 3.19 Ce/Yb v. Ce for Vulcano older series lavas, shows a weak negative correlation in contrast with the positive correlation predicted for fractional crystallisation.

A rather extreme example of this model is illustrated (fig. 3.20), which emphasises the suitability of such a model to the older series REE patterns. Numerous variables are difficult to constrain *eg.* composition of LREE enriching agent, degree of partial melting *etc.*, which preclude the formulation of a unique model of the data. However this example does adequately demonstrate the potential of the model to fractionate the REE in the manner required. Moreover, the model is consistent with the predicted enrichment process within the mantle wedge above a subduction zone. During subduction, it seems likely that enrichment by fluids or melts will be intimately associated with melting of the wedge. Both are likely to be episodic and as such likely to fulfill the requirements of the model.

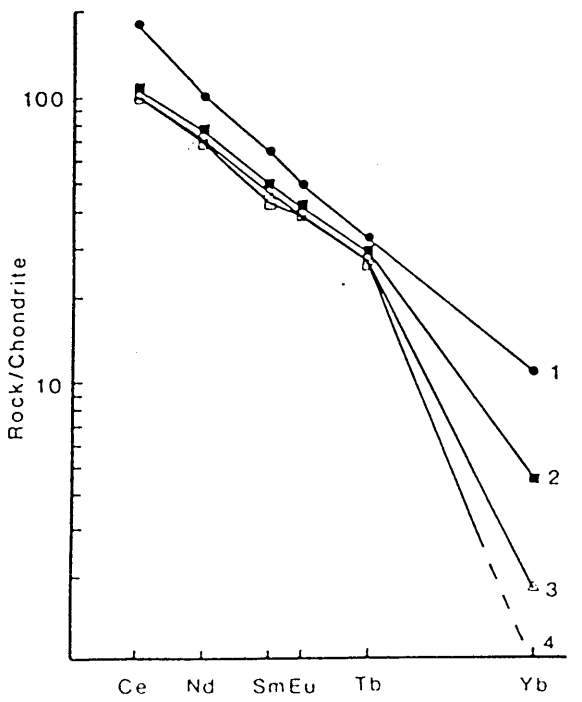

Fig. 3.20 Vulcano older series REE model. Figures indicate successive batches of melting.

3.4.4 Older Series: Trace Element Component Recognition

The component recognition method (Pearce, 1983) has been applied to one of the most basic Vulcano lavas. (fig. 3.21). The LILE are again dominantly subduction derived, consistent with their low $^{87}Sr/^{86}Sr$ (0.7043 - 0.7046). A range of Ta/Yb does exist,

however as shown above, this is related to Yb content, it does not reflect an increased within - plate component so much as this should be representative of HFSE enrichment. This point is emphasised by figure 3.22a,b,c which show that Ta/Yb is not strongly related to Ta content (fig. 3.22a), but rather shows a negative correlation with Yb (fig. 3.22b). This is in contrast with Stromboli lavas which display a good positive correlation between Ta/Yb and Ta content (fig. 3.22c), which is indicative of within - plate enrichment.

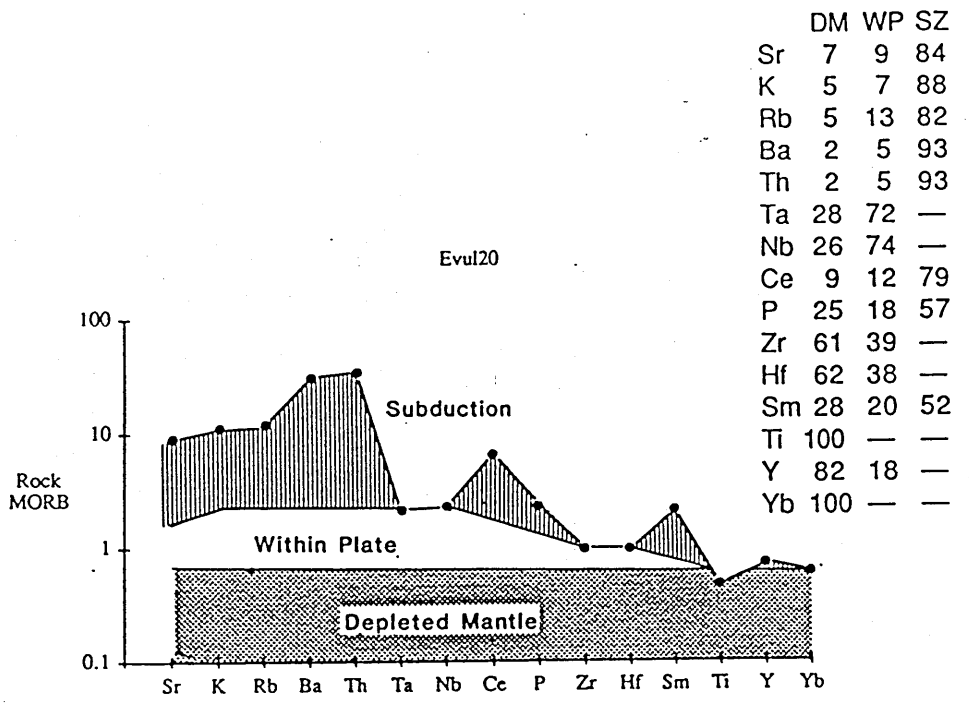

	DM	WP	SZ
Sr	7	9	84
K	5	7	88
Rb	5	13	82
Ba	2	5	93
Th	2	5	93
Ta	28	72	—
Nb	26	74	—
Ce	9	12	79
P	25	18	57
Zr	61	39	—
Hf	62	38	—
Sm	28	20	52
Ti	100	—	—
Y	82	18	—
Yb	100	—	—

Fig 3.21 MORB normalised trace element abundance pattern of a Vulcano older series lava (EVUL 20) showing trace element components after Pearce (1983). DM, depleted mantle, WP, within plate, SZ, subduction zone

The best representative of the original Vulcano source Ta/Yb must therefore be the lowest observed value, which is within the range for Salina lavas whose isotopic compositions are similar to those of the Vulcano older series.

3.4.5 Younger Series: The Effects of Fractional Crystallisation

As shown in chapter two, the younger group of lavas define what appears to be an extensive fractional crystallisation sequence from leucite tephrite through to rhyolite. In modelling the lava sequence it was divided into two sections; the basic to intermediate and the intermediate to acidic stages of evolution. Whilst this is likely to be an oversimplification, it does allow the effects of changing mineral assemblage and variable Kd to be considered. Equating the most incompatible elements to Kd = 0 (table 3.6), the

first stage of fractional crystallisation represents around 35% solidification, whilst the second stage is consistent with a further 40% crystallisation of the intermediate liquid.

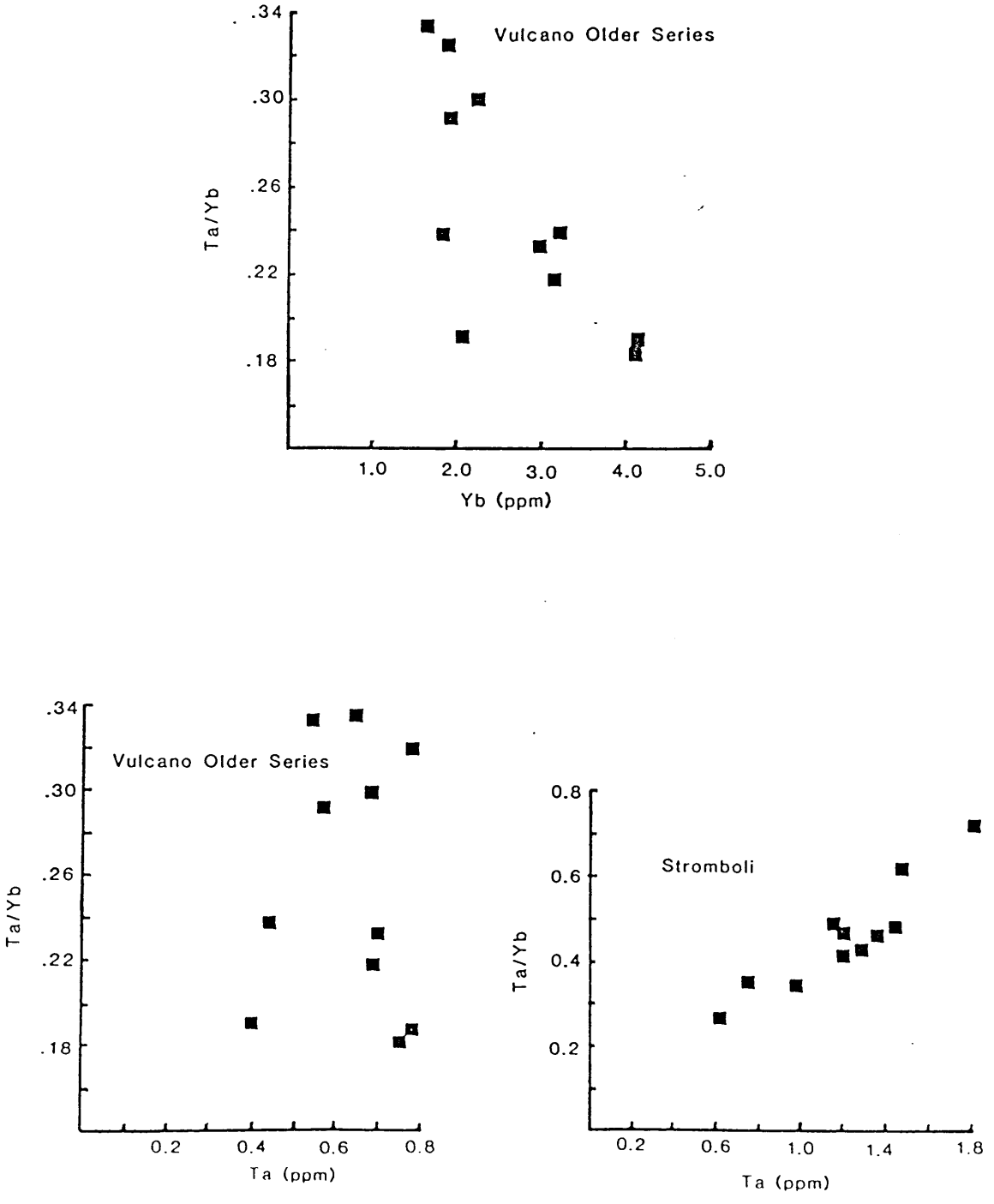

Fig 3.22 Negative correlation of Ta/Yb with Yb (a) and lack of correlation between Ta/Yb and Ta (b) in Vulcano older series lavas, contrasts with positive correlation between Ta/Yb and Ta in Stromboli lavas (c).

	Basic - Intermediate (EVUL 11 -EVUL 09)	Intermediate - Acidic (EVUL 09 - EVUL 23)
Th	0.59	0.63
Ta	0.69	0.58
Nb	0.66	0.60
Zr	0.59	

Table 3.6 Calculated F (proportion of liquid remaining) for incompatible elements in the Vulcano younger series lavas, assuming Kd = 0

Having assumed that F = 0.65 and 0.6 for the first and second stages of evolution respectively, the Kds of other trace elements may be calculated (table 3.7). Elements which behave compatibly include Ba, Sr, Ni and Cr which may well imply fractionation of alkali feldspar (and/or leucite), plagioclase, olivine and pyroxene respectively. Furthermore an increase in Kd_{Ba} and Kd_{Sr} along with a decrease in Kd_{Cr}, Kd_{Y} and Kd_{Yb} during stage two, implies an increased importance for feldspar and a diminishing role for olivine and pyroxene in the later stages of evolution.

	STAGE ONE F = 0.65	STAGE TWO F = 0.6
Ba	1.8	5.4
Sr	1.6	5.8
Ni	4.2	
Cr	3.1	0.73
Y	0.38	0
Yb	0.44	- 0.17

Table 3.7 Calculated Kds from the Vulcano younger series fractional crystallisation model

The mineral assemblage implied by the compatible trace elements is consistent with the observed phenocryst phases in the younger series lavas. Attempts were therefore made to model the major element variations within these younger series lavas in terms of fractional crystallisation of those observed phenocrysts, using the least squares approach

introduced in the previous chapter, and successfully applied to the Salina lavas. A variety of mineral assemblages was modelled but in the majority of cases the best fit model gave only a poor approximation to the target composition. This was especially so when an attempt was made to constrain the least squares models to the F value implied by incompatible trace elements. Clearly a simple closed system fractionation model is inadequate in accurately describing the evolution of the younger series lavas. More complex open systems must be examined.

3.4.6 Younger Series : A Role for the RTF Magma Chamber ?

If closed system evolution is to be rejected then perhaps a periodically replenished, periodically tapped, continuously fractionating (RTF) magma chamber (O'Hara & Matthews, 1981) may be invoked to explain the data.

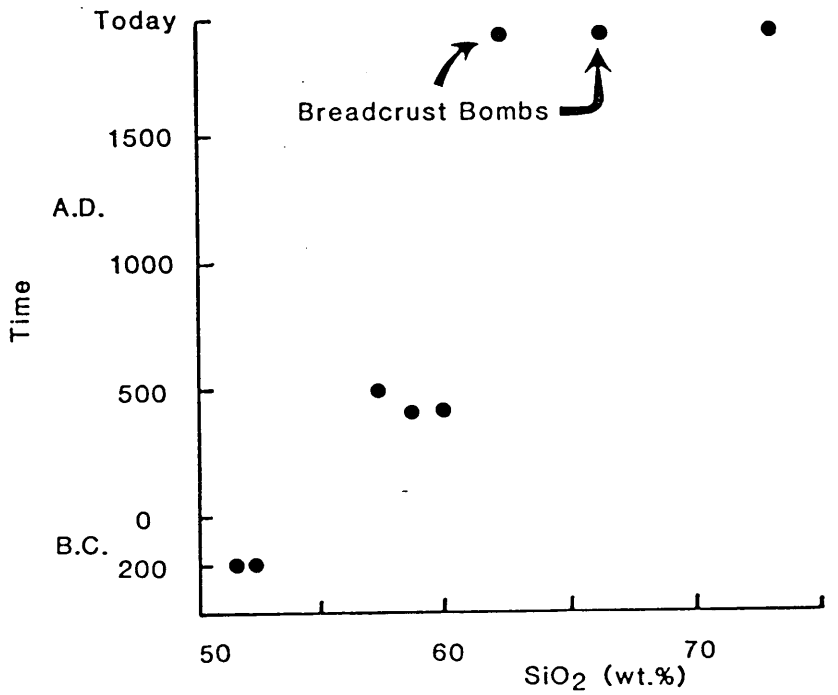

Fig. 3.23 Age v. SiO_2 of Vulcano younger series lavas. *N.B.* Breadcrust bombs of the 1889/90 eruption may be reworked products of previous eruptions. (Keller, 1980b).

Certainly such a system is capable of decoupling the major and trace elements. However, the nature of that decoupling would be to relatively enrich elements whose Kds are low, as low Kd implies a longer period of time to achieve a steady state concentration. Many of the least squares solutions require larger degrees of crystallisation to satisfy the relatively compatible major elements than that required by highly incompatible trace elements. Clearly this situation conflicts with the predicted effects of an RTF chamber. Furthermore,

the Vulcano younger series lavas show a strong correlation between SiO_2 and time (fig. 3.23). The youngest lavas are the most siliceous which implies progressive evolution of a single magma body, with no episodes of replenishment with fresh magma.

3.4.7 Younger Series: A Role for Crustal Contamination ?

Another commonly invoked open system process is addition of crustal material to evolving magmas. Crustal contamination tends to increase $^{87}Sr/^{86}Sr$, as many crustal rocks have very radiogenic Sr isotope ratios. Vulcano younger series lavas display only a very narrow range in $^{87}Sr/^{86}Sr$ (0.7045 - 0.7049). This would usually be interpreted as reflecting a negligable role for contamination. However basic lavas from this series have very high Sr contents (>1000 ppm), compared with the likely composition of a crustal component (<500 ppm). It may be possible that the isotopic effects of contamination are hidden by the high initial Sr contents of the basic lavas of this series, until the later stages of crystallisation when the Sr content of the liquid has been reduced by fractional crystallisation of feldspar.

An assimilation fractional crystallisation (AFC) model (De Paolo, 1981) is presented (fig. 3.24) which shows the young series lavas to be consistent with an assimilation to crystallisation ratio of 0.1. Clearly the simple two stage model is an over - simplification of the real system, it does however illustrate the manner in which the effects of assimilation are hidden during the early stages of crystallisation. Table 3.8 illustrates the minor deviation from perfect Rayleigh fractionation that this AFC model will induce on incompatible element abundances, this may explain why trace element variations are apparently consistent with closed system evolution whilst major element variations are not.

The effect on the major elements of adding small quantities of crust to a magma is likely to be significant and may be sufficient to invalidate the least squares modelling of fractional crystallisation. A simple demonstration of this may be obtained by considering a 5% addition of sample 85/SAL/04, a crustal xenolith from Salina to basic lava EVUL 11 (table 3.9). Evidently, the SiO_2 content of a magma may be altered quite significantly by small amounts of crustal contamination. Such a change may well be sufficient to produce erroneous least squares models if the effects of contamination are not considered.

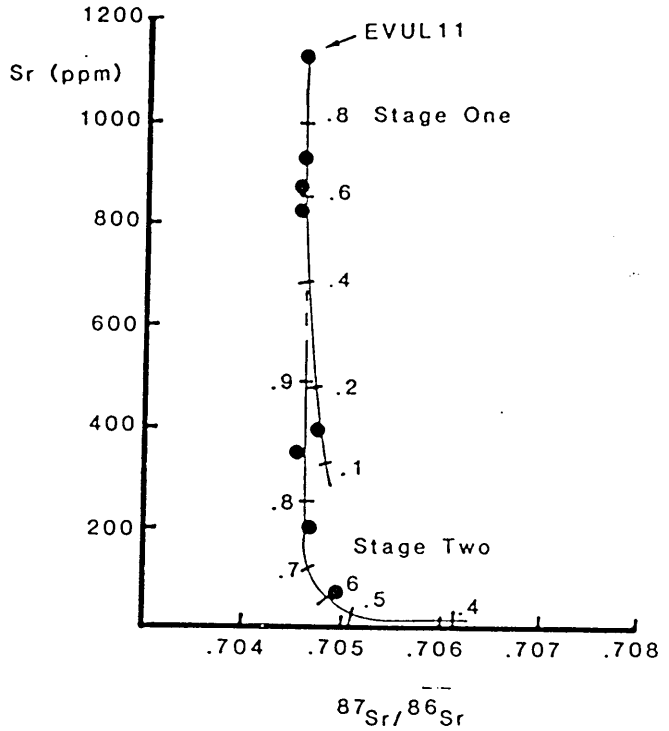

Fig 3.24 Vulcano younger series two stage AFC model.

Stage One Sr: C_O= 1127 ,C_A= 200 ,$^{87}Sr/^{86}Sr$: C_O= 0.70411 , C_A= 0.7140 , D_{Sr}=1.6

Stage Two Sr C_O=819 ,C_A=200 ,$^{87}Sr/^{86}Sr$ C_O=0.70466 , C_A= 0.714 , D_{Sr}= 5.8

r=0.1

	C_O	C_A	Kd
Th	23.8	5.0	0.001
Nb	18	12	0.01
Ce	109.0	50.0	0.1
Yb	2.3	1.5	0.5

R = 0.1

F	Th		Nb		Ce		Yb	
	AFC	FC	AFC	FC	AFC	FC	AFC	FC
0.9	26.5	26.4	20.1	20.0	120.3	120.0	2.4	2.4
0.7	34.2	34.0	25.2	25.6	152.0	150.3	2.8	2.7

Table 3.8 Comparison of assimilation fractional crystallisation (AFC) and Rayleigh fractional crystallisation (FC) for the early stages of crystallisation. C_O is original liquid composition, C_A is assimliant composition and Kd the bulk partition coefficient.

	EVUL 11	85/SAL/04	MIXTURE
SiO_2	51.79	74.42	52.92
TiO_2	0.66	0.24	0.64
Al_2O_3	14.96	14.20	14.92
Fe_2O_3	9.03	1.01	8.63
MnO	0.17	0.01	0.17
MgO	4.78	1.21	4.60
CaO	8.60	2.65	8.30
Na_2O	3.51	2.96	3.48
K_2O	4.53	2.22	4.41
P_2O_5	0.44	0.50	0.44

Table 3.9 The effect of 5% contamination with crustal xenolith 85/SAL/04 on the major element composition of leucite tephrite EVUL 11

3.4.8 Younger Series: REE Geochemistry

REE patterns of the younger series lavas (fig. 3.25) reveal patterns for the basic lavas similar to those from Salina and Stromboli with enriched LREE and only small negative Eu anomalies. More evolved trachytes and rhyolites show progressive development of large negative Eu anomalies, which is in contrast to the tiny anomalies found in the Salina Lavas.The growth of Eu anomalies is consistent with the relationship between increasing D_{Eu} in plagioclase and decreasing temperature as well as with an increasing proportion of feldspar in the fractionating assemblage at more evolved stages of fractionation. Comparison of lavas with similar SiO_2 and Mg number from Salina and Vulcano younger series, reveals larger Eu anomalies in the latter. This is thought to reflect the presence of alkali feldspar as a relatively early fractionating phase in the Vulcano lavas. Modelling using the partition coefficients shown in table 3.10 shows that for 50% fractional crystallisation, an assemblage of 50% plagioclase + 50% clinopyroxene would produce $Eu/Eu^* = 0.93$, whereas replacing half the plagioclase with alkali feldspar gives $Eu/Eu^* = 0.81$ for the same degree of crystallisation, a larger negative Eu anomaly.

	Plagioclase	Clinopyroxene	Alkali Feldspar
Sm	0.14	0.9	0.02
Eu	0.32	0.9	1.0
Gd	0.10	0.9	0.01

Table 3.10 MREE Kds for the fractional crystallisation model described in the text.

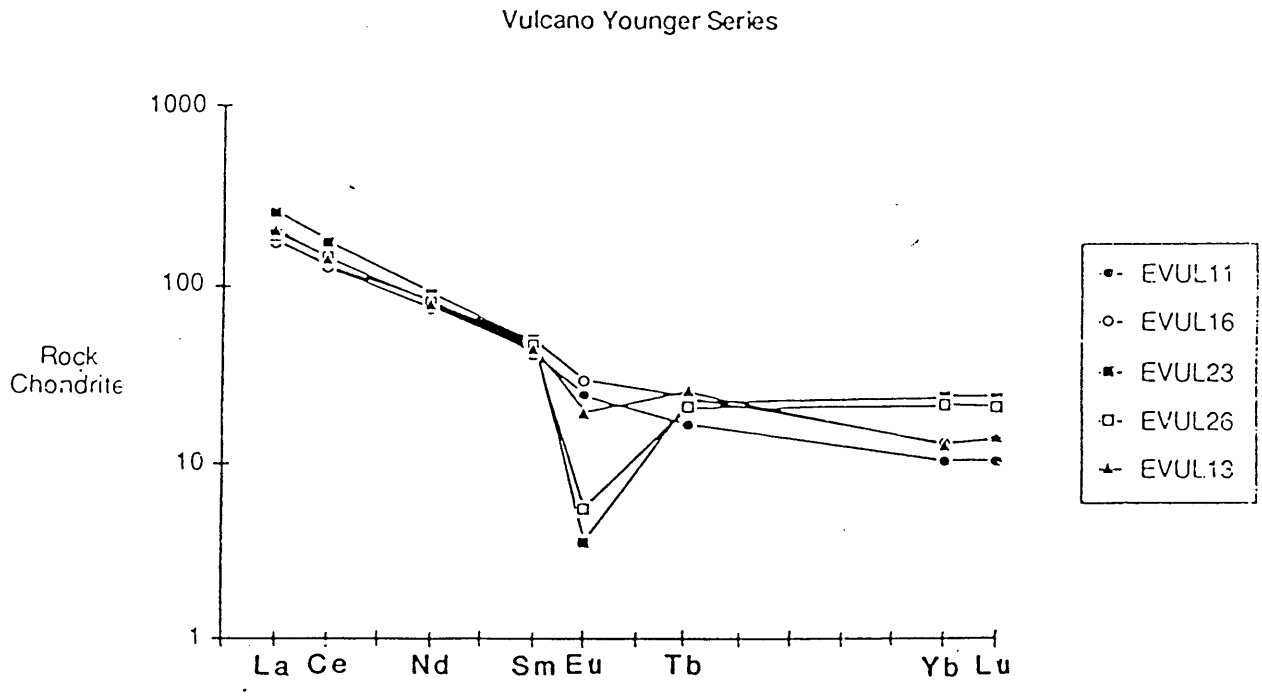

Fig. 3.25 REE patterns of Vulcano younger series lavas.

3.4.9 Younger Series: Trace Element Component Recognition

Despite the fairly elevated Ta/Yb in these lavas the calculation of Pearce (1983) (fig. 3.26) shows that all the LILE are dominantly subduction derived. In contrast to the lavas of Stromboli, the Vulcano lavas do not show a large within - plate contribution to their Sr and K budget. This would appear to be consistent with their relatively low $^{87}Sr/^{86}Sr$ which is apparently dominated by low $^{87}Sr/^{86}Sr$ material derived from subduction zone processes. This observation is important as it demonstrates that whilst the within - plate component may be important in the genesis of potassic lavas, as appears to be the case at Stromboli, it is by no means necessary to invoke within - plate enrichment to explain all the Aeolian Islands potassic lavas. Clearly within the model of Pearce (1983) the Vulcano potassic lavas appear to derive their potassium dominantly from a subduction related component.

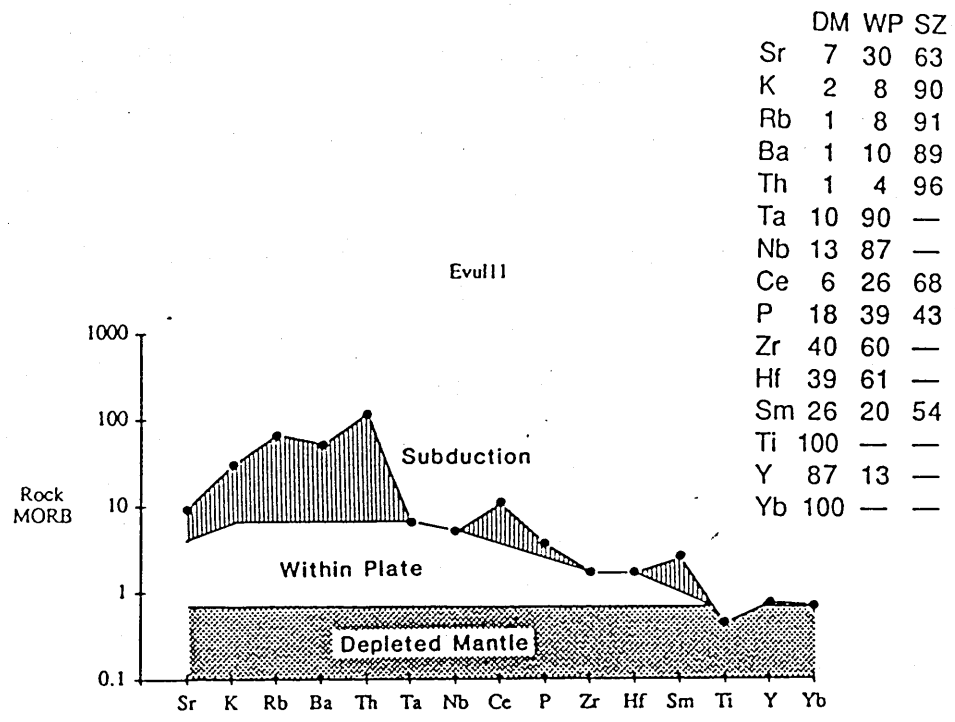

Fig. 3.26 MORB normalised trace element abundance pattern of a Vulcano younger series lava EVUL 11, showing trace element components after Pearce (1983). DM, depleted mantle, WP, within plate, SZ, subduction zone.

3.5 Summary of Trace Element Data

Consideration of the trace element geochemistry of Aeolian Islands lavas has revealed a number of important features. The fractional crystallisation model developed on the basis of major element variations within the lavas of Salina, has been shown to be consistent with much of the trace element evidence and constraints have been placed on the physical conditions pertaining during the evolution of this series of lavas. This model may well have implications for the genesis of similar lavas in other subduction related environments.

Salina lavas have trace element abundances similar to those which characterise the products of destructive plate margin magmatism throughout the world. In contrast lavas from Vulcano and, in particular Stromboli are enriched in the HFSE which is believed to be inconsistent with subduction processes. At Vulcano it appears that the HFSE enrichment may be an artefact of a complex regime of melting acting on a "normal" subduction zone

mantle source. However at Stromboli the HFSE enrichment appears to pre-date subduction related LILE enrichment and a component of mantle enrichment similar to that seen in within-plate lavas has been inferred.

The effects of crustal contamination have been considered and it is possible that this process may have a minor role to play in the evolution of some of the lava series.

In the following chapter the hypotheses developed above are tested and developed with the aid of a range of radiogenic istope data.

CHAPTER FOUR

Radiogenic Isotope Variations

4.1 Introduction

4.1.1 Aims & Methodology

Within this chapter the variations of Sr Nd and Pb isotopic composition will be described and interpreted. The approach adopted is a response to increasing evidence of the equivocality of radiogenic isotope ratios. Variations will be assessed primarily in terms of their elemental components, as developed in the previous chapter, before examination of their isotopic characteristics. In essence this approach develops the elemental component recognition technique of Pearce (1983), not least to evaluate whether such a technique may be shown to be consistent with isotope data. Rather than using the components identified by Pearce (*op. cit.*), the present approach concentrates more directly on the trace element ratios which provide the keys to discrimination of the different components. In this manner, no geological significance is attached to a component before all the available evidence has been considered.

4.1.2 Terminology

Although there is no immediate need to interpret the geological processes which are responsible for particular elemental components, it is often useful in the discussion to bear in mind the tectonic significance of particular styles of elemental enrichment. Towards this end the following terminology will be adopted to describe the various elemental components. Where possible the terms are identical to those used by Pearce (1983).

(a) **The Subduction Component:** This represents the component of LILE (relative to HFSE) enrichment which is found in subduction related lavas worldwide. It is geochemically well established and characterised, but its origin is highly controversial (see chapter six). In later discussion it may be necessary to appeal to two components which both have some characteristics typical of a subduction component (*eg.* low HFSE, high LILE), but which vary in detail. In this eventuality these components will be simply termed subduction components A and B.

(b) **The Within - Plate Component:** This represents the HFSE rich component which was recognised above in the lavas of Stromboli. It is not thought to be related to

subduction processes, but typifies lavas erupted in intraplate environments. No distinction is drawn here between the (enriched) within - plate and depleted mantle components as recognised by Pearce (1983), as it would appear likely that a continuum exists between depleted MORB and enriched within - plate lavas.

4.2 Sr & Nd Isotope Variations

4.2.1 Introduction

Sr and Nd isotope variations within the Aeolian Islands are illustated in figure 4.1. Rocks from Salina and Vulcano display a limited range close to bulk earth values ($^{87}Sr/^{86}Sr$ = 0.7041 - 0.7049, $^{143}Nd/^{144}Nd$ = 0.51282 - 0.51254), whilst Stromboli lavas show a much wider range towards more enriched compositions, ($^{87}Sr/^{86}Sr$=0.7050-0.7075, $^{143}Nd/^{144}Nd$=0.51265-0.51242). A simple mixing curve calculated between the lowest and highest $^{87}Sr/^{86}Sr$ samples (fig. 4.1 inset) is consistent with the remaining data, which might suggest an origin by two component mixing.

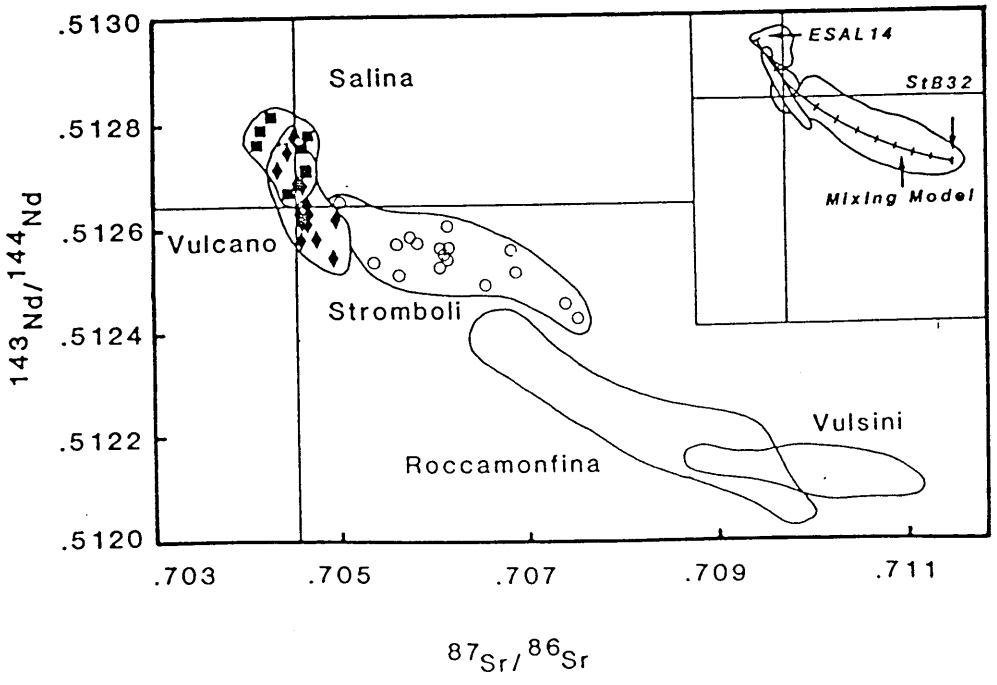

Fig. 4.1 $^{143}Nd/^{144}Nd$ v. $^{87}Sr/^{86}Sr$ for Aeolian lavas with Roman province lavas (Hawkesworth & Vollmer, 1979, Rogers *et al.* 1985) shown for comparison. Inset: simple two component mixing model between highest (StB32) and lowest (ESAL14) $^{87}Sr/^{86}Sr$ samples

4.2.2 A Role for Crustal Contamination ?

The continental crust is a major reservoir of radiogenic Sr and unradiogenic Nd. Lavas which plot in the bottom right-hand or enriched quadrant of the Nd-Sr isotope diagram have often been assumed to have interacted with the continental crust (*e.g.* Allegre *et al.* 1981). However the discovery of similar isotopic signatures in oceanic basalts (*e.g.* Dosso & Murthy, 1980) and mantle xenoliths (*e.g.* Menzies & Murthy, 1980), has illustrated that the continental crust is not a unique source of high $^{87}Sr/^{86}Sr$ and low $^{143}Nd/^{144}Nd$. It is believed that such features represent mantle processes such as partial melting and fluid/melt migration which fractionate parent and daughter elements. In areas of the mantle which remain isolated from the main convective circulation for long periods of time, notably the sub-continental lithosphere, these elemental fractionations lead to the generation of anomalous isotope ratios.

Therefore elevated $^{87}Sr/^{86}Sr$ and low $^{143}Nd/^{144}Nd$ may not be interpreted as unambiguous evidence of crustal involvement in magmatism. However consideration of the elemental variations which accompany isotopic enrichment may allow the role of continental crust to be assessed. In the destructive continental plate margin environment two potential processes of continental crustal involvement exist:

(a) Crust may be recycled into the mantle as a terrigenous sedimentary component from the subducted oceanic plate. This type of crustal incorporation will be dealt with as a subduction zone component as defined above.

(b) Continental crust may be incorporated into ascending magmas during their passage through the crust. This is the process implied here by the phrase "crustal contamination."

The Aeolian Islands sit upon distended continental crust, which is composed of a complex mixture of rock types. Crustal xenoliths from the pyroclastic units of Salina reveal a wide range of crustal lithologies (appendix A). At least in part the sub-arc crust is composed of refractory metabasites, although more readily fusible acidic igneous and sedimentary rocks also occur, as do carbonates and metamorphic calc-silicates. Many of these xenoliths are small (<5 cm) and highly altered by weathering and hydrothermal processes, as a result their chemistry may demonstrate the effects of this alteration (LILE depletion ?) which limits their use as representatives of potential crustal contaminants. Instead average crustal values (*e.g.* Weaver & Tarney, 1984) are preferred in models of

contamination.

Perhaps the most commonly demonstrated contamination process is that of assimilation, fractional crystallisation (AFC), formalised by De Paolo (1981). Assimilation of crust is accompanied by, and indeed promoted by the latent heat of, fractional crystallisation. In AFC systems a positive relationship is produced between indices of contamination (*e.g.* $^{87}Sr/^{86}Sr$) and differentiation (*e.g.* SiO_2), as fractional crystallisation is accompanied by addition of radiogenic Sr to the remaining liquid. At Stromboli no such relationship exists (fig. 4.2), however it seems likely that small isotopic variations observed at Salina and Vulcano are the result of AFC, as was modelled above for the Vulcano younger series.

An alternative method of crustal contamination may be considered in which assimilation is not necessarily accompanied by fractional crystallisation, but crust is simply melted by hot uprising magmas. In this case higher temperature basaltic magmas are more likely to become contaminated than cooler more differentiated magmas. An elemental test for such a process is available in the form of the diagram $^{87}Sr/^{86}Sr$ v. $^{1}/_{Sr}$ (fig. 4.3). In this graph fractional crystallisation will change $^{1}/_{Sr}$ but not $^{87}Sr/^{86}Sr$ producing horizontal trends. Crustal contamination by this bulk assimilation process, on the other hand, would produce a mixing trend between uncontaminated (low $^{87}Sr/^{86}Sr$) lavas and crust (high $^{87}Sr/^{86}Sr$, high $^{1}/_{Sr} \geq 0.002$ *ie.* Sr≤500 ppm). Aeolian lavas from Salina and Stromboli however define a trend towards high $^{87}Sr/^{86}Sr$ and *low* $^{1}/_{Sr}$, with $^{87}Sr/^{86}Sr$=0.710

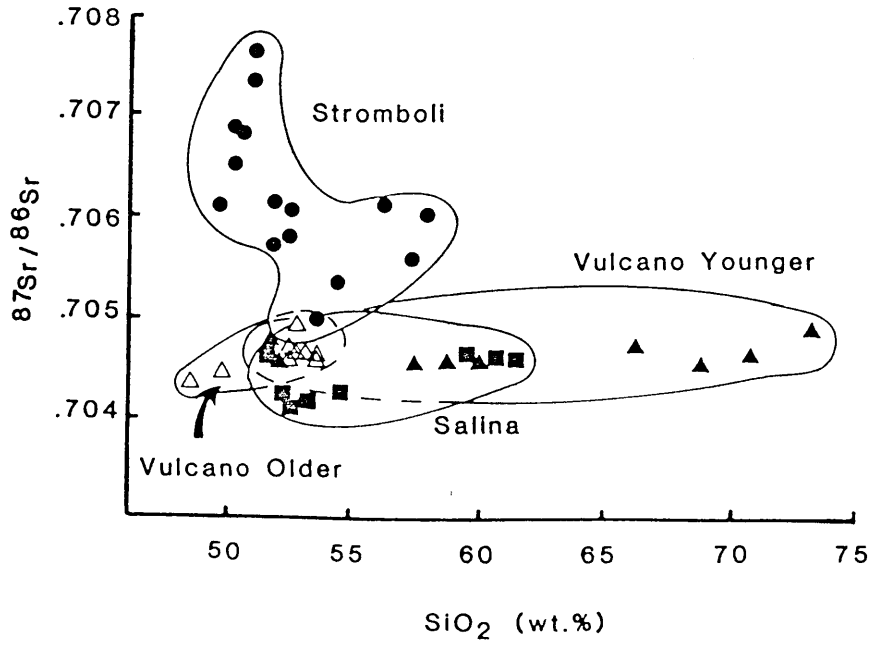

Fig. 4.2 $^{87}Sr/^{86}Sr$ v. SiO_2 for Aeolian Islands lavas

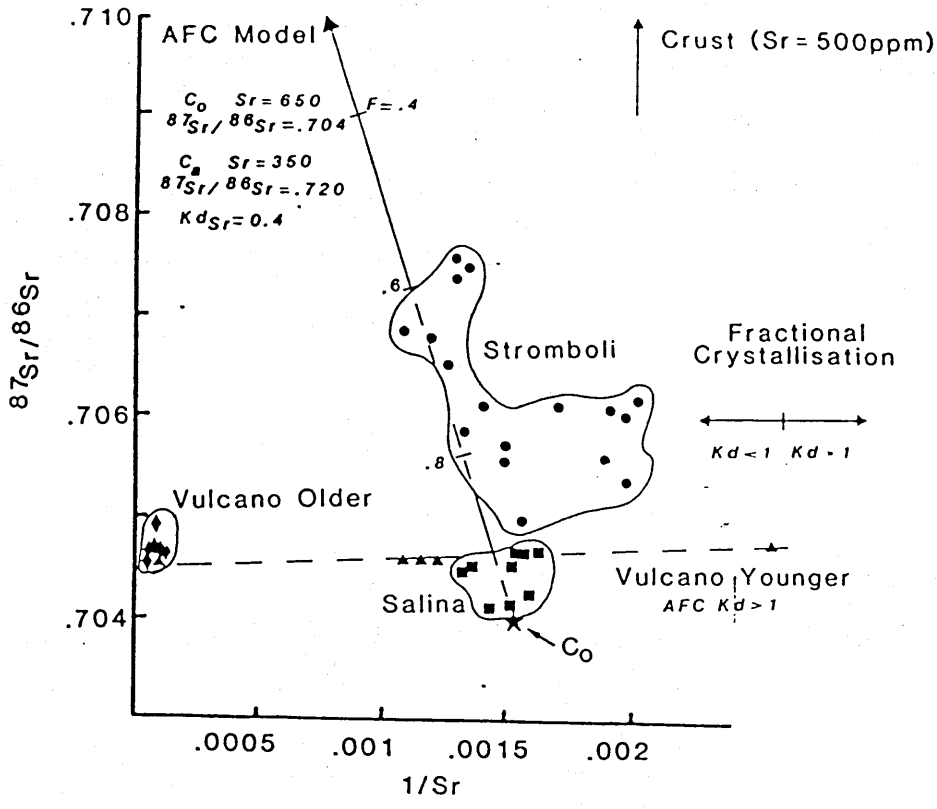

Fig. 4.3 $^{87}Sr/^{86}Sr$ v. $^{1}/_{Sr}$ for Aeolian Islands lavas

roughly corresponding to Sr=1000 ppm. Continental crust is not so rich in Sr and hence bulk assimilation may also be rejected as the source of high $^{87}Sr/^{86}Sr$ in the Stromboli lavas. Within individual fractionation trends, as defined by the K_2O v. SiO_2 diagram (chapter two) some small scale contamination may be inferred. It is also notable that the Sr rich younger series lavas of Vulcano are consistent with small amounts of AFC, as was proposed above.

As shown (fig. 4.3) a negative correlation between $^{87}Sr/^{86}Sr$ and $^{1}/_{Sr}$ is not inconsistent with an AFC process. Such a model may mimic the Salina - Stromboli trend on this diagram. However, there are important constraints on such a model which are unlikely to be satisfied by these lavas.

(a) Sr must behave highly incompatibly, therefore plagioclase is unlikely to be part of the fractionating assemblage. Its ubiquitous presence in Aeolian Islands lavas suggests that plagioclase does fractionate and this is supported by major element modelling (chapter two)

(b) If Sr were to behave highly incompatibly, this would tend to reduce the amount of isotopic variation produced by assimilation of low Sr, high $^{87}Sr/^{86}Sr$ crust. For a given $^{87}Sr/^{86}Sr$ assimilant, a play-off exists between Sr content enrichment due to

fractional crystallisation and $^{87}Sr/^{86}Sr$ enrichment by assimilation. Only by assimilation of very $^{87}Sr/^{86}Sr$ rich crust is both high Sr content and high $^{87}Sr/^{86}Sr$ attainable.

(c) The crystallisation dominated system required to enrich Sr to an extent greater than the dilutant effect of assimilation is highly favourable to the development of a positve relationship between differentiation and contamination indices (*e.g.* SiO_2 and $^{87}Sr/^{86}Sr$). As noted above, such a relationship is not observed in the Stromboli lavas.

It therefore appears that crustal contamination during magma ascent is not a suitable process by which to generate the isotopic shift observed between Salina and Stromboli and within the Stromboli lavas. It is however possible that minor amounts of contamination have occurred at all the Aeolian volcanic centres. This latter possibility will be discussed below with reference to Pb isotope data.

4.2.3 The Relationship Between Isotopic and Trace Element Enrichment

In chapter three a distinction was made between subduction related LILE enrichment and within-plate enrichment of all the incompatible elements, in the Aeolian lavas. The nature of the subduction and within-plate components may now be further investigated using isotopes. A diagram of $^{87}Sr/^{86}Sr$ v. Ta/Yb (fig.4.4) reveals a correlation for lavas from Salina and Stromboli which suggests that the Ta-rich within-plate component is associated with radiogenic Sr. Furthermore, the lavas are consistent with a simple mixing curve calculated between the lowest and highest $^{87}Sr/^{86}Sr$ samples.

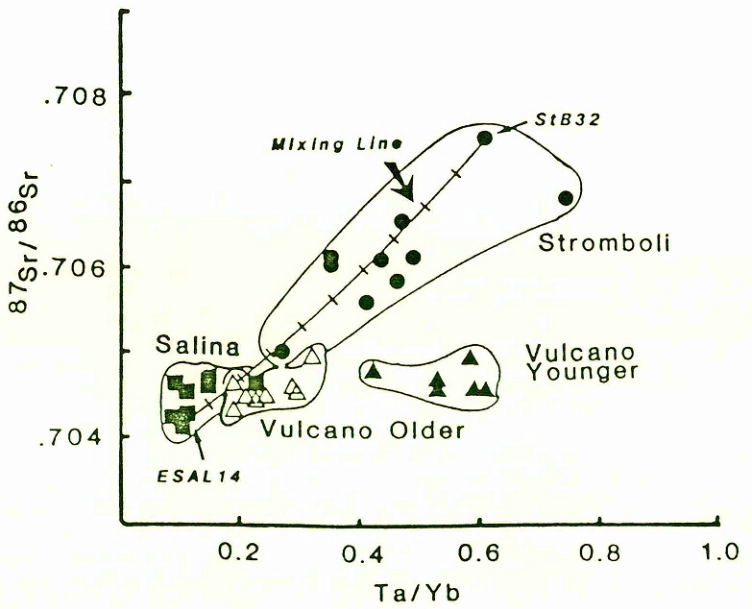

Fig. 4.4 $^{87}Sr/^{86}Sr$ v. Ta/Yb for Aeolian lavas. Mixing line is between highest and lowest $^{87}Sr/^{86}Sr$ samples.

In contrast, lavas from Vulcano do not lie on the Salina - Stromboli trend, being displaced towards higher Ta/Yb at given $^{87}Sr/^{86}Sr$. As discussed above this Ta/Yb increase is thought to arise from Yb depletion during multiple melting of a garnet-free source. In contrast the Salina - Stromboli trend is likely to reflect addition of Ta in the within-plate component. Despite their high Ta/Yb, there is no reason to suggest that the Vulcano lavas require a large contribution from the within-plate component.

The ratio Ta/Yb has revealed interesting information about the within-plate component, however it does not supply useful constraints on the subduction component as this is thought to contain negligable quantities of both Ta and Yb. It is more useful to consider one of the LILE which are believed to be highly concentrated in the subduction component. Of particular interest is the ratio Ta/Sr. When this is plotted against $^{87}Sr/^{86}Sr$ (fig. 4.5a) two component mixing lines are constrained to be straight (Langmuir *et al.* 1978). A problem arises from the compatible behaviour of Sr during plagioclase fractionation which will tend to increase Ta/Sr as shown by the Vulcano younger series data. However if low CaO (< 8%) Stromboli lavas are excluded, a positive relationship emerges. Again the Ta-rich within-plate component is associated with high $^{87}Sr/^{86}Sr$, but now an estimate of the isotopic composition of the subduction zone component may be made by assuming it contains no Ta. In this case the y axis intercept (~0.7040) represents the subduction component.

A similar treatment may be applied to the Nd isotope variations (fig. 4.5b). This diagram is free from the problem caused by plagioclase fractionation, as Nd is incompatible in plagioclase. The results of this treatment agree well with those produced from Sr isotopes. The low Ta/Nd subduction component is inferred to have high $^{143}Nd/^{144}Nd$ (~0.5129) whilst more enriched isotopic compositions occur in lavas with a significant within-plate component. It should be noted that Vulcano basic lavas show far greater consistency with Salina and Stromboli in figures 4.5 a, b than in figure 4.4. This is further evidence in support of Yb depletion being the cause of high Ta/Yb at Vulcano. Notably Ta/Sr and Ta/Nd are not similarly enriched.

It would appear that Aeolian lavas may be explained in terms of a two component mixture between an isotopically depleted subduction component and an enriched within-plate component. However such a hypothesis implies no variation in these components throughout the arc, other than in their relative contribution to the mixture.

Such an assumption warrants further discussion.

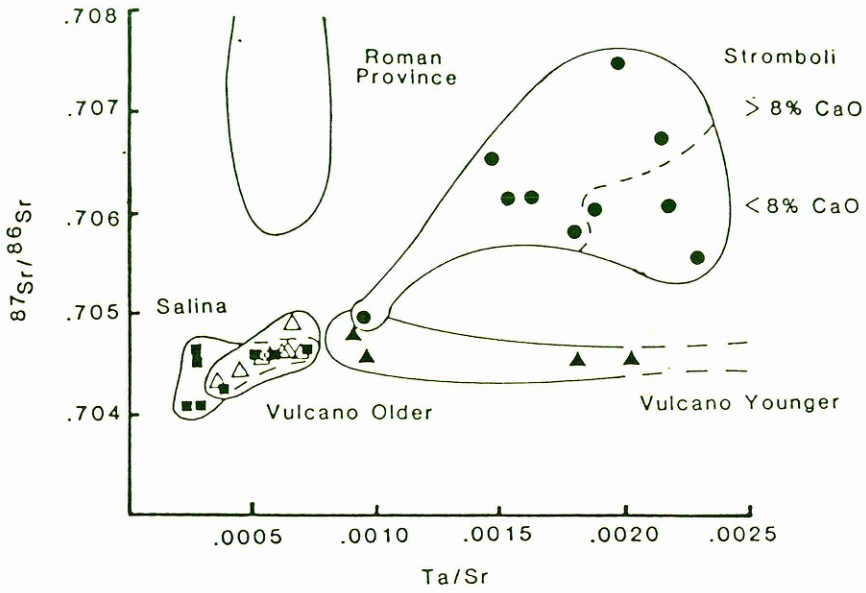

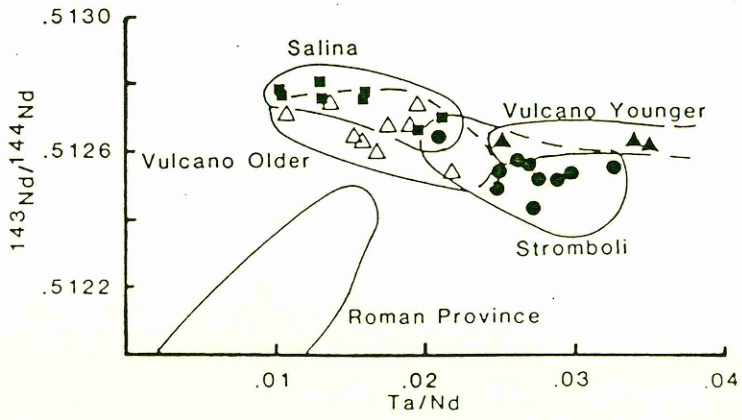

Fig. 4.5 $^{87}Sr/^{86}Sr$ v. Ta/Sr (a) and $^{143}Nd/^{144}Nd$ v. Ta/Nd (b) for Aeolian lavas *nb.* contrast with Roman province lavas.

An approach similar to that used above may be applied to various trace element ratios in order to gain further information as to the nature of the components. A diagram of Sm/Nd v. Ta/Nd (fig. 4.6 a) may be used in a similar manner to that of $^{143}Nd/^{144}Nd$ v. Ta/Nd, in an attempt to infer the trace element characteristics of the end members. For basic Salina and Stromboli lavas a trend may be recognised (fig. 4.6) which suggests a high Sm/Nd subduction component and a low Sm/Nd within-plate component. If the within-plate component is arbitrarily assumed to have Ta/Nd = 1.5 x chondrite (0.048) then a Sm/Nd of around 0.163 is implied for this component. Whilst such a value is low, it is not beyond the range of alkalic magmas which might be thought of as potential agents of within-plate enrichment. Furthermore if the within-plate component is assumed to have $^{143}Nd/^{144}Nd$ between 0.5124 and 0.5125 then a model age (T_{CHUR}) may be calculated for the enrichment. This yields between 400 and 200 Ma and is therefore consistent with enriched lithosphere of relatively young (Hercynian ?) age, as might be expected in this tectonically complex region.

A similar treatment of Rb/Sr ratios (fig. 4.6 b) does not yield such encouraging results. Again only the basic lavas are plotted to diminish the effects of fractional cystallisation. A trend exists, but if Ta/Sr is assumed to be 1.5 x chondrite (0.0025) a Rb/Sr of around 0.13 is inferred for the within-plate component. Such a value is extremely high, and well outside the range of alkali basalts *etc.* Even the extremely enriched lamproites and kimberlites do not have such elevated Rb/Sr. Indeed even if the within-plate component were to have very high Rb/Sr, as implied by this model, it would still require a long period of time (> 1Ga) to achieve the high $^{87}Sr/^{86}Sr$ (> 0.709) required in the within-plate component. It seems unlikely that stable lithosphere has existed for such a long period of time beneath such a tectonically active region. Hence whilst the within-plate component shows many characteristics of an enriched mantle source, it also dispays very high Rb/Sr which appears inconsistent with such an origin, but is characteristic of the upper continental crust. It therefore appears feasible that the component recognised as within-plate by virtue of its HFSE enrichment, is itself a mixture of a true within-plate (enriched mantle) component and a continental crustal component. Crustal contamination has been rejected as the source of large scale variations, however addition of subducted crust to the source of Stromboli lavas is a potential process by which the crustal component could be introduced.

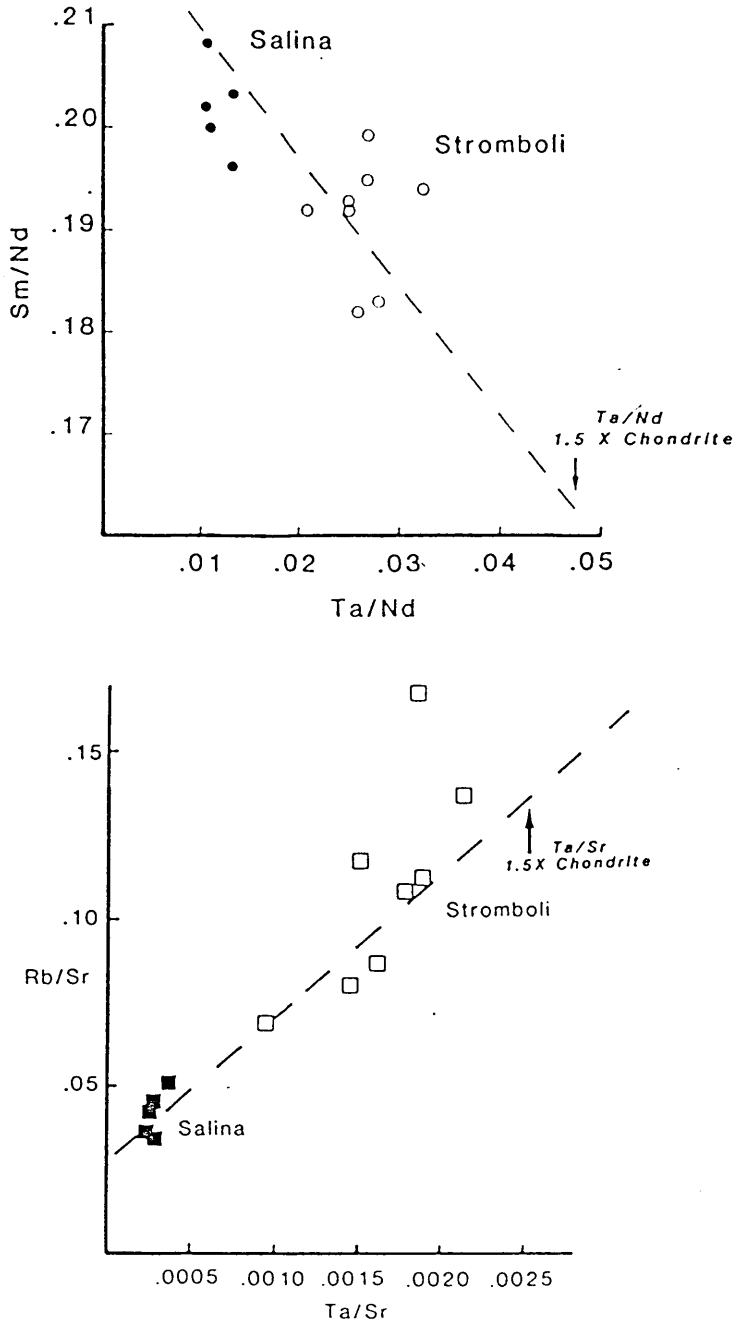

Fig 4.6 Sm/Nd v. Ta/Nd (a) and Rb/Sr v. Ta/Sr (b) for basic (>10% CaO) lavas form Salina and Stromboli. Arrows indicate values of Sm/Nd and Rb/Sr for Ta/Nd and Ta/Sr = 1.5 x chondrite.

Clearly a high Rb/Sr crustal component is required by the Stromboli lavas to explain their anomalously high Rb/Sr, even in relatively primitive lavas. It is however unclear to what extent this crustal component has affected Sm/Nd and $^{143}Nd/^{144}Nd$. The timing of within-plate enrichment calculated above seems geologically reasonable, the age of

lithosphere require agrees well with the age of the oldest exposed crust in this region (Hercynian). However the likely effect of addition of a crustal component would be to reduce the age of the within-plate component. This is believed to be geologically quite acceptable.

The discussion above has introduced the possibility that two subduction components may be recognised within the Aeolian Islands lavas. It is therefore prudent to distinguish between these prior to further discussion. Subduction component A (SCA) is that which dominates the Salina lavas, and is the normal component seen in arc lavas. It is of course LILE enriched but has relatively low Rb/Sr and high Sm/Nd. It would appear to be isotopically depleted. Subduction component B (SCB) has its characteristics largely hidden by the within plate component, with which it is associated at Stromboli. It is recognisable however by virtue of its high Rb/Sr. It is also likely to preserve high $^{87}Sr/^{86}Sr$ and is most likely derived from subducted terrigenous sediment.

The apparent need for two subduction components in the Aeolian Islands lavas may be investigated more thoroughly using other trace element ratios. A diagram of Sr/Nd v. Th/Ta (fig. 4.7) is particularly useful in this respect. Rogers *et.al.* (1985) have shown that MORB and within-plate lavas occupy a very restricted area of this diagram (the within-plate field). In contrast subduction related lavas tend to display elevated Sr/Nd (~50) and Th/Ta (~20). Clearly the normal subduction component (SCA) has high Sr/Nd and Th/Ta. Rogers *et al.* (*op.cit.*) used this diagam to establish a mixing relationship between such a normal subduction component (their low-K component) and a second (high-K) component with relatively low Sr/Nd (17) but extemely high Th/Ta (>100). This high-K end member was though to originate from subducted terrigenous material.

Basic lavas from Salina and Vulcano show enrichment in both Sr/Nd and Th/Ta compared with within-plate lavas, consistent with their including a significant contribution from a normal subduction component (SCA). In contrast Stromboli lavas have much lower Sr/Nd at a given Th/Ta. Such a variation may reflect low Sr/Nd due to plagioclase fractionation. However all the lavas plotted (with the exception of those from Vulcano) have similar high CaO (>10%), also Stromboli lavas have higher Mg numbers than the Salina lavas which rather precludes the derivation of the former from the latter by fractional crystallisation. Furthermore, the required decrease in Sr/Nd would imply around 50% fractional crystallisation of pure plagioclase if it were to be achieved in this manner. In

addition Nd/Sr correlates with $^{87}Sr/^{86}Sr$ (fig. 4.8) for Salina and Stromboli lavas. Simple fractional crystallisation is unlikely to induce such a variation in $^{87}Sr/^{86}Sr$.

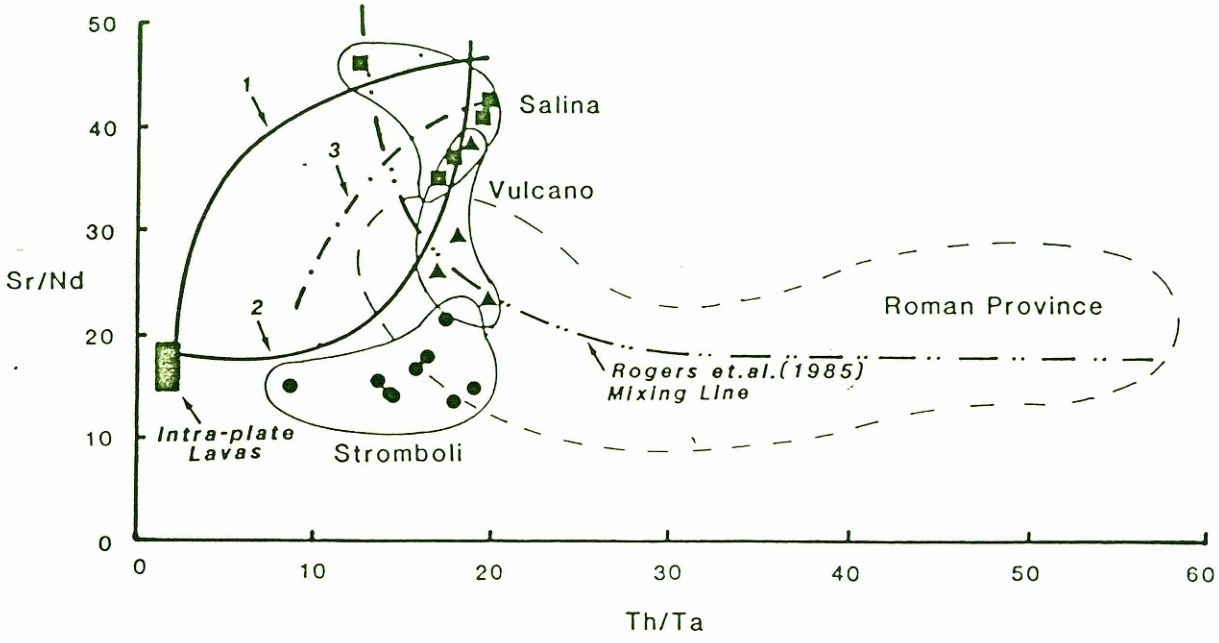

Fig. 4.7 Sr/Nd v. Th/Ta for Aeolian Islands basic lavas (>10 % CaO, except Vulcano <52% SiO_2) Roman province field and mixing line from Rogers *et.al.* (1985). For discussion of mixing lines 1-3, see text.

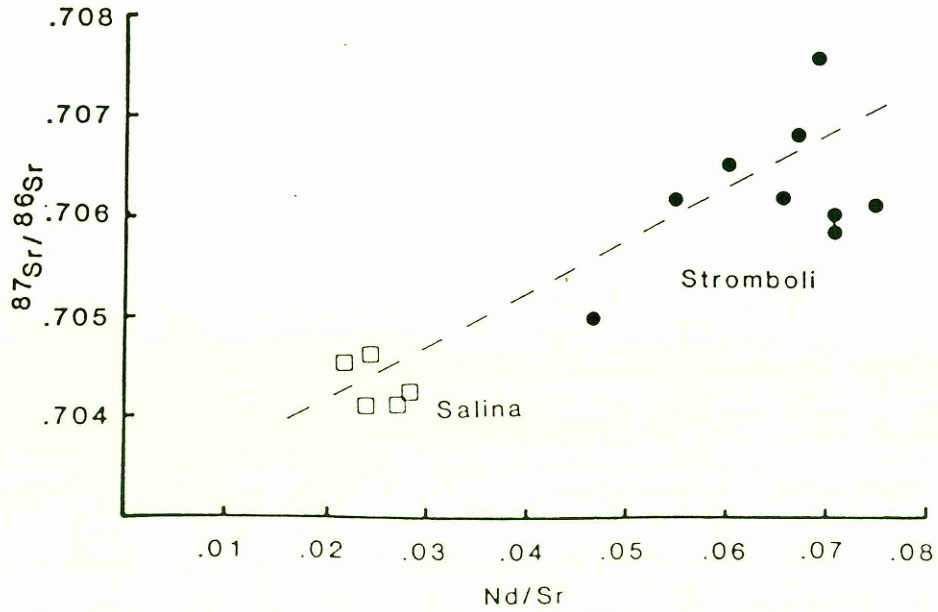

Fig 4.8 $^{87}Sr/^{86}Sr$ v. Nd/Sr for basic (>10% CaO) lavas fom Salina and Stromboli.

It seems therefore, that the distribution of Aeolian basic lavas must be explained by some other means. The most simple alternative is two component mixing between a within-plate component and a subduction component, as already discussed. Such a mixture is required to produce a strongly convex downwards mixing hyperbola in figure 4.7. Modelling reveals that such a variation is difficult to achieve, in order to produce such a curve, one must constrain the within-plate component to have lower Ta/Nd than the subduction component. As the subduction component contains negligable Ta by definition, this is unlikely to be realistic. Hence, if Nd is added in the subduction component convex upwards hyperbolae are produced (model 1). Only if Nd is constrained to be negligable (Nd≤ Ta) in the subduction component is it possible to produce high Ta/Nd (≥1) in this end member (model 2) Such a model is obviously difficult to constrain as it is most dependant on two very low concentrations (Nd and Ta in the subduction component) to determine the shape of the mixing curves. Furthermore the required lack of Nd in the subduction component is inconsistent with the apparent LREE contribution from this component calculated in chapter three. This two component model also requires that the within-plate component have elevated $^{87}Sr/^{86}Sr$ which was considered unlikely above.

It may also be noted at this stage that continental crustal contamination of Salina lavas cannot produce the required shape of mixing curve to explain the Stromboli data. Model 3 illustrates that contamination with average continental crust (Weaver & Tarney, 1984[1]) will result in convex upward hyperbolae, which are inconsistent with the observed variation.

Apparently a more complex model is required to explain the Stromboli lavas. The evidence for three components has already been introduced, high Ta implies a within-plate component, a coherence with Salina data on several diagrams suggests a normal subduction component (SCA) similar to that required in Salina basalts, and evidence for a high Rb/Sr crustal component has been found. In addition low Sr/Nd is associated with low Eu/Eu* (fig. 4.9). Plagioclase fractionation is unlikely to be the source of this Eu anomaly particularly as Nd/Sr correlates with $^{87}Sr/^{86}Sr$ (fig. 4.8). However the Eu anomaly is highly unlikely to be a mantle enrichment phenomenon as plagioclase is unlikely to be a stable mantle phase. More likely, the Eu anomaly is a feature inherited from a subducted crustal component.

[1]Chondrite normalised Ta abundance assumed to equal chondrite normalised Nb

Comparison with Rogers *et.al.* (1985) data for the Roman province, reveals that Stromboli data are displaced from the mixing curve proposed by these authors towards lower values of Th/Ta (fig. 4.7). It is believed that the Roman province lavas define a mixing hyperbola between two subduction components whose elemental characteristics are similar to those implied at Stromboli. The mantle prior to subduction beneath the Roman province was depleted (E-type MORB, Rogers *et al. op. cit.*). Therefore this depleted mantle contributes little to the final mixture and the observed mixing relationship is produced. At Stromboli however, elementally enriched mantle exists which contributes significant amounts of HFSE to the final mixture. Hence Stromboli lavas are displaced away from the Roman province mixing curve towards the low Th/Ta within-plate field.

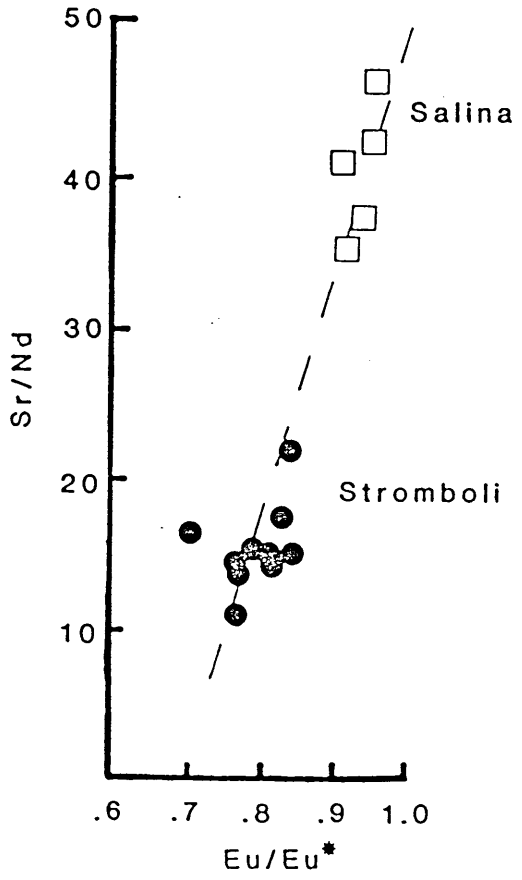

Fig. 4.9 Sr/Nd v. Eu/Eu* for basic (>10% CaO) lavas from Salina and Stromboli.

The recognition of a third component (SCB) at Stromboli is an important discovery. Immediately, conclusions drawn from the simple two component scenario are called into question. It is no longer necessary (nor possible) to assume that the within-plate component had high $^{87}Sr/^{86}Sr$. Moreover, it explains some of the inadequacies of the two

component model, such as the relatively poor correlations for some pairs of element ratios. For example the discovery that high Ta/Yb and high $^{87}Sr/^{86}Sr$ whilst being related, are derived from distinct components explains why sample StB32 has the highest $^{87}Sr/^{86}Sr$ but not the highest Ta/Yb. Features such as these emphasise the danger of the simplified two component interpretation.

Using the SCA derived from two component modelling, and largely constrained by the Salina data, and the SCB taken as the high-K end member of the Roman Province mixing model (Rogers *et al.* 1985), it is now possible to assess the need for an isotopically enriched within-plate end member. For two Stromboli samples (StD1 and StB42) the relative contribution of the subduction and within-plate components[1] were taken from the method of Pearce (1983). In each case the following values were assumed:

	$^{87}Sr/^{86}Sr$
Within-Plate Component	0.7035
Subduction Component A	0.7040
Subduction Component B	0.7105

For StD1 to meet these criteria the bulk subduction component is required to be almost 100% SCB whereas for StB42 only around 20% SCB is required, the more normal SCA being dominant. Important points to be drawn from this are that the within-plate component is not required to be isotopically enriched, and the subduction component is apparantly highly variable, but explicable in terms of two end members. Further constraints on the nature of the observed variations may be placed by using Pb isotope data which will be described below.

4.3 Pb Isotope Variations

4.3.1 Introduction

The continental crust is a major reservoir of Pb. It is therefore important to establish whether the Pb isotope data are consistent with the hypothesis developed above. In particular it is necessary to determine the effect of the postulated subducted crustal component (SCB) on Pb isotope ratios. All Aeolian Islands lavas show radiogenic $^{208}Pb/^{204}Pb$ and $^{207}Pb/^{204}Pb$ compared with MORB (Dupre & Allegre, 1980, Sun, 1980, Cohen & O'Nions, 1982a) and other subduction related provinces (*eg.* Kay *et al.*, 1978).

1 Within plate component = within plate + depleted mantle component of Pearce (1983)

The measured Aeolian Islands ranges are:

$^{208}Pb/^{204}Pb$	38.74 - 39.50
$^{207}Pb/^{204}Pb$	15.50 - 15.69
$^{206}Pb/^{204}Pb$	18.93 - 19.77

It should be noted that the radiogenic nature of these samples is such that average continental crust and many oceanic sediments (White *et al.*, 1985) are less radiogenic than these lavas.

4.3.2 The Effects of Crustal Contamination

As Pb is around two orders of magnitude more abundant in the continental crust than in the upper mantle, it is likely to be an excellent indicator of crustal contamination. It is therefore prudent to examine any evidence for or against contamination prior to discussion of other processes which may affect Pb isotope composition. It should be borne in mind that small degrees of contamination which may be of little significance to Sr and Nd isotopes, might produce important Pb variations.

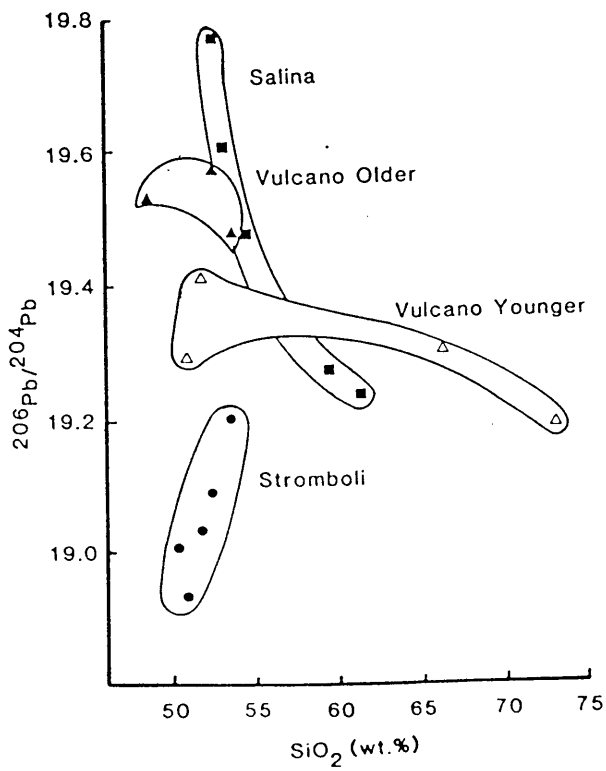

Fig. 4.10 $^{206}Pb/^{204}Pb$ v. SiO_2 for Aeolian Islands lavas. *nb.* Negative correlations for Salina and Vulcano younger series and positive correlation for Stromboli.

A diagram of $^{206}Pb/^{204}Pb$ v. SiO_2 (fig. 4.10) provides the necessary plot of contamination index against fractionation index, which allows recognition of AFC processes. Vulcano younger series lavas show a small range in $^{206}Pb/^{204}Pb$ (19.41-19.19) which is negatively correlated with SiO_2. This suggests an AFC trend which is consistent with the small degree of contamination inferred for these lavas in chapter three. The model illustrated (fig. 4.11) shows that an AFC treatment similar to that shown in chapter three is indeed consistent with the data. However, with the ratio of assimilation to crystallisation (r) fixed at 0.1(from the previous model) and Kd_{Pb}=0.5, which is likely to be roughly correct in feldspar dominated fractionation (Henderson, 1982), then to generate the required drop in $^{206}Pb/^{204}Pb$ requires either very low $^{206}Pb/^{204}Pb$ in the assimilant (~17.5) or a Pb-rich (~60 ppm) assimilant. In the former case this would imply old crust with an ancient depletion in U, whereas the latter requires anomalously Pb rich crust or some mechanism of preferentially incorporating Pb. No evidence for ancient crust exists in the region and the fact that both Pb and Sr are concentrated in the feldspars reduces the possibility that they may be fractionated during assimilation.

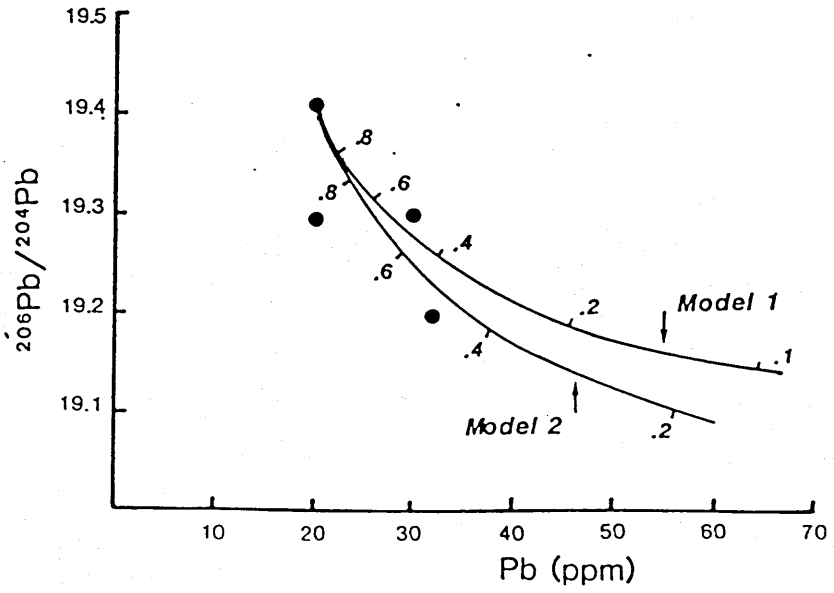

Fig. 4.11 Vulcano younger series AFC model.

Model One Pb: C_O=20, C_A=20, $^{206}Pb/^{204}Pb$: C_O=19.41, C_A=17.5, Kd_{Pb}=.5 ,r =.1

Model Two Pb: C_O=20, C_A=60, $^{206}Pb/^{204}Pb$: C_O=19.41, C_A=18.3, Kd_{Pb}=.5 ,r =.1

Lavas from Salina also display a negative relationship between $^{206}Pb/^{204}Pb$ and SiO_2. An AFC model may be used to explain the Sr-Pb isotope variations (fig. 4.12). The

wide variation in $^{206}Pb/^{204}Pb$ (19.77-19.24) but only minor variation in $^{87}Sr/^{86}Sr$ (0.7041-0.7047) may be explained by incorporation of relatively Pb-rich, Sr-poor crust into comparatively Pb-poor, Sr-rich magma.

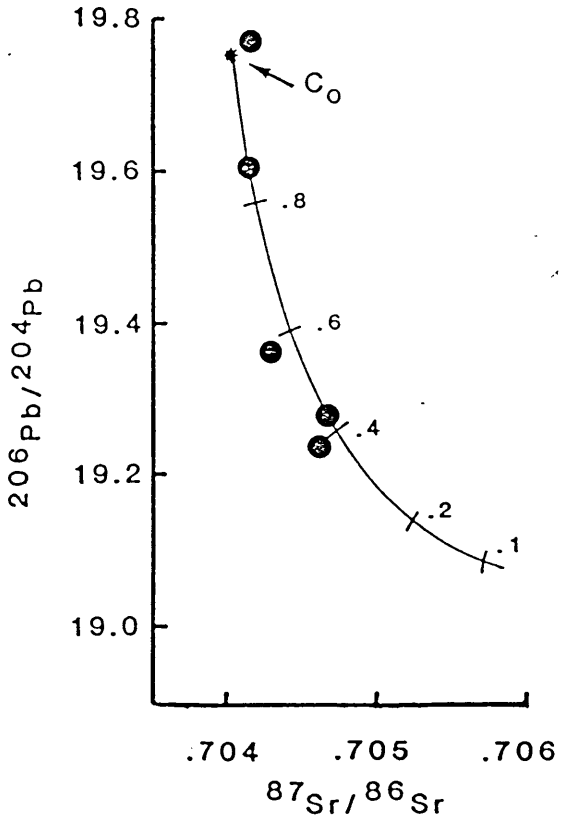

Fig. 4.12 Salina AFC model

C_O: Pb =8ppm, Sr =650ppm, $^{206}Pb/^{204}Pb$ =19.75, $^{87}Sr/^{86}Sr$ =0.704

C_A: Pb =15ppm, Sr =200ppm, $^{206}Pb/^{204}Pb$ =17.5, $^{87}Sr/^{86}Sr$ =0.714

D_{Sr} =0.9, D_{Pb}=0.001, r =0.2

It should be emphasised that the model presented is in no way unique, it is capable of explaining the required isotopic variations but requires an assimilant with low Sr content and low $^{206}Pb/^{204}Pb$ (≈17.5). As discussed above no evidence for the latter exists. Moreover the model presented is not fully consistent with trace element abundances in evolved Salina lavas (table 4.1). It is therefore unclear to what entent crustal contamination has affected the Salina lavas. Trace element and Sr isotope evidence implies only a very minor role for contamination but this is not likely to be consistent with the large range of Pb isotope ratios. Given the lack of conclusive evidence in favour of crustal contamination as the source of isotopic variations within the Aeolian lavas, it is now of interest to explore the

nature of Pb isotope variations, with reference to the hypotheses developed above from Sr and Nd isotope and trace element data.

CRYSTALLISING ASSEMBLAGE

		Orthopyroxene	19%		
		Clinopyroxene	28%		
		Plagioclase	46%		
		Magnetite 7%			
	Rb	Ba	Hf	Eu	Yb
D_{OPX}	0.025	0.013	0.11	0.05	0.34
D_{CPX}	0.04	0.07	0.8	0.9	1.0
D_{PLAG}	0.1	0.23	0.08	0.32	0.07
MAGNETITE IGNORED IN Kd CALCULATION					
Kd	0.06	0.13	0.28	0.41	0.38
ESAL14 (C_O)	25	386	1.61	1.09	1.77
C_A	110	700	5.8	0.88	2.2

F	Rb	Ba	Hf	Eu	Yb
0.8	37.5	508.3	2.2	1.3	2.1
0.6	58.1	703.6	3.1	1.5	2.6
0.4	98.0	1072.7	4.7	2.0	3.5
0.2	212.8	2081.2	8.7	2.9	5.5
ESAL 24	62	565	2.54	1.21	2.44

Table 4.1 Salina AFC model showing inconsistencies with the trace element data

4.3.3 Other Controls on Pb Isotope Data

The range of Pb isotope ratios which are found within basaltic lavas is large, and as with the Sr and Nd systems it is not possible to unequivocally distinguish between crustal and mantle derived isotopic signatures, let alone discriminate distinct reservoirs within the mantle. Whilst it may be tempting to use Pb isotopes to infer mixing between preferred end members, such models are rarely unique and the source of their end members is often unclear. A more thorough approach is to explain the isotopic variations in terms of the trace element framework already developed.

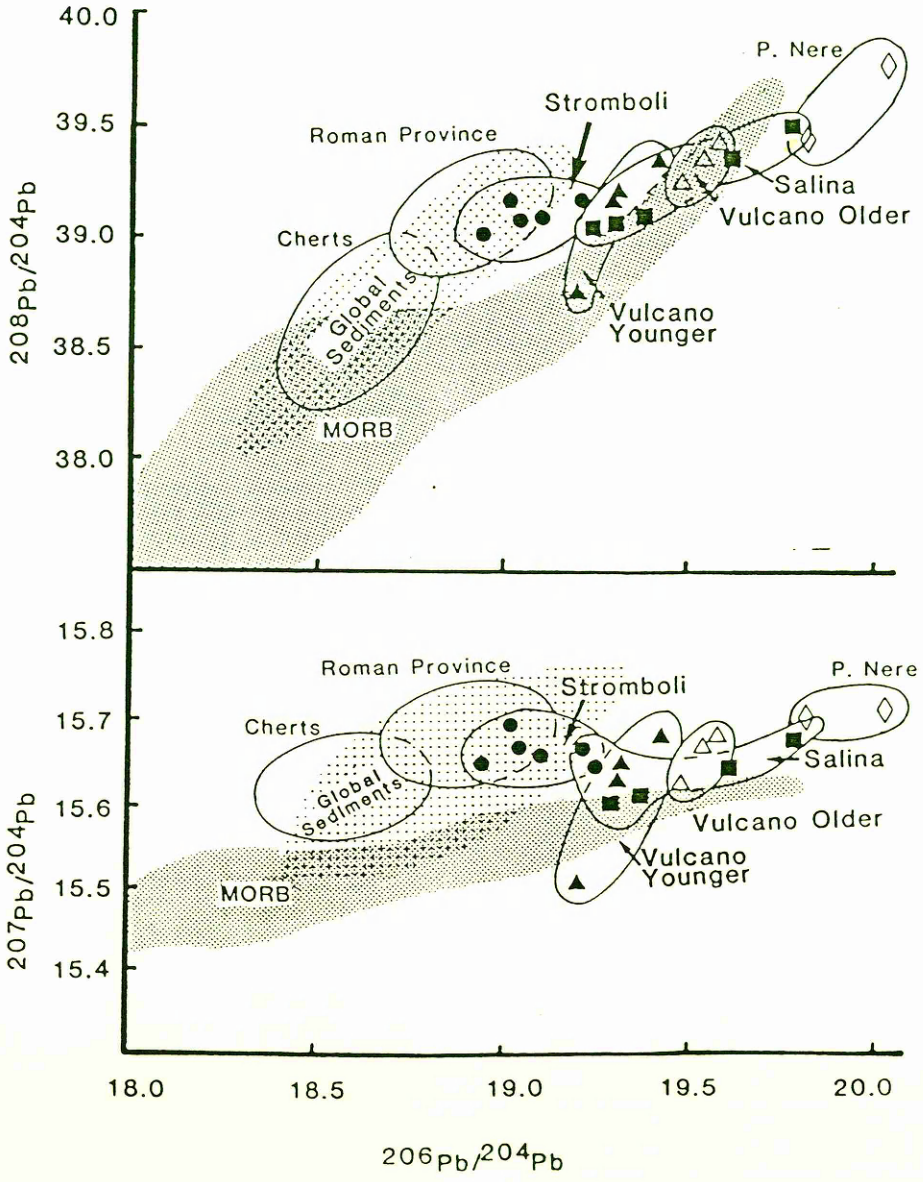

Fig 4.13 Pb isotope diagrams of Aeolian Islands lavas and comparison with Roman Province/Pietre Nere. (Vollmer, 1976, Vollmer & Hawkesworth, 1980), MORB (Dupre & Allegre, 1980, Sun, 1980, Cohen & O'Nions, 1982a), Apennine ophiolitic cherts (Barrett, 1980) and global sediments (White *et al.*, 1985.)

Pb isotope diagrams (fig.4.13 a,b) show a largely coherent variation within the Aeolian Islands lavas. The main exception to this is the Vulcano younger series rhyolite which is most likely contaminated with relatively unradiogenic crustal Pb. Lavas from Salina have highly radiogenic Pb isotopes ($^{208}Pb/^{204}Pb > 39.04$, $^{207}Pb/^{204}Pb > 15.60$, $^{206}Pb/^{204}Pb > 19.24$). Such values are inconsistent with derivation from oceanic crust, terrigenous material or pelagic sediment, however similarly radiogenic ratios do occur in the mantle, as illustrated by ocean island basalts (OIB). This observation suggests that Salina lavas derive their Pb isotope characteristics from their mantle source. Moreover it would imply that the subduction component (SCA) has not significantly altered the Pb isotope signature of the lavas. The implication of this observation are discussed in chapter six.

Lavas from Vulcano lie between Salina and Stromboli in Pb isotope diagrams (Fig 4.13 a,b). Stromboli lavas show lower $^{208}Pb/^{204}Pb$ and $^{206}Pb/^{204}Pb$ than Salina and Vulcano rocks. In previous discussion it was argued that Stromboli lavas include a contribution from a subducted terrigenous sediment component (SCB). Such a component is likely to be extremely rich in Pb in comparison with the mantle wedge. (~ 2 orders of magnitude richer). Pb isotopes should therefore provide a sensitive test for this crustal component. Even when it is insignificant in term of the volume of sediment subducted it is likely to be important in terms of the amount of Pb added to the mantle wedge. Therefore if a subducted sediment component does affect the Stromboli lavas, it is expected to dominate their Pb isotope composition. It is significant that Stromboli lavas have Pb isotope ratios that overlap those of oceanic sediments (White *et al.*, 1985) and are similar to those of cherts associated with Apennine ophiolites (Barrett, 1980) which are perhaps, ideal examples of the types of sediment likely to be involved in subduction.

It would appear that the Pb isotope data agree well with the model established above. To emphasise the suitability of this model a diagram of $^{206}Pb/^{204}Pb$ v. $^{87}Sr/^{86}Sr$ is plotted (fig. 4.14) which shows a coherent mixing relationship between two components, one with low $^{87}Sr/^{86}Sr$, high $^{206}Pb/^{204}Pb$ and high Sr/Pb, the second with high $^{87}Sr/^{86}Sr$, low $^{206}Pb/^{204}Pb$ and relatively low Sr/Pb. These components represent the mantle wedge and subducted terrigenous sediment component (SCB). Such a simple mixing relationship is believed to exist because the trace element enrichments associated with the normal subduction component (SCA) and the within plate component do not appear to be related to major isotopic variations.

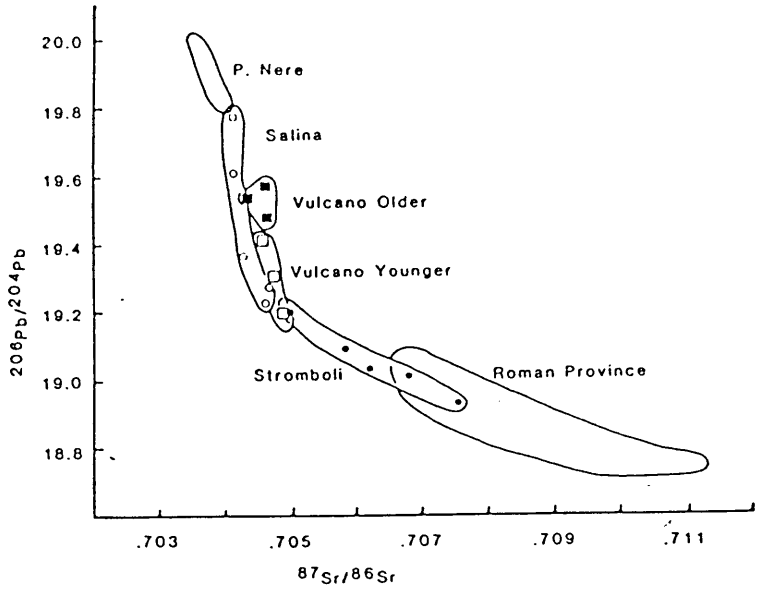

Fig 4.14 $^{206}Pb/^{204}Pb$ v. $^{87}Sr/^{86}Sr$ for Aeolian Islands and Italian mainland lavas (Vollmer, 1976, Vollmer & Hawkesworth, 1980).

4.4 Summary

By way of a summary one may tabulate the key features of the three proposed components of enrichment.

Normal Subduction Component (SCA)

Th/Ta > 20

Sr/Nd > 45

Eu/Eu* = 1

$^{87}Sr/^{86}Sr \leq 0.7040$

$^{143}Nd/^{144}Nd \geq 0.5129$

$^{206}Pb/^{204}Pb \approx 19.7$

$^{207}Pb/^{204}Pb \approx 15.7$

$^{208}Pb/^{204}Pb \approx 39.5$

Terrigenous Sediment Subduction Component (SCB)

This has many elemental features which are similar to the SCA and suggest a subduction related origin, in addition:

Sr/Nd is low (~15)

$Eu/Eu^* < 1$

Rb/Sr is very high (> 0.1)

$^{87}Sr/^{86}Sr < 0.710$

$^{143}Nd/^{144}Nd < 0.5125$

$^{206}Pb/^{204}Pb \approx 18.9$

$^{207}Pb/^{204}Pb \approx 15.5$

$^{208}Pb/^{204}Pb \approx 38.7$

Within-Plate Component

Sr/Nd ~ 17

Ta/Yb (high) > 0.75

Rb/Sr ~0.03

There is no evidence to suggest that this component requires enriched isotopic compositions.

CHAPTER FIVE

A Comparison Between the Aeolian Islands and the Roman Magmatic Province

5.1.1 Introduction

This chapter aims to compare the calc-alkaline to potassic volcanism of the Aeolian Islands with the potassic to ultra-potassic magmatism of the Italian mainland. Included within the Roman province, for the purposes of this discussion are the volcanic centres around Rome and also those of the Campania region to the south (fig. 5.1). This comparison is not only of geographical significance, but is also of geotectonic importance. The Aeolian Islands are clearly related to subduction processes, recently strong evidence has been presented, (Alvarez, 1972, Thompson, 1977, Rogers *et al.*, 1985) for a subduction related origin for the Roman province also. Opinions differ as to whether these subduction related provinces are in any way linked, a comparative study of their magmatic products may therefore provide further constraints on the relationship, or lack of such, between the two regions.

5.1.2 Timing of Magmatic Activity.

Active volcanism persists to the present day in both the Aeolian Islands (Stromboli and Vulcano) and the Roman province (Vesuvius and Campi Flegrei). The onset of volcanism would also appear to have been similarly timed. Radiometric ages from Vulsini range from 0.9-0.15 Ma for the various products (Ferrara *et al.*, 1986), and dates on other Roman centres extend back to around 1Ma (Gasparini & Adams, 1969, Everden & Curtis, 1965). Exposed rocks from the Aeolian Islands are all less than 0.5 Ma (Gillot & Villari,1980), but lavas as old as 1.3 ± 0.2 Ma (Beccaluva *et al.*, 1982) have been dredged from seamounts to the west of the exposed arc. Roman and Aeolian volcanism is therefore temporally related and would appear to largely post-date Tuscan Province magmatism (7.0-0.43 Ma, Taylor & Turi, 1976).

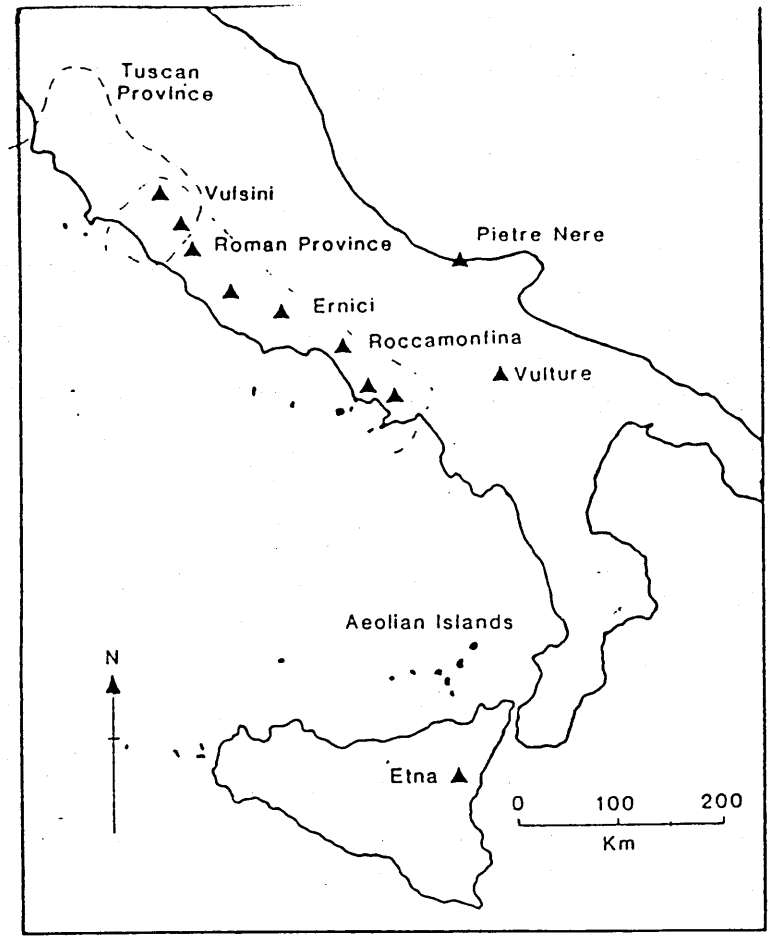

Fig. 5.1 Location of Italian volcanic provinces.

5.2 Petrography of Roman Province Lavas

The study of Roccamonfina lavas by Appleton (1972), provides a suitable example with which to compare other Roman centres. At Roccamonfina, in the high potassium series (HKS) the earliest assemblage to fractionate is biotite pyroxenite, followed by biotite gabbro. Appleton (*op. cit.*) argued that this was achieved at $P_{H2O} \approx 2.6$ Kb, where $P_{H2O} < P_{TOTAL}$. Plagioclase entered the fractionating assemblage at around 8% CaO, 48% SiO_2. After rapid release of pressure, intermediate lavas were developed along two fractionation schemes:

(a) The highest K_2O lavas fractionated leucite, clinopyroxene, plagioclase and magnetite.

(b) Slightly lower K_2O lavas produced the assemblage biotite clinopyroxene, plagioclase and magnetite.

Minor leucite flotation was believed to have occurred in lavas with >10% K_2O.

In the low potassium series (LKS), Appleton (*op. cit.*) recognised the following fractionation sequence. Clinopyroxene and spinel, thought to occur at pressures

between 10 and 15 kb, followed by olivine gabbro. Intermediate lavas were produced by separation of clinopyroxene, plagioclase, biotite and magnetite, with alkali feldspar a late crystallising phase.

Subsequent workers have modified these fractionation trends slightly for individual volcanoes. For example Rogers *et al.* (1985) reported olivine in primitive HKS lavas from Vulsini and Civetta *et al.* (1981) have recognised barkevikitic amphibole, fayalitic olivine and interstitial nepheline in HKS lavas from Ernici. In addition a number of exotic minerals occur as accessory phases in evolved Roman province lavas, these include hauyne, sodalite, sphene and apatite which Rogers *et. al* (*op.cit.*) have shown to be an important control on REE abundances.

Clearly the mineralogy and evolution paths of Roman province lavas are quite distinct from those of the Aeolian Islands. Leucite occurs much more frequently in the Roman province and it is found in much larger modal abundances. Plagioclase is almost ubiquitous in Aeolian Islands lavas, although it was argued in chapter two that plagioclase was not amongst the earliest fractionating phases. Appleton (1972) argued that the "plagioclase in" point for Roccamonfina lavas was around 48% SiO_2, 8% CaO, this is both lower CaO and SiO_2 than plagioclase phyric Salina lavas. Such an observation might suggest that plagioclase entered the fractionating assemblage at a different degree of evolution in the two provinces. However comparison of Mg numbers shows that the Salina lavas are actually more evolved (lower Mg number) than the likely Roccamonfina "plagioclase in" point (Mg number ≈0.65). Hence, plagioclase may first occur on the liquidus at similar degrees of evolution in otherwise quite different liquid lines of descent. It should be noted that relatively low SiO_2 and CaO in Roman province basic lavas probably reflects the dominance of pyroxene over olivine in the fractionation process in comparison to calc-alkaline lavas. Furthermore the high K_2O content of Roman lavas will of course slightly reduce their SiO_2 and CaO percentages.

Orthopyroxene has not been reported in any Roman province lavas. This is a reflection of the SiO_2 undersaturated nature of basic Roman lavas. A similar feature is found in the Aeolian Islands, whereby SiO_2 saturated lavas crystallise orthopyroxene, but none is found in undersaturated potassic lavas.

Hydrous phases are rare in the Aeolian Islands lavas, occuring as phenocrysts of biotite and amphibole in quite evolved lavas or as biotite xenocrysts. Roman lavas

commonly contain hydrous phases and biotite is an important fractionating phase in the HKS basic-intermediate lavas and in the intermediate lavas of the LKS. It would appear that P_{H2O} was higher during evolution of the Roman lavas than during Aeolian lava evolution. A possible effect of higher P_{H2O} would be to reduce the stability field of plagioclase, which is perhaps consistent with the absence of plagioclase as an early fractionating phase in Roman lavas.

5.3 Experimental Petrology

No data are available on experimental melting of Aeolian Islands lavas. However, it is of interest to review the experimental study of Roman province lavas carried out by Thompson (1977), as this has important implications for Roman province magma genesis. In this study a mafic leucitite fron the Alban Hills (EU13), was investigated by anhydrous high pressure melting experiments. It was found that only at high pressures (~12 kb) do leucite and clinopyroxene coexist on the liquidus. As these are the only two phenocryst phases in EU13, it was inferred that they coprecipitated, and therefore implied a final position of equilibrium for this lava at a pressure of around 12 kb, *ie.* within the mantle.

Clearly the conclusion drawn is critically dependant on the assumption that leucite and clinopyroxene coprecipitated, this would appear likely given the small phenocryst content of EU13 (<4%) which would imply efficient separation of fractionating phases. Furthermore, important evidence may be gained by considering the major element composition of EU13. The lava is clearly not primary; despite low SiO_2 (46.85%), it also has low MgO (3.42%), low CaO (9.23%) and high K_2O (9.26%). These features are particularly striking when compared with a magnesian leucitite from Vulsini (Rogers *et al.* 1985, table 5.1). Low MgO and CaO are obviously consistent with removal of clinopyroxene and high K_2O content suggests that removal of leucite has been very minor indeed. Such a situation may be explained by reference to the phase diagram of EU13 (Thompson *op.cit.* fig. 4). At pressures greater than 12 Kb the first liquidus phase will be clinopyroxene, it would appear that EU13 underwent significant high pressure fractionation of clinopyroxene before coprecipitating only a small volume of leucite and clinopyroxene at around 12 Kb. This would support the conclusion of Thompson (*op. cit.*) that this lava last equilibrated within the upper mantle and was rapidly erupted avoiding interaction with the continental crust.

	EU13	7601
SiO_2	46.85	47.25
TiO_2	3.25	0.74
Al_2O_3	15.30	12.15
Fe_2O_3	4.40	3.08
FeO	3.52	4.54
MnO	0.17	0.17
MgO	3.42	9.26
CaO	9.23	15.61
Na_2O	2.97	1.10
K_2O	9.26	4.49
P_2O_5	0.65	0.35
H_2O^-	0.81	0.19
LOI		0.93
Total	99.83	99.86

Table 5.1 Comparison of Alban Hills leucitite EU13 with Vulsini magnesian leucitite (7601) (Rogers *et al.*,1985).

However, a number of points may be raised which cast doubt on the applicability of the conclusions drawn from EU13 to the rest of the Roman province. Anhydrous experiments may be suitable for EU13 which does not contain hydrous phenocrysts, although groundmass biotite does occur. However anhydrous melting is unlikely to be relevant to the majority of Roman province lavas which have apparently fractionated biotite at a very early stage (Appleton, 1972). EU13 is also unusual in its TiO_2 content (3.25%). This is very high for a Roman province lava which normally contain less than 1% TiO_2. High TiO_2 is inconsistent with the subduction related origin proposed by Thompson (1977). However, normal Roman province TiO_2 values are consistent with such an origin.

It would therefore appear that EU13 is unlikely to be representative of Roman province lavas in general, however for this individual sample, evidence suggests that it last equilibrated within the upper mantle. This is strong evidence of isotopically enriched mantle beneath Italy as EU13 has $^{87}Sr/^{86}Sr=0.71024$ and $^{143}Nd/^{144}Nd=0.51220$ (Hawkesworth & Vollmer, 1979) which is constrained by the experimental petrology to be a mantle derived signature.

5.4 Major Element Variations.

5.4.1 K_2O v. SiO_2 Comparison

Aeolian and Roman lavas may be compared on a diagram of K_2O v. SiO_2 (fig 5.2). Representative Aeolian fractionation trends are superimposed upon Roman province data. LKS lavas have K_2O and SiO_2 contents similar to the Aeolian shoshonitic and leucite tephritic series. However the Roman HKS is much richer in K_2O at a given SiO_2 than any Aeolian lavas. In general Roman province fractionation trends extend to much lower SiO_2 values than Aeolian trends. Within the HKS some of the low SiO_2 lavas may have fractionated to lower SiO_2 by removal of relatively SiO_2-rich leucite. The dominance of pyroxene over leucite in the early stages of fractional crystallisation of the Roman province magmas tends to limit the SiO_2 enrichment produced in evolved lavas. Clearly SiO_2 is not a particularly useful index of differentiation in the Roman lavas.

5.4.2 CIPW Normative Compositions.

The projection of the normative basalt tetrahedron used in chapter two is plotted (fig. 5.3). This diagram indicates the presence of a thermal divide in the Diopside-olivine-nepheline portion of the tetrahedron. Although HKS and LKS lavas from Ernici (Civetta *et al.* 1981) have similar normative compositions, more evolved lavas from

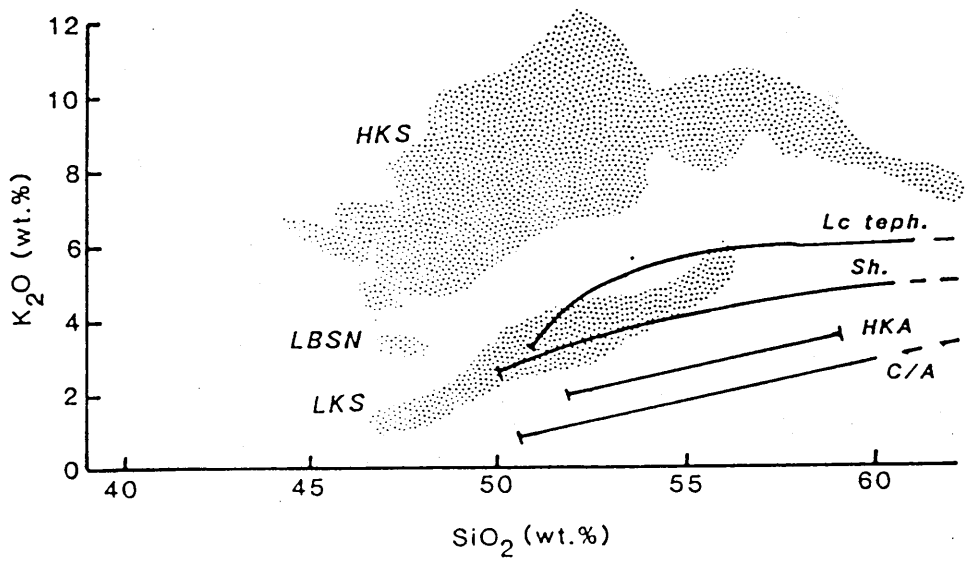

Fig. 5.2 Comparison of Roman province lavas (stippled) with Aeolian Islands lavas series. Abreviations: HKS high potassium series, LKS low potassium series, LBSN leucite basanite series (Rogers *et al.* 1985), Lc teph. leucite tephrite series, Sh. shoshonitic series, HKA high potassium andesites, C/A calc-alkaline series (Barberi *et al.* 1974)

Roccamonfina, (Appleton, 1972) reveal quite distinct fractionation trends. HKS lavas evolve to highly nepheline normative compositions, whilst LKS lavas show trends similar to Aeolian lavas towards quartz normative compositions. In basaltic systems the join olivine-diopside (critical plane of silica undersaturation) is a thermal divide, it was shown in chapter two that this was not so for potassic Aeolian lavas. However, clearly a thermal divide does occur at more nepheline normative compositions. This is likely to be consistent with a thermal divide along the join Mg_2SiO_4-$KAlSi_2O_6$ in the system Mg_2SiO_4-$KAlSiO_4$-SiO_2 (Luth, 1967).

Clearly the presence of this thermal divide is a strong control on the end product of fractional crystallisation. Furthermore it provides a useful discriminant of mildly nepheline normative Aeolian and Roman LKS lavas from the highly undersaturated HKS lavas.

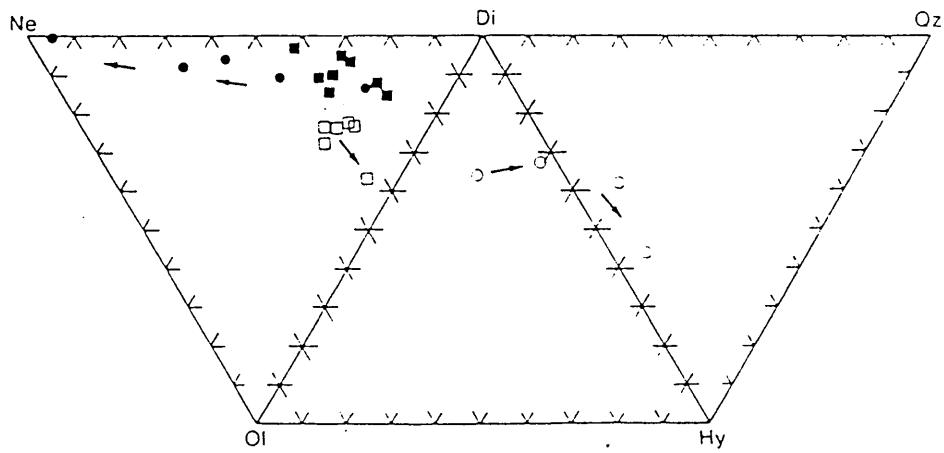

Fig 5.3 Projection from plagioclase of the normative basalt tetrahedron, simplified to include Fe-bearing end members. Filled dots Roccamonfina HKS, filled squares Ernici HKS, open circles Roccamonfina LKS, open squares Ernici LKS. Arrows indicate direction of fractionation (*ie.* decreasing MgO). Data sources: Appleton (1972), Civetta *et al.* (1981).

5.5 Trace Element Variations.

MORB normalised trace element patterns (fig. 5.4) provide a useful comparison between Roman and Aeolian lavas. Both provinces display similar patterns with enrichment of the LILE and negative anomalies for the HFSE. Such patterns are typical of subduction related rocks. This observation strongly suggests a role for subduction processes in the source of the Roman lavas, particularly when compared with the more demonstrably subduction related Aeolian Islands. It should be noted that elevated K_2O content in the Roman province is not associated with relative HFSE enrichment as is the case at Stromboli. Indeed Rogers *et.al.* (1985) have shown that the transition from LKS to HKS in the Roman province is associated with an increase in Th/Ta. Such a variation is entirely consistent with subduction related enrichment and contrasts with the variations observed at Stromboli. Furthermore, Rogers *et al.* (*op. cit.*) have shown that basic Roman lavas have low Ta/Yb which is consistent with subduction related enrichment. Notably the Roman province lavas display a negative Ba anomaly in their trace element patterns. Such a feature is absent in all the Aeolian Islands lavas, and will be discussed below.

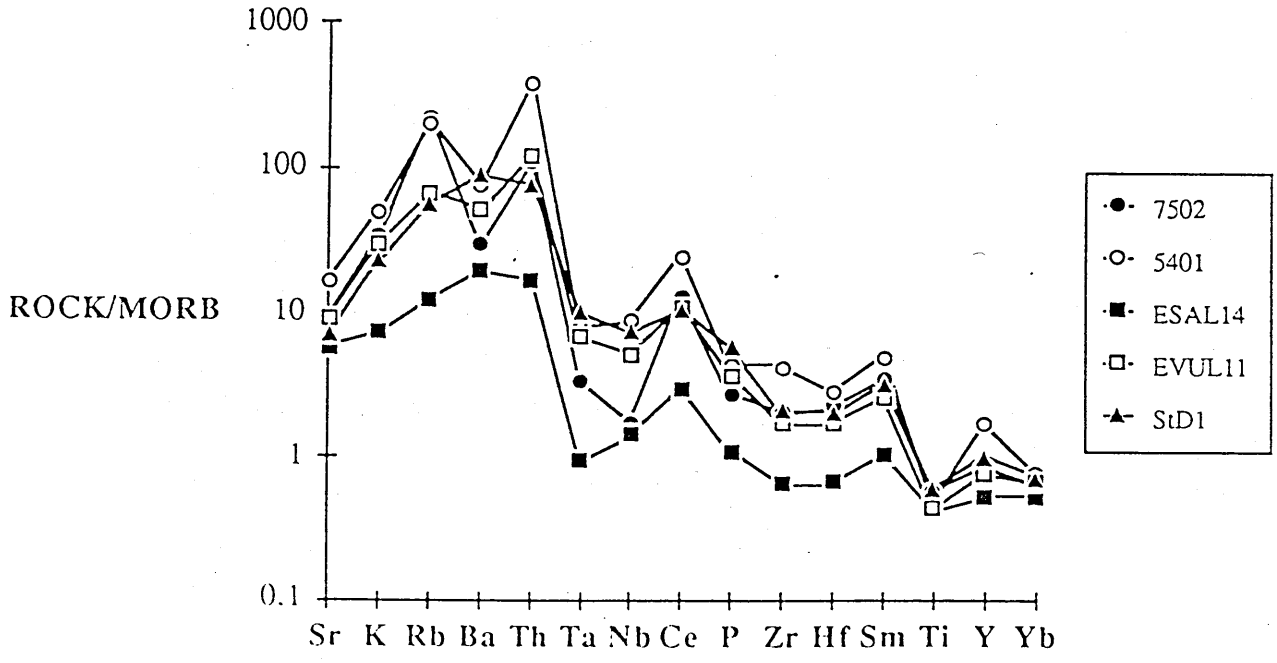

Fig. 5.4 MORB normalised trace element abundance patterns of Roman and Aeolian lavas. 7502 and 5401 are Vulsini HKS lavas (Rogers *et al.*, 1985)

Perhaps the most useful discriminant of the elemental components present in the Aeolian rocks was the diagram of Sr/Nd v. Th/Ta (fig. 5.5). As discussed in the previous chapter, this diagram was used by Rogers *et al.* (*op.cit.*) to show that Roman province lavas may be explained by a two component mixture between a normal subduction component with high Sr/Nd and Th/Ta and a second subduction derived component with relatively low Sr/Nd but extremely high Th/Ta. It was also established that the mantle prior to these subduction related enrichments was of *relatively* depleted E-type MORB composition, the contribution of the original mantle to the eventual mixture was therefore considered negligible.

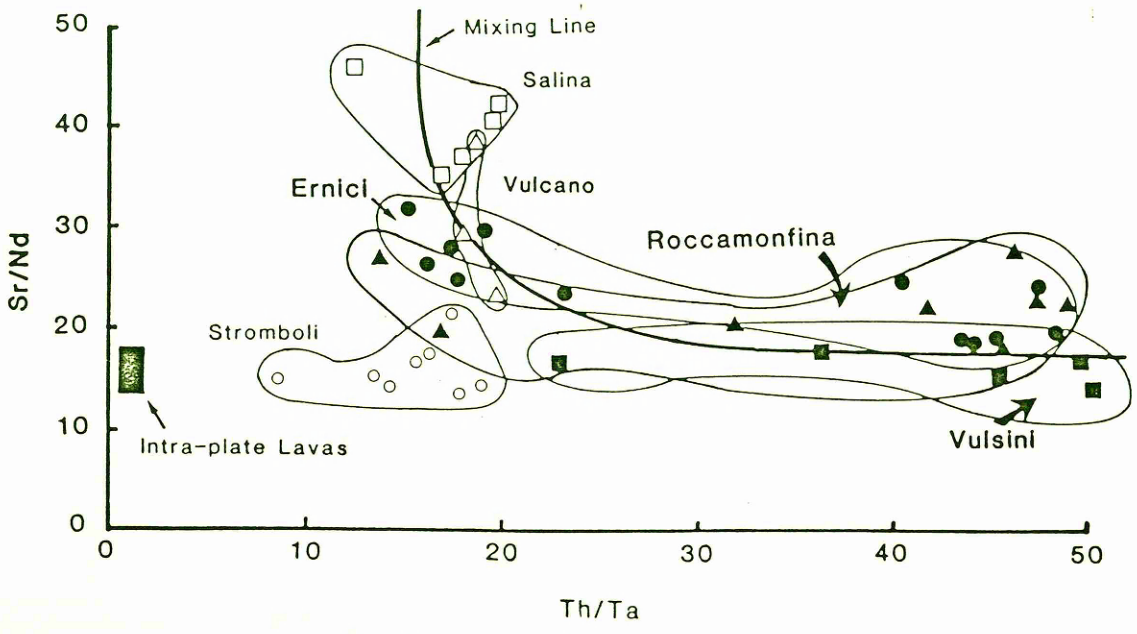

Fig. 5.5 Sr/Nd v. Th/Ta for Aeolian Islands basic lavas (>10% CaO, except Vulcano <52% SiO_2) and Roman province lavas (Rogers *et al.*, 1985, Civetta *et al.*, 1981). Mixing line after Rogers *et al.*, 1985)

Comparison with the previous chapter reveals a number of similarites between the Roman and Aeolian regions. The subduction components of Rogers *et al.* (1985) are similar to those (SCA and SCB) recognised in Aeolian lavas. Accordingly lavas from Salina

and Vulcano are consistent with the Roman province mixing hyperbola. In contrast Stromboli lavas are markedly displaced towards low Th/Ta values, away from the Roman province mixing curve. This displacement is believed to represent the effect of an enriched mantle component, rich in HFSE in the Stromboli lavas. Apparently the original mantle beneath Stromboli was richer in HFSE than the E-type MORB source proposed beneath the Roman province.

Although it has been possible to recognise two subduction related components in the lavas of the Aeolian Islands and the Roman province, it remains unclear to what extent the composition of these components reflects their source or the effects of processes active within that source. The origin of the normal subduction component is highly controversial and will be discussed in the following chapter. The second subduction component (SCB) is also rather enigmatic. Its relatively low Sr/Nd is consistent with a terrigenous sedimentary origin as average upper crust has an estimated Sr/Nd ratio of 13.5 (Weaver & Tarney, 1984). However the highly elevated Th/Ta of this component is not a feature of the continental crust, the average upper crustal Th/Ta being around 7.4[1]. It is notable however that high Th/Ta is a feature common to most subduction related rocks. It is conceivable that the high Th/Ta of this component is a reflection of processes active within the subduction zone which increase Th/Ta, rather than an actual reservoir of very high Th/Ta material.

A significant difference between Roman and Aeolian lavas is found in their Rb/Ba ratios. Roman province lavas have extremely high Rb/Ba in many cases, which contrasts them with Aeolian lavas. Indeed, Hawkesworth *et al.* (1984) have recognised the Roman province as a representative of a relatively rare style of mantle enrichment which produces high Rb/Ba, high Rb/Sr and low Ti/K. This enrichment style is similar to that observed in phlogopite and K-richterite bearing mantle xenoliths. A diagram of Sr/Nd v. Rb/Ba (fig. 5.6) illustates the differences between Aeolian and Roman lavas. This diagram implies that high Rb/Ba is a feature of the low Sr/Nd, high Th/Ta component, the subducted crustal component. Despite the recognition of a similar component at Stromboli, no Rb enrichment relative to Ba is indicated. Striking however is the similarity of this diagram (fig. 5.6) to that of Sr/Nd v. Th/Ta (fig. 5.5). Relatively low Th/Ta at Stromboli was ascribed to the effects of the Ta rich within-plate component. It may be that the lack of elevated Rb/Ba

[1]Assumes Ta normalised to chondrite is equal to Nb normalised to chondrite

in Stromboli lavas is attributable to significant Rb and Ba contribution from a relatively low Rb/Ba within-plate component.

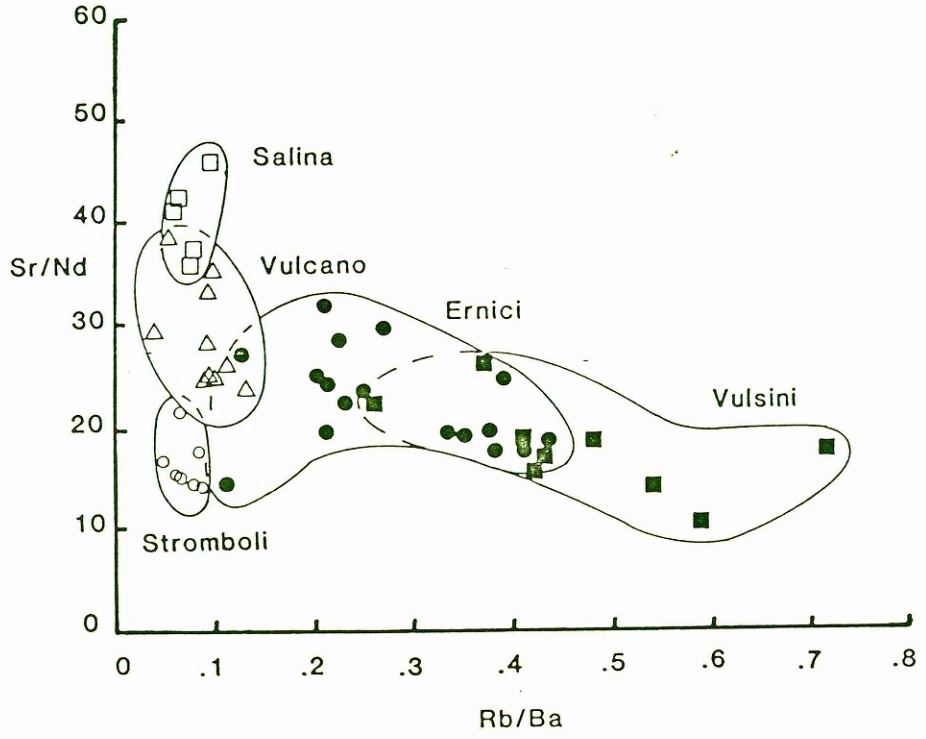

Fig. 5.6 Sr/Nd v. Rb/Ba for Aeolian Islands and Roman province lavas. Data sources Civetta *et al.* (1981), Rogers *et al.* (1985).

5.6 Isotopic Variations.

A large body of isotope data is available on the Roman province lavas. Over the past fifteen years or so much controversy has surrounded the interpretation of these results. Some workers (*eg.* Turi & Taylor,1976) have invoked major crustal contamination as the source of high $^{87}Sr/^{86}Sr$ and $\partial^{18}O$. Others however, have suggested a role for mantle enrichment in the in the generation of enriched isotopic signatures, *e.g.* Hawkesworth & Vollmer, (1979). In recent years a concensus appears to have emerged, which although not rejecting crustal contamination within individual fractionation sequences, does imply that the major isotopic variations result from mantle processes (Rogers *et al.*, 1985. Ferrara *et al.*, 1986). The purpose of this section is to review the most important evidence that

leads to this consensus, and to compare these isotopic variations with those in the Aeolian Islands lavas.

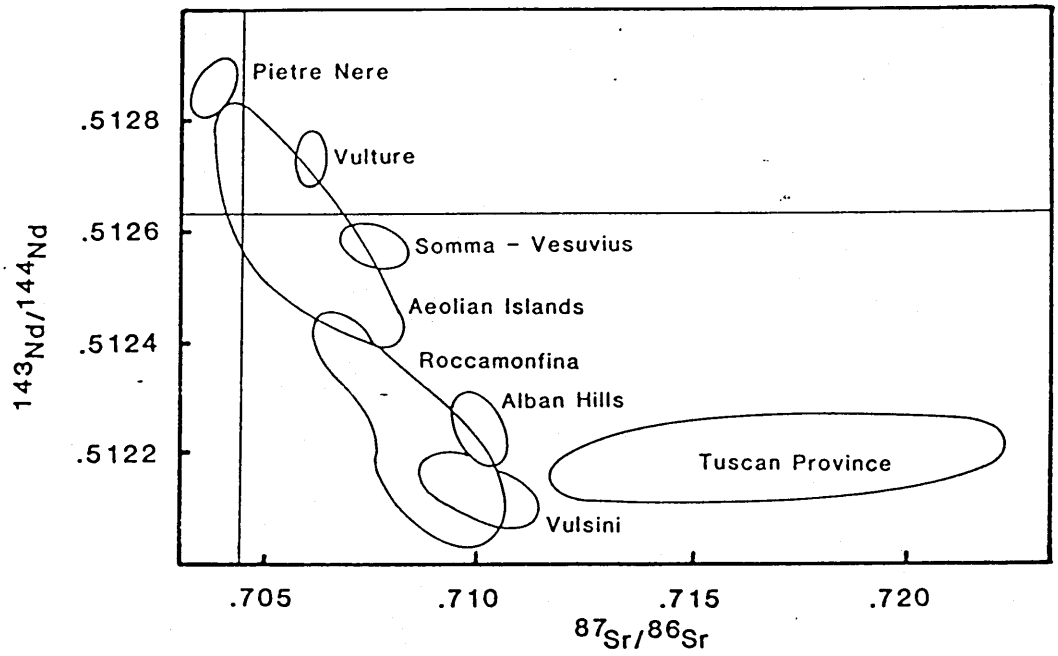

Fig. 5.7 $^{143}Nd/^{144}Nd$ v. $^{87}Sr/^{86}Sr$ for Italian lavas. Data sorces Hawkesworth & Vollmer (1979), Rogers *et al.* (1985).

Sr and Nd isotope ratios from Roman and Tuscan province lavas all show enriched compositions. Indeed the only samples from the Italian mainland with $^{87}Sr/^{86}Sr$ <bulk earth and $^{143}Nd/^{144}Nd$ >bulk earth are those from Pietre Nere, a 56 Ma alkali trachyte centre which is considerably to the east of the Roman province. The apparent coherent variation (fig. 5.7) of the Roman lavas led Vollmer & Hawkesworth (1980) to suggest an origin by mixing between a mantle component similar to Pietre Nere and a crustally derived component similar to the Tuscan province rhyolites. However it was also shown (Hawkesworth & Vollmer, 1979) that crustal contamination of uprising magmas is an unlikely process to produce the observed elemental variations. The main objection to contamination within the crust is the observation that Sr behaves incompatibly throughout the enrichment process, *i.e.* Sr increases as $^{87}Sr/^{86}Sr$ increases (fig. 5.8). As was discussed for Stromboli in chapter four, such a variation rules out bulk assimilation of

Sr-poor crust. Whilst AFC may produce such a variation (if plagioclase doesn't fractionate) there is a play-off between large degrees of fractional crystallisation to generate high Sr content and large amounts of assimilation (of Sr-poor material) to produce elevated $^{87}Sr/^{86}Sr$. As these two have opposite effects on the "effective partition coefficient " of the enrichment process it seems unlikely that both high Sr content and high $^{87}Sr/^{86}Sr$ would be achieved by AFC. It is notable that basic lavas from the Aeolian Islands lie on a similar trend to Roccamonfina and Ernici (fig. 5.8). This may imply only minor isotopic variation associated with within-plate enrichment at Stromboli, as was suggested in chapter four. Also, the Aeolian Islands lavas tend to fill the gap in isotopic composition between the lavas of Pietre Nere and those of the Roman province, perhaps supporting the genetic link between these two provinces suggested by Vollmer & Hawkesworth, (1980).

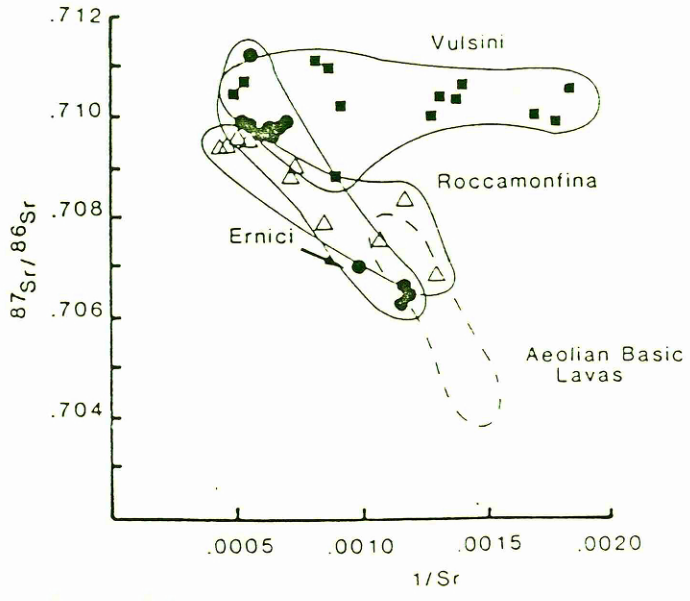

Fig. 5.8 $^{87}Sr/^{86}Sr$ v. $^{1}/_{Sr}$ for Roman province lavas. Data sources: Hawkesworth & Vollmer (1979), Civetta *et al.* (1981), Rogers *et al.* (1985).

Oxygen isotopes have been used extensively to imply a crustal component in the Roman magmas (*eg.* Turi & Taylor,1976, Taylor *et al.*,1979). Roman lavas were shown to have high $\partial^{18}O$, characteristic of crustal involvement. Such an observation does not however imply a mechanism for crustal incorporation. Until recently Sr and O isotope data

on the same samples was not available, so that comparisons between the two isotope systems could not be made with full confidence. Recent data (Ferrara *et al.*,1985, Ferrara *et.al.*, 1986) allow such a comparison to be made.

James (1981) has shown that the higher Sr/O ratio of a primitive magma than that of the solid mantle induces quite different trends for crustal contamination and mantle enrichment on a diagram of $\partial^{18}O$ v. $^{87}Sr/^{86}Sr$ (fig. 5.9). During crustal assimilation the basalt has higher or similar Sr/O to the assimilant (crustal melt) therefore mixing lines are convex upwards (1) or roughly straight. In mantle enrichment the crustally derived component is added to a low Sr/O mantle to produce convex downwards mixing curves. (2) Vulsini and Alban Hills lavas are clearly inconsistent with crustal contamination of a low $^{87}Sr/^{86}Sr$, low $\partial^{18}O$ melt by high $^{87}Sr/^{86}Sr$, high $\partial^{18}O$ crust.

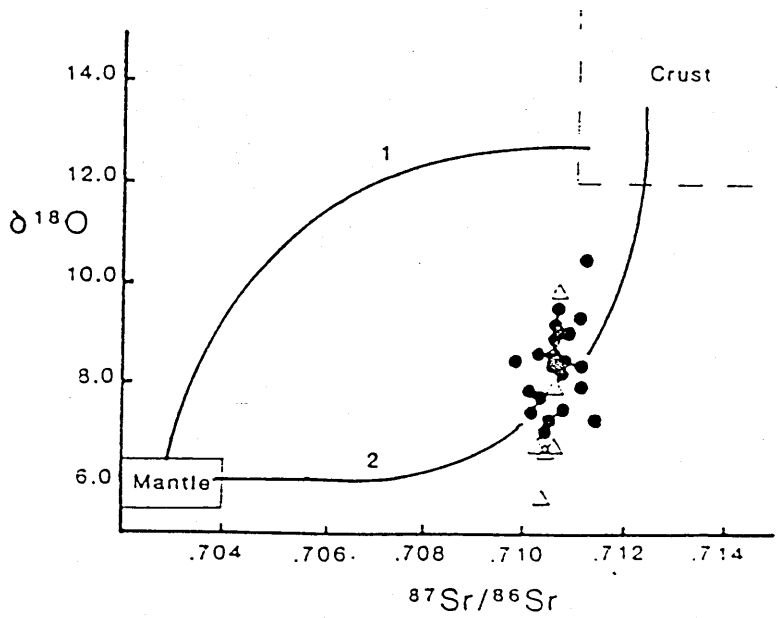

Fig 5.9 $\partial^{18}O$ v. $^{87}Sr/^{86}Sr$ for Roman province lavas showing the effects of intra-crustal contamination and addition of crust to the mantle, after James (1981). Details in the text. Dots are Vulsini (Ferrara *et al.* ,1986), triangles are Alban Hills (Ferrara *et al.* 1985)

The evidence for a crustal component would therefore appear overwhelming, it is also clear that such a component was incorporated in a sub-crustal environment, rather than by crustal assimilation. The recognition of subduction related trace element patterns in the

Roman lavas provides a mechanism for adding crustal material into the mantle.

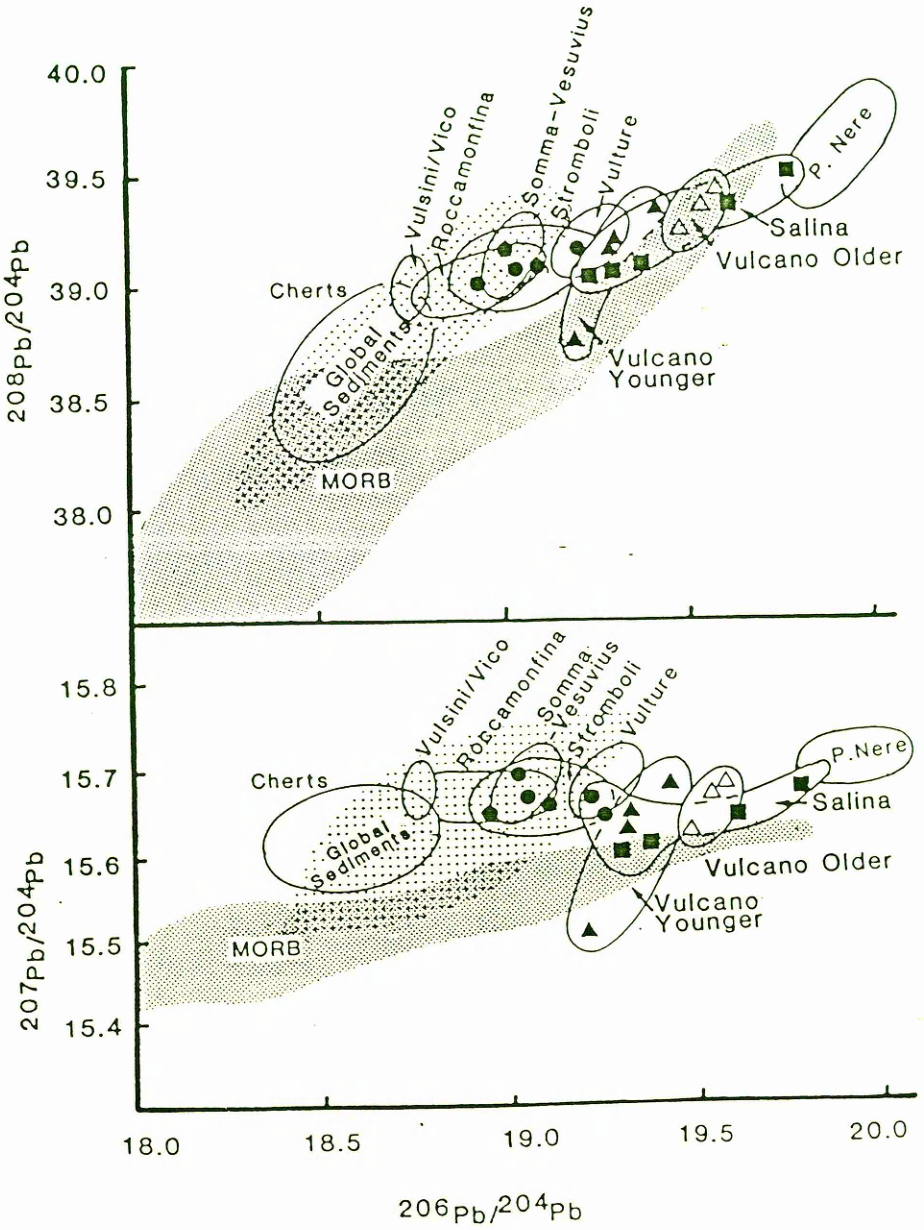

Fig. 5.10 Pb isotope variations of Italian lavas. Data sources: Roman province, Pietre Nere, Vulture, Vollmer (1976), Vollmer & Hawkesworth (1980), MORB, Dupre & Allegre (1980),Sun (1980), Cohen & O'Nions (1982a), Apennine cherts, Barrett (1980), global sediments, White *et al.* (1985).

Pb isotope evidence (fig. 5.10) is consistent with the hypothesis developed above. Roman province and Stromboli lavas have values within the range of global sediments (White *et al.*,1985) and approach the composition of cherts associated with Apennine ophiolites (Barrett, 1980). In contrast Salina and Vulcano lavas which are thought to

contain a much smaller contribution from a subducted crustal component have much more radiogenic $^{208}Pb/^{206}Pb$ and $^{206}Pb/^{204}Pb$ and approach the composition of Pietre Nere, which may perhaps be taken as representative of the mantle beneath Italy prior to recent enrichments. It should be noted that Salina lavas preserve this Pietre Nere-like signature despite having a significant trace element subduction component. It would appear that where sediment is not involved in subduction, little isotopic change is produced. Obviously this observation has important implications regarding the nature of subduction related enrichment which will be discussed further in the following chapter.

The available Roman province data provide an opportunity to test the method developed above (chapter four) for defining the isotopic composition of the subduction zone component. In a diagram of $^{87}Sr/^{86}Sr$ v. Ta/Sr (fig. 5.11), Roman lavas define rather a diffuse trend. All have low Ta/Sr with a range in $^{87}Sr/^{86}Sr$, this is consistent with the hypothesis of Rogers *et al.* (1985) that Roman lavas include two subduction components of differing isotopic composition, but both with low Ta/Sr. A weak trend towards a high $^{87}Sr/^{86}Sr$ intercept for Ernici data agrees with the hypothesis of a very high Th/Ta, high $^{87}Sr/^{86}Sr$ component in these lavas.

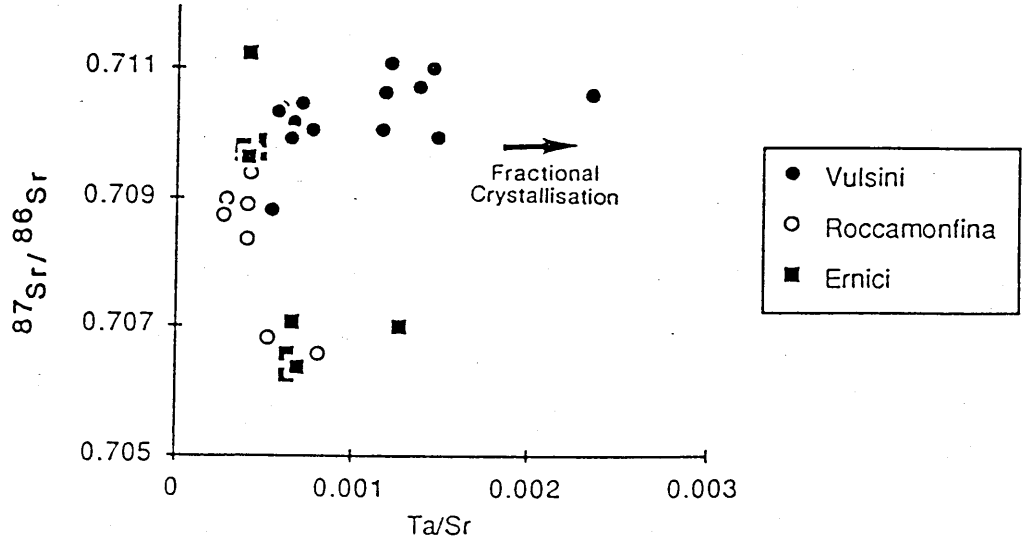

Fig. 5.11 $^{87}Sr/^{86}Sr$ v. Ta/Sr for Roman province lavas. Arrow indicates direction of fractional crystallisation ($Kd_{Sr} > Kd_{Ta}$). Data sources: Rogers *et al.* (1985), Civetta *et al.* (1981)

5.7 Summary.

Whilst the Aeolian and Roman province lavas are petrographically quite distinct and have rather different major element compositions, they can be shown to have strong similarities and relationships in terms of their trace element and isotopic compositions. It would appear that similar components and processes have been involved in both provinces. Furthermore, Aeolian lavas appear to bridge the gap between the Roman province and the alkalic volcanism of Pietre Nere, enforcing a genetic link between the two. However it should be remembered that important differences do exist between the two regions. The dominant subduction component in Salina lavas (SCA) is isotopically depleted ($^{87}Sr/^{86}Sr \approx 0.704$) in contrast to that proposed by Rogers *et al.* (1985) for the Roman province ($^{87}Sr/^{86}Sr \approx 0.7062$). Moreover, a within-plate component is recognised at Stromboli but not required by Roman province lavas. Perhaps the within-plate component is related to the currently active intraplate volcanism of M.Etna on Sicily. The within-plate component is found in lavas which are isotopically enriched, however this is believed to be due to the presence of a second subduction component derived from continental sediments. There is little evidence to suggest that the within-plate component need be isotopically enriched. It seems likely that within-plate enrichment beneath Stromboli is a relatively recent phenomenon which has caused significant trace element variation, but little isotopic enrichment within the pre-subduction mantle. In terms of Sr, Nd and Pb isotopes the mantle wedge prior to subduction may have varied little from the values recorded by Pietre Nere lavas. Furthermore, it appears that only when the trace element subduction component contains a contribution from the sediment component (SCB), is a significant isotopic shift away from the inferred pre-subduction composition of the mantle wedge produced. However this may perhaps be a phenomenon restricted to the Aeolian arc, where the inferred mantle wedge is likely to be different isotopically from that found beneath island arcs in less tectonically complex areas. The following chapter discusses evidence from subduction zone lavas throughout the world in order to compare the Aeolian and Roman lavas with those found in more typical subduction related provinces, to investigate the origin of subduction related enrichment and to study the nature of petrogenetic processes in the subduction zone environment.

CHAPTER SIX

Subduction Related Petrogenesis

6.1 Introduction

Despite a large number of geochemical studies, the origin of subduction related magmatism remains controversial. The unique association of potential source materials at destructive plate margins is widely recognised, but little consensus exists as to the relative contribution of these components. It has become widely accepted that the mantle wedge which forms the hanging wall of the subduction zone is the likely location of magma formation, however there is little agreement as to the nature of the wedge. Despite the important geodynamic implications it remains unclear whether the mantle wedge prior to subduction is similar to the source of mid ocean ridge basalts (MORB) (Perfit *et al.*,1980), the ocean island basalt (OIB) source (Morris & Hart, 1983), or distinct from both these well established global reservoirs. Uncertainty as to the nature of the wedge leads to differing assessments of the role of the subducted oceanic lithosphere in subduction related petrogenesis. This also has important consequences for the chemical differentiation of the earth as it places constraints on the potential of subducted oceanic lithosphere and continental detritus to be carried beyond the region of arc magma formation and perhaps contribute to the OIB source(White & Hofmann, 1982). Furthermore the destructive plate margin is the dominant environment of continental growth, at least at the present day. Radiogenic isotope studies require the continental crust to have undergone enrichment of Rb/Sr and depletion of Sm/Nd relative to the upper mantle. It remains unclear how such marked fractionation of similarly incompatible elements was achieved, and whether it still accompanies modern continental crust formation, or was restricted to an earlier differentiation process.

The following discussion uses trace element and radiogenic isotope data from subduction related provinces throughout the world in order to address the points raised above. Where elemental abundances or ratios are compared with one another or with isotope ratios, only basaltic samples (SiO_2<53%) have been considered in an attempt to minimise the effects of fractional crystallisation. In many provinces this criterion severely depletes the available data set, but it is thought necessary in order to maintain confidence in the interpretation of these data.

The distinctive trace element geochemistry of subduction related basalts is well documented (Hawkesworth *et al.*, 1979a, Saunders *et al.*, 1980), arc lavas are enriched in large ion lithophile elements (LILE) relative to high field strength elements (HFSE) (fig. 6.1). Indeed this characteristic has been exploited as a tectonic discriminant (Pearce, 1983). Subduction zone basalts also have high LILE/LREE (light rare earth element) ratios compared with MORB and OIB lavas (fig. 6.1). The interpretation of this distinctive trace element signature is controversial, however it is clearly not produced by processes controlled by lherzolite mantle - melt partition coefficients, but requires an environment in which the HFSE are relatively compatible compared with the LILE, in contrast to their behaviour in other tectonic environments. Therefore models which aim to explain the characteristic trace element signature must satisfy two criteria; they must provide a source of incompatible elements of appropriate isotopic composition, and invoke a means of producing the required fractionation of LILE from HFSE and LREE. Such models may be discussed in terms of two idealised end members which arise from comparison of the trace element characteristics of subduction related basalts with those of MORB and OIB (fig. 6.1).

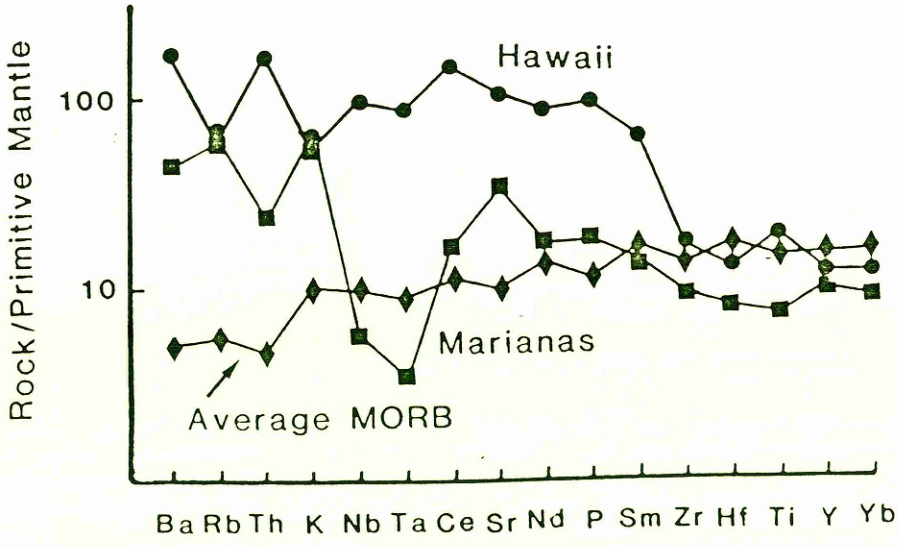

Fig. 6.1 Mantle normalised trace element abundance patterns of average MORB (Pearce *et al.*, 1981), an OIB from Hawaii, (Clague & Frey, 1982) and a subduction related basalt from the Marianas arc. (Hole *et al.*, 1984)

(a) Models which invoke a depleted mantle source similar to that of MORB and hence require enrichment by a subduction component with high LILE/HFSE ratios *e.g.* Ba/Nb, Th/Ta, high LILE/LREE ratios *e.g.* Ba/La, Sr/Nd and low concentrations of HFSE and LREE. This component is generally thought to originate within the subducted oceanic lithosphere. (Hawkesworth *et al.*, 1977)

(b) Alternatively, models may infer a source or process similar to that responsible for incompatible element enrichment in OIB. In this case anomalous LILE enrichment is not required, but depletion of LREE and HFSE is necessary. A minor phase phase rich in HFSE which is residual during melting, may be postulated as the cause of this depletion *e.g.* perovskite (Morris& Hart, 1983), sphene, rutile (Green, 1981)

6.2 LILE Variations: Implications for Magma Genesis

In this section the significance and implications of variations in the abundance of the LILE relative to one another are considered, and the relationship of these variations with more conspicuous elemental and isotopic features are investigated. Diagrams of Rb/Ba and Rb/Sr versus Rb content are useful in this context (figs. 6.2 and 6.3). These show quite striking linear trends for a number of subduction related provinces. Perhaps these may be interpreted in terms of mixing models or as variations due to other petrogenetic processes such as partial melting. The mantle wedge is highly unlikely to contain such high Rb abundances as the 50 ppm or more required in the high Rb end member on these diagrams and therefore the wedge may be equated with the low Rb component if it is to be incorporated into these models, either as an end member during mixing or as the site of LILE fractionation by melting *etc.*, In either case the wedge is not characterised by Rb/Ba and Rb/Sr typical of average MORB (Pearce *et al.*, 1981) or the primitive mantle (Hofmann White, 1983, DePaolo & Wasserburg, 1976). It would appear that the wedge is required to be depleted in Rb relative to the other LILE.

Mixing models are also inhibited by the problem that two component mixing lines on diagrams of X/Y versus X are only linear under very special circumstances (Langmuir *et al.*, 1978). Either the Y (Ba, Sr) composition must be very similar in both end members, or alternatively the two end members must have highly different X (Rb) compositions such that the observed linear trends are merely artefacts of much longer mixing curves. Hence,

addition of a highly LILE rich slab-derived fluid to a Rb depleted wedge may be consistent with the observed trends. Alternatively one may totally reject the mantle wedge as an end member, and postulate another low Rb component. A suitable end member might be pelagic sediment, as this has low Rb/Ba, low Rb/Sr and has a considerably lower Rb content than a proposed slab dehydration product (Hole *et al.*, 1984). However, it is unlikely that a mixture between slab-derived fluid and pelagic sediment could be consistent with Sr isotope data for subduction related basalts. Clearly any mixture is likely to have its Sr isotope composition dominated by the high Sr, high $^{87}Sr/^{86}Sr$ pelagic sediment component, this is inconsistent with the relatively depleted isotopic compositions of arc lavas. Moreover there is little evidence of a strong relationship between $^{87}Sr/^{86}Sr$ and Rb/Sr in subduction related lavas (fig. 6.4), which implies that the observed range in Rb/Sr and Rb/Ba is unlikely to result from mixing of isotopically distinct components. Only in the lavas of Grenada where assimilation of the arc crust has been proposed (Thirlwall & Graham, 1984) do Rb/Sr and $^{87}Sr/^{86}Sr$ show a reasonably strong positive correlation.

Given the apparent inconsistencies between the observed variations and those predicted by mixing models, it is of interest to examine the likely effects of other petrogenetic processes on the LILE. Fractional crystallisation and small degree batch partial melting will be discussed. It is believed that the latter is useful as an approximation to other more complex processes which may have similar effects on the LILE distributions *eg.* zone refining. The observed fractionations of Rb/Ba and Rb/Sr are unlikely to be due to fractional crystallisation, even if Ba is considered to be compatible (fig. 6.2), adequate fractionation of Rb/Ba will only be achieved by large amounts of crystallisation (~90%). If both Ba and Rb are considered to be incompatible albeit with different bulk partition coefficients then fractionation will only be significant during the very final stages of solidification ($F<0.01$). Such high degrees of crystallisation are inappropriate to basaltic systems. However it should be noted that Rb and Ba contents are undoubtably increased by fractional crystallisation, and as such the trends in figures 6.2 and 6.3 represent minimum gradients, the trends induced by the original process having been flattened by fractional crystallisation.

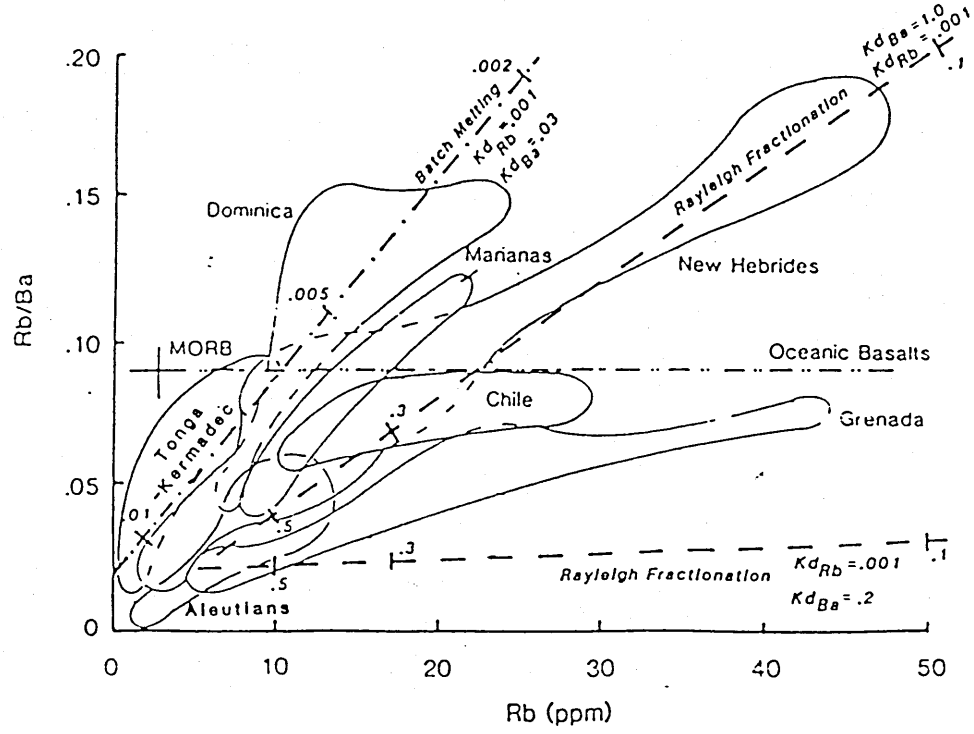

Fig. 6.2 Rb/Ba v. Rb for subduction related basalts. MORB values is from Pearce *et al.* (1981), oceanic basalt trend from Hofmann & White (1983). Partition coefficients in melting model refer to residual assemblage. Data sources: Ewart *et al.* (1977), Thirlwall & Graham (1984), Dupuy *et al.* (1982), Hole *et al.* (1984), Hickey *et al.* (1986), Hawkesworth & Powell (1980), McCulloch & Perfit (1981), Nye & Reid (1986). Marianas data include samples with SiO_2 <55%

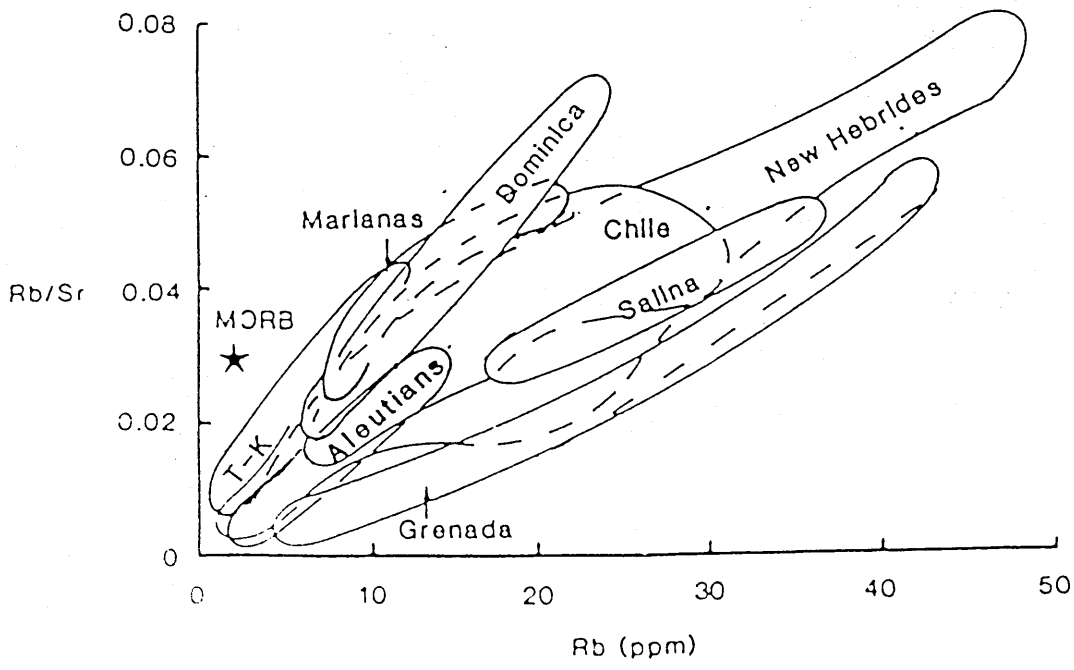

Fig. 6.3 Rb/Sr v. Rb MORB value is from Pearce *et al.* (1981), T-K is Tonga-Kermadec. Data sources as in fig. 6.2.

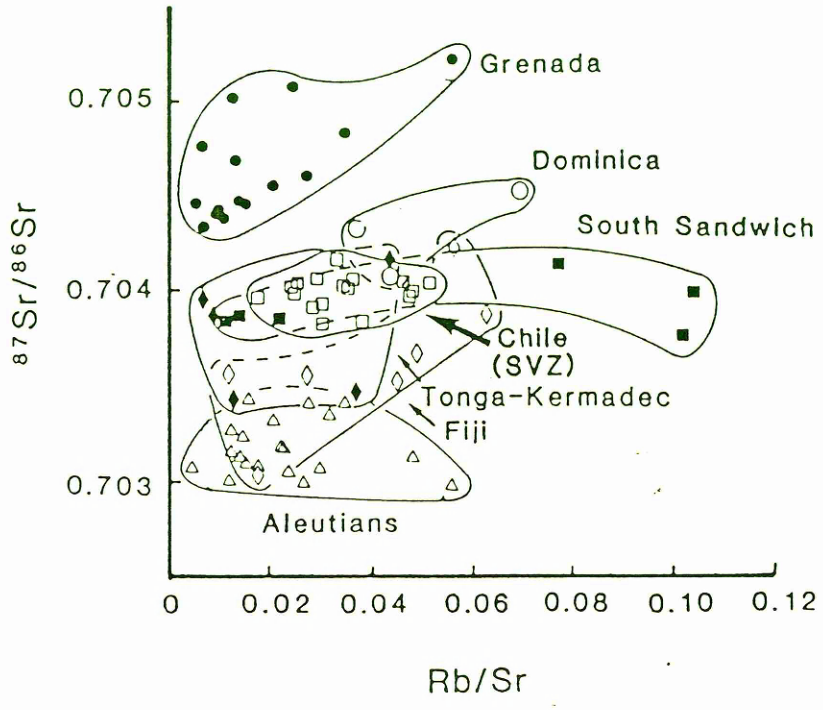

Fig. 6.4 $^{87}Sr/^{86}Sr$ v. Rb/Sr showing a lack of correlation. Data sources as in fig. 6.2 plus Gill (1984), Hawkesworth *et al.* (1977), Ewart & Hawkesworth (in press)

Open system fractional crystallisation (O'Hara & Mathews, 1981) may also be invoked as a mechanism to fractionate LILE ratios. However modelling reveals that very extreme conditions must be postulated to produce Rb/Ba fractionations of the magnitude required. If the same bulk distribution coefficients are used as in the partial melting modelling (fig. 6.2) then an extremely high ratio of crystallisation of cumulates to eruption of lava is necessary to generate the required fractionation even at steady state. O'Hara and Mathews (*op. cit.*) demonstrate that subject to a number of simplifications, open system fractional crystallisation may be related to equilibrium partial melting by the equation:

$$f=y/x+y$$

where f is the degree of partial melting, x is the mass fraction of cumulate crystallised in any cycle of replenishment, fractionation and tapping, and y is the mass fraction of lava erupted during each cycle. Hence in order to produce an effect similar to that of the 0.2% partial melting inferred for the observed Rb/Ba fractionation (fig. 6.2) requires that $y/x+y = 0.002$. Therefore if between 1 and 100% of the magma chamber is crystallised during each cycle,

the erupted flows would represent between 0.2 and 0.002% of the magma chamber, values which do not seem unlikely.

This model may be investigated further by fixing the mass fraction of cumulate in each cycle at 10% (x = 0.1) which implies for the required fractionation of Rb/Ba that the mass fraction of erupted lava is 0.02% (y =0.0002). The number of cycles required for Rb (the most incompatible of the two elements) to closely approach its steady state concentration may then be calculated from the equation:

$$n = \log \{ \delta C / (1 - x - y).(1 - x)^{D-1} \} \Big/ \log (1 - x - y).(1 - x)^{D-1}$$

where n is the number of cycles and δC the fractional departure from the steady state composition. For δC of 1% the nominal steady state is attained after 14,679 cycles, and for a 10% departure from steady state 7,005 cycles are required. Hence even to approach within 10% of steady state Rb/Ba requires around 700 times the volume of the magma chamber to be deposited as cumulates. Even for fairly small magma chambers there will be a considerable space problem in accommodating such a large cumulate pile, and for volcanoes which erupt very large lava flows or ignimbrite sheets, which in the Andes may reach volumes in excess of 100 Km^3 (Francis *et al.* 1978), the problem is immense and open system fractional crystallisation is unlikely to achieve the required LILE fractionations. Attainment of the required fractionation prior to steady state being closely approached would imply even more extreme conditions. It should also be noted that highly compatible elements are likely to reach steady state conditions very rapidly, this is clearly in contrast with the wide range of Cr and Ni observed in subduction related basalts.

At very low degrees of partial melting (as at high degrees of fractional crystallisation) it is possible to fractionate incompatible element ratios. In the illustrated model (fig. 6.2) the partition coefficient of Rb (in the residuum) is lower than that of Ba by an order of magnitude, but both lie within the range recorded in basaltic systems (Henderson, 1982). The observed fractionation requires very low degrees of partial melting, but as this is model dependant its significance is limited. More complex models may achieve similar

fractionation under less stringent physical conditions, *e.g.* zone refining could produce the required fractionation after less than 500 zone lengths had been processed. Alternatively presence of a phase with highly different partition coefficients for Rb and Ba may facilitate fractionation of Rb/Ba and Rb/Sr either by contributing to the melt, or by remaining in the residuum during melting. However it is clear that the ability of a phase to remain residual or its significance in the melting assemblage both diminish with increasing degree of melting. Furthermore the nature of a potential mineral phase remains speculative, as even when phases are observed to be associated with high Rb/Ba *e.g.* K-richterite it is not clear whether this reflects differences in the partition coefficients of Rb and Ba or is a feature inherited from the fluid from which they precipitated (Hawkesworth *et al.*, 1984). Therefore the small degree melting hypothesis is preferred and is supported by modelling of melt extraction (McKenzie, 1985) and complex regimes of melting, which suggests that small degree melts may dominate the trace element composition of basic lavas (O'Hara, 1985).

Diagrams of Rb/Nb and Rb/Zr against Rb (fig. 6.5) also show quite coherent linear variations for the available data, these appear to intersect predicted primitive mantle values and imply that the wedge was not depleted in Rb relative to the HFSE. However there is no strong relationship between Rb/Ba and HFSE/LILE ratios *e.g.* Nb/Ba (fig. 6.6) nor does Rb/Ba appear to be strongly associated with LILE/LREE fractionation *e.g.* Sr/Nd (fig. 6.7). Hence whilst it is likely that the process responsible for Rb/Ba variations may well cause fractionation of other incompatible element ratios, it is clear that this is not the dominant process responsible for LILE enrichment relative to the LREE and HFSE. This would appear to rule out the stabilisation of a Ti-rich minor phase in the mantle during melting as the cause of HFSE depletion and agrees with the conclusions of other studies which have rejected the wedge as the site of a residual HFSE- rich phase (Arculus & Powell, 1986, Norry & Saunders, in press).

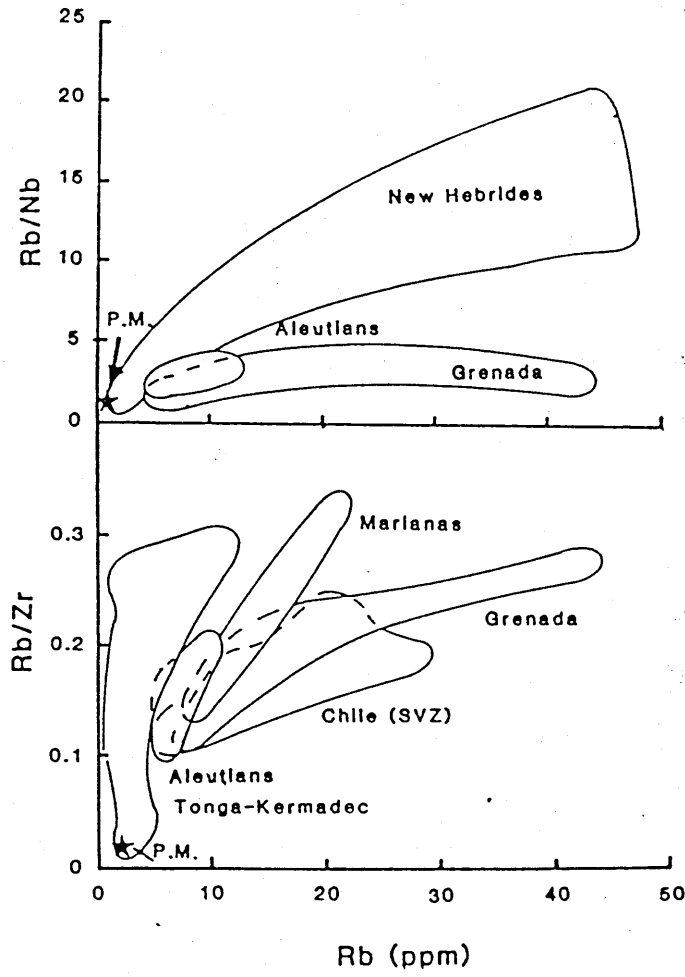

Fig. 6.5 Rb/Nb and Rb/Zr v. Rb. Note that trends intersect primitive mantle (P.M.) values.

Data sources as in fig. 6.2.

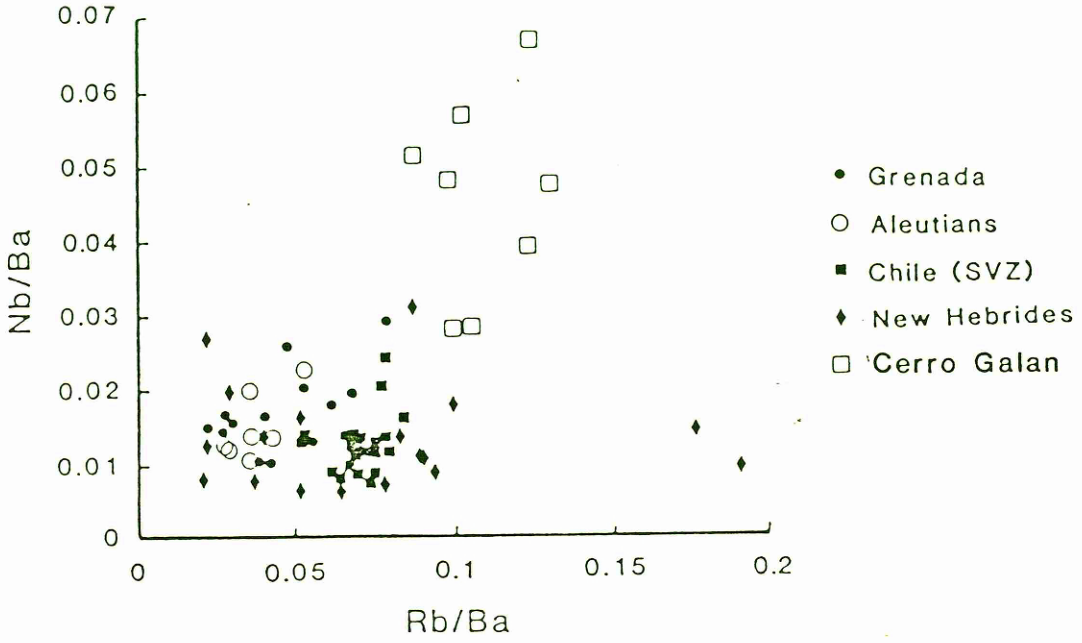

Fig. 6.6 Nb/Ba v. Rb/Ba showing lack of strong relationship. Note that high Rb/Ba is associated with both high and low Nb/Ba. Data sources as in fig. 6.2 plus Thorpe *et al.* (1984), R.S. Thorpe (pers. comm.)

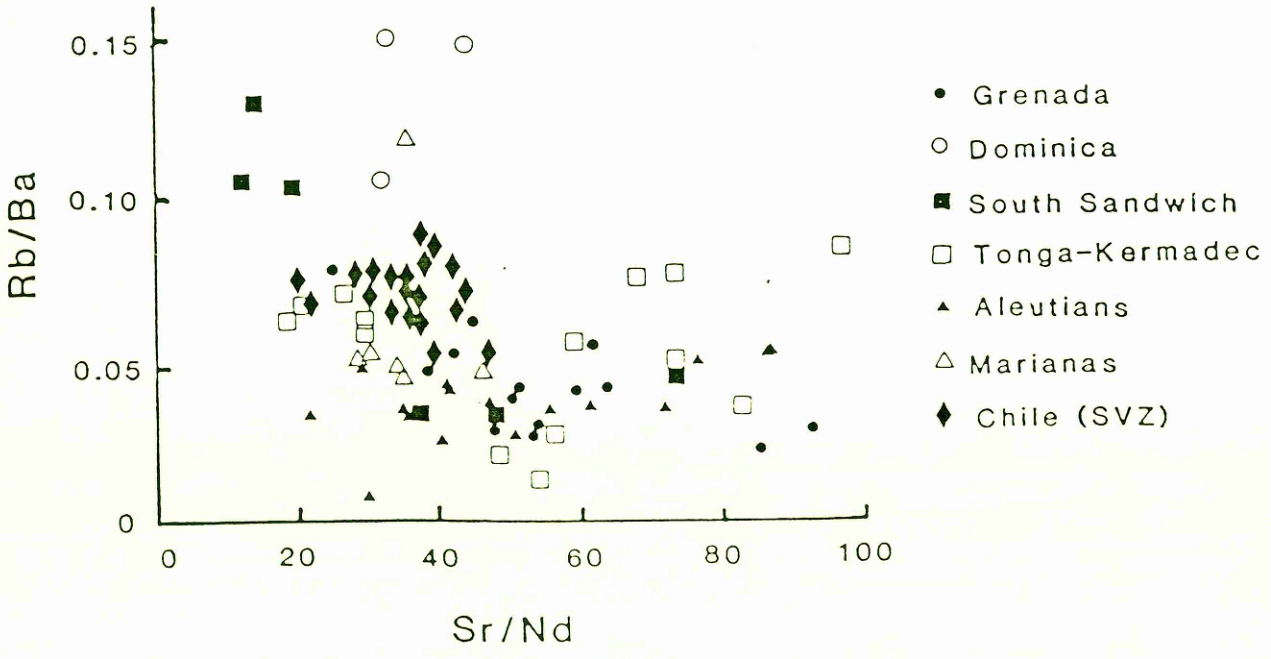

Fig. 6.7 Rb/Ba v Sr/Nd showing lack of any strong relationship. Data sources as in fig. 6.2

6.3 Origin of LILE Enrichment and Isotopic Variation

Having demonstrated significant fractionation between Rb and other LILE in arc basalts, and having established that this is apparently unrelated to LILE enrichment relative to HFSE and LREE and isotopic variability, it is appropriate to investigate the origin of these more conspicuous elemental and isotopic features. Subduction related lavas show a wide range of $^{87}Sr/^{86}Sr$ and $^{143}Nd/^{144}Nd$, however this range is only occasionally outside that recorded by OIB which is represented by the "mantle fan" (fig. 6.8a,b). Indeed the similarity between subduction related lavas and OIB has been interpreted in terms of a common source (Morris & Hart, 1983). Whilst such a conclusion may be overstating the relationship between these two groups of lavas, there is a notable lack of island arc lavas with isotopic characteristics similar to the most depleted MORB. Clearly if a MORB-like mantle wedge is preferred, then an additional component with low $^{143}Nd/^{144}Nd$ and high $^{87}Sr/^{86}Sr$ is required to cause a shift away from the MORB field. Moreover this component is either present in all subduction zone lavas, or alternatively is only absent in lavas derived from slightly enriched E-type MORB wedges (Morris & Hart *op. cit.*). Although the latter possibility may reflect unknown geodynamic controls, it does appear to require an unrealistic degree of special pleading.

Two dominant vectors of Sr-Nd isotopic shift away from the MORB field may be recognised. Lavas from some Atlantic arcs *e.g.* St. Kitts (Hawkesworth & Powell, 1980), South Sandwich (Hawkesworth *et al.*, 1977), Grenada (Hawkesworth *et al.*, 1979b, Thirlwall & Graham, 1984), and a single dacite from the Marianas (DePaolo & Wasserburg, 1977) show displacement towards high $^{87}Sr/^{86}Sr$ at a given $^{143}Nd/^{144}Nd$ (fig. 6.8a). Such a trend is consistent with addition of a high Sr/Nd component with higher $^{87}Sr/^{86}Sr$ than MORB and this is thought to originate from dehydration of the subducting plate. The observation that back-arc lavas from the Scotia Sea have lower $^{87}Sr/^{86}Sr$ than the South Sandwich arc tholeiites with which they are associated, supports this hypothesis (Hawkesworth *et al.*, 1977, Cohen & O'Nions, 1982b). Other arcs, particularly in the Pacific show a dominant displacement along the mantle array towards high $^{87}Sr/^{86}Sr$ and low $^{143}Nd/^{144}Nd$ (fig. 6.8b). Such a trend is difficult to reconcile with addition of a high Sr/Nd component. However in common with other arc lavas (DePaolo & Johnson, 1979) these do show high Sr/Nd. This apparent dilemma is of great interest and makes the variation in

$^{143}Nd/^{144}Nd$ particularly important. This is further emphasised when the likely source of low $^{143}Nd/^{144}Nd$ material is considered. Clearly fresh MORB within the subducted oceanic lithosphere is unsuitable to produce trends away from the MORB field. Altered MORB does not show low $^{143}Nd/^{144}Nd$ (DePaolo & Wasserburg, 1977) as seawater is very poor in Nd. Hence the only likely sources of low $^{143}Nd/^{144}Nd$ material are subducted sediment or inherent heterogeneity within the mantle wedge.

Another feature of particular interest is the relationship between $^{143}Nd/^{144}Nd$ and Zr/Y (fig. 6.9). Although combined Zr, Y and Nd isotope data on subduction related lavas are rare, for those provinces where appropriate data are available a negative relationship exists between $^{143}Nd/^{144}Nd$ and Zr/Y. Furthermore lavas from the Aleutians,the Tonga-Kermadec arc and Dominica which show only minor variation in $^{143}Nd/^{144}Nd$ also have quite restricted Zr/Y. In the Chile and Grenada provinces, crustal contamination may be proposed as the cause of low $^{143}Nd/^{144}Nd$ (Hickey *et al.*, 1986, Thirlwall & Graham, 1984). This may perhaps also increase Zr/Y, but in the basic Chilean southern volcanic zone lavas the reduction in $^{143}Nd/^{144}Nd$ is accompanied by increasing Sr content, and similar variations in Cerro Galan basalts have been attributed to the uppermost mantle rather than to high level crustal contamination (Leeman & Hawkesworth, 1986). Complete evaluation must await more complete data sets, but if this relationship is upheld it would have important implications. As Zr and Y are not highly enriched relative to MORB in arc basalts it is inferred that they have only very minor abundance in the subduction zone component responsible for relative LILE enrichment (Pearce, 1983). A relationship between Zr/Y and $^{143}Nd/^{144}Nd$ tentatively suggests that LILE enrichment and isotopic variation are not simply related. However it is likely that both subducted sediment and enriched mantle have high Zr/Y relative to MORB and further investigation is required to distinguish between the likely effects of these two possible sources.

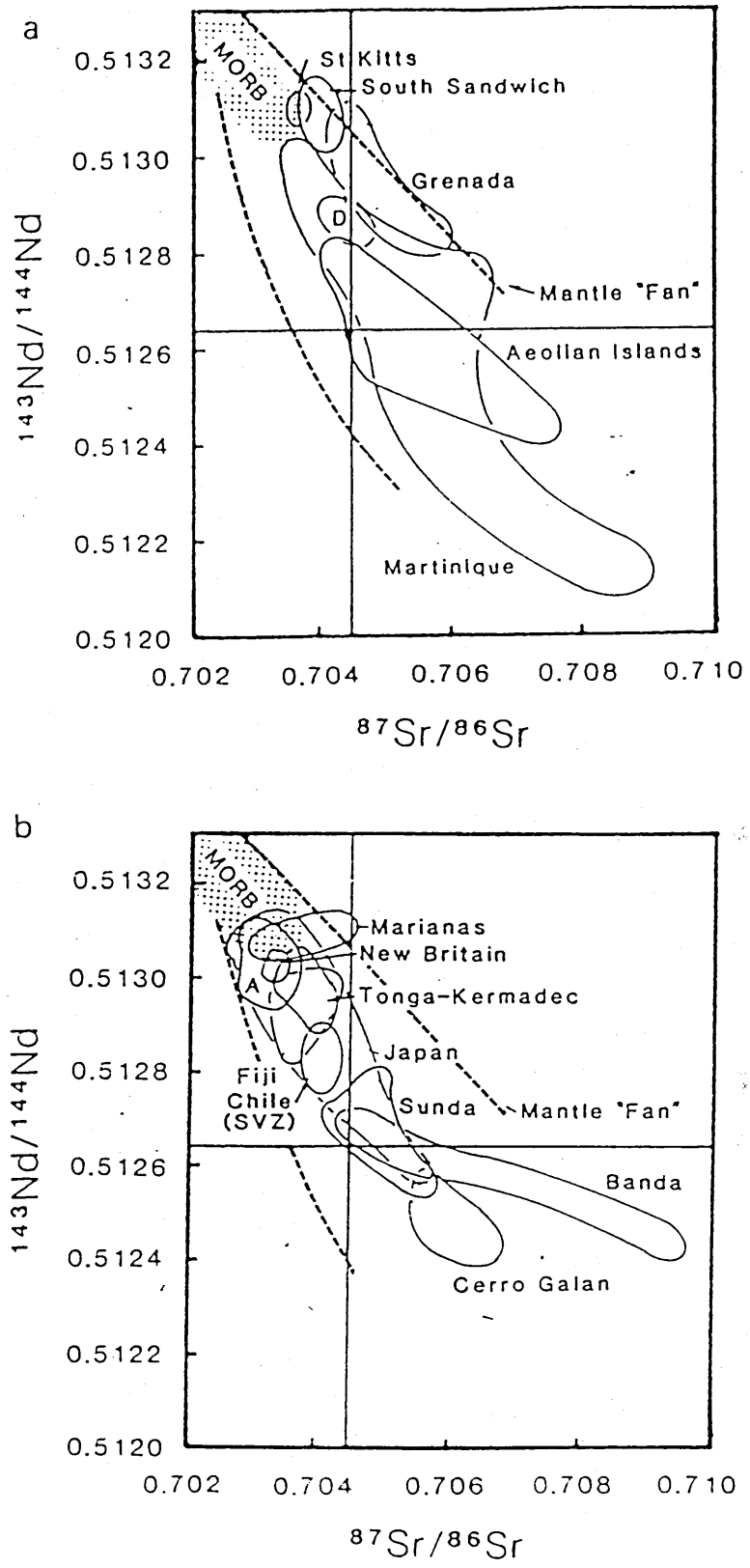

Fig. 6.8 $^{143}Nd/^{144}Nd$ v. $^{87}Sr/^{86}Sr$ of Atlantic and Mediterranean (a) and Pacific (b) arc lavas. D is Dominica, A is Aleutians. Mantle fan represents the range of OIB and is constrained at its upper boundary by MORB and Samoa, and at its lower boundary by St. Helena and Walvis Ridge. Data sources as in fig. 6.2 plus this study, Davidson (1986), De Paolo & Wasserburg (1977), Nohda & Wasserburg (1986), Whitford & Jezek (1979), Whitford *et al.* (1979), Whitford *et al.* (1981), Hawkesworth *et al.* (1979b).

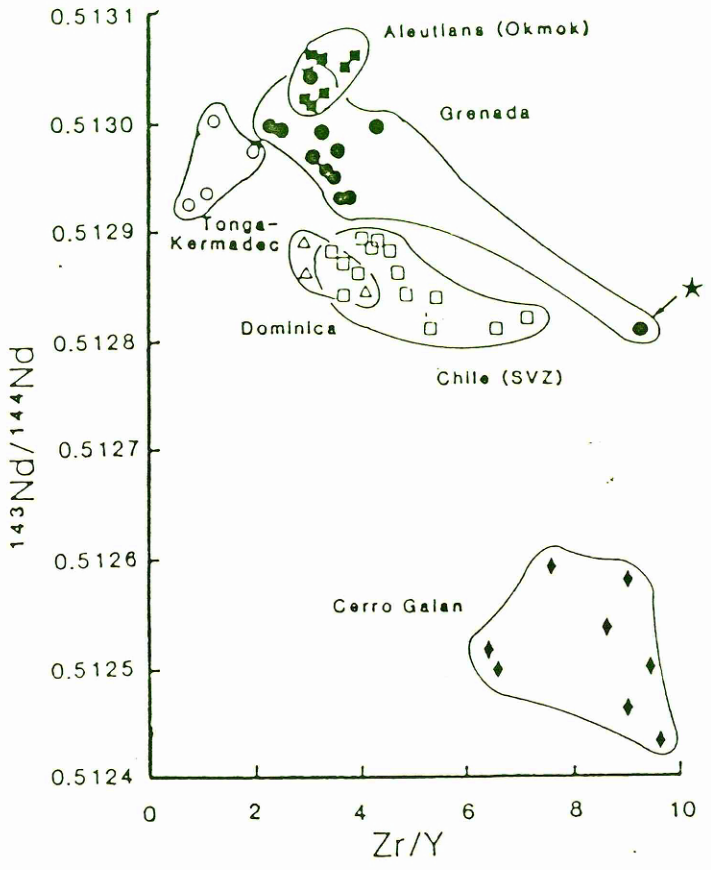

Fig. 6.9 $^{143}Nd/^{144}Nd$ v. Zr/Y showing negative correlation. Dominica samples and Grenada lava marked with a star are calculated from Yb content assuming chondrite normalised Y is equal to normalised Yb.

Evidence for the involvement of sediment in subduction related petrogenesis is strong. The discovery of ^{10}Be in some subduction zone basalts (Tera *et al.*, 1986) appears to support a role for sediment. ^{10}Be is a short-lived (half life = 1.5×10^6 years) natural radioactive isotope. It is produced by cosmic ray irrradiation in the upper atmosphere, and as such only achieves significant concentration in soils and sediments. The presence of ^{10}Be in some subduction related lavas and its apparent absence in intraplate continental basalts, implies a role for subducted sediment in magma genesis. However lack of ^{10}Be in some subduction related lavas does not preclude a role for sediment, because subduction may have taken place slowly enough to allow decay of the isotope below detectable levels prior to introduction of the sediment component into the mantle wedge.

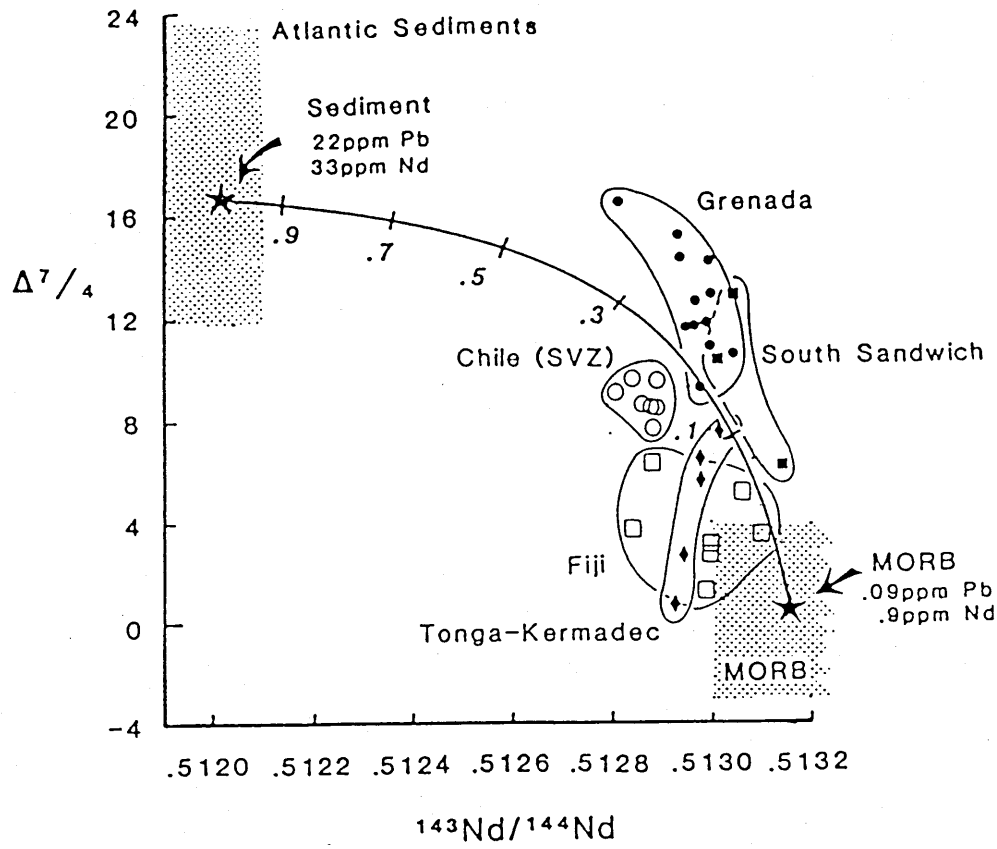

Fig. 6.10 Δ7/4 v. $^{143}Nd/^{144}Nd$ showing mixing model between MORB source mantle wedge and average Atlantic sediment (White *et al.* 1985)

Pb isotope data have also been used to suggest the presence of a sediment component in many subduction related provinces (Hickey *et al.*, 1986). This component has been recognised by steep trends on diagrams of $^{207}Pb/^{204}Pb$ v. $^{206}Pb/^{204}Pb$ (Kay, 1977) hence if a sediment component were responsible for the $^{143}Nd/^{144}Nd$ variation then one would expect to see a relationship between the vertical displacement *ie.* Δ7/4 (Hart, 1984) and Nd isotopic composition (fig. 6.10) Whilst trends for individual provinces are relatively weak, it is striking that arc lavas lie close to a two component mixing curve between mantle and sediment. However sediment is not a unique source of high Δ7/4. Some OIBs show high Δ7/4 and therefore similar Pb isotope compositions in arc lavas may perhaps be derived from an OIB source mantle wedge. However simply tapping an OIB-like wedge will not induce steep trends on $^{207}Pb/^{204}Pb$ v. $^{206}Pb/^{204}Pb$ diagrams, as high Δ7/4 in OIB reflects an ancient process and is associated with relatively flat lying vectors in $^{207}Pb/^{204}Pb$ v. $^{206}Pb/^{204}Pb$ space. In contrast steep trends reflect recent addition of high $^{207}Pb/^{204}Pb$ material, this does not preclude recent mixing between

MORB and high Δ7/4 OIB. However if OIB mantle were responsible for ^{207}Pb enrichment in subduction related lavas, one might expect this signature to appear only in arcs which are found in the area centred on latitude 30°S in which high Δ7/4 OIBs have been recognised, *ie.* the Dupal anomaly (Hart, 1984). In actual fact high Δ7/4 and steep trends on the $^{207}Pb/^{204}Pb$ v. $^{206}Pb/^{204}Pb$ diagram are found outside the Dupal area, as far away as the Aleutians arc (Kay, 1977). It is also notable that some of the lower Δ7/4 values recorded in arc basalts are from arcs inside the area of the Dupal anomaly *e.g.* Fiji, Tonga-Kermadec. Hence it seems more likely that the high Δ7/4 component in subduction related lavas is derived from subducted sediment rather than from a mantle source similar to that of anomalous Dupal OIB.

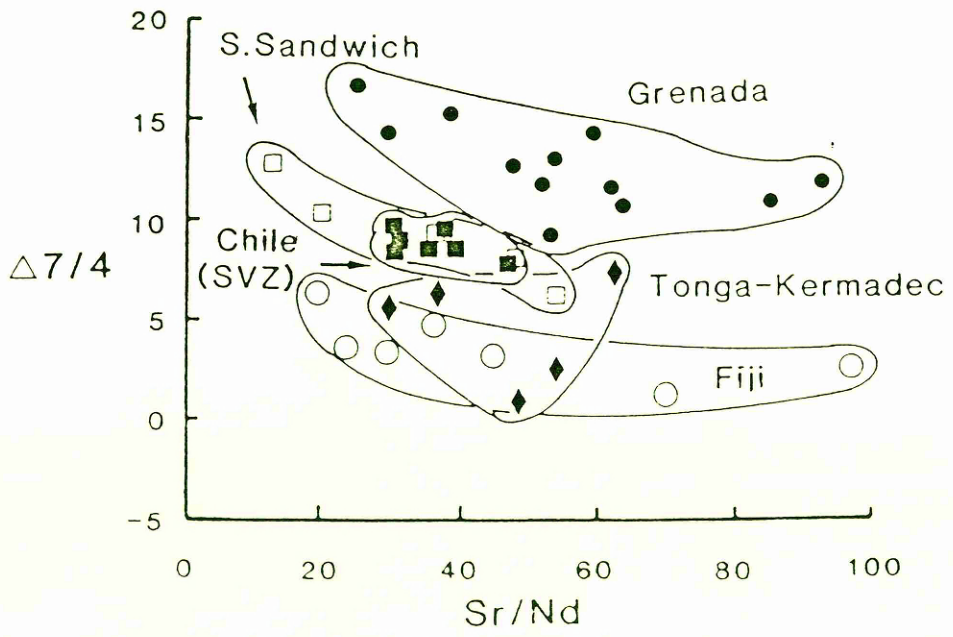

Fig. 6.11 Δ7/4 v. Sr/Nd showing negative correlations for various island arcs. South Sandwich Pb isotope data from Cohen & O'Nions (1982b), other data as in previous figures.

Comparison of Δ7/4 and Sr/Nd (fig. 6.11) reveals how the sediment component is related to the high Sr/Nd trace element subduction component. Clearly high Sr/Nd and high Δ7/4 are not associated. This implies that the sediment component is distinct from the source of high Sr/Nd. As the latter is thought to be derived from dehydration of the subducted oceanic lithosphere (Hawkesworth *et al.*,1977), this implies that there are two geochemically distinguishable components derived from the subducted oceanic slab. This observation is consistent with the Sr-Nd isotope dilemma mentioned above, in which it was considered unlikely that binary mixtures of mantle and sediment could be responsible for the high Sr/Nd observed in arc basalts.

Clearly more complex models are required, the recognition of two slab-derived components implies that a three component mixing model is required. Such a mixture has been modelled (fig. 6.12) and is shown to be in good agreement with basalts from a number of island arcs. Notably Grenada lavas appear to be inconsistent with the model having higher Δ7/4 for a given Sr/Nd than predicted, however this may be due to high level assimilation of arc crust (Thirlwall & Graham, 1984). The three component model may also be applied to Sr and Nd isotopic variations (fig. 6.13). It is apparent that the model can explain the two vectors of isotopic shift recognised above by reference to the same three components. Trends along the mantle array are found in arcs which contain a significant (>10%) contribution from the sediment component. In this case the third component with high Sr/Nd causes mixing away from the sediment component onto the mantle array towards its own isotopic composition which is likely to have $^{143}Nd/^{144}Nd$ similar to MORB but slightly elevated $^{87}Sr/^{86}Sr$, representing a mixture between fresh and altered oceanic crust. The strong concavity of mixing curves associated with this third component allows generation of high Sr/Nd with little change in $^{143}Nd/^{144}Nd$. Trends towards high $^{87}Sr/^{86}Sr$ at relatively constant $^{143}Nd/^{144}Nd$ reflect a very minor role for sediment (<~5%), and the consequent dominance of the high Sr/Nd component. On a global scale this component may well be somewhat heterogeneous. In some arcs *e.g.* South Sandwich, Marianas, a high Sr/Nd component with $^{87}Sr/^{86}Sr$ in excess of 0.704 is required, whilst in others *e.g.* Aleutians it is most likely MORB-like in its isotopic composition. This is easily reconcilable with a component derived from the dehydration of subducted oceanic crust, its Sr isotope composition being a function of the degree of alteration of the subducted material.

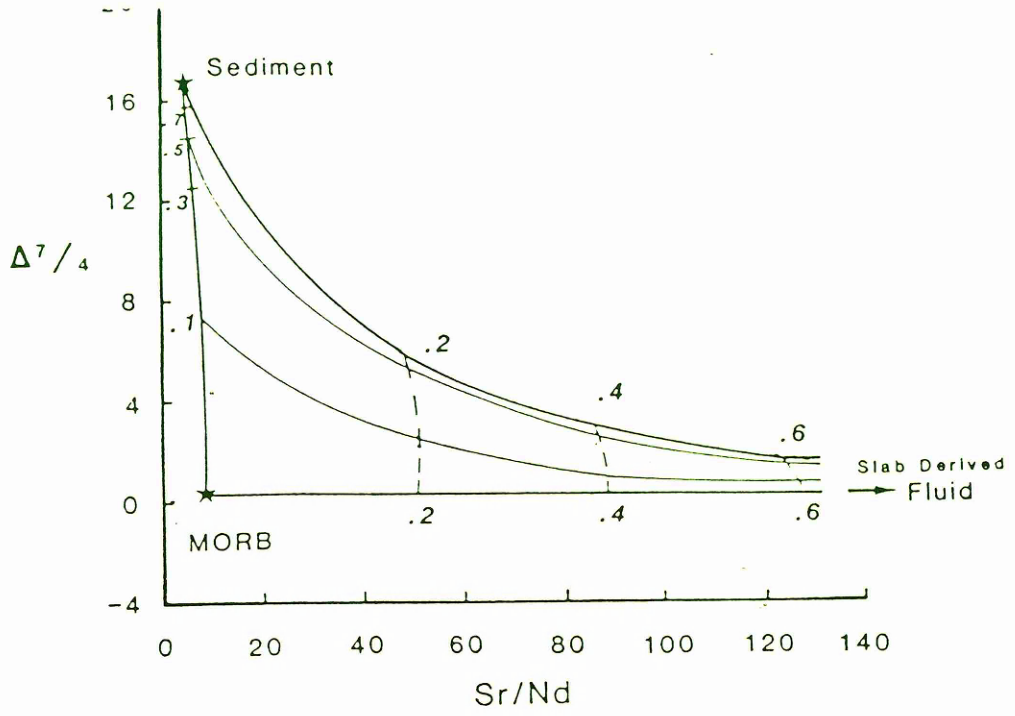

Fig. 6.12 Three component mixing model between MORB source mantle wedge (Pb=0.09ppm, Sr=12ppm, Nd=0.9ppm, $^{207}Pb/^{204}Pb$=15.5, $^{206}Pb/^{204}Pb$=18.5), Atlantic average sediment (White *et al.*, 1985) (Pb=22ppm, Nd=33ppm, Sr=298ppm, $^{207}Pb/^{204}Pb$=19.21, $^{206}Pb/^{204}Pb$=15.74) and slab derived fluid (Pb=0.5ppm, Nd=0.1ppm, Sr=20ppm, $^{207}Pb/^{204}Pb$=15.5, $^{206}Pb/^{204}Pb$=18.5). Figures in italics are mixing proportions.

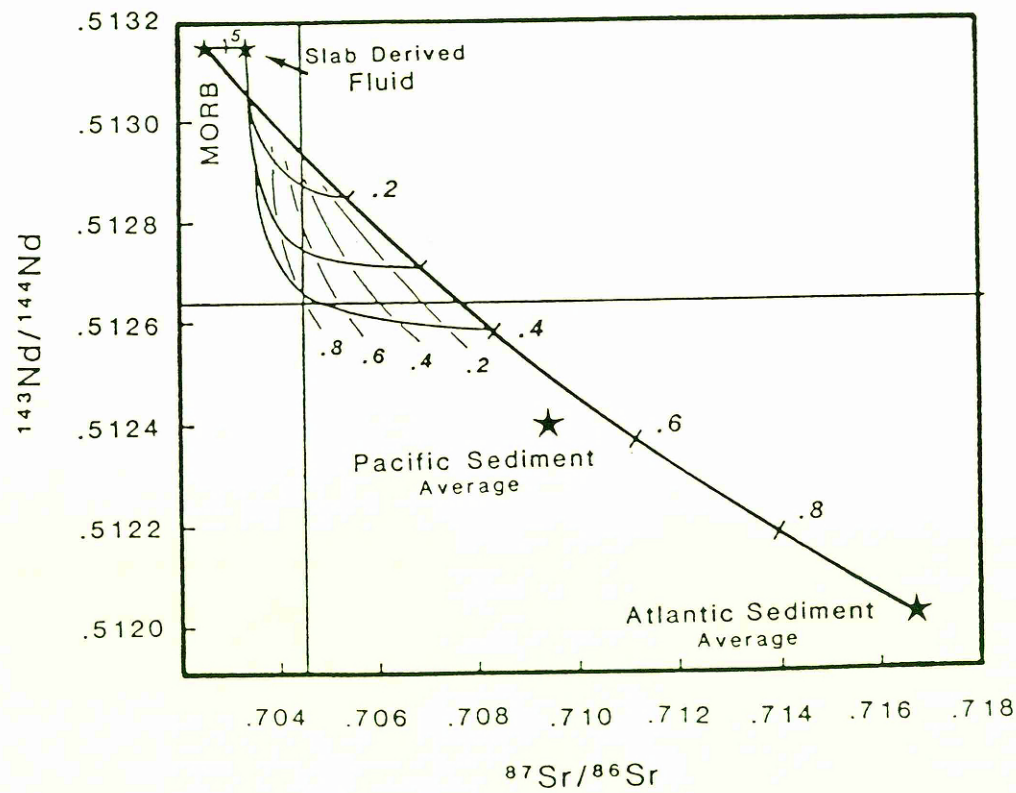

Fig. 6.13 Three component mixing model between MORB source, average Atlantic sediment (White *et al.* 1985) and slab derived fluid. Components as in fig. 6.12. Also included is a Pacific average sediment (O'Nions *et al.*, 1978, Elderfield *et al.*, 1981, Goldstein & O'Nions, 1981). Slab component $^{87}Sr/^{86}Sr$ is from Hawkesworth & Elderfield (1978). Figures in italics are mixing proportions.

Comparison of the two representations of the model (figs. 6.12, 6.13) reveals that in both cases a similar ratio of MORB wedge to sediment is indicated for subduction zone basalts, with a range of 0 to 50% sediment contribution being appropriate for most arc lavas. However a small discrepancy exists in the contribution of the high Sr/Nd fluid component required. Much of this arises from uncertainty about the likely concentration of Sr, Nd and Pb in this component. Some error may also be attributed to variation in the isotopic composition of the sediment component. The modelled sediment is an average of Atlantic sediments (White *et al.*, 1985), Pacific sediments tend to have lower $^{87}Sr/^{86}Sr$ and higher $^{143}Nd/^{144}Nd$ and lie closer to an extension of the mantle array (O'Nions *et al.*, 1978, Elderfield *et al.*, 1981, Goldstein & O'Nions, 1981). This may help to slightly reduce the required contribution from the high Sr/Nd fluid component, and may explain why Atlantic island arc lavas tend to have higher $^{87}Sr/^{86}Sr$ at given $^{143}Nd/^{144}Nd$ than those found in the Pacific.

6.4 Summary of Petrogenetic Model

Geochemical evidence suggests that the trace element and isotopic characteristics of subduction related lavas are inconsistent with simple two component mixing between the mantle wedge and a subducted oceanic lithosphere component. Neither is it likely that arc lavas derive their characteristics exclusively from within the mantle wedge. However a three component mixing model does seem to fulfill many of the requirements of subduction zone petrogenesis. The components involved in this mixture are mantle wedge, subducted sediment and a fluid component derived from dehydration of the descending oceanic lithosphere. The mantle wedge is MORB-like in its isotopic composition and in many of its trace element features. It differs from MORB (and OIB) in its relative distribution of the LILE elements, being depleted in Rb relative to other LILE such as Ba and Sr. The sediment component is characterised by low Sr/Nd (~9), moderately high LILE/HFSE ratios and elevated Zr/Y compared with MORB. It has high $^{87}Sr/^{86}Sr$, low $^{143}Nd/^{144}Nd$ and is enriched in ^{207}Pb relative to ^{206}Pb *ie.* high $\Delta 7/4$. The slab derived fluid component is characterised by high LILE/LREE *eg.* Sr/Nd, high LILE/HFSE *eg.* Ba/Nb, Th/Ta, but on a global scale is isotopically variable as it is itself derived from a mixture of isotopically distinct fresh and altered oceanic lithosphere. This component is

responsible for the dominant trace element fractionation observed in subduction related lavas *ie.* LILE enrichment relative to the HFSE and LREE. However it it apparently unrelated to fractionation of Rb relative to the other LILE which is thought to be more directly related to magma formation and/or extraction. The trace element characteristics of this fluid phase are believed to reflect the enhanced mobility of LILE in aqueous solution compared with the LREE and HFSE (Tatsumi *et al.*, 1986). It is thought unnecessary to invoke a Ti-rich phase in the slab *e.g.* rutile as the source of HFSE depletion, particularly as it is unclear that a minor phase would cause significant fractionation of Sr/Nd.

Therefore it appears that the proposed fluid component is characterised by the features which were used in previous chapters to define a "subduction zone component." The proposed sediment component has some features similar to the slab derived fluid, *e.g.* high LILE/HFSE ratios, but differs by having low Sr/Nd and apparently being associated with enrichment of Zr/Y. These features are inconsistent with the subduction component of Pearce (1983). Hence, the three component recognition technique (Pearce *op. cit.*) would appear to be an oversimplification as the subducted sediment component has some features typical of the subduction zone component *e.g.* high Th/Ta and Ba/Nb and some characteristics of the within-plate component *e.g.* low Sr/Nd and perhaps high (relative to MORB) Zr/Y. This is not accounted for in the model of Pearce (*op. cit.*) which recognises a single subduction zone component, but fails to appreciate its potential variability for different relative contributions of slab derived fluid and sediment.

6.5 Implications for the Aeolian Islands

The recognition of two subduction zone component in worldwide subduction related lavas is similar to the conclusions drawn for Aeolian Islands and Roman province lavas in chapters four and five. The proposed fluid component may be equated with the subduction zone component defined on trace element grounds (SCA), and the sediment component is similar to that proposed as a second subduction component in Italian rocks (SCB). However the sediment component inferred for worldwide island arc lavas does not require the extremely high Th/Ta proposed for the sediment end member in Roman province lavas (Rogers *et al.* 1985). This high Th/Ta was demanded by the high values of this ratio in the Roman lavas, however Aeolian lavas do not have such high Th/Ta (fig. 5.5).

Therefore although it is possible to explain the Aeolian and Roman provinces in terms of the same subduction components, it is evident that Aeolian lavas may be equally well explained by reference to a sediment component with much lower Th/Ta, more akin to likely sediment values and hence similar to the proposed model for worldwide subduction related petrogenesis. It seems unlikely that one can uniquely establish on geochemical grounds which of these two potential "sediment" components is present in the Aeolian lavas, because the shape of mixing curves between slab derived fluid and sediment are difficult to constrain. These curves are highly dependent on the Nd/Ta ratio of the slab derived fluid component to define their curvature, whilst it is thought that both Nd and Ta have low concentration in this component, their exact concentrations and hence the Nd/Ta ratio are unconstrained.

The proposed model does appear to be somewhat in conflict with the rather qualitative observation that Salina lavas have similar Sr, Nd and Pb isotopic compositions to lavas from Pietre Nere (Vollmer, 1976, Hawkesworth & Vollmer, 1979, see chapter five). As Sr and Nd isotopic characteristics of Salina lavas are unremarkable for subduction related rocks, this similarity may be merely coincidental in a similar manner to the apparently coincidental relationship between subduction zone lavas in general and OIB. However the geographical association encourages further consideration of this isotopic similarity. In the absence of a significant sediment component as indicated by Salina Pb isotope data (chapter four), the source of Salina lavas represents a mixture between mantle wedge and slab derived fluid. The former is may be similar to the source of Pietre Nere lavas ($^{87}Sr/^{86}Sr$ ~ 0.70355-0.70401) and the latter is constrained by the calculated "subduction zone component" (~ 0.704) which is within the range proposed for the fluid component from consideration of island arc lavas throughout the world. Hence it seems likely that addition of fluid to the wedge will not radically alter the Sr isotope composition of the mantle and as was shown by modelling (fig. 6.13) addition of this component even in large amounts does not drastically alter $^{143}Nd/^{144}Nd$. Hence it may well be possible that Salina lavas may represent enrichment of a Pietre Nere-like mantle wedge with a slab derived fluid component yet retain Sr and Nd isotope compositions similar to Pietre Nere.

Pb isotope data are more difficult to reconcile with the preferred model. Salina lavas have Pb isotope compositions similar to Pietre Nere and quite distinct from typical MORB.

It would seem that this precludes a significant contribution from MORB-like slab derived Pb. This implies that either an unusual Pb isotope composition of the descending lithosphere, or that much of the Salina Pb is scavenged from within the mantle wedge, rather than being added in a slab derived component. Also of interest is the ability of Salina lavas to apparently tap the same mantle source as the lavas of Pietre Nere. The isotopic composition of the latter implies an OIB type source (Hawkesworth & Vollmer, 1979), and hence it is inferred that Salina lavas also sample the OIB source. While this may perhaps reflect the geodynamic complexity of the Mediterranean region, it provides circumstantial evidence that an OIB source should not be rejected as a component in the generation of subduction related magmatism elsewhere.

6.6 Geodynamic Implications of the Petrogenetic Model.

In addition to satisfying many of the geochemical constraints on magma genesis in subduction zones, the model developed above has important geodynamic implications. At the present day it would appear that continental growth by arc accretion will not lead to the elevation in Rb/Sr relative to the upper mantle which is a necessary feature of the continental crust from Sr isotope considerations. However this merely reflects the Rb depleted nature of the mantle wedge relative to MORB. If similar processes to those active in subduction zones today were operative on primordial mantle material, then the crust formed would have higher Rb/Sr than its source. Moreover if the Rb depletion of the wedge is itself in some way complementary to the continental crust, perhaps by escape of Rb-rich fluids from mantle to crust, then another mechanism of generating high Rb/Sr is available.

The recognition of a crustally derived sediment component in arc basalts also has important consequences, as it implies a component of old crust is involved in the generation of new crust. Hence chemical differentiation of the crust and mantle may well be considerably slower than is implied by the rate of crustal growth at active continental margins. The important role implied for sediment in arc basalt genesis suggests that subducted sediment is efficiently removed from the oceanic slab by subduction zone processes, thus precluding large amounts of sediment subduction deep into the upper mantle to participate in OIB genesis (cf. White & Hofmann, 1982). However the slab would

appear to act as a geochemical filter, losing the LILE to the mantle wedge, but transporting the HFSE and LREE beyond the zone of subduction related magma generation deep into the upper mantle,. Thus subduction may produce on-going differentiation of the OIB and MORB sources (Hofmann *et al.*, 1986), and the HFSE and LREE budget of oceanic lithosphere may eventually become involved in the generation of OIB (Norry & Saunders, in press).

Chapter Seven

Concluding Remarks

A geochemical study of lavas from the Aeolian Islands southern Italy and comparison of these rocks with lavas from the Roman province and worldwide subduction related volcanism has revealed a number of conclusions of both local and global significance.

(a) Within the Aeolian region a range of lavas with variable SiO_2 and K_2O has been recognised. These may be classified into four different series whose range in SiO_2 is dominantly produced by fractional crystallisation. Variation in K_2O between these series is however unlikely to be due to fractional crystallisation and appears to reflect variation in the compositions of the primary magmas. Evidence suggests that K_2O content may be the only major element criterion by which this change in parental liquid can be recognised.

(b) The evolution of calc-alkaline lavas was probably a polybaric phenomenon. Basaltic lavas appear to have evolved from the primary magma by fractional crystallisation of olivine and orthopyroxene at a pressure greater than 10 Kb, perhaps in an environment approaching H_2O saturation. Basalt to andesite evolution probably occurred by fractional crystallisation of the observed phenocryst phases; clinopyroxene, orthopyroxene, plagioclase and magnetite at a pressure of around 5 Kb. Olivine is unlikely to have been involved during this stage of evolution.

(c) The leucite tephrite to rhyolite series defies simple interpretation in terms of closed system fractional crystallisation. Crustal contamination may have a minor but significant role in the evolution of this series. Involvement of leucite is required and implies low pressure (<2.5 Kb) evolution.

(d) Elevated K_2O content in Aeolian lavas is not diagnostic of a single source or process. Vulcano lavas derive their high K_2O content dominantly from a normal subduction zone component, albeit assisted by a relatively complex regime of melting involving periodic small degree partial melting and concomitant enrichment of the mantle. In contrast Stromboli lavas derive potassium from a number of sources:

(i) normal subduction component

(ii) subducted terrigenous sediment

(iii) within-plate enriched mantle component.

(e) At Stromboli it appears that the within-plate component pre-dates the subduction zone component. The within-plate component is not simply the result of variable degrees of partial melting in a single stage process. If the within-plate component were solely responsible for the low $^{143}Nd/^{144}Nd$ in Stromboli lavas, an age of 200-400 Ma would be implied for the within-plate enrichment. However, much of this low $^{143}Nd/^{144}Nd$ signature is likely to be derived from the terrigenous sediment component, and hence the within-plate enrichment may be a much more recent phenomenon. Perhaps within-plate enrichment is related to a hot spot which is now the cause of volcanism at M. Etna. An isotopically depleted within-plate component is not inconsistent with the Stromboli data.

(f) The component of subduction related trace element enrichment *ie.* high Ba/Nb, high Sr/Nd *etc.* in Aeolian Islands lavas is characterised by low $^{87}Sr/^{86}Sr$, high $^{143}Nd/^{144}Nd$ and radiogenic Pb isotope compositions. Its Sr and Nd signature is consistent with derivation from dehydration of subducted oceanic lithosphere, but it is unlikely that its Pb isotope composition may be reconciled with such an origin. However it is notable that Salina lavas share their rather unusual Pb isotope composition with lavas from Pietre Nere which may represent the composition of the mantle beneath Italy unaffected by Pliocene to Recent subduction. Not only does this imply derivation of Pb from within the mantle rather than from the subducting slab, but also implies a role for OIB-like material in subduction related petrogenesis.

(g) Similar subduction components to those present in Aeolian lavas may also be recognised in Roman province lavas although it is not clear that these components are isotopically alike in the two provinces. The within-plate component is however apparently restricted to Stromboli.

(h) Subduction related lavas worldwide are unlikely to be derived from pristine MORB or OIB source mantle with Ba/Rb =11. Rather, they appear to originate from mantle which is depleted in Rb relative to the other LILE.

(i) Subduction related lavas display a wide range of Rb/Ba and Rb/Sr. This variation is consistent with the range of basic arc lavas having been produced by processes involving variable but small degrees of partial melting. However this melting process is not responsible for LILE enrichment compared with HFSE and LREE

(j) A three component mixing model involving mantle wedge, subducted sediment and slab derived fluid is capable of explaining many of the trace element and isotopic

features of subduction related lavas throughout the world. The model is particularly strong in that it is able to reconcile the observation of high Sr/Nd in all subduction related basalts with variations in Sr and Nd isotopes along the mantle array, whilst within the same framework predicting the trend observed in some arcs towards high $^{87}Sr/^{86}Sr$ at fairly constant $^{143}Nd/^{144}Nd$, when little or no sediment component is involved. The model proposed is similar to that developed for the Roman and Aeolian lavas.

(k) The observation of significant fractionation of Rb/Sr in arc basalt genesis and the hypothesis that this may reflect variable but small degree partial melting during the genesis of subduction related magmas, has important implications for the growth of the continental crust. At the present day these processes act on mantle which is anomalously depleted in Rb, however were they to have acted on primordial souces during a period of early crust - mantle differentiation, then the crust produced would have higher Rb/Sr than its source, causing the required time integrated enrichment of the continental crust and depletion of the upper mantle implied from radiogenic isotope studies.

(l) The recognition of a sediment component in many subduction related provinces implies a role for recycled crustal material in the genesis of new continental crust. Moreover it also suggests that sediment is efficiently removed from the slab during destructive plate margin magmatism and hence unlikely to contribute to OIB genesis. In contrast the slab appears to preferentially retain HFSE and REE and these may ultimately contribute to the budgets of these elements in OIB.

BIBLIOGRAPHY

Abbey, S. (1980) "Studies in "standard samples" for use in the general analysis of silicate rocks and minerals." *Geostand. Newslett.* 4, 163-190

Allegre, C.J., Dupre,B., Lambret,B., & Richard,P. (1981) "The sub-continental versus sub-oceanic debate. I. Lead-neodymium-strontium isotopes in primitive alkali basalts from a shield area: the Ahaggar volcanic suite. *Earth Planet. Sci. Lett.* 52, 85-92

Arculus, R.J. & Powell, R. (1986) "Source component mixing in the regions of arc magma generation." *J. Geophys. Res.* 91 (B6), 5913-5926

Alvarez, W., (1972) "Rotation of the Corsica - Sardinia micro-plate." *Nature Phys. Sci.* 235, 103-105

Appleton, J.D., (1972) "Petrogenesis of potassium-rich lavas from the Roccamonfina volcano, Roman region, Italy." *J. Petrol.* 13 (3), 425-456

Baker, D.R. & Eggler, D.H. (1982) "Anhydrous phase relations of island-arc high-alumina basalts from 1 bar to 20 Kbar." (abstract) *Geol. Soc. Am. abstr. programs* 14, 437

Barberi, F., Innocenti,F., Ferrara,G., Keller,J. & Villari,L. (1974) "Evolution of Eolian arc volcanism (southern Tyrrhenian Sea)." *Earth Planet. Sci. Lett.* 21, 269-276

Barrett, T.J., (1980) "The Pb isotopic composition of Jurassic cherts overlying ophiolites in the north Apennines, Italy. *Earth Planet. Sci. Lett.* 49, 193-204

Beccaluva,L., Rossi,P.L. & Serri, G. (1982) "Neogene to Recent volcanism of the southern Tyrrhenian - Sicilian area: implications for the geodynamic evolution of the Calabrian arc." *Earth Evolution Sciences* 3, 222-238

Bender, J.F., Hodges,F.N. & Bence, A.E. (1978) "Petrogenesis of basalts from the project FAMOUS area: experimental study from 0-15 Kbars." *Earth Planet. Sci. Lett.* 41, 277-302

Bergeat, A. (1899) "*Die Äolischen Inseln (Stromboli, Panarea, Salina, Lipari, Vulcano, Filicudi und Alicudi) Abh. math. phys. Kl.* Klg. bayer Akad. Wiss. 20, I Abt. p.274 München.

Caputo, M., Panza,G.F. & Postpischl, D. (1972) "New evidences about the deep structure of the Lipari arc." *Tectonophysics* 15, 219-231.

Civetta, L., Innocenti, F., Manetti, P., Peccerillo, A., & Poli, G. (1981). "Geochemical characteristics of potassic volcanics from Mnts. Ernici (southern Latium, Italy)." *Contrib. Mineral. Petrol.* 78, 37-47

Clague, D.A. & Frey, F.A. (1982) "Petrology and trace element geochemistry of the Honolulu volcanics, Oahu: implications for the oceanic mantle beneath Hawaii." *J. Petrol.* 23(3) 447-504

Cohen, R.S. & O'Nions, R.K. (1982a) "The Pb, Nd and Sr isotopic structure of ocean ridge basalts." *J. Petrol.* 23(3), 299-324

Cohen, R.S. & O'Nions, R.K. (1982b) "Identification of recycled continental material in the mantle from Sr, Nd and Pb isotopic investigations." *Earth Planet. Sci. Lett.* 61, 71-84

Cortese, E. & Sabatini, V. (1892) "*Descrizione geologico - petrographica delle Isole Eolie." Mem. descritt. d. Carta Geol. d'Italia* 7, 131 S., Roma.

Cortini, M. (1981) "Aeolian island arc (southern Tyrrhenian Sea) magma heterogeneities in historical lavas: Sr and Pb isotopic evidence. *Bull. Volcanol.* 44(4), 712-722

Cortini, M & van Calsteren, P.W.C. (1985) "Lead isotope differences between whole-rock and phenocrysts in recent lavas from southern Italy. *Nature* 314, 343-345

Davidson, J.P. (1986) "Isotopic and trace element constraints on the petrogenesis of subduction related lavas from Martinique, Lesser Antilles." *J. Geophys. Res.* 91 (B6) 5943-5962

Deer, W.A., Howie, R.A. & Zussmann, J. (1966) "An introduction to the rock forming minerals." p.528 Longman, London

De Fiore O. (1922) *"Vulcano (Isole Eolie)" Z. Vulk. Erg.*, Bd IIIs. Berlin

DePaolo, D.J. (1981) "Trace element and isotopic effects of combined wall-rock assimilation and fractional crystallisation." *Earth Planet. Sci. Lett.* 53, 189-202

DePaolo, D.J. & Johnson, R.W. (1977) "Magma genesis in the New Britain island arc: constraints from Sr and Nd isotopes and trace element patterns." *Contrib. Mineral. Petrol.* 70, 367-379

DePaolo, D.J. & Wasserburg,G.J. (1976) "Inferences about mantle sources and mantle structure from variations of $^{143}Nd/^{144}Nd$." *Geophys. Res. Lett.* 3, 743-743

DePaolo, D.J. & Wasserburg,G.J. (1977) "The sources of island arcs as indicated by Nd and Sr isotope studies." *Geophys. Res. Lett.* 4, 465-468

Dodson, M.H. (1978) "A linear method for second-degree interpolation in cyclical data collection." *J. Phys. E. Sci. Instrum.* 11, 296

Dosso, L. & Murthy, V.R. (1980) " A Nd isotope study of the Kerguelen islands: inferences on enriched oceanic mantle sources." *Earth Planet. Sci. Lett.* 48, 268-276

von Drach, V., Marsh, B.D. & Wasserburg, G.J. (1986) "Nd and Sr isotopes in the Aleutians: multicomponent parenthood of island arc magmas." *Contrib. Mineral. Petrol.* 92, 13-34

Drake, M.J. & Weill, D.F. (1975) "Partition of Sr, Ba, Ca, Y, Eu^{2+}, Eu^{3+}, and other REE between plagioclase feldspar and magmatic liquid: an experimental study. *Geochim. Cosmochim. Acta* 39,689-712

Dupre, B. & Allegre, C.J. (1980) " Pb - Sr - Nd correlations and the chemistry of the North Atlantic mantle." *Nature* 286, 17-21

Dupuy, C., Dostal, J., Girod, M. & Liotard, M. (1981) "Origin of volcanic rocks from Stromboli (Italy)." *J. Volcanol. Geotherm. Res.* 10, 49-65

Dupuy, C., Dostal, J., Marcelot, G., Bougault, H., Joron, J.L. & Treil, M. (1982) "Geochemistry of basalts from central and southern New Hebrides arc: implications for their source rock composition." *Earth. Planet. Sci. Lett.* 60 207-225

Eggler, D.H. (1972) "Water saturated and undersaturated melting relations in a Paracutin andesite and an estimate of the water content in the natural magma." *Contrib. Mineral. Petrol.* 34 261-271

Eggler, D.H. & Burnham, C.W. (1973) "Crystallisation and fractionation trends in the system andesite-H_2O-CO_2-O_2 at pressures to 10 Kb." *Geol. Soc. Am. Bull.* 84,2517-2532

Elderfield, H., Hawkesworth, C.J. & Greaves, M.J. (1981) "Rare earth geochemistry of oceanic ferromanganese nodules and associated sediments." *Geochim Cosmochim. Acta* 45, 513-528

Evernden, J.F. & Curtis, G.H. (1965) "Potassium - argon dating of late Cenozoic rocks in East Africa and Italy." *Current Anthropology* 6, 343-385

Ewart, A. (1982) "Petrogenesis of the Tertiary anorogenic volcanic series of southern Queensland, Australia in the light of trace element geochemistry and O, Sr and Pb isotopes." *J. Petrol.* 23, 344-382

Ewart, A., Brothers, R.N. & Mateen, A. (1977) "An outline of the geology and geochemistry, and the possible petrogenetic evolution of the volcanic rocks of the Tonga - Kermadec - New Zealand island arc." *J. Volcanol. Geotherm. Res.* 2, 205-250

Ewart, A. & Hawkesworth, C.J. (1986) "The Pleistocene to Recent Tonga - Kermadec arc lavas. Re-evaluation of new isotopic and rare earth data in terms of a depleted mantle source model." in press *Contrib. Mineral. Petrol.*

Ferrara, G., Laurenzi, M.A., Taylor, H.P. Jr., Tonarini, S. & Turi, B. (1985) "Oxygen and strontium isotope studies of the K- rich volcanic rocks from the Alban Hills, Italy" *Earth Planet. Sci. Lett.* 75, 13-28

Ferrara, G., Preite-Martinez, M., Taylor, H.P. Jr., Tonarini, S. & Turi, B. (1986) "Evidence for crustal assimilation, mixing of magmas and a ^{87}Sr rich upper mantle." *Contrib. Mineral. Petrol.* 92, 269-280

Francis, P.W., Hammill, M., Kretzschmar,G. & Thorpe, R.S. (1978) "The Cerro Galan caldera, North-west Argentina and its tectonic setting." *Nature* 274 749-751

Fraser, K.J., Hawkesworth, C.J., Erlank, A.J., Mitchell, R.H. & Scott-Smith, B.H. (1985) "Sr, Nd, and Pb isotope and minor element geochemistry of kimberlites and lamproites." *Earth Planet. Sci. Lett.* 76, 57-70

Gasparini, C., Innaccone, G., Scandone, P. & Scarpa, R. (1982) "Seismotectonics of the Calabrian arc" *Tectonophysics* 84, 267-286

Gasparini, P. & Adams, J.A.S. (1969) "K/Ar dating of Italian Plio -Pleistocene volcanic rocks." *Earth Planet. Sci. Lett.* 6, 225-230

Gill, J.B. (1984) "Sr - Pb - Nd isotopic evidence that both MORB and OIB sources contribute to oceanic island arc magmas in Fiji." *Earth Planet. Sci. Lett.* 68, 443-458

Gillot, P. & Villari, L. (1980) "K - Ar geochronological data on the Aeolian arc volcanism. A preliminary report. Open File 3/80 I.I.V., Catania

Goldstein, S.L. & O'Nions,R.K. (1981) "Nd and Sr isotopic relationships in pelagic clays and ferromanganese deposits." *Nature* 292, 324-327

Green, T.H. (1981) "Experimental evidence for the role of accessory phases in magma genesis." *J .Volcanol. Geotherm. Res.* 10, 405-422

Grove, T.L. & Baker, M.B. (1984) "Phase equilibrium controls on the tholeiite versus calc-alkaline differentiation trends." *J. Geophys. Res.* 89 (B5) 3253-3274

Harris, P.G. (1957) "Zone refining and the origin of potassic basalts." *Geochim. Cosmochim. Acta* 12, 195-208

Hart, S.R. (1984) "A large-scale isotopic anomaly in the southern hemisphere mantle." *Nature* 309, 752-757

Harvey, P.K. & Atkin, B.P. (1981) "The rapid determination of Rb, Sr and their ratios in geological materials by X-ray fluoresence spectrometry using a rhodium X-ray tube." *Chem. Geol.* 32, 291-301

Hatherton, T. & Dickinson, W.R. (1969) "The relationship between andesitic volcanism and seismicity in Indonesia, the Lesser Antilles and other island arcs." *J. Geophys. Res.* 74 5301-5310

Hawkesworth, C.J. & Elderfield, H. (1978) "The strontium isotopic composition of interstitial waters from sites 245 and 336 of the deep sea drilling project." *Earth Planet. Sci. Lett.* 40, 423-432

Hawkesworth, C.J., O'Nions, R.K., Pankhurst, R.J., Hamilton, P.J. & Evenson, N.M. (1977) "A geochemical study of island arc and back arc tholeiites from the Scotia Sea." *Earth Planet. Sci. Lett.* 36 253-263

Hawkesworth, C.J., Norry, M.J., Roddick, J.C., Baker, P.E., Francis, P.W. & Thorpe,R.S. (1979a) "$^{143}Nd/^{144}Nd$, $^{87}Sr/^{86}Sr$ and incompatible element variations in calc-alkaline andesites and plateau lavas from South America." *Earth Planet. Sci. Lett.* 42, 45-57

Hawkesworth, C.J., O'Nions, R.K. & Arculus, R.J. (1979b) " $^{143}Nd/^{144}Nd$ and $^{87}Sr/^{86}Sr$ geochemistry of the alkalic rock suite, Grenada, Lesser Antilles." *Earth Planet. Sci. Lett.* 45, 237- 248

Hawkesworth, C.J. & Powell, M. (1980) "Magma genesis in the Lesser Antilles island arc." *Earth Planet. Sci. Lett.* 51,297-308

Hawkesworth, C.J., Rogers, N.W., van Calsteren, P.W.C. & Menzies, M.A. (1984) "Mantle enrichment processes." *Nature* 311, 331-335

Hawkesworth, C.J. & Vollmer, R. (1979) "Crustal contamination versus enriched mantle: $^{143}Nd/^{144}Nd$ and $^{87}Sr/^{86}Sr$ evidence from the Italian volcanics." *Contrib. Mineral. Petrol.* 69, 151-165

Henderson, P. (1982) "Inorganic geochemistry." p.353 Pergammon, Oxford

Hickey, R.L., Frey, F.A. & Gerlach, D.C. (1986) "Multiple sources for basaltic rocks from the southern volcanic zone of the Andes (34° - 41° S): trace element and isotopic evidence for contributions from subducted oceanic mantle and continental crust. *J. Geophys. Res.* 91 (B6) 5943-5962

Hofmann, A.W., Jochum,K.P, Seufert, M. & White, W.M. (1986) "Nb and Pb in oceanic basalts: new constraints on mantle evolution." *Earth Planet. Sci. Lett.* 79, 33-45

Hofmann, A.W. & White, W.M. (1983) "Ba, Rb and Cs in the earth's mantle." *Z. Naturforsch* 38a 256-266

Hole, M.J., Saunders, A.D., Marriner, G.F. & Tarney, J. (1984) "Subduction of pelagic sediments: implications for the origin of Ce-anomalous basalts from the Mariana Islands." *J. geol. Soc. London* 141 453-472

James, D.E. (1981) "The combined use of oxygen and radiogenic isotopes as indicators of crustal contamination." *Ann. Rev. Earth Planet. Sci.* 9, 311-344

Kay, R.W. (1977) "Geochemical constraints on the origin of Aleutian magmas." In *Island arcs, deep sea trenches and back arc basins.* M.Ewing Ser. 1. (Eds. M. Talwani & W.W. Pitman III), pp229-242. Amer. Geophys. Union.

Kay, R.W., Sun, S-S & Lee-Hu, C-N (1978) "Pb and Sr isotopes in volcanic rocks from the Aleutian Islands and Pribiloff Islands, Alaska." *Geochim .Cosmochim. Acta* 42, 263-273

Keller, J. (1967) *"Ater und abfolge des vulkanischen ereignisse auf den Äolischen Inseln/Sizilien." Ber. Natruf. Ges.Freiburg* i.B., 57, 33-67

Keller, J. (1974) "Petrology of some volcanic rock series of the Aeolian arc, southern Tyrrhenian Sea: calc-alkaline and shoshonitic associations." *Contrib. Mineral. Petrol.* 46, 29-47

Keller, J. (1980a) "The Island of Salina." In: Villari (Ed) "The Aeolian Islands an active volcanic arc in the Mediterranean Sea I.I.V. C.N.R. Catania 149-184

Keller, J. (1980b) "The Island of Vulcano." In: Villari (Ed) "The Aeolian Islands an active volcanic arc in the Mediterranean Sea I.I.V. C.N.R. Catania 29-74

Klerkx, J., Deutsch, S., Hertogen, J., De Winter, J., Gijbels, R. & Pichler, H. (1974) "Comment on "Evolution of Eolian arc volcanism, southern Tyrrhenian Sea." by Barberi *et al.*" *Earth Planet. Sci. Lett.* 23, 297-303

Kushiro, I. (1969) "The system forsterite - diopside - silica with and without water at high pressures." *Am. J. Sci.* 267A, 269-294

Kushiro, I. (1974) "On the nature of silicate melt and its significance in magma genesis. Regularities in the shift of the liquidus boundaries involving olivine, pyroxene and silica minerals." *Am. J. Sci.* 275, 411-431

Langmuir, C.H., Vocke, R.D. Jr., Hanson, G.N. & Hart, S.R. (1978) "A general mixing equation with applications to Icelandic basalts." *Earth Planet. Sci. Lett.* 37, 380-392

Leeman, W.P. & Hawkesworth, C.J. (1986) "Open magma systems: trace element and isotopic constraints." *J. Geophys. Res.* 91 (B6) 5901-5912

Le Roex, A.P., Dick, H.J.B., Erlank, A.J., Reid, A.M., Frey, F.A. & Hart, S.R. (1983) "Geochemistry, mineralogy and petrogenesis of lavas erupted along the south west Indian ridge between the Bouvet triple junction and 11 degrees east. *J. Petrol.* 24(3), 267-318

Luth, W.C. (1967) "Studies in the system $KAlSiO_4$ - Mg_2SiO_4 - SiO_2 - H_2O: pt.1 Inferred phase relations and petrologic applications." *J. Petrol.* 8, 372-416

Mattey, D.P. (1982) "The minor and trace element geochemistry of volcanic rocks from Truk, Ponape and Kusaie, eastern Caroline Islands: the evolution of a young hot-spot trace across old Pacific Ocean crust." *Contrib. Mineral. Petrol.* 80, 1-13

McCulloch, M.T. & Perfit, M.R. (1981) "$^{143}Nd/^{144}Nd$, $^{87}Sr/^{86}Sr$ and trace element constraints on the petrogenesis of Aleutian island arc magmas." *Earth Planet. Sci. Lett.* 56 167-179

McKenzie, D. (1985) "The extraction of magma from the crust and mantle." *Earth Planet. Sci. Lett.* 74, 81-91

Menzies, M. & Murthy, V.R. (1980) "Nd and Sr isotope geochemistry of hydrous mantle nodules and their host alkali basalts: implications for local heterogeneities in metasomatically veined mantle." *Earth Planet. Sci. Lett.* 46. 323-334

Mercalli, G. & Silvestri, O. (1891) *"Le eruzioni dell' isola di Vulcano 1888-1890." Ann. Uff. Cenr. Meteor. e Geodyn. Ital.* 10, 4a

Morris, J.D. & Hart, S.R. (1983) "Isotopic and incompatible element constraints on the genesis of island arc volcanics from Cold Bay and Amark Island, Aleutians and implications for mantle strucure." *Geochim. Cosmochim. Acta* 47, 2015-2030

Nakamura, N. (1974) "Determination of REE, Ba, Fe, Mg, Na and K in carbonaceous and ordinary chondrites." *Geochim. Cosmochim. Acta* 38, 757-775

Nohda, A.S. & Wasserburg, G.J. (1986) "Trends of Sr and Nd isotopes through time near the Japan Sea in northeastern Japan." *Earth Planet. Sci. Lett.* 78,157-167

Norry M.J. & Saunders A.D. "The significance and consequence of Nb and Ta anomalies in terrestrial magmas." in press *Earth. Planet. Sci. Lett.*

Nye, C.J. & Reid, M.R. (1986) "Geochemistry of primary and least fractionated lavas from Okmok volcano, central Aleutians: implications for arc magmagenesis." *J. Geophys. Res.* 91 (B10) 10,271-10,287

O'Hara, M.J. (1977) "Geochemical evolution during fractional crystallisation of a periodically refilled magma chamber." *Nature* 266, 503-507

O'Hara, M.J. (1985) "Importance of the "shape" of the melting regime during partial melting of the mantle." *Nature* 314, 58-62

O'Hara, M.J. & Mathews, R.E. (1981) "Geochemical evolution in an advancing, periodically replenished, periodically tapped, continuously fractionated magma chamber." *J. geol. Soc. London* 38, 237-277

O'Nions,R.K., Carter,S.R., Cohen,R.S., Evenson, N.M. & Hamilton, P.J. (1978) "Pb, Nd and Sr isotopes in oceanic feromanganese deposits and ocean floor basalts." *Nature* 273, 435-436

Oxburgh, E.R. (1972) "Flake tectonics and continental collision." *Nature* 239, 202-204

Pearce, J.A. (1983) "Role of the subcontinental lithosphere in magma genesis at active continental margins." In: Continental basalts and mantle xenoliths. (Eds. Hawkesworth, C.J. & Norry, M.J.) Shiva Publishing, Nantwich 230-249

Pearce, J.A., Alabaster, T., Shelton, A.W. & Searle, M.P. (1981) "The Oman ophiolite as a Cretaceous arc - basin complex: evidence and implications. *Phil. Trans. R. Soc. Lond.* A300, 299-317

Peccerillo, A. & Taylor, S.R. (1976) "Geochemistry of Eocene calc-alkaline volcanic rocks from the Kastamonu area, northern Turkey. *Bull. Volcanol.* 39, 557-569

Perfit, M.R., Gust, D.A., Bence, A.E., Arculus,R.J. & Taylor,S.R. (1980) "Chemical characteristics of island-arc basalts: implications for mantle sources." *Chem. Geol.* 30 227-256

Pichler, H. (1968) *"Zur alkersfrage des Vulkanismus des Äolischen archipels und der inseln Ustica (Sizilien)." Geol. Mitt.* 7, 299-322

Pichler, H. (1980) "The island of Lipari." In: Villari (Ed.) "The Aeolian Islands an active volcanic arc in the Mediterranean Sea." I.I.V. C.N.R. Catania 75-100

Potts, P.J., Thorpe, O.W. & Watson, J.S. (1981) "Determination of the rare-earth element abundances in 29 international rock standards by instrumental neutron activation analysis: a critical appraisal of calibration errors." *Chem. Geol.* 34, 331-352

Potts, P.J., Thorpe, O.W., Isaacs, M.C. & Wright, D.W. (1985) "High precision instrumenral neutron activation analysis of geological samples employing simultaneous counting with both planar and coaxial detectors." *Chem. Geol.* 48, 145-155

Potts, P.J., Webb, P.C., & Watson, J.S. (1984) "Energy dispersive X-ray fluoresence analysis of silicate rocks for major and trace elements." *X-Ray Specrometry* 13, 2-15

Rogers, N.W., Hawkesworth, C.J., Parker, R.J. & Marsh, J.R. (1985) "The geochemistry of potassic lavas from Vulsini, central Italy and implications for mantle enrichment processes beneath the Roman region. *Contrib. Mineral. Petrol.* 90, 244-257

Romano, R. (1973) *"Le Isole di Panarea e Basiluzzo, contributa alla conoscenza geo-volcanologica e magmatologica delle Isole Eolie." Riv. Min. Sic.* 24, 139-141

Rosi, M. (1980) "The island of Stromboli." In: Villari (Ed.) "The Aeolian Islands an active volcanic arc in the Mediterranean Sea." I.I.V. C.N.R. Catania 1-28

Saunders, A.D., Tarney, J. & Weaver,S.D. (1980) "Transverse geochemical variations across the Antarctic Peninsula: implications for the genesis of calc-alkaline magmas. *Earth Planet. Sci. Lett.* 46, 344-360

Scandone, P. (1979) "Origin of the Tyrrhenian Sea and Calabran arc." *Boll. Soc. Geol. It.* 98, 27-34

Schenk, V. (1984) "Petrology of felsic granulites, metapelites, metabasics, ultramafics and metacarbonates from southern Calabria (Italy). Prograde metamorphism, uplift and cooling of a former lower crust." *J. Petrol.* 25 255-298

Schutte, K-G. (1978) "Crustal structure of southern Italy." in Closs, H., Roeder, D. & Schmidt, K. (Eds.) "Alps, Apennines, Hellenides." Scweizerbart, Stuttgart 315-321

Stothers, R.B. & Rampino, M.R. (1983) "Volcanic eruptions in the Mediterranean before AD 630 from written and archaeological sources." *J. Geophys. Res.* 88 (B8), 6357-6371

Sun, S-S. (1980) "Lead isotope study of young volcanic rocks from mid ocean ridges, ocean islands and island arcs. *Phil. Trans. R. Soc. Lond.* A297, 409-455

Tatsumi, Y., Hamilton, D.L. & Nesbitt, R.W. (1986) "Chemical characteristics of fluid phase released from a subducted lithosphere and origin of arc magmas: evidence from high-pressure experiments and natural rocks." In: I Kushiro (Editor), M. Sakuyama and H. Fukuyama Memorial Volume. *J. Volcanol. Geotherm. Res.* 29: 293-309

Taylor, H.P. Jr., Gianetti, B. & Turi, B. (1979) "Oxygen isotope geochemistry of the potassic igneous rocks from the Roccamonfina volcano, Roman comagmatic region, Italy." *Earth Planet. Sci. Lett.* 46, 81-106

Taylor, H.P. Jr., & Turi, B. (1976) "High ^{18}O igneous rocks from the Tuscan magmatic province, Italy." *Contrib. Mineral. Petrol.* 55, 33-56

Tera, F., Brown, L., Morris, J., Sacks, I.S., Klein,J. & Middleton, R. (1986) "Sediment incorporation in island arc magmas: inferences from ^{10}Be." *Geochim. Cosmochim. Acta* 50,535-550

Thirlwall, M.F. & Graham, A.M. (1984) "Evolution of high-Ca, high-Sr C-series basalts from Grenada, Lesser Antilles: the effects of intra-crustal contamination." *J. geol. Soc. London* 141, 427-445

Thompson, R.N. (1977) "Primary basalts and magma genesis III: Alban Hills, Roman comagmatic province, central Italy." *Contrib. Mineral. Petrol.* 68,91-108

Thompson, R.N. (1982) "Magmatism of the British Tertiary volcanic province." *Scottish Journal of Geology* 18(1), 49-107

Thompson, R.N., Morrison, M.A., Hendry, G.L. & Parry, S.J. (1984) "An assessment of the relative roles of crust and mantle in magma genesis; an elemental approach." *Phil. Trans. R. Soc. Lond.* A310, 549-590

Thorpe, R.S., Francis, P.W. & O'Callaghan, L. (1984) "Relative roles of source composition, fractional crystallisation and crustal contamination in the petrogenesis of Andean volcanic rocks." *Phil. Trans. R. Soc. Lond.* A310, 675-692

Turi, B. & Taylor, H.P. Jr. (1976) "Oxygen isotope studies of potassic volcanic rocks of the Roman province, central Italy." *Contrib. Mineral. Petrol.* 55, 1-31

Villari, L. (1972) *"L' Isole di Filicudi ed il suo sinificato magmatologico." Rend. Soc. It. Min. Pet.* 28,475-506

Villari, L. (Ed.) (1980) "The Aeolian Islands an active volcanic arc in the Mediterranean Sea." p.191 I.I.V. C.N.R. Catania

Villari, L. (1980a) "The island of Filicudi." In: "The Aeolian Islands an active volcanic arc in the Mediterranean Sea." p.191 I.I.V. C.N.R. Catania 127-148

Villari, L. (1980b) "The island of Alicudi." In: "The Aeolian Islands an active volcanic arc in the Mediterranean Sea." p.191 I.I.V. C.N.R. Catania 101-126

Vollmer, R. (1976) "Rb - Sr and U - Th - Pb systematics of alkaline rocks: the alkaline rocks from Italy." *Geochim. Cosmochim. Acta* 40, 283-295

Vollmer, R. & Hawkesworth, C.J. (1980) "Lead isotope composition of potassic rocks from Roccamonfina (south Italy). *Earth Planet. Sci. Lett.* 47, 91-101

Vollmer, R., Johnston, K., Ghiara, M.R., Lirer, L. & Munno, R. (1981) "Sr isotope geochemistry of megacrysts from continental rift and convergent plate margin alkaline volcanism in south Italy." *J. Volcanol. Geotherm. Res.* 11, 317-327

Weaver, B.L. & Tarney, J. (1984) "Empirical approach to estimating the composition of the continental crust." *Nature* 310, 575-577

White, W.M., Dupre, B. & Vidal, P. (1985) "Isotope and trace element geochemistry of sediments from the Barbados ridge and Demerara Plain region, Atlantic Ocean." *Geochim. Cosmochim. Acta* 49,1875-1886

White, W.M. & Hofmann, A.W. (1982) "Sr and Nd isotope geochemistry of oceanic basalts and mantle evolution." *Nature* 296, 821-825

Whitford, D.J. & Jezek, P.A. (1979) "Origin of late Cenozoic lavas from the Banda arc, Indonesia: trace element and Sr isotope evidence." *Contrib. Mineral. Petrol.* 68,141-150

Whitford, D.J., Nicholls, I.A. & Taylor, S.R. (1979) "Spatial variations in the geochemistry of Quaternary lavas across the Sunda arc in Java and Bali." *Contrib. Mineral. Petrol.* 70, 341-356

Whitford, D.J., White, W.M. & Jezek, P.A. (1981) "Neodymium isotopic composition of Quaternary island arc lavas from Indonesia." *Geochim. Cosmochim. Acta* 45,989-995

Wood, D.A., Tarney, J., Varet, J., Saunders, A.D., Bougault, H., Joron, J.L., Treuil, M., & Cann, J.R. (1979) "Geochemistry of basalts drilled in the North Atlantic by IPOD leg 49: Implications for mantle heterogeneity." *Earth Planet. Sci. Lett.* 42, 77-97

Wright, T.L. & Doherty, P.C. (1970) A linear programming and least squares computer method for solving petrographic mixing problems. *Geol. Soc. Am. Bull.* 81, 1995-2008

Yoder, H.S. jnr. & Tilley, C.E. (1962) "Origin of basalt magmas: an experimental study of natural and synthetic rock systems." *J. Petrol.* 3, 342-532

APPENDIX A

Sample Petrography

SAMPLE	LOCATION	PHENOCRYSTS	MATRIX	TEXTURE	LITHOLOGY
		SALINA			
ESAL01	Vne. Martello	Cpx, Plag	Plag, Glass	Porphyritic	Basalt
ESAL02	Caldara	Ol (red rims) Cpx, Opx, Plag	Ol?, Px,Plag Op	Porphyritic	Basalt
ESAL03	P. di Menarento	1. Cpx, Opx plag,micro-perthite, Op	1. glass, Fspr, Op	Mixed Rock 1. f.g. glassy	Basalt/ Andesite Hybrid
		2. as 1. but more Opx & Fspr		2.Porphyritic	
ESAL04	P. di Menarento	Cpx, Opx plag, Op, AF	Fspr, Op glass	Porphyritic (altered)	Andesite
ESAL05	P. Brigantino	Cpx, Opx (black rims), Plag, San	Fspr, Op glass	Porphyritic	Andesite
ESAL06	Serro Spinnato	Opx, Cpx, Plag> AF, Bt (corroded)	Fspr (v.f.g)	Porphyritic Numerous glomerocrysts	Andesite
ESAL07	nr. Serro Spinnato	as ESAL03 plus olivine in both textures.			
ESAL08	Erbe Bianche	Opx, Cpx Plag rare untwinned AF & Sanidine	Vitreous	V.f.g	Andesite
ESAL09	Erbe Bianche	as ESAL04 plus rare olivine			
ESAL11	Belvedere	Cpx, Opx (rare) Plag, AF (rare) Opaque	Px, Plag, Op	Porphyritic	Andesite
ESAL12	nr. M. Rivi	Cpx, Opx,Ol (orange rims) Plag, AF	V.f.g. but crystalline Opaque	f.g Porph.	Basalt
ESAL13	M. Rivi	Cpx, Opx,Ol (serpentinised) Plag,San, Op	Plag, Op & alterred ferro-magnesian minerals	Porphyritic	Basalt
ESAL14	M. Rivi	as ESAL13 but the matrix is much fresher. Olivines still have thick black rims & serpentine along fractures.			
ESAL15	nr. Ospizio (Valdichiesa)	as ESAL03 but only the fine grained vitreous texture is represented in this sample. Olivine is present.			

ESAL16	nr. Malfa	Opx (pleochroic in fawn-green-colourless), Cpx Plag, rare AF,Op	Px, plag,Op	Porphyritic	Basaltic andesite
ESAL17	Pollara	Ol, (orange rims) Cpx, Plag	Vitreous	Porphyritic	Basalt
ESAL18	Pollara	Ol (v. altered), Cpx, Plag	v.f.g altered	Porphyritic	Basalt
ESAL19	P. di Perciato	Cpx, Opx, Amp (pleochroic in green-yellow-brown) AF>> Plag, Op	vitreous AF microliths	Porphyritic Glomerocrysts	Andesite/ Dacite
		Glomerocrysts are amphibole free. Amphiboles show black rims and are occasionally rounded & resorbed.			
ESAL20	Pollara	as ESAL11- numerous glomerocrysts (cumulate xenoliths)			
ESAL21	Capo		Cpx, Opx (rare),Plag Opaque	Hypabyssal Equigrained	Dolerite
			Contains gabbroic xenolith		
ESAL22	Gramignazzo	Px (rare), F'mags v. altered, Plag AF (rare)	v.f.g. altered (red)	Porphyritic	Basaltic andesite
ESAL23	Torricella	Opx, Cpx, Ol (altered), Plag AF	Op, glass	Porphyritic V. rich in phenocrysts	Basaltic andesite
ESAL24	nr. Scogliazzo	as ESAL06 but slightly finer grained and no Bt xenocrysts.			
ESAL25	V. Borrello	as ESAL11 but richer in olivine with orange rims. Very complex plagioclase intergrowths.			
ESAL26	V. Olivio Grande	as ESAL16			
ESAL27	M. Porri	as ESAL11			

STROMBOLI

StA1	P. dei Corvi	Cpx, Ol, Plag	glass	Porphyritic	Absarokite
StA2	Fili di Baraona	Cpx, Ol, Plag	Cpx, plag, Opaque	Porphyritic	Absarokite
StA3	Ginostra	Cpx, Plag, AF (rare), Lc	glass, Cpx & Plag micro-liths	Porphyritic	Absarokite
StB5	Malpasseddu	Cpx, Plag, AF Op. Plag> Cpx ≥ AF	glass, Op V.f.g. Cpx, fspr	Porphyritic	Basalt

StB10	la Petrazza	Cpx, Opx, Plag > AF, Op (rare)	V.f.g glass, Px, Fspr	Porphyritic	Basalt
StB12	la Petrazza	Cpx, Opx, Plag AF, Op Bt (rare, corroded)	Px, Fspr, glass, Op	Porphyritic	Basaltic
StB20	Filo del Fuoco	Cpx, Opx, Ol Plag>> AF	glass, Fspr Px (micro-liths)	Vesicular Porphyritic	Absarokite
StB24	i Vancori	Cpx, Plag, AF	Cpx, Ol (rare) Plag, AF	Porphyritic Quite coarse matrix.	Basaltic andesite
StB29	P. dei Corvi	Cpx, Opx, Plag AF (rare)	Px, Plag, glass	Porphyritic	Absarokite
StB32	Ginostra	Cpx, Ol, Plag AF	Px, Fspr, glass	Porphyritic	Absarokite
StB34	nr. Ginostra	Cpx, Opx, Bt Plag, AF,Op (Bt: dark rims)	v.f.g. Px, Fspr, glass minor Op	Porphyritic	Basaltic andesite
StB35	i Vancori	Ol, Cpx, Plag AF	F'mags, Fspr, Op	Porphyritic Glomero-crysts (cumulate xenoliths)	Basaltic andesite
StB38	i Vancori	Plag > AF, Cpx	Cpx, Fspr,	Porphyritic Glomerocrysts (Cpx, Ol, Fspr)	Basalt
StB42	Malo Passo	Cpx, Opx (orange rims), Plag, AF (rare)	Px, Fspr, Opaque	Non Porph. range in grainsize.	Basaltic andesite
StB45	P. del Monaco	Cpx, Plag, AF minor Bt with ragged and altered rims.	Cpx, Ol, Fspr,Op glass	Porphyritic	Andesite
StC5	P. dell' Omo	Cpx, Plag, AF	Px, Fspr altered glass	Rather equi-grained	Basaltic Andesite
StC9	Bastimento	Cpx, Ol, Plag analcite after Lc	Px, Fspr Opaque	Vesicular	Absarokite
StC14	i Vancori	Cpx, Plag>AF (Fspr> F'mag) minor Opaque	Px, Fspr glass	Porphyritic	Basalt

StC18	Sciara del Fuoco	Cpx, Ol,Plag AF	Px,Fspr Opaque	Porphyritic	Basalt/ Absarokite
StC19	Sciara del Fuoco	Cpx, Ol,Plag AF (Ol included In Cpx)	Px, Plag, Opaque	Equigrained	Basalt
StD1	Bastimento	Cpx, Ol, Plag Lc	Px, Plag Opaque	Porphyritic	Absarokite
StD4	Filo del Fuoco	Cpx, Ol,Plag AF	Px, Fspr Op, glass	Porphyritic Cumulate Xenoliths	Absarokite
StD5	Stromboli	Cpx, Plag AF (rare)	Px, Fspr, Op, glass	Porphyritic	Basalt
StD6	la Petrazza	Opx, Cpx, Plag AF, Op (minor).	v.f.g	Porphyritic	Basalt
StD7	la Petrazza	Rare (Cpx, Plag, AF, amp? Very feldspathic	glass	Vitreous, Micro-crystalline "clots"	Andesite
StD8	Stromboli	Cpx, Ol, Opx Plag, AF (rare)	glass	f.g.	Basalt
StD10	nr. Pisciata	Cpx, Opx, Plag AF	glass	Porphyritic	Basalt
ESTR01	Pizzo la Fossa	Cpx, Plag, (rare) Bt	minor cpx & Op, PLag	Porphyritic Glomerocrysts	Basalt
ESTR02	nr. Malpassedu	Cpx, Opx,Plag Bt (altered), Op	Plag, Op	Porphyritic Glomerocrysts	Basalt
ESTR03	nr. Malpassedu	Cpx, Amp,Opx Plag, AF, Op	Glass, Op	Porphyritic	Andesite
ESTR04	la Petrazza	Cpx, plag, Op	Plag, Op glass	Porphyritic	Basalt
ESTR05	la Petrazza	Cpx,Opx,Plag	Plag Op glass	Porphyritic	Basaltic andesite
ESTR06	Sciara del Fuoco	as StC18			
ESTR07	Filo di Fuoco	Cpx, Ol, Plag	Cpx, Ol, Plag., Op	Porphyritic	Absarokite
ESTR08	P. Labronzo (Sill)		Cpx, Ol,Plag AF (rare)	Hypabyssal Equigrained	Absarokitic Dolerite

VULCANO

EVUL01	C. Amendola	Cpx, Ol (altered rims) Plag, cubic opaque Small microcystalline Fspr/Qtz xenoliths.	Fspr, glass	Porphyritic Op included by Cpx but not by Plag.	Shoshonite
EVUL02	C. Amendola	Ol, Cpx, Plag, Opaque	Cpx,Plag Op. v.f.g	Porphyritic	Shoshonite
EVUL03	nr. La Portella	Ol, Cpx, Plag Opaque	Ol (altered) Cpx, Plag, Op	Porphyritic	Shoshonite
EVUL04	Fossa di Vulcano			Aphyric Vitreous	Obsidian
EVUL05	Fossa di Vulcano (Breadcrust bomb)	Cpx, Plag, AF	glass	Porphyritic Basic inclusions (? Xenoliths)	Trachyte
EVUL06	Fossa di Vulcano (Breadcrust bomb)	1. Bulk of T.S. Cpx, Plag, AF 2. Cpx, Ol, Plag & AF	v.f.g feldspathic feldspathic	Mixed 1. Porphyritic 2. Coarser grained, no evidence of chilling along the contact.	Rhyolite
EVUL07	Fossa di Vulcano	Cpx, Plag (xenocrysts?)	Devitrified glass (cpx & AF)	Vitreous	Obsidian
EVUL08	Fossa di Vulcano	Cpx, minor Ol Fspr	Plag Cpx, opaque	Crystalline	Trachyte
EVUL09	Fossa di Vulcano	Cpx, AF (san, an, & untwinned), plag Glomerocrysts (cumulate xenoliths) also contain Olivine and are richer in plagioclase.	Px, Fspr, Op	Porphyritic	Trachyte
EVUL10	Fossa di Vulcano	Cpx, AF (as in EVUL09) > Plag V. small Ol, Op	Px,Fspr,Op	Porphyritic	Trachyte
EVUL11	Vulcanello (Porto Ponente)	Cpx, Ol, Lc, Plag Opaque	accicular Plag, analcite after Lc, Op	Porphyritic	Tephrite
EVUL12	Vulcanello (Porto Ponente)	as EVUL11			
EVUL13	Vulcanello (P. del Roveto)	Cpx, Plag, (rare) AF, opaque	Px,Fspr, Op	Porphyritic	Trachyte
EVUL14	Vulcanello	as EVUL11 but slightly richer in plag, quite altered especially olivine.			

EVUL15	Vulcanello	as EVUL11 but contains large (~1mm) fresh olivine phenocrysts.			
EVUL16	M. Rosso		Px, fspr	Aphyric	Shoshonitic scoria
EVUL17	M. Rosso		Cpx, plag,	v.f.g.	Absarokite
EVUL18	M. Molineddo	Ol, Cpx, Plag	Plag, analcite, glass	Porphyritic	Absarokite
EVUL19	M. Molineddo	as EVUL18			
EVUL20	Piano	Rare Cpx	Cpx, Plag Analcite?	f.g.	Absarokite
EVUL21	M. Saraceno	Cpx, Ol, Plag, opaque	Cpx, Plag opaque	Porphyritic	Absarokite
EVUL22	Fossa di Vulcano	Rare Cpx,Plag Minor phase with large pleochroic radiation haloes.	glass	largely aphyric	Obsidian
EVUL23	Fossa di Vulcano	as EVUL22			
EVUL24	Fossa di Vulcano	Cpx, Plag, AF Op, rare resorbed Ol	Cpx, Fspr (quite altered)	Porphyritic	Trachyte
EVUL25	Lentia	Cpx (brown rims) Plag	AF> Plag, Opaque	Vitreous Glomerocrysts	Rhyolite
EVUL26	Lentia	Cpx, Plag, AF (all are often rounded and resorbed)	Brown glass Fspr laths	Porphyritic	Rhyolite
EVUL27	Lentia	Cpx (often resorbed) AF, Plag	Fspr, Op	Porphyritic v.f.g. matrix	Rhyolite
EVUL28	Lentia	Cpx (Ol, Cpx, Plag cumulate xen-oliths), Op	f.g. Fspr AF> Plag	Largely Aphyric	Rhyolite
EVUL29	S. Vulcano	Ol, Cpx, Plag Opaque	Cpx, Plag, Opaque	Porphyritic Op often included in Cpx	Shoshonite
EVUL30	S. Vulcano	as EVUL29			
85/VUL/02	Sc^{o} di Capo Secco, Lentia	Cpx, AF, Plag Opaque	Vesic. glass	Porphyritic	Banakite
85/VUL/03	S. Vulcano	Cpx, Ol, Opx Plag, Op	Cpx, Plag	Porphyritic	Absarokite

85/VUL/04	Capo Secco	Ol, Cpx, Plag AF, Op	Cpx, Plag, glass	Porphyritic	Absarokite
85/VUL/05	M. Saraceno	Cpx, Ol, Plag Op	Cpx, Plag	Trachytic	Absarokite
85/VUL/06	P. di Levante	Cpx, AF, Plag	glass	Porphyritic	Shoshonite

CRUSTAL XENOLITHS (Salina)

85/SAL/04	Pollara	Qtz, acc. Hem?	Qtz, AF, Bt Plag	f.g. Gneissic	Leucogneiss
85/SAL/06	Pollara	Gt (serp. on fractures), Bt after Gt	Opx, AF, Plag, Mullite?	Porphyro-blastic	Garnet Gneiss
85/SAL/07	Pollara	Calcite, Gt, Cpx Melilite (after Gt & Cpx)		Equigrained	Marble
85/SAL/08	Pollara	Qtz, sericitised Fspr		Banded f.g	Leucogneiss
85/SAL/12	Rinella		Qtz, Epidote	f.g. equi-grained	Metapelite
GX1	Pollara		Qtz, Plag AF, Bt, Amp	Granitic	Granodiorite
SA270	Pollara	Gt, Amp	Qtz, Chl, AF	Minor Schistosity	Pelite
SA309	Pollara		Chl, Qtz, Bt, Op, AF	v.f.g.	Chlorite mica Schist
ST12	Pollara		Qtz, AF, Plag Bt, Epidote		Pelite

Abbreviations

Cpx	Clinopyroxene	Opx	Orthopyroxene
Px	Pyroxene (non specific)	Plag	Plagioclase
Ol	Olivine	AF	Alkali feldspar
Op	Opaque	Fspf	Feldspar (non specific)
Bt	Biotite	San	Sanidine
f.g.	Fine grained	V.f.g	Very fine grained
Porph.	Porphyritic	Amp	Amphibole
F'mags	Ferromagnesian minerals	Lc	Leucite
Qtz	Quartz	An	Anorthoclase
Hem	Hematite	Serp	Serpentine
Gt	Garnet		

APPENDIX B

Geochemical Data

Major Element Data

SALINA

	ESAL01	ESAL02	ESAL03	ESAL05	ESAL13	ESAL14	ESAL17	ESAL18
SiO_2	49.55	52.14	54.48	61.35	50.95	52.45	51.80	51.59
TiO_2	0.64	0.65	0.61	0.55	0.65	0.63	0.63	0.60
Al_2O_3	18.56	19.19	17.45	17.08	17.07	17.43	18.42	17.35
Fe_2O_3	11.72	9.16	8.99	6.35	9.67	9.46	9.09	9.28
MnO	0.16	0.17	0.17	0.15	0.17	0.15	0.15	0.15
MgO	4.81	4.03	4.53	2.15	6.57	5.67	4.75	5.78
CaO	10.59	10.40	9.23	6.00	11.23	10.33	10.32	10.74
Na_2O	2.15	2.27	2.75	3.41	2.49	1.99	0.00	2.09
K_2O	1.28	1.08	1.35	2.34	1.00	1.10	2.60	0.89
P_2O_5	0.18	0.19	0.17	0.23	0.20	0.13	0.19	0.17
L.O.I	0.38	-0.03	0.04	0.37	0.00	0.18	0.93	1.02
Total	100.02	99.25	99.77	99.98	100.00	99.52	98.88	99.66

	ESAL06	ESAL08	ESAL09	ESAL12	ESAL15	ESAL16	ESAL19	ESAL20
SiO_2	57.11	58.63	59.79	52.51	58.03	53.55	59.44	56.51
TiO_2	0.60	0.62	0.57	0.64	0.65	0.70	0.51	0.73
Al_2O_3	17.20	16.54	16.99	17.43	17.12	18.90	16.98	17.54
Fe_2O_3	8.07	8.03	6.89	9.38	7.70	8.43	6.03	8.74
MnO	0.16	0.18	0.15	0.16	0.16	0.15	0.15	0.16
MgO	3.66	2.98	2.58	5.42	3.37	3.21	3.06	3.26
CaO	8.10	6.96	6.49	10.11	7.61	9.18	7.18	7.96
Na_2O	2.80	3.75	3.63	2.75	3.13	2.67	3.03	3.22
K_2O	1.69	2.10	2.18	1.15	1.80	1.57	2.01	1.60
P_2O_5	0.14	0.21	0.22	0.18	0.20	0.22	0.15	0.22
L.O.I	-0.07	0.00	0.06	0.02	0.03	0.11	0.65	0.20
Total	99.46	100.00	99.55	99.75	99.80	98.69	99.19	100.14

	ESAL21	ESAL22	ESAL23
SiO_2	55.25	54.08	53.17
TiO_2	0.59	0.72	0.67
Al_2O_3	16.10	18.80	17.67
Fe_2O_3	8.72	9.51	9.56
MnO	0.17	0.19	0.16
MgO	6.02	3.31	4.52
CaO	9.60	8.52	10.35
Na_2O	2.58	2.76	2.27
K_2O	1.25	1.16	1.19
P_2O_5	0.18	0.18	0.20
L.O.I	0.02	0.34	0.04
Total	100.48	99.57	99.80

	ESAL25	ESAL27	ESAL24
SiO_2	54.31	53.82	60.56
TiO_2	0.70	0.68	0.55
Al_2O_3	19.05	19.13	17.09
Fe_2O_3	8.50	8.71	6.71
MnO	0.15	0.15	0.15
MgO	3.09	3.39	2.49
CaO	9.17	9.58	6.25
Na_2O	3.12	2.59	3.33
K_2O	1.55	1.48	2.43
P_2O_5	0.21	0.25	0.22
L.O.I	0.43	0.02	0.16
Total	100.28	99.80	99.94

STROMBOLI OLDER SERIES

	StC5	StC14	StD5	StD6	StD7	StD8	StB38	StB42
SiO_2	54.24	52.33	51.68	52.18	57.38	51.71	51.89	53.49
TiO_2	0.67	1.04	0.74	0.98	0.70	0.75	1.01	0.78
Al_2O_3	14.70	18.91	16.78	17.16	17.05	16.81	17.59	17.00
Fe_2O_3	8.32	8.70	8.25	8.49	6.17	8.22	9.01	8.07
MnO	0.17	0.16	0.15	0.16	0.16	0.15	0.16	0.14
MgO	6.62	3.24	6.87	5.06	3.24	7.05	4.16	5.55
CaO	10.18	8.83	10.78	9.25	6.62	10.82	8.79	9.81
Na_2O	1.86	3.16	2.62	3.13	3.43	2.57	2.73	2.83
K_2O	1.47	2.89	1.78	2.56	3.01	1.75	2.65	1.68
P_2O_5	0.22	0.75	0.28	0.37	0.32	0.30	0.61	0.27
L.O.I	1.03	0.17	0.04	0.18	1.82	-0.01	0.31	0.11
Total	99.48	100.18	99.97	99.52	99.90	100.12	98.91	99.73

	StD10	StD12	StB5	StB14	StB12	StB34	StB45	ESTR05
SiO_2	51.60	52.97	52.40	57.94	56.12	54.64	56.12	54.26
TiO_2	0.75	0.82	0.95	0.77	0.88	0.78	0.80	0.68
Al_2O_3	16.68	17.62	17.53	16.96	17.17	16.77	17.75	14.92
Fe_2O_3	8.24	8.12	8.67	6.68	7.70	7.27	7.35	8.32
MnO	0.15	0.15	0.14	0.15	0.16	0.14	0.14	0.16
MgO	6.84	4.81	4.81	2.98	3.71	4.31	3.26	6.56
CaO	10.83	9.31	9.55	6.69	7.70	8.43	7.36	9.94
Na_2O	2.65	2.63	2.95	3.45	3.42	2.77	3.55	2.51
K_2O	1.74	2.97	1.78	2.94	2.57	2.75	3.07	1.51
P_2O_5	0.30	0.43	0.31	0.29	0.35	0.38	0.36	0.20
L.O.I	0.03	0.14	1.06	0.50	0.21	1.42	0.45	0.10
Total	99.81	99.97	100.15	99.35	99.99	99.66	100.21	99.16

STROMBOLI YOUNGER SERIES

	StA1	StA3	StB20	StB29	StD4	StD11
SiO_2	50.87	51.21	50.24	50.88	51.16	52.97
TiO_2	0.92	0.89	0.91	0.90	0.91	0.82
Al_2O_3	16.52	15.94	16.37	15.93	15.58	16.48
Fe_2O_3	8.60	8.50	8.47	8.53	8.60	8.54
MnO	0.16	0.15	0.15	0.15	0.15	0.15
MgO	5.79	5.96	5.59	6.04	6.13	5.73
CaO	10.01	10.12	9.84	10.10	10.18	10.04
Na_2O	2.48	1.96	2.31	2.42	2.09	2.52
K_2O	3.58	3.81	3.54	3.65	3.49	3.73
P_2O_5	0.68	0.71	0.66	0.69	0.57	0.66
L.O.I	0.12	0.39	1.07	0.15	0.50	-0.15
Total	99.73	99.64	99.15	99.44	99.36	101.49

	StB32	StC9	StC19	StD1	ESTR08
SiO_2	50.82	50.48	51.30	50.44	50.73
TiO_2	0.89	0.91	0.89	0.90	0.94
Al_2O_3	15.86	16.46	15.77	16.21	15.79
Fe_2O_3	8.48	8.53	8.57	8.62	8.92
MnO	0.15	0.16	0.16	0.17	0.16
MgO	5.99	5.52	6.14	5.80	5.77
CaO	10.05	9.84	10.20	9.92	9.97
Na_2O	2.41	2.15	2.20	2.29	2.50
K_2O	3.95	3.50	3.49	3.45	3.68
P_2O_5	0.59	0.65	0.58	0.69	0.67
L.O.I	0.37	0.82	0.33	1.27	0.07
Total	99.56	99.02	99.63	99.76	99.20

STROMBOLI RECENT LAVAS

	St72	StC18	ESTR06
SiO_2	49.70	50.05	49.53
TiO_2	0.90	0.87	0.86
Al_2O_3	16.59	16.78	15.21
Fe_2O_3	8.76	9.05	8.63
MnO	0.16	0.16	0.16
MgO	6.61	6.47	7.63
CaO	11.43	11.44	11.80
Na_2O	2.43	2.52	2.37
K_2O	2.15	2.24	1.99
P_2O_5	0.58	0.46	0.50
L.O.I	0.34	0.02	0.16
Total	99.65	100.06	98.84

VULCANO OLDER SERIES

	EVUL01	EVUL02	EVUL03	EVUL10	EVUL29	85/VUL/03	85/VUL/06
SiO_2	53.43	53.58	53.00	52.55	53.61	52.25	55.25
TiO_2	0.72	0.74	0.76	0.79	0.73	0.72	0.63
Al_2O_3	17.93	17.89	17.53	16.27	18.37	16.17	18.64
Fe_2O_3	8.50	8.55	9.12	9.19	8.50	9.48	7.04
MnO	0.20	0.13	0.15	0.17	0.20	0.16	0.08
MgO	3.17	3.85	3.99	4.83	3.08	5.21	1.28
CaO	7.69	7.63	7.91	8.94	7.14	9.08	3.51
Na_2O	3.50	3.23	3.75	3.27	3.49	2.95	3.92
K_2O	3.54	3.21	3.41	2.71	3.56	2.87	5.88
P_2O_5	0.38	0.35	0.38	0.28	0.42	0.32	0.45
L.O.I	0.33	0.67	0.00	0.69	0.99	0.36	1.85
Total	99.39	99.83	100.00	99.69	100.09	99.57	98.53

	EVUL17	EVUL18	EVUL20	EVUL21	85/VUL/04	85/VUL/05
SiO_2	49.62	52.70	48.51	52.53	51.64	52.46
TiO_2	0.75	0.82	0.70	0.73	0.68	0.74
Al_2O_3	15.52	16.31	13.79	16.76	16.93	16.46
Fe_2O_3	9.95	9.35	10.07	9.29	8.70	8.97
MnO	0.20	0.16	0.20	0.23	0.15	0.16
MgO	6.26	4.35	7.66	4.51	4.75	4.45
CaO	10.79	8.51	12.54	8.44	8.95	8.05
Na_2O	2.73	2.72	1.84	3.32	3.66	3.20
K_2O	1.97	2.93	1.69	3.19	2.95	3.19
P_2O_5	0.32	0.33	0.28	0.37	0.37	0.35
L.O.I	1.35	1.03	1.55	0.06	0.37	0.35
Total	99.46	99.21	98.83	99.43	99.15	98.38

VULCANO YOUNGER SERIES

	EVUL06	EVUL08	EVUL09	EVUL11	EVUL24	EVUL25	EVUL26
SiO_2	66.17	62.20	58.64	51.79	59.82	69.46	70.60
TiO_2	0.29	0.41	0.51	0.66	0.48	0.19	0.18
Al_2O_3	14.86	15.20	15.97	14.96	16.15	13.77	13.87
Fe_2O_3	4.15	5.37	6.69	9.03	6.33	3.18	2.96
MnO	0.10	0.12	0.12	0.17	0.13	0.07	0.09
MgO	1.17	2.08	2.47	4.78	2.14	1.05	0.85
CaO	2.66	4.04	5.13	8.60	4.58	2.06	2.02
Na_2O	4.27	4.21	3.85	3.51	4.06	4.01	3.99
K_2O	5.53	5.40	5.51	4.53	5.68	4.98	5.01
P_2O_5	0.18	0.27	0.32	0.44	0.31	0.15	0.10
L.O.I	0.40	0.39	0.26	0.36	0.36	0.43	0.62
Total	99.78	99.69	99.47	98.83	100.04	99.35	100.29

	EVUL13	EVUL14	EVUL16	EVUL23	EVUL30	85/VUL/01	EVUL28
SiO_2	57.32	52.35	50.86	73.16	58.39	66.75	68.74
TiO_2	0.53	0.67	0.77	0.12	0.52	0.24	0.24
Al_2O_3	15.14	15.32	16.16	14.03	16.01	13.96	14.29
Fe_2O_3	7.40	9.02	10.06	2.23	6.75	3.62	3.63
MnO	0.14	0.17	0.17	0.08	0.12	0.08	0.08
MgO	3.49	4.79	3.69	0.27	2.35	1.38	1.27
CaO	6.38	8.41	8.06	0.98	5.24	2.32	2.57
Na_2O	3.80	3.86	2.71	4.20	4.24	4.31	4.16
K_2O	5.04	4.68	4.22	5.36	5.47	4.96	5.03
P_2O_5	0.34	0.46	0.51	0.03	0.35	0.14	0.11
L.O.I	0.05	0.02	1.41	0.10	0.13	1.26	0.08
Total	99.63	99.75	98.62	100.56	99.57	99.02	100.20

CRUSTAL XENOLITHS (SALINA)

	SA270	SA156	85/SAL/07	SA309
SiO_2	55.02	47.99	30.14	45.37
TiO_2	0.90	1.44	0.37	2.04
Al_2O_3	20.12	18.39	8.85	14.55
Fe_2O_3	7.42	8.55	3.48	10.24
MnO	0.11	0.17	0.07	0.23
MgO	3.27	6.88	3.38	6.99
CaO	2.64	12.03	33.82	14.33
Na_2O	5.34	2.26	0.47	2.07
K_2O	2.78	0.36	0.08	0.45
P_2O_5	0.15	0.20	0.07	0.30
L.O.I	2.57	1.60	20.25	1.37
Total	100.32	99.87	99.98	98.01

	ST12	85/SAL/04	GXSALI	GXSAL II
SiO_2	48.18	74.42	64.26	68.80
TiO_2	1.41	0.24	0.52	0.39
Al_2O_3	20.60	14.20	16.68	15.03
Fe_2O_3	7.51	1.01	3.80	3.20
MnO	0.13	0.01	0.08	0.03
MgO	5.08	1.21	1.64	1.23
CaO	11.31	2.65	5.12	3.20
Na_2O	4.25	2.96	3.86	3.75
K_2O	0.35	2.22	2.66	3.30
P_2O_5	0.18	0.18	0.18	0.12
L.O.I	0.49	0.50	1.19	0.70
Total	99.49	99.60	99.99	99.78

Rb, Sr, Y, Zr, Nb, Pb are averages of analyses by EDXRF (O.U.) and XRF (University of Nottingham).
Ba, Ni, Cr, V analysed by XRF (University of Nottingham)
Samples with no Ba, Ni, Cr, V analyses were analysed only by EDXRF (O.U.)
La, Ce, Nd, Sm, Eu, Tb, Yb, Lu, Sc, Co, Hf, Ta, Th, U analysed by INAA.

SALINA

Trace Element Data

	ESAL02	ESAL03	ESAL05	ESAL06	ESAL08	ESAL09	ESAL12	ESAL13	ESAL14
Ba	270	398	585	493	513	545	393	314	386
Rb	26	32	58	40	52	56	26	18	25
Sr	737	629	648	600	650	647	712	614	398
Y	18	20	24	20	23	23	15	16	16
Zr	64	71	107	84	95	106	59	60	58
Nb	4	5	8	6	6	7	4	5	5
Pb	10	12	12	14	12	14	10	10	8
Ni	12	6	5		2		19	38	21
Cr	27	32	10	18	33	23	52	140	64
V	236	231	111	191	165	121	268	253	265
La	13.4	16.9	24.2						17.00
Ce	26.8	31.6	45.7						29.9
Nd	16	17.9	23.3						16.5
Sm	3.24	3.51	4.35						3.43
Eu	1.05	1.08	1.21						1.09
Tb	0.56	0.57	0.64						0.53
Yb	1.86	2.04	2.49						1.77
Lu	0.31	0.34	0.42						0.28
Sc	13	14	7						17
Co	26	25	13						30
Hf	1.54	1.76	2.66						1.61
Ta	0.21	0.23	0.37						0.17
Th	2.6	3.9	6.03						3.4
U	0.9	1.5	2.2						1

	ESAL15	ESAL16	ESAL17	ESAL18	ESAL19	ESAL20	ESAL21	ESAL22	ESAL23
Ba	459	461	376	350	649	471	403	374	373
Rb	45	38	30	22	54	40	28	26	30
Sr	581	782	710	647	616	662	570	614	658
Y	23	20	17	16	18	24	18	18	18
Zr	94	78	64	60	108	84	66	63	64
Nb	6	6	5	4	10	7	4	6	5
Pb	11	10	12	10	13	12	10	10	8
Ni	5	2	17	20	6	6	28	2	18
Cr	32	24	85	64	24	35	123	45	32
V	183	213	247	261	132	214	230	235	279
La				14.4	26.4				15.9
Ce				27.7	48.2				30.7
Nd				15.8	20.9				17.6
Sm				3.15	3.83				3.56
Eu				0.99	1.08				1.13
Tb				0.58	0.47				0.58
Yb				1.81	1.93				1.93
Lu				0.27	0.33				0.30
Sc				16	8				18
Co				30	16				30
Hf				1.47	2.53				1.34
Ta				0.17	0.44				0.18
Th				3.3	8.02				3.2
U				1.1	2.4				1 4

	ESAL24	ESAL25	ESAL27
Ba	565	463	433
Rb	62	37	33
Sr	660	778	750
Y	24	20	16
Zr	108	77	74
Nb	8	6	6
Pb	16	11	10
Ni	3	6	8
Cr	16	45	26
V	113	230	230
La	23.1		19.4
Ce	45.2		37.7
Nd	22.6		20.7
Sm	4.36		3.87
Eu	1.21		1.21
Tb	0.65		0.63
Yb	2.44		1.90
Lu	0.40		0.31
Sc	7		11
Co	14		22
Hf	2.54		1.73
Ta	0.36		0.40
Th	5.9		4.6
U	2.6		1.7

STROMBOLI OLDER SERIES

	StB14	StB12	StB34	StB38	StB42	StB45	ESTR05
Ba	889	745	960	1011	656	968	507
Rb	90	79	88	81	44	96	44
Sr	508	597	655	670	641	590	506
Y	27	28	27	36	23	30	20
Zr	195	177	187	192	121	212	108
Nb	16	18	24	22	12	22	10
Pb	12	14	18	18	12	19	13
Ni	8	7	27	22	33	9	49
Cr	17	40	72	62	121	30	200
V	152	178	192	241	237	170	199
La	47.7				32.8	54.7	
Ce	85.00				62.1	97.4	
Nd	34.7				29.6	43.2	
Sm	6.32				5.67	7.50	
Eu	1.64				1.54	1.83	
Tb	0.83				0.77	0.93	
Yb	2.68				2.28	3.00	
Lu	0.44				0.39	0.49	
Sc	15				14	17	
Co	16				25	18	
Hf	4.64				2.85	4.92	
Ta	0.95				0.61	1.28	
Th	18				10.6	22.7	
U	4.4				2.9	5.7	

	StC5	StC14	StD5	StD6	StD7	StD8	StD10	StD12	StB5
Ba	507	1054	732	837	929	709	717	1102	522
Rb	44	83	62	78	99	59	58	96	52
Sr	506	759	502	632	530	498	502	646	524
Y	20	33	22	30	31	23	23	28	28
Zr	108	210	123	182	213	120	122	187	147
Nb	10	23	14	20	22	13	14	22	14
Pb	13	20	16	17	20	15	20	20	12
Ni	49	9	55	27	22	58	56	24	24
Cr	200	22	137	73	65	159	144	69	52
V	199	244	217	226	118	210	213	201	219
La		47.7			55.1	30.9			
Ce		85.00			102.7	57.4			
Nd		34.7			42.6	28.2			
Sm		6.32			7.57	5.50			
Eu		1.64			1.84	1.49			
Tb		0.83			1.03	0.80			
Yb		2.68			2.94	2.16			
Lu		0.44			0.51	0.36			
Sc		17			7	34			
Co		22			18	31			
Hf		4.80			5.07	2.89			
Ta		1.36			1.21	0.75			
Th		19.2			20.1	12.2			
U		4.5			5.4	3.2			

STROMBOLI YOUNGER SERIES

	StA1	StA3	StB20	StB29	StB32	StC9	StC19	StD1	StD4
Ba	1748	1547	1732	1606	1543	1754	1419	1776	1442
Rb	110	134	102	98	132	115	119	115	120
Sr	875	780	846	778	776	876	708	842	689
Y	30	31	32	29	29	36	30	30	30
Zr	192	192	189	194	192	194	180	186	182
Nb	26	25	26	26	25	28	22	26	23
Pb	28	26	26	26	27	26	26	28	20
Ni	35	36	37	37	38	35	46	56	43
Cr	89	114	76	105	105	79	142	91	121
V	237	223	233	31	234	226	218	223	228
La					55.4			5.03	
Ce					106.3			106.4	
Nd					53.9			55.7	
Sm					10.70			10.80	
Eu					2.53			2.81	
Tb					1.16			1.17	
Yb					2.38			2.43	
Lu					0.36			0.41	
Sc					31			32	
Co					29			32	
Hf					4.74			4.76	
Ta					1.45			1.80	
Th					20.6			15.4	
U					6.1			3.6	

STROMBOLI RECENT LAVAS

	StD11	ESTR08	St72	StC18	ESTR06
Ba	1750	1760	944	1307	987
Rb	116	127	70	65	62
Sr	884	882	762	816	712
Y	31	32	30	28	28
Zr	191	192	172	160	159
Nb	28	27	22	21	20
Pb	28	26	20	20	18
Ni	34	31	47	36	92
Cr	73	58	126	79	200
V	231	227	242	260	232
La				59.2	44.8
Ce				108	91.1
Nd				48.6	46.3
Sm				9.40	8.91
Eu				2.34	2.25
Tb				1.14	1.18
Yb				2.52	2.33
Lu				0.39	0.40
Sc				34	14
Co				32	35
Hf				3.94	3.65
Ta				1.19	1.15
Th				18.5	15.4
U				4.7	4.5

VULCANO OLDER SERIES

	EVUL01	EVUL02	EVUL03	EVUL10	EVUL17	EVUL18	EVUL20	EVUL21	EVUL29
Ba	916	803	892	703	725	742	621	869	940
Rb	90	82	86	68	37	68	24	80	88
Sr	1258	1130	1102	1092	1223	1174	1074	1112	1137
Y	30	54	44	30	20	26	22	34	53
Zr	138	144	138	118	102	138	88	128	136
Nb	12	12	12	11	9	12	8	12	12
Pb	16	16	14	12	12	16	12	14	16
Ni	15	13	15	21	23	13	37	21	14
Cr	48	30	49	66	56	52	154	43	41
V	180	192	207	208	244	219	261	223	178
La		47.3	49.4		32.7	37.6	34.00	48.5	51.1
Ce		91.8	91.00		61.3	72.8	66.3	91.00	87.7
Nd		46.2	44.1		31.8	35.1	36.5	44.7	45.8
Sm		9.80	8.52		6.38	6.97	7.05	8.71	9.16
Eu		2.46	2.07		1.72	1.77	1.83	2.08	2.42
Tb		1.37	1.13		0.81	0.85	0.84	1.15	1.55
Yb		4.11	2.98		1.81	2.37	2.04	3.14	4.09
Lu		0.65	1.51		0.30	0.38	0.35	0.52	0.73
Sc		9	10		16	11	15	12	8
Co		21	25		33	25	39	32	26
Hf		3.44	3.19		2.44	3.42	2.31	3.14	3.30
Ta		0.77	0.69		0.43	0.76	0.39	0.68	0.75
Th		12.2	11.5		8	9.7	7	11.2	12.5
U		3.9	3.6		2.4	3.1	2.2	3.7	4.1

	85/VUL/03	85/VUL/05	85/VUL/04
Ba			
Rb	75	83	79
Sr	1113	1128	1313
Y	19	20	16
Zr	122	137	112
Nb	9	11	9
Pb	8	11	13
Ni			
Cr			
V			
La	36.7	38.7	36.00
Ce	69.7	71.9	65.9
Nd	32.1	33.3	27.3
Sm	6.36	6.13	5.42
Eu	1.61	1.59	1.50
Tb	0.77	0.75	0.64
Yb	1.92	1.88	1.59
Lu	0.31	0.31	0.26
Sc	15	11	11
Co	27	25	27
Hf	2.94	3.06	2.58
Ta	0.56	0.63	0.53
Th	10	10.8	9.3
U	2.8	3.1	1.9

VULCANO YOUNGER SERIES

	EVUL06	EVUL08	EVUL09	EVUL11	EVUL13	EVUL14	EVUL16	EVUL23	EVUL24
Ba	394	585	722	1020		1027	1075	75	724
Rb	253	236	196	134	193	153	122	306	211
Sr	392	647	869	1127	923	1214	1366	74	827
Y	40	36	30	23	30	26	38	50	33
Zr	243	238	259	153	208	164	157	228	278
Nb	33	32	27	18	24	20	21	45	28
Pb	30	28	20	20	27	25	20	32	26
Ni	4	7	5	20		19	15		7
Cr	32	29	27	66		65	27	31	39
V	38	75	105	184		178	248	9	89
La			71.2	59.4	67.3		57.00	84.7	
Ce			129.4	109.4	122.2		111.4	152.2	
Nd			51.3	48.00	50.6		52.5	57.9	
Sm			8.91	8.53	9.12		10.11	10.14	
Eu			1.43	1.89	1.51		2.27	0.28	
Tb			1.22	0.87	1.34		1.23	1017.00	
Yb			2.92	2.29	2.85		2.93	5.30	
Lu			0.51	0.35	0.48		0.47	0.80	
Sc			6	11	8		9	1	
Co			16	29	22		33	2	
Hf			6.55	4.11	5.44		4.00	7.54	
Ta			1.78	1.21	1.69		1.23	3.08	
Th			40.3	23.8	35.9		20.8	64	
U			12.2	6	10.8		6.4	20.2	

	EVUL25	EVUL26	EVUL28	EVUL30	85/VUL/01	85/VUL/06
Ba	163	152	270	758		
Rb	264	270	249	185	254	121
Sr	226	202	349	918	351	1588
Y	35	47	40	31	43	51
Zr	190	196	182	250	174	205
Nb	32	34	30	26	28	24
Pb	24	28	27	24	20	23
Ni	5	4	7	11		
Cr	34	32	33	33		
V	40	30	52	102		
La		63.3				
Ce		124.8				
Nd		52.2				
Sm		9.51				
Eu		0.43				
Tb		1.09				
Yb		4.81				
Lu		0.72				
Sc		3				
Co		5				
Hf		6.63				
Ta		2.57				
Th		51.3				
U		16.1				

CRUSTAL XENOLITHS (SALINA)

	SA270	SA156	85/SAL/07	SA309	ST12	85/SAL/04	GXSALI
Ba							
Rb	64	13	3	17	6	108	75
Sr	547	376	2688	375	284	209	751
Y	34	22	22	42	23	16	21
Zr	169	102	150	200	124	62	126
Nb	17	17	8	8	7	9	11
Pb	27	3	6	4	3	10	6
Ni							
Cr							
V							
La	51.4	12.9		8.92	5.1	11.8	28.7
Ce	98.2	31.3		23.5	14.7	25	54
Nd	45.2	19.6		19.6	12	12.7	23
Sm	8.85	4.4		5.6	3.49	2.8	4.39
Eu	2.14	1.74		1.92	1.36	0.57	1.28
Tb	1.26	0.71		0.65	0.68	0.49	0.67
Yb	3.65	2.09		4.16	2.33	1.36	2.19
Lu	0.6	0.36		0.69	0.38	0.22	0.4
Sc		18		15	14	2	6
Co		25		27	35	1.6	4
Hf		2.51		4.49	2.71	2.07	2.99
Ta		1.02		0.58	0.36	1.41	0.51
Th		0.65		0.54	0.3	4.75	8.5
U		1.14		0.65		7.6	2.8

Isotope Data

	$^{87}Sr/^{86}Sr$	$^{143}Nd/^{144}Nd$	$^{206}Pb/^{204}Pb$	$^{207}Pb/^{204}Pb$	$^{208}Pb/^{204}Pb$
STROMBOLI OLDER SERIES					
StC5	0.70352±40	0.512537±18			
StC14	0.705805±30	0.512574±24	19.093±7	15.697±7	39.08±2
StD7	0.705599±26	0.512509±14			
StD8	0.706153±32	0.512564±8	19.034±5	15.666±4	39.068±6
StB5	0.706064±42	0.512564±14			
StB14	0.706031±26	0.512527±20			
StB38	0.705722±46	0.512583±18			
StB42	0.704985±28	0.512649±14	19.200±14	15.665±12	39.16±4
StB45	0.706102±30	0.5512545±10			
STROMBOLI YOUNGER SERIES					
StB20	0.706859±38	0.512515±20			
StB29	0.707369±38	0.512455±16			
StB32	0.707508±28	0.512426±12	18.934±8	15.644±8	39.01±2
StD1	0.706785±38	0.512558±20	19.010±1	15.691±1	39.157±5
StC18	0.706537±38	0.512493±20			
ESTR06	0.706116±20	0.512544±20			
SALINA					
ESAL02	0.704524±22	0.512758±16			
ESAL03	0.704262±44	0.512817±12	19.365±11	15.610±10	39.08±5
ESAL05	0.704602±40	0.512759±8	19.235±9	15.644±8	39.04±2
ESAL14	0.704112±44	0.512774±26	19.770±16	15.676±14	39.50±3
ESAL18	0.704634±32	0.512716±16			
ESAL19	0.704660±36	0.512707±24	19.275±11	15.599±9	39.05±2
ESAL23	0.704221±22	0.512788±16	19.608±10	15.643±9	39.36±2
ESAL24	0.704645±44	0.512779±26			
ESAL27	0.704493±26	0.512669±28			
VULCANO OLDER SERIES					
EVUL01	0.704569±46				
EVUL02	0.704625±30	0.512604±14	19.477±10	15.625±12	39.27±3
EVUL03	0.704641±28	0.512634±10			
EVUL17	0.704453±22	0.512752±10			
EVUL18	0.704937±34	0.512544±12			
EVUL20	0.704315±34	0.512716±12	19.532±5	15.671±5	39.358±11
EVUL21	0.704610±38				
85/VUL/03	0.704521±32	0.512681±16			
85/VUL/05	0.704592±26	0.512680±12	19.572±4	15.681±3	39.426±8
85/VUL/04		0.512748±12			
VULCANO YOUNGER SERIES					
EVUL06	0.704740±38	0.512580±10	19.302±10	15.645±8	39.330±8
EVUL09	0.704568±48	0.512616±20			
EVUL11	0.704578±32	0.512645±22	19.414±3	15.686±5	39.330±8
EVUL13	0.704578±24	0.512628±24			
EVUL16			19.292±22	15.626±17	39.16±5
EVUL23	0.704942±26	0.512617±10	19.194±10	15.503±9	38.74±2
EVUL24	0.704578±26	0.512578±16			
EVUL26	0.704654±28	0.512630±16			
EVUL28	0.704524±38	0.512686±12			
CRUSTAL XENOLITHS (SALINA)					
ST12	0.7035±5	0.5130±3			
85/SAL/04	0.7142±3	0.5123±2			
GXSAL1	0.70548±6	0.512685±10			

CIPW NORMATIVE COMPOSITIONS

STROMBOLI OLDER SERIES

	StB5	StB12	StB14	StB34	StB38	StB42	StB45	StC5
Q	0.68	4.00	7.22	3.88	0.46	1.76	2.65	6.90
Or	10.53	15.20	17.39	16.27	15.67	9.94	18.16	8.69
Ab	24.93	28.90	29.16	23.41	23.07	23.92	30.00	15.72
An	29.29	23.86	22.06	25.15	27.86	28.68	23.38	27.38
Lc								
Ne								
C								
Wo	6.72	5.04	3.86	5.93	4.92	7.62	4.51	9.07
En	3.58	2.54	1.88	3.23	2.44	4.36	2.19	5.39
Fs	2.91	2.38	1.91	2.48	2.38	2.92	2.24	3.20
En	8.44	6.73	5.57	7.54	7.96	9.52	5.96	11.16
Fs	6.86	6.31	5.64	5.79	7.77	6.37	6.10	6.64
Fo								
Fa								
Mt	1.88	1.68	1.45	1.58	1.96	1.75	1.59	1.81
Il	1.80	1.67	1.46	1.48	1.92	1.48	1.52	1.27
Ap	0.72	0.81	0.67	0.88	1.41	0.63	0.83	0.51
Pl	54.22	51.77	51.22	48.56	50.94	52.59	53.38	43.10
Di	13.22	9.96	7.66	11.65	9.74	14.90	8.94	17.66
Hy	15.30	13.04	11.21	13.33	15.73	15.88	12.05	17.80
Ol								

	StC14	StD5	StD6	StD7	StD8	StD10	StD12	ESTR05
Q				6.45				3.85
Or	17.09	10.53	15.14	17.80	10.35	10.25	17.57	8.93
Ab	26.71	22.14	26.45	28.99	21.72	22.40	22.23	21.21
An	28.82	28.72	25.16	22.19	29.12	28.43	27.45	24.94
Lc								
Ne								
C								
Wo	4.22	9.58	7.65	3.58	9.45	9.75	6.66	9.64
En	1.91	5.80	4.20	1.86	5.77	5.90	3.62	5.72
Fs	2.29	3.24	3.16	1.62	3.13	3.31	2.80	3.42
En	4.48	5.81	3.06	6.24	6.44	5.62	7.54	10.68
Fs	5.36	3.25	2.30	5.41	3.49	3.15	5.83	6.39
Fo	1.20	3.89	3.78		3.79	3.90	0.61	
Fa	1.58	2.40	3.14		2.27	2.41	0.52	
Mt	1.90	1.80	1.84	1.35	1.78	1.78	1.77	1.81
Il	1.98	1.41	1.86	1.33	1.42	1.42	1.56	1.29
Ap	1.74	0.65	0.86	0.74	0.70	0.70	1.00	0.46
Pl	55.53	50.86	51.62	51.18	50.84	50.83	49.67	46.16
Di	8.42	18.63	15.02	7.07	18.35	18.96	13.09	18.77
Hy	9.84	9.06	5.36	11.65	9.94	8.77	13.37	17.07
Ol	2.78	6.30	6.92		6.05	6.31	1.13	

STROMBOLI YOUNGER SERIES

	StA1	StA3	StB20	StB29	StB32	StC9	StC19
Q							
Or	21.18	22.54	20.94	21.59	23.36	20.7	20.64
Ab	18.83	16.57	19.32	18.25	15.71	18.17	18.59
An	23.32	23.39	23.79	21.77	20.74	24.87	22.79
Lc							
Ne	1.15		0.11	1.19	2.53		
C							
Wo	9.16	9.27	8.66	9.96	10.56	8.42	10.04
En	5.22	5.36	4.91	5.78	6.11	4.63	5.84
Fs	3.53	3.48	3.38	3.71	3.94	3.26	3.72
En		2.86				2.44	1.59
Fs		1.86				1.72	1.01
Fo	6.48	4.68	6.35	6.53	6.2	4.71	5.55
Fa	4.83	3.35	4.82	4.62	4.42	3.65	3.9
Mt	1.87	1.86	1.84	1.86	1.84	1.86	1.87
Il	1.75	1.69	1.73	1.71	1.69	1.73	1.69
Ap	1.58	1.64	1.53	1.6	1.37	1.51	1.34
Pl	42.15	39.95	43.1	40.02	36.45	43.04	41.39
Di	17.9	18.11	16.95	19.45	20.62	16.13	19.59
Hy		4.72				4.16	2.59
Ol	11.31	8.03	11.16	11.15	10.62	8.36	9.45

RECENT LAVAS

	StD1	StD4	StD11	ESTR08	ST72	StC18	ESTR06
Q							
Or	20.41	20.64	22.06	21.77	12.72	13.25	11.77
Ab	19.35	17.66	21.3	18.27	20.45	19.55	19.09
An	23.71	22.77	22.59	20.94	27.96	27.81	24.94
Lc							
Ne				1.55	0.05	0.95	0.51
C							
Wo	8.78	10.04	9.58	10.09	10.43	10.84	12.68
En	5	5.84	5.46	5.68	6.16	6.28	7.84
Fs	3.39	3.72	3.69	3.99	3.74	4.05	4.07
En	0.65	2.76	0.82				
Fs	0.44	1.76	0.55				
Fo	6.19	4.71	5.63	6.02	7.25	6.93	7.86
Fa	4.64	3.31	4.21	4.67	4.85	4.93	4.51
Mt	1.87	1.87	1.86	1.91	1.9	1.97	1.87
Il	1.71	1.73	1.75	1.79	1.71	1.65	1.63
Ap	1.6	1.32	1.53	1.55	1.34	1.07	1.16
Pl	43.06	40.43	43.88	39.21	48.41	47.36	44.04
Di	17.17	19.59	18.73	19.76	20.33	21.17	24.59
Hy	1.1	4.52	1.37				
Ol	10.84	8.02	9.84	10.69	12.11	11.86	12.38

SALINA

	ESAL01	ESAL02	ESAL03	ESAL05	ESAL06	ESAL08	ESAL09
Q		4.52	5.24	14.60	9.71	8.07	11.06
Or	7.57	6.39	7.99	13.84	10.00	12.42	12.89
Ab	18.17	19.19	23.24	28.82	23.66	31.69	30.68
An	37.16	38.93	31.24	24.34	29.33	22.05	23.58
Lc							
Ne							
C							
Wo	5.94	4.78	5.62	1.65	4.16	4.64	3.00
En	2.70	2.26	2.81	0.69	2.00	2.03	1.32
Fs	3.19	2.46	2.69	0.96	2.10	2.61	1.67
En	8.22	7.82	8.51	4.68	7.15	5.42	5.13
Fs	9.72	8.51	8.12	6.54	7.52	6.97	6.48
Fo	0.77						
Fa	1.01						
Mt	2.55	1.99	1.96	1.38	1.75	1.74	1.49
Il	1.22	1.23	1.16	1.04	1.14	1.18	1.08
Ap	0.42	0.44	0.39	0.53	0.32	0.49	0.51
Pl	55.33	58.11	54.48	53.16	52.99	53.75	54.26
Di	11.84	9.50	11.12	3.30	8.26	9.28	6.00
Hy	17.94	16.32	16.64	11.22	14.67	12.39	11.60
Ol	1.78						

	ESAL16	ESAL17	ESAL18	ESAL19	ESAL20	ESAL21	ESAL22
Q	5.66	1.58	3.42	13.06	7.73	5.48	6.98
Or	9.29	7.33	5.26	11.89	9.46	7.39	6.86
Ab	22.57	21.97	17.66	25.61	27.21	21.81	23.33
An	34.90	34.88	35.28	26.75	28.64	28.62	35.43
Lc							
Ne							
C							
Wo	3.86	6.31	7.06	3.30	3.94	7.46	2.37
En	1.72	3.21	3.84	1.67	1.74	4.21	1.01
Fs	2.12	2.94	2.97	1.56	2.19	2.93	1.37
En	6.31	8.66	10.61	5.98	6.41	10.84	7.27
Fs	7.79	7.92	8.19	5.59	8.07	7.56	9.94
Fo							
Fa							
Mt	1.83	1.97	2.02	1.30	1.90	1.90	2.07
Il	1.33	1.20	1.14	0.97	1.39	1.12	1.37
Ap	0.51	0.44	0.39	0.35	0.51	0.42	0.42
Pl	57.46	56.85	52.95	52.36	55.85	50.42	58.76
Di	7.69	12.46	13.87	6.53	7.87	14.59	4.75
Hy	14.10	16.59	18.80	11.57	14.48	18.40	17.21
Ol							

	ESAL12	ESAL13	ESAL14	ESAL15
Q	1.47		4.51	10.02
Or	6.80	5.91	6.51	10.65
Ab	23.24	21.04	16.82	26.45
An	31.77	32.40	35.33	27.30
Lc				
Ne				
C				
Wo	7.19	9.20	6.30	3.83
En	3.81	5.16	3.38	1.82
Fs	3.16	3.65	2.71	1.96
En	9.74	8.62	10.79	6.61
Fs	8.07	6.10	8.63	7.11
Fo		1.85		
Fa		1.44		
Mt	2.04	2.10	2.06	1.68
Il	1.22	1.23	1.20	1.23
Ap	0.42	0.46	0.30	0.46
Pl	55.02	53.45	52.15	53.76
Di	14.16	18.01	12.39	7.60
Hy	17.81	14.72	19.43	13.72
Ol		3.29		

	ESAL23	ESAL24	ESAL25	ESAL27
Q	5.22	12.91	4.36	5.64
Or	7.04	14.37	9.17	8.75
Ab	19.19	28.14	26.37	21.89
An	34.46	24.46	33.35	36.15
Lc				
Ne				
C				
Wo	6.52	2.14	4.51	4.08
En	3.18	0.94	1.96	1.83
Fs	3.21	1.20	2.54	2.22
En	8.12	5.29	5.76	6.64
Fs	8.20	6.75	7.45	8.06
Fo				
Fa				
Mt	2.07	1.46	1.86	1.90
Il	1.27	1.04	1.33	1.29
Ap	0.46	0.51	0.49	0.58
Pl	53.65	52.60	59.72	58.04
Di	12.91	4.28	9.01	8.14
Hy	16.32	12.03	13.21	14.70
Ol				

VULCANO OLDER SERIES

	EVUL01	EVUL02	EVUL03	EVUL10	EVUL17	85/VUL/05
Q						
Or	20.94	18.99	20.17	16.03	11.65	18.87
Ab	29.58	27.30	28.59	27.64	22.10	27.05
An	22.71	24.78	20.88	21.67	24.23	21.08
Lc						
Ne			1.68		0.53	
C						
Wo	5.42	4.51	6.64	8.72	11.37	6.93
En	2.38	2.18	3.16	4.49	6.23	3.48
Fs	3.02	2.26	3.39	4.00	4.72	3.29
En	1.50	5.95		1.99		2.83
Fs	1.90	6.15		1.77		2.68
Fo	2.83	1.05	4.77	3.92	6.60	3.38
Fa	3.96	1.19	5.65	3.86	5.52	3.53
Mt	1.86	1.86	1.99	2.00	2.16	1.96
Il	1.37	1.41	1.44	1.50	1.42	1.41
Ap	0.88	0.81	0.88	0.65	0.74	0.81
Pl	52.29	52.08	49.47	49.30	46.33	48.12
Di	10.83	8.95	13.18	17.20	22.31	13.70
Hy	3.40	12.10		3.77		5.50
Ol	6.78	2.24	10.42	7.78	12.11	6.91

	EVUL18	EVUL20	EVUL21	EVUL29	85/VUL/03	85/VUL/04
Q	0.46					
Or	17.33	10.00	18.87	21.06	16.98	17.45
Ab	22.99	15.55	28.06	29.50	24.93	25.09
An	23.59	24.34	21.36	23.89	22.36	21.01
Lc						
Ne						3.17
C						
Wo	6.89	15.06	7.56	3.68	8.61	8.77
En	3.37	8.78	3.73	1.60	4.49	4.57
Fs	3.38	5.54	3.68	2.08	3.87	3.95
En	7.50	1.52	0.08	3.28	2.70	
Fs	7.52	0.96	0.07	4.27	2.33	
Fo		6.20	5.23	1.98	4.08	5.12
Fa		4.32	5.69	2.84	3.89	4.88
Mt	2.03	2.19	2.02	1.86	2.06	1.90
Il	1.56	1.33	1.39	1.39	1.37	1.29
Ap	0.76	0.65	0.86	0.97	0.74	0.86
Pl	46.58	39.89	49.42	53.39	47.29	46.10
Di	13.64	29.39	14.98	7.35	16.97	17.28
Hy	15.02	2.47	0.15	7.56	5.03	
Ol		10.51	10.91	4.82	7.97	10.00

VULCANO YOUNGER SERIES

	EVUL06	EVUL08	EVUL09	EVUL11	EVUL13
Q	12.49	5.67	0.67		
Or	32.71	31.94	32.59	26.79	29.81
Ab	36.09	35.58	32.54	16.30	32.12
An	5.00.	6.58	9.97	11.64	9.32
Lc					
Ne				7.25	
C					
Wo	2.93	4.89	5.60	11.76	8.40
En	1.10	2.18	2.44	6.02	4.10
Fs	1.89	2.69	3.14	5.43	4.15
En	1.82	3.02	3.73	0.00	1.48
Fs	3.12	3.73	4.80	0.00	1.50
Fo				4.15	2.21
Fa				4.13	2.47
Mt	0.90	1.17	1.45	1.96	1.61
Il	0.55	0.78	0.97	1.25	1.01
Ap	0.42	0.63	0.74	1.02	0.79
Pl	41.09	42.16	42.51	27.93	41.44
Di	5.92	9.75	11.18	23.22	16.65
Hy	4.96	6.75	8.53		2.97
Ol				8.28	4.68

	EVUL24	EVUL25	EVUL26	EVUL28	EVUL30
Q	1.44	20.73	22.19	17.65	4.69
Or	33.60	29.46	29.63	29.75	29.75
Ab	34.31	33.89	33.72	35.16	35.16
An	9.01	4.82	5.10	5.42	10.11
Lc					
Ne					
C					
Wo	4.88	1.85	1.79	2.76	0.81
En	2.04	0.75	0.67	1.16	0.24
Fs	2.87	1.11	1.15	1.61	0.60
En	3.31	1.87	1.46	2.01	2.93
Fs	4.67	2.77	2.50	2.79	7.32
Fo					
Fa					
Mt	1.38	0.70	0.64	0.78	1.46
Il	0.91	0.36	0.34	0.46	0.99
Ap	0.72	0.35	0.23	0.25	0.25
Pl	43.33	38.71	38.82	40.58	45.26
Di	9.79	3.71	3.60	5.54	1.65
Hy	7.89	4.64	3.96	4.81	10.25
Ol					

	EVUL14	EVUL16	EVUL23
Q			24.79
Or	27.68	24.96	31.70
Ab	15.79	21.85	35.50
An	10.61	19.41	3.55
Lc			
Ne	9.12	0.57	
C			
Wo	11.74	7.21	0.47
En	6.03	3.14	0.10
Fs	5.41	4.05	0.40
En			0.58
Fs			2.41
Fo	4.16	4.26	
Fa	4.13	6.06	
Mt	1.96	2.19	0.48
Il	1.27	1.46	0.23
Ap	1.07	1.18	0.07
Pl	26.39	41.27	39.05
Di	23.18	14.41	0.96
Hy			2.99
Ol	8.29	10.32	

	85/VUL/01	85/VUL/06
Q	15.50	
Or	29.34	34.78
Ab	36.43	33.13
An	4.05	14.49
Lc		
Ne		
C		
Wo	2.73	
En	1.20	
Fs	1.53	
En	2.25	1.05
Fs	2.86	2.65
Fo		1.51
Fa		4.21
Mt	0.78	1.55
Il	0.46	1.20
Ap	0.32	1.04
Pl	40.48	47.62
Di	5.46	
Hy	5.11	3.69
Ol		

APPENDIX C

Analytical Techniques

C1. Powder Preparation

In all cases (except the crustal xenoliths), fresh rock samples in excess of 1 Kg were collected. A hydraulic splitter was used to break these down into around 3 cm cubes. Any weathered surfaces or amygdaloidal fragments were discarded and the remainder crushed to around 0.5 cm in a hardened steel jaw crusher. After cone and quartering, approximately 100g of crushed rock were powdered to 200 mesh in an agate "Tema" mill. The small (5-10 cm) crustal xenoliths were treated in a similar manner except that the initial splitting was carried out with a diamond saw in an effort to preserve as much relatively fresh rock as possible.

C2. X-Ray Fluoresence Techniques (Open University)

Energy dispersive X-ray fluoresence (EDXRF) techniques were used to analyse major elements and the trace elements; Rb, Sr, Y, Zr, Nb and Pb. Major elements were analysed using glass discs, made by mixing a 4:1 lithium metaborate:tetraborate mixture (Spectraflux 100B) with rock powder, dried overnight at 105°C, in the ratio 6:1. This mixture was fused in a Pt-Au alloy crucible in a muffle furnace at 1200°C for 15 minutes. Daily correction for flux weight loss was made and the flux : rock ratio adjusted accordingly. Loss on ignition data were obtained by heating pre-dried rock powder in a silica crucible at 1000°C for 20 minutes. Trace element analyses were performed on pressed powder pellets made by thoroughly mixing 6-8g of powder with a binding agent (Moviol), compressing into a 3cm diameter disc using a hydraulic press and drying overnight at 105°C.

Samples were analysed using a Link Systems 10-44 EDXRF spectrometer. This consisted of a low power (maximum 49 W) silver anode side window X-ray tube operated in pulsed mode with maximum setting of 49KV or 1mA, and a Si(Li) detector with a resolution of 165KeV at 5.9KeV. The EDXRF was calibrated using international standards covering a wide range of compositions. For major elements glass discs were counted in duplicate for 500 seconds at 10KV, 0.2mA with no primary beam filter. Pressed powder pellets were counted twice for 800 seconds at 45KeV, 0.3mA with a 127μm silver primary beam filter. Instrumental drift was monitored by analysis of international standards USGS AGV-1 (major elements) and USGS GSP-1 (trace elements) several times during each run. All major

element analyses were performed on duplicate discs prepared and analysed within the same batch of samples. Data presented are averages of duplicate analyses.

Full details of the EDXRF system are given in Potts *et al.* (1984) including precision and detection limits. The results for international standards analysed as unknowns are compared with the values given by Abbey (1980) in table C1. Results for several analyses of an internal reference rock (CMV120, a leucitite from M. Vico, Italy) are also given in this table.

	GSP-1 (this study)		GSP-1 (Abbey, 1980)	CMV120	
	n=9	2σ		n=7	2σ
SiO_2	67.22	(0.46)	67.32	54.35	(0.38)
TiO_2	0.68	(0.016)	0.66	0.70	(0.01)
Al_2O_3	15.20	(0.24)	15.28	17.06	(0.20)
Fe_2O_3	4.43	(0.038)	4.30	6.39	(0.054)
MnO	0.04	(0.008)	0.04	0.11	(0.01)
MgO	1.00	(0.09)	0.97	2.89	(0.19)
CaO	2.02	(0.014)	2.03	6.17	(0.05)
Na_2O	2.90	(0.28)	2.81	2.25	(0.82)
K_2O	5.54	(0.12)	5.51	8.19	(0.058)
P_2O_5	0.29	(0.054)	0.28	0.37	(0.032)

	AGV-1 (this study)		AGV-1 (Abbey, 1980)	CMV120	
	n=7	2σ		n=8	2σ
Rb	69	(4.2)	67	631	(11.6)
Sr	672	(7.8)	660	1325	(26.0)
Y	21	(0.74)	19	35*	(1.66)
Zr	238	(0.14)	230	374	(7.0)
Nb	15	------	16	22	(1.0)
Pb	36	(2.8)	33	71	(2.8)

* In high Rb samples such as CMV120, Y may be unreliable due to Rb interference

Table C1. Major and trace element standard data for EDXRF analyses.

C3. X-Ray Fluoresence Techniques (University of Nottingham)

The trace elements Ba,Cr, Ni, Nb, Rb, Sr, V, Y and Zr were analysed on the same powder pellets described above at the University of Nottingham using a Phillips PW1400 wavelength dispersive X-ray fluoresence spectrometer. A rhodium X-ray tube was utilised throughout. Operating conditions are as listed in table C2. Rb and Sr were analysed

separately from the other elements following the method of Harvey & Atkin (1981). Operating conditions for Rb and Sr determination were 75KV, 40mA using a LiF22O crystal.

Element	KV	mA	Crystal	Ct. (peak)	Ct (background)
Ba	50	60	LiF22O	20	10
Co	60	50	LiF22O	20	10
Cr	50	60	LiF22O	20	8
Ni	70	40	LiF22O	10	4
Nb	75	40	LiF22O	20	16
Y	75	40	LiF22O	20	16
Zr	75	40	LiF22O	20	20

Table C2 Operating conditions for XRF (University of Nottingham)

Ct. (peak) is normal counting time in seconds on peak position.

Ct (background) is normal counting time in seconds on background.

C4 Instrumental Neutron Activation Analysis.

Selected samples were analysed by instrumental neutron activation analysis (INAA) for: La, Ce, Nd, Sm, Eu, Tb, Yb, Lu, Sc, Co, Hf, Ta, Th and U. Detailed descriptions of the analytical technique are given in Potts *et al.* (1981, 1985).

0.3g of rock powder was dried overnight at 105°C and loaded into polythene capsules which were then heat sealed. Eleven samples were loaded into a polythene tube, with two of these being the standards which were positioned half way along the tube. The standards used were the Ailsa Craig microgranite laboratory irradiation standard and another internal standard (Whin Sill dolerite) which was analysed as an unknown. Data for this standard are compared with the values reported by Potts *et al.* (1985) in table C3. Laquered iron foils were placed between the samples as neutron flux monitors.

Samples were irradiated in the 270° core tube facility at the Imperial College reactor centre, Ascot. They were subjected to a thermal flux of 10^{12} $ncm^{-2}s^{-1}$ for 16 hours of reactor time. Following one week of "cooling" samples were counted at the Open University, using two detectors; a low energy photon spectrometer (LEPS) and a coaxial Ge(Li) detector. An automatic sample changer was employed and the counting procedure was as follows:

(a) The Fe foils were counted on the coaxial detector for 1000 seconds each. This provides data which enables a neutron flux correction to be made.

(b) Each sample was counted for around 2 hours on both the LEPS and the

coaxial detector.

(c) Each sample was counted for 6-8 hours again using both the LEPS and coaxial detector.

An EG and G ORTEC 7032A multichannel analyser system was used to calculate the photopeak areas, using the peak-fitting software supplied. Corrections were then made for neutron flux variations and weight of sample.

C5 Mass Spectrometry Techniques

C5.1 General Chemistry

All chemical separation and analysis was performed in a laboratory with a small positive pressure generated by an air make-up unit with particle filters. Sample dissolutions were performed in teflon beakers and bombs within laminar flow cupboards. Teflon laboratory ware was cleaned by thorough washing in distilled water, soaking for 24 hours in concentrated HNO_3, followed by soaking in distilled water for at least 24 hours on a hotplate. RO water is supplied from a Milli Q reverse osmosis purification system. HCl and HNO_3 were double distilled in quartz stills and further purified in sub-boiling teflon stills (TD). HF and HBr were purified in similar teflon stills as was the H_2O used in Pb separations.

C5.2 Sr Chemistry

Around 100 mg of rock powder was weighed into a teflon beaker, a small drop of RO water was added to prevent loss of powder due to static charge build-up upon the teflon. About 2ml of 16M HNO_3 and 5 ml of 40% HF was added and evaporated to dryness in a teflon oven at 80°C with clean air circulation. When dry a further 2 ml of 16M HNO_3 was added and evaporated, after which 2 ml 6M HCl was added. At this stage the sample was closely inspected to ensure complete dissolution and the HCl was evaporated down. The sample was then redissolved in 2.5M HCl and left overnight in a covered beaker. Occasionally the dissolution process was repeated to achieve a complete digestion. On rare occasions complete dissolution was only achieved after 6M HCl treatment in a teflon bomb placed in a metal jacket in an oven at 180°C overnight. The sample, dissolved in 1 ml 2.5M HCl was then centrifuged to remove any residue and the solution was loaded onto a pre-conditioned cation exchange column containing 10 ml Bio-Rad AGW 50 X 8, 200- 400

mesh resin. The sample was washed in with 2 x 1 ml 2.5M HCl and eluted with 40 ml 2.5M HCl. Sr was then collected in 10 ml 2.5M HCl in a clean teflon beaker, and evaporated to dryness. The total procedure blank for Sr analyses was less than 7 ng which is negligible for the samples studied.

C5.3 Nd Chemistry

Nd was extracted from the same dissolution as Sr. Following collection of Sr, elutions of 1 ml H_2O and 21 ml 3M HNO_3 were then made and 20 ml of 3M HNO_3 was collected. This fraction contains the MREE (and Ba), following collection it was evaporated to dryness. Two methods of Nd extraction were used during the course of this study. In the early stages the sample was dissolved in 1 ml of a solution of 75% CH_3OH - 10% 8M CH_3OOH - 10% 5M HNO_3 - 5% H_2O (solution 1) and left overnight in a covered beaker. This was loaded onto a preconditioned anion exchange column containing 3 ml Bio-Rad AG 1 X 8 200-400 mesh resin encased in a thermostatically controlled water jacket set at 25°C. The sample was washed in with 2 x 1 ml of solution 1 and 32 ml of solution 1 eluted. The temperature of the water bath was then increased to 35°C and the column eluted with 15 ml of a solution of 75% CH_3OH - 10% 8M CH_3OOH - 5% 5M HNO_3-10% H_2O. (solution 2). A further 29 ml of solution 2 was collected and evaporated to dryness. In the latter half of this study the MREE extract from the cation exchange column was dissolved in 1 ml 0.25M HCl and left standing overnight in a covered beaker. The sample was loaded onto a preconditioned reverse chromatography column which was prepared by mixing 1g of teflon powder (Voltalef 300LD PL micro) with 100 mg HDEHP ((Di(2-ethylhexyl) orthophosphoric acid). After washing in with 2 x 1 ml 0.25M HCl, 10 ml 0.25M HCl was eluted and Nd was collected with 4 ml 0.25M HCl which was evaporated to dryness. This teflon column procedure is preferable to the resin columns used previously because it achieves more efficient separation of Ba from Nd, the separation is faster and requires no temperature control. The total procedure blank for Nd analysis was less than 2ng which is negligible for the samples studied.

C5.4 Pb Chemistry

Pb chemistry was carried out in a separate low blank laboratory within the mass spectrometry suite. A laboratory coat, hood and gloves were worn at all times. All the

reagents used in Pb chemistry were sub-boiling teflon distilled and the whole procedure was performed inside a laminar flow cupboard. Separate dissolutions were performed for Pb extraction. The amount of rock powder digested was modified according to Pb concentration of the sample to achieve approximately equal yield of Pb for all samples. Approximately 50 mg for 20ppm samples to 100 mg for 10ppm samples was weighed into a savilex bomb. These bombs were cleaned in the same manner as teflon beakers prior to a RO H_2O wash separate from general chemistry utensils. The bombs were finally cleaned by standing on a hot plate (80°C) approximately two thirds full of 16M HNO_3, with the lids screwed down firmly for 24 hours and immediately prior to use they were rinsed in teflon distilled water. Samples were dissolved in 1 ml 16M HNO_3 and 2-3 ml 40% HF and evaporated to dryness. 2 ml HNO_3 was then added and evaporated and this process was repeated with 3 ml 6M HCl and 1 ml 1M HBr. This was left overnight at which stage the sample should be fully dissolved.

Fritted 1 ml polypropylene pipette tips were used as columns. They were stored in concentrated HCl and washed with 16M HNO_3 and H_2O prior to addition of around 10 µl of Bio- Rad 1 X 8 200-400 mesh anion exchange resin. The column was then washed with 1 column volume (cv) 6M HCl, 1 cv RO H_2O, 1 cv 6M HCl, 1 cv TD H_2O and 0.5 cv 1M HBr. The sample was then added dropwise to the column and washed in with 1 ml 1M HBr. 3 x 1 cv 1M HBr was then eluted and Pb was collected with 2-3 cv TD H_2O in a clean savilex bomb and evaporated to dryness. The total procedure blank for Pb samples was less than 1.5 ng which is negligible for the samples studied.

C5.5 Mass Spectrometry

Sr and Nd were loaded in a filtered loading bay, laboratory coat and gloves were worn throughout. Pb samples were loaded in a laminar flow cupboard within the Pb laboratory. Filament assemblies were boiled in RO water prior to outgassing. Single filaments were outgassed for 5 minutes at 4.5A in a vacuum of 10^{-6} torr, triple filament assemblies were outgassed for 5 minutes at 4.5A in a vacuum of10^{-5} torr and then immediately outgassed again at 10^{-6} torr. Sr was dissolved in a drop of TD H_2O and loaded onto an outgassed single Ta filament onto which about1 µl of H_3PO_4 had been placed. A small current was passed through the filament to slowly dry the sample and then gradually increased until the H_3PO_4 fumed off and the filament glowed dull red. Nd was dissolved in a drop of TD H_2O

and loaded onto the Ta side filaments of a triple filament assembly with a Re centre filament. The sample was dried out gently and the side filaments placed orthogonally to the centre filament. The Pb sample was dissolved in a drop of H_3PO_4 and Pb was loaded using the silica gel method. A drop of silica gel was placed on the filament, and evaporated slowly by passing a current through the filament until the gel was almost (but not quite) dry. The sample was then added and evaporated down. When dry, the current was slowly increased until excess H_3PO_4 was given off and the filament glowed dull red.

Loaded filaments were placed in a six sample turret and analysed on a Vacuum Generators Isomass 54E solid source mass spectrometer. Samples were run automatically by software developed at the Open University by D.W. Wright and P.W.C. van Calsteren, using a HP9845T computer. All analyses are carried out at an accelerating potential of 8KV at 10^{-7}torr.

C5.6 Isotope Measurement

C5.6.1 Sr

Sr isotope abundances were measured with a beam intensity of 15 pA at a filament current of 2.5 A. Peaks were counted for four periods of 1.28 seconds, after which the magnet was stepped to the next position. The measuring cycle was 88, 87, 86, 85.5, 85, 84. The 84 peak was eliminated after the first set and the 85 peak when the Rb contribution to the 87 peak was less than 0.01%. Peak intensities were calculated using a double interpolation algorithm (Dodson, 1978) and were corrected for zero, dynamic memory and Rb interference where necessary. Mass fractionation was corrected for by assuming that $^{86}Sr/^{88}Sr$ =0.1194 and that there is a linear dependance on mass difference. The isotope ratios were stored in sets of ten and the mean and error calculated for each set. Any ratios which did not satisfy Chauvenet's criterion were rejected and the mean and error re-calculated. Sets whose total error (1σ) was 100 ppm or more were rejected and those with total error of 500 ppm or greater were ignored. Chauvenet's criterion was then applied to all the stored ratios, including those rejected but not those ignored, and a running mean was formed. The analysis continued until at least 100 ratios had been accepted and the error was 20ppm or less. Repeat analyses of the NBS 987 standard give $^{87}Sr/^{86}Sr$ = 0.71018±4, all data in this work, both original and quoted are normalised to this value.

C5.6.2 Nd

Nd isotope measurement and data reduction was similar to that for Sr. Beams were managed to give a beam intensity of 7pA with a centre filament current of 3.9 A and side filament currrents of 2.0 A. The purpose of a triple filament assembly is to allow ionisation of the Nd on the centre filament at a higher temperature to that at which it is released off the side filaments. The measuring cycle for Nd analysis was 146, 144, 143, 142.5, 142, 147, the 142 peak was eliminated after the first set and the 147 peak was eliminated when the Sm contribution to the 144 peak was less than 0.01%. Mass fractionation was corrected by assuming linear dependance on mass difference and $^{146}Nd/^{144}Nd = 0.7219$. Sets of ratios were rejected when the error on $^{143}Nd/^{144}Nd$ was 100 ppm or worse and ignored when the error was 500 ppm. Analysis was continued until at least 200 ratios were accepted and the error (1σ) was 10 ppm or less. The standard BCR-1 gives $^{143}Nd/^{144}Nd = 0.512620 \pm 20$ and all the data presented here are normalised to this value.

C5.6.3 Pb

As there is no non-radiogenic reference isotope ratio of Pb, the problem of mass fractionation must be addressed in a different manner. In order to minimise fractionation between runs, all samples were run with a filament current of 2.25 A which ensured a filament temperature of 1150-1200°C. The measuring cycle was 207, 206, 204, 204.5, 208. Sets of ratios were rejected when the error on $^{207}Pb/^{206}Pb$ was 200 ppm and rejected if it was 500 ppm. Analysis continued until the error was better than 50ppm and 100 ratios had been accepted. All samples were carefully monitored to assess the extent of any mass fractionation during the run. A correction for mass fractionation was made by performing multiple analyses of the standard NBS 981which gave:

$^{206}Pb/^{204}Pb = 16.8961$ $^{207}Pb/^{204}Pb = 15.4317$

$^{207}Pb/^{206}Pb = 0.91333$ $^{208}Pb/^{204}Pb = 36.513$

samples were then normalised to the "accepted" values of this standard:

$^{206}Pb/^{204}Pb = 16.9371$ $^{207}Pb/^{204}Pb = 15.4913$

$^{208}Pb/^{204}Pb = 36.7213$ $^{207}Pb/^{206}Pb = 0.91464$

All the Pb isotope data presented here, both original and quoted are normalised in a similar manner which eliminates inter-laboratory bias.

APPENDIX D

Normalised Trace Element Abundance Diagrams

D1 MORB Normalised

The MORB normalising factors used are those of Pearce *et al.* (1981):

Sr	120
K_2O	0.15%
Rb	2
Ba	20
Th	0.2
Ta	0.18
Nb	3.5
Ce	10
P_2O_5	0.12%
Zr	90
Hf	2.4
Sm	3.3
TiO_2	1.5%
Y	30
Yb	3.4

all values are ppm unless otherwise indicated

D2 Trace Element Component Recognition.

The method used is similar to that proposed by Pearce (1983) but is slightly modified to better suit Aeolian lavas.

(a) Depleted Mantle Component:- A proportion of all the elements is assigned to this component such that the normalised abundance of all element, in this component, is equal to the normalised abundance of Yb.

(b) Within Plate Component:- All excess Ta, Nb, Zr, Hf, Ti and Y is assigned to this component. In all Aeolian lavas, Ti is insufficient to satisfy the depleted mantle component (*i.e.* $Ti_n<Yb_n$). Therefore Sm is obtained by linear interpolation between Hf and a point above Ti equal to the normalised value of Yb. Ce and P are obtained by linear interpolation between the averaged normalised value of Nb and Ta, and

Zr. Th, Ba and Rb are given a normalised value in this component equal to the averaged normalised abundance of Ta and Nb. Sr is assigned a normalised value equal to that of Ce and K is obtained by linear interpolation between Sr and Rb.

(c) Subduction Zone Component:- Any remaining Sr, K, Rb, Ba, Th, Ce,P and Sm is assigned to this component.

Relative contributions of each component to the overall budget of a particular element are expressed as percentages.

D3 Mantle Normalised Diagrams

The primitive mantle normalising factors employed are:

Ba	3.85
Rb	0.35
Th	0.042
K_2O	0.01446%
Nb	0.35
Ta	0.02
Ce	0.865
Sr	11.8
Nd	0.63
P_2O_5	0.01053%
Sm	0.203
Zr	6.84
Hf	0.20
TiO_2	0.10333%
Y	2
Yb	0.22

All values are ppm unless otherwise indicated. These values are those of Thompson (1982) except Ba. Thompson's values are chondritic, except for Rb, K and P. A value of 3.85 is preferred for Ba to maintain Ba/Rb =11 in the mantle (Hofmann & White, 1983)

D4 REE Diagrams

REE data are normalised to the chondritic values of Nakamura, (1974):

La	0.328
Ce	0.865
Nd	0.63
Sm	0.203
Eu	0.077
Tb	0.052
Yb	0.22
Lu	0.034

All ppm.

APPENDIX E

COMPUTER PROGRAMS

A number of the computer programs written during the course of this work are included in this appendix. The software was written in the FORTRAN 77 language on a DEC-20 computer at the Open University. This language is widely available on mainframe computers and as such the programs are designed to be machine portable. However it should be noted that the software is not suitable for use with versions of FORTRAN other than 77. The data from these programs is output either on-line to the stream 5 device or to a stream 20 data file which is named in an OPEN statement. No graphical output is produced by any of the programs listed, however they are written so that graph plotting routines appropriate to the environment in which the programs are being used may be quite easily added. Data which are not stored within the program *ie.* which changes with each run, is input interactively from stream five, following prompts generated by the software.

NEWRTF.FOR

This is a program to simulate the products of a periodically replenished, periodically tapped, continuously fractionating magma chamber as it evolves through 500 cycles. The program uses the formulae developed by O'Hara & Mathews (1981). The program will calculate variations for up to 10 elements in a single run, and the concentration of these elements in the liquid is output after every ten cycles Also output are the original composition, bulk partition coefficient and the mass fractions of erupted lava , cumulate and added magma in each cycle. **Warning** In some cases this program will encounter FORTRAN underflow errors as a variable in the equations assumes a value less than the range accomodated by FORTRAN. On the DEC-20 this effect is not significant as the very small number is equated to zero and execution continues, however this may not be the case on all computers.

PLAGSAT.FOR

This is a program to calculate the plotting parameters of a plagioclase saturated

pseudoternary projection of the CMAS system (Grove *et al.*, 1985). If data for the ferrous: ferric ratio are not available then Fe should be entered as Fe_2O_3 and FeO enterred as 0.0. Fe_2O_3 is then calculated as 15% of total Fe. The program calculates a single sample during each run but subject to a prompt may be looped around several times during a single run.

VULCAN.FOR

This is the program used to model the effects of repeated batch partial melting of a source being enriched by addition of a fluid between each batch of melting. Data required to run the program are the partition coefficients of the solid and of the melting assemblage, composition of the solid, composition of the fluid, the proportion of fluid during mixing into the solid source region and the degree of partial melting. Up to 10 elements may be modelled in any one run which simulates 10 cycles of melting and enrichment. The output shows the conditions pertaining to the model and the composition of the magmas produced during each cycle.

3COMP.FOR

This program performs mixing between three components. The prompt sequence is designed to deal with the general case which refers to trace element or isotope ratios and two ratios are modelled, these are referred to as x and y axis ratios although no graphical output is produced. The program first performs a mixture between the first two components, calculating the ratio and denominator values of mixtures at intervals of 10%. These are then individually mixed with the third component. The program does not produce the coordinates of the 2 component mixture between end members 2 and 3, but this is easily available by using a two component mixing model similar to that in DO-loop 20 of this program.

NEWRTF.FOR

```
      DIMENSION D(10),CO(10)
      DIMENSION XMN1(1000),XMN2(1000),XMN3(1000)
      DIMENSION XMN4(1000),XMNT(1000)
      DIMENSION CM1(1000,10),CM2(1000,10),CM3(1000,10)
      DIMENSION CM4(1000,10),CM5(1000,10)
C
C CHARACTER ARRAY FOR ELEMENT NAMES
C
      CHARACTER*2 L1(10)
C
C  DIRECT OUTPUT TO FILE "RTF.TXT"
C
      OPEN (UNIT=20,FILE='RTF.TXT')
C
C  PROMPT SEQUENCE FOR DATA INPUT
C
      WRITE(5,*) '****************************************'
      WRITE(5,*) 'HOW MANY ELEMENTS TO BE MODELLED?'
      READ(5,*) K
      WRITE(5,*) '****************************************'
      WRITE(5,*) 'PLEASE INPUT NAMES OF THESE ELEMENTS'
      WRITE(5,*) '****************************************'
      READ(5,200) (L1(I),I=1,K)
  200 FORMAT(10(A2,1X))
      DO 5 I=1,K
      WRITE(5,*) '******************************'
      WRITE(5,100) L1(I)
  100 FORMAT(1X,A2,1X,'PLEASE INPUT CO AND BULK KD')
      WRITE(5,*) '******************************'
    5 READ(5,*) CO(I),D(I)
      WRITE(5,*) '*********************************************'
      WRITE(5,*) 'INPUT X (MASS FRACTION OF CUMULATE'
      WRITE(5,*) 'Y (MASS FRACTION OF ERUPTED LAVA'
      WRITE(5,*) 'AND Z (MASS FRACTION OF REPLENISHING MAGMA'
      WRITE(5,*) '*********************************************'
      READ(5,*) X,Y,Z
      WRITE(20,*) '+++++++++++++++++++++++++++++++++++++++++++++++++'
      WRITE(20,*) 'THIS IS A PROGRAM TO SIMULATE EVOLUTION'
      WRITE(20,*) 'OF A RTF MAGMA CHAMBER,EQUATIONS ARE FROM'
      WRITE(20,*) 'OHARA & MATTHEWS,(1981) AND REFER TO'
      WRITE(20,*) 'SPECIAL CASE WHEN MO=0,AND X,Y,Z ARE CONSTANT'
      WRITE(20,*) 'WRITTEN BY R.M.ELLAM NOV.1985'
      WRITE(20,*) '-------------------------------------------------'
C
C  X AMOUNT OF CUMULATES
C  Y MAGMA ERUPTED
C  Z REPLENISHING MAGMA
C
C  MAIN ITERATIVE DO LOOP COMMENCING
C  CALCULATE MIXING TERM
```

```
C
      DO 10 I=1,500
C
C INCREMENT COUNTER
C
      XN=FLOAT(I)
      XMN1(I)=(1.0-X-Y)**(XN+1.0)
      XMN2(I)=1.0-((1.0-X-Y)**(XN+1.0))
      XMN3(I)=1.0-(1.0-X-Y)
      XMN4(I)=(XMN2(I)/XMN3(I))*Z
      XMNT(I)=XMN1(I)+XMN4(I)
C
C CALCULATE COMPOSITION OF "EVOLVED" LIQUID
C SET UP  DO LOOP TO CALCULATE CL VALUES
C
      DO 20 J=1,K
      CM1(I,J)=((((1.0-X-Y)*((1.0-X)**(D(J)-1.0)))**XN)/XMNT(I))
      CM2(I,J)=1.0-(((1.0-X-Y)*((1.0-X)**(D(J)-1.0)))**XN)
      CM3(I,J)=CM2(I,J)/(1.0-((1.0-X-Y)*((1.0-X)**(D(J)-1.0))))
      CM4(I,J)=CM3(I,J)*(Z/XMNT(I))
      CM5(I,J)=CO(J)*(CM1(I,J)+CM4(I,J))
   20 CONTINUE
C
   10 CONTINUE
C
C OUTPUT RESULTS
C
      WRITE(20,*) 'MASS FRACTION OF CUMULATES=',X
      WRITE(20,*) 'MASS FRACTION OF ERUPTED LAVA=',Y
      WRITE(20,*) 'MASS FRACTION OF ADDED MAGMA=',Z
      DO 40 I=1,K
   40 WRITE(20,4000) L1(I),CO(I),D(I)
 4000 FORMAT(1X,A2,2X,'ORIGINAL COMPOSITION=',F6.2,2X,'BULK KD=',F9.6)
      WRITE(20,5000) (L1(I),I=1,K)
 5000 FORMAT(1X,'CYCLE',5X,10(A2,8X))
      DO 50 I=1,500,10
      WRITE(20,6000) I,(CM5(I,J),J=1,K)
 6000 FORMAT(2X,I3,1X,10(F7.1,3X))
   50 CONTINUE
      WRITE(20,6000) I,(CM5(500,J),J=1,K)
      STOP
      END
```

PLAGSAT.FOR

```
      WRITE(5,*) 'THIS IS A PROGRAM TO CALCULATE THE PLOTTING'
      WRITE(5,*) 'PARAMETERS OF THE PLAGIOCLASE SATURATED, '
      WRITE(5,*) 'PSEUDOTERNARY PHASE DIAGRAM OF GROVE ET.AL.'
      WRITE(5,*) '(1985). DIAGRAM IS A PROJECTION FROM'
      WRITE(5,*) 'PLAGIOCLASE INTO THE PLANE OLIVINE-CLINOPYROXENE'
      WRITE(5,*) '-QUARTZ'
      DIMENSION XMW(11),WP(11),WO(11),RO(11),XMP(11)
C
C  CHARACTER VARIABLES FOR ELEMENT NAMES, SAMPLE NAME & YES/NO PROMPT
C
      CHARACTER*5 LEL(11)
      CHARACTER*6 LNAM
      CHARACTER*1 LA
C
C  ELEMENT NAMES
C
      DATA (LEL(I),I=1,11) /'SIO2','TIO2','AL2O3','FE2O3','FEO','MNO',
     1'MGO','CAO','NA2O','K2O','P2O5'/
C
C  MOLECULAR WEIGHTS
C       DATA (XMW(I),I=1,11) /60.08,79.9,101.96,159.69,71.85,70.94,40.31
     1,56.08,61.98,94.19,141.94/
    1 WRITE(5,*) 'INPUT SAMPLE NAME'
      READ(5,1000) LNAM
 1000 FORMAT(A6)
      SM1=0.0
      WRITE(5,*) 'INPUT OXIDES AS PROMPTED,NOTE IF ONLY FE2O3'
      WRITE(5,*) 'IS AVAILABLE ENTER FEO=0.0, FE2O3 IS THEN'
      WRITE(5,*) 'SET TO 15% OF TOTAL FE'
      DO 10 I=1,11
      WRITE(5,2000) LEL(I)
 2000 FORMAT(1X,A5)
      READ(5,*) WP(I)
      WO(I)=WP(I)
      SM1=WO(I)+SM1
   10 CONTINUE
      IF (WP(5).NE.0.00) GOTO 15
C
C  RECALCULATE FE2O3 TO 0.15 FEOT
C
      WO(5)=(WO(4)/1.1113)-(WO(4)*0.08998)
      WO(4)=WO(4)*.1
   15 SM2=0.0
      DO 20 I=1,11
      SM2=SM2+WO(I)
   20 CONTINUE
      SM6=0.0
      DO 30 I=1,11
      RO(I)=WO(I)*(SM1/SM2)
      XMP(I)=RO(I)/XMW(I)
      SM6=SM6+XMP(I)
   30 CONTINUE
      DO 40 I=1,11
      XMP(I)=(XMP(I)/SM6)*1.
   40 CONTINUE
```

```
C
C CALCULATE CMAS COMPONENTS
C
      AG=XMP(3)+XMP(9)-XMP(10)
      CG=XMP(8)+(2.0*XMP(9))
      XMG=XMP(7)+XMP(5)+(2.0*XMP(4))-(2.0*XMP(2))
      SG=XMP(1)-(2.0*XMP(9))-(6.0*XMP(10))
C
C CALCULATE COORDINATES FOR PROJECTION
C
      PLAG=AG
      CPX=CG-AG
      OL=(XMG-CG+AG)/2.0
      SIL=SG-((XMG+AG+(3.0*CG))/2.0)
      TOT=PLAG+CPX+OL+SIL
      PLAG=(PLAG/TOT)*100.0
      CPX=(CPX/TOT)*100.0
      OL=(OL/TOT)*100.0
      SIL=(SIL/TOT)*100.0
C
C PROJECT FROM PLAGIOCLASE
C
      TOT2=CPX+OL+SIL
      CPX=(CPX/TOT2)*100.0
      OL=(OL/TOT2)*100.0
      SIL=(SIL/TOT2)*100.0
C
C  OUTPUT RESULTS
C
      WRITE(5,3000) LNAM
 3000 FORMAT(1X,A6)
      WRITE(5,*) 'CPX=',CPX
      WRITE(5,*) 'OLIVINE=',OL
      WRITE(5,*) 'SILICA=',SIL
      WRITE(5,*) 'ANOTHER SAMPLE?'
      READ(5,4000) LA
 4000 FORMAT(A1)
      IF (LA.EQ.'Y') GOTO 1
      STOP
      END
```

VULCAN.FOR

```
      DIMENSION CO(10),D(10),P(10),CF(10)
      DIMENSION CL(10,10),CRS(10,10),CM(10,10),CO1(10,11)
      DIMENSION CRS1(10,10),CRS2(10,10)
      CHARACTER*2 L1(10)
C
C  DIRECT OUTPUT TO FILE "OP1.TXT"
C
   OPEN (UNIT=20,FILE='OP1.TXT')
      WRITE(5,*) 'HOW MANY ELEMENTS?'
      READ(5,*) K
      WRITE(5,*) 'INPUT ELEMENT NAMES'
      READ(5,1000) (L1(I),I=1,K)
 1000 FORMAT (10(A2,1X))
C
C  ALPHA IS THE PROPORTION OF FLUID IN THE MIXTURE
C  F IS THE DEGREE OF PARTIAL MELTING
C
      WRITE(5,*) 'INPUT ALPHA AND F'
      READ(5,*) ALFA,F
      DO 10 I=1,K
      WRITE(5,2000) L1(I)
C
C  CO ORIGINAL SOLID COMPOSITION, D KD OF SOLID, P KD OF
C  MELTING ASSEMBLAGE AND CF COMPOSITION OF FLUID
C
 2000 FORMAT (1X,A2,1X,'INPUT CO,D,P,CF')
      READ(5,*) CO(I),D(I),P(I),CF(I)
      CO1(I,1)=CO(I)
   10 CONTINUE
C
C  BEGIN DO LOOP TO CALCULATE LIQUIDS
C
      DO 20 I=1,K
      DO 20 J=1,10
C
C  BATCH MELTING CALCULATIONS
C
      CL(I,J)= CO1(I,J)/(D(I)+(F*(1.0-P(I))))
      CRS(I,J)=CO1(I,J)/(1.0-F)
      CRS1(I,J)=D(I)-(F*P(I))
      CRS2(I,J)=D(I)+(F*(1.0-P(I)))
      CRS(I,J)=CRS(I,J)*(CRS1(I,J)/CRS2(I,J))
C
C  MIXING CALCULATION
C
      CM(I,J)=(CRS(I,J)*(1.0-ALFA))+(CL(I,J)*ALFA)
      N=J+1
      CO1(I,N)=CM(I,J)
   20 CONTINUE
```

```
C
C  OUTPUT RESULTS
C
      WRITE(20,*) 'ALPHA=',ALFA
      WRITE(20,*) 'F=',F
      DO 40 L=1,K
      WRITE(20,3000) L1(L)
 3000 FORMAT (1X,A2)
      WRITE(20,*) 'CO=',CO(L),' ','D=',D(L),' ','P=',P(L),' ',
     1'CF=',CF(L)
   40 CONTINUE
      WRITE(20,*) 'COMPOSITIONS OF LIQUIDS PRODUCED'
      WRITE(20,4000) (L1(I),I=1,K)
 4000 FORMAT (5X,10(A2,8X))
      DO 50 J=1,10
      WRITE(20,5000) (CL(I,J),I=1,K)
 5000 FORMAT (1X,10(F7.1,3X))
   50 CONTINUE
      STOP
      END
```

3COMP.FOR

```
      DIMENSION AX(11),EM4A(11),EM4B(11),BX(11)
      DIMENSION CA(11),CB(11),CC(11),CD(11),EM4Y(11),EM4X(11)
      DIMENSION CINC(11), CX(11,11),CY(11,11)
      CHARACTER*6 IMONE
      CHARACTER*6 IMTWO
      CHARACTER*6 IMTHR
      CHARACTER*11 IXNAME
      CHARACTER*11 IYNAME
      CHARACTER*2 IXDEN
      CHARACTER*2 IYDEN
C
C  DIRECT OUTPUT TO FILE "OPT.TXT"
C
   OPEN (UNIT=20,FILE='OPT.TXT')
C
C  INTERACTIVE DATA INPUT ROUTINE FROM STREAM FIVE
C
      WRITE(5,*) 'NAME OF END MEMBER ONE?'
      READ(5,1000) IMONE
 1000 FORMAT(A6)
      WRITE(5,*) 'NAME OF END MEMBER TWO?'
      READ(5,1000) IMTWO
      WRITE(5,*) 'NAME OF END MEMBER THREE?'
      READ(5,1000) IMTHR
      WRITE(5,*) 'WHAT IS X AXIS RATIO?'
      READ(5,500) IXNAME
      WRITE(5,*) 'WHAT IS Y AXIS RATIO?'
      READ(5,500) IYNAME
  500 FORMAT(A11)
      WRITE(5,*) 'PLEASE INPUT X AND Y AXIS DENOMINATORS'
      READ(5,600) IXDEN,IYDEN
  600 FORMAT(A2,1X,A2)
      WRITE(5,*) '************************************'
      WRITE(5,2000) IMONE
 2000 FORMAT(10X,A6)
      WRITE(5,*) '************************************'
      WRITE(5,3000) IXNAME,IYNAME
 3000 FORMAT(1X,'PLEASE INPUT',1X,A11,1X,'AND',1X,A11)
      WRITE(5,4000) IXDEN,IYDEN
 4000 FORMAT(20X,A2,1X,'AND',1X,A2)
      READ(5,*) X1,Y1,B1,A1
      WRITE(5,*) '************************************'
      WRITE(5,2000) IMTWO
      WRITE(5,*) '************************************'
      WRITE(5,3000)IXNAME,IYNAME
      WRITE(5,4000)IXDEN,IYDEN
      READ(5,*) X2,Y2,B2,A2
      WRITE(5,*) '************************************'
      WRITE(5,2000) IMTHR
      WRITE(5,*) '************************************'
      WRITE(5,3000)IXNAME,IYNAME
      WRITE(5,4000)IXDEN,IYDEN
      READ(5,*) X3,Y3,B3,A3
```

```
C
C  OUTPUT DETAILS OF COMPONENTS
C
      WRITE(20,4500) IMONE,IXNAME,X1,IYNAME,Y1,IXDEN,B1,IYDEN,A1
      WRITE(20,4500) IMTWO,IXNAME,X2,IYNAME,Y2,IXDEN,B2,IYDEN,A2
      WRITE(20,4500) IMTHR,IXNAME,X3,IYNAME,Y3,IXDEN,B3,IYDEN,A3
 4500 FORMAT(1X,A6,1X,A11,1X,F13.7,1X,A11,1X,F13.7,1X,A2,1X,
     1F13.7,1X,A2,F13.7)
C
C  CALCULATE A,C,D COEFFICIENTS FOR ELEMENTAL MIXING OF DENOMINATORS
C  B=0 FOR ELEMENT-ELEMENT MIXTURES
C
      AA=A2-A1
      AC=B1-B2
      AD=(B2*A1)-(B1*A2)
C
C  MIX DENOMINATORS OF FIRST TWO COMPONENTS
C
      AINC=(B2-B1)/10.0
      EM4B(1)=B1+AINC
      DO 10 I=1,10
      EM4A(I)=(0.0-AD-(AA*EM4B(I)))/AC
      EM4B(I+1)=EM4B(I)+AINC
   10 CONTINUE
C
C  CALCULATE A,B,C,D COEFFICIENTS FOR MIXING 2 COMPONENTS
C
      BA=(((A2*B1)*Y2)-((A1*B2)*Y1))
      BB=((A1*B2)-(A2*B1))
      BC=(((A2*B1)*X1)-((A1*B2)*X2))
      BD=((A1*B2*X2*Y1)-(A2*B1*X1*Y2))
C
C  MIX FIRST 2 COMPONENTS
C
      BINC=(X2-X1)/10.0
      EM4X(1)=X1+BINC
      DO 20 I=1,10
      EM4Y(I)=(0.0-BD-(BA*EM4X(I)))/((BB*EM4X(I))+BC)
      EM4X(I+1)=EM4X(I)+BINC
   20 CONTINUE
C
C  MIX WITH THIRD COMPONENT
C
C  CALCULATE A,B,C,D COEFFICIENTS
C
      DO 30 I=1,10
      CA(I)=((A3*EM4B(I))*Y3)-((EM4A(I)*B3)*EM4Y(I))
      CB(I)=(EM4A(I)*B3)-(A3*EM4B(I))
      CC(I)=((A3*EM4B(I))*EM4X(I))-((EM4A(I)*B3)*X3)
      CD(I)=(EM4A(I)*B3*X3*EM4Y(I))-(A3*EM4B(I)*EM4X(I)*Y3)
```

```
C
C  OUTPUT DETAILS OF COMPONENTS
C
      WRITE(20,4500) IMONE,IXNAME,X1,IYNAME,Y1,IXDEN,B1,IYDEN,A1
      WRITE(20,4500) IMTWO,IXNAME,X2,IYNAME,Y2,IXDEN,B2,IYDEN,A2
      WRITE(20,4500) IMTHR,IXNAME,X3,IYNAME,Y3,IXDEN,B3,IYDEN,A3
 4500 FORMAT(1X,A6,1X,A11,1X,F13.7,1X,A11,1X,F13.7,1X,A2,1X,
     1F13.7,1X,A2,F13.7)
C
C  CALCULATE A,C,D COEFFICIENTS FOR ELEMENTAL MIXING OF DENOMINATORS
C  B=0 FOR ELEMENT-ELEMENT MIXTURES
C
      AA=A2-A1
      AC=B1-B2
      AD=(B2*A1)-(B1*A2)
C
C  MIX DENOMINATORS OF FIRST TWO COMPONENTS
C
      AINC=(B2-B1)/10.0
      EM4B(1)=B1+AINC
      DO 10 I=1,10
      EM4A(I)=(0.0-AD-(AA*EM4B(I)))/AC
      EM4B(I+1)=EM4B(I)+AINC
   10 CONTINUE
C
C  CALCULATE A,B,C,D COEFFICIENTS FOR MIXING 2 COMPONENTS
C
      BA=(((A2*B1)*Y2)-((A1*B2)*Y1))
      BB=((A1*B2)-(A2*B1))
      BC=(((A2*B1)*X1)-((A1*B2)*X2))
      BD=((A1*B2*X2*Y1)-(A2*B1*X1*Y2))
C
C  MIX FIRST 2 COMPONENTS
C
      BINC=(X2-X1)/10.0
      EM4X(1)=X1+BINC
      DO 20 I=1,10
      EM4Y(I)=(0.0-BD-(BA*EM4X(I)))/((BB*EM4X(I))+BC)
      EM4X(I+1)=EM4X(I)+BINC
   20 CONTINUE
C
C  MIX WITH THIRD COMPONENT
C
C  CALCULATE A,B,C,D COEFFICIENTS
C
      DO 30 I=1,10
      CA(I)=((A3*EM4B(I))*Y3)-((EM4A(I)*B3)*EM4Y(I))
      CB(I)=(EM4A(I)*B3)-(A3*EM4B(I))
      CC(I)=((A3*EM4B(I))*EM4X(I))-((EM4A(I)*B3)*X3)
      CD(I)=(EM4A(I)*B3*X3*EM4Y(I))-(A3*EM4B(I)*EM4X(I)*Y3)
```

```
C
C  CALCULATE MIXTURES
C
      CINC(I)=(X3-EM4X(I))/10.0
      CX(I,1)=EM4X(I)+CINC(I)
      DO 40 J=1,10
      CY(I,J)=(0.0-CD(I)-(CA(I)*CX(I,J)))/((CB(I)*CX(I,J))+CC(I))
      CX(I,J+1)=CX(I,J)+CINC(I)
   40 CONTINUE
C
C  OUTPUT DATA
C
      WRITE(20,5000) I
 5000 FORMAT (1X,'MIXTURE',I2)
      WRITE(20,6000) IXNAME,EM4X(I),(CX(I,J),J=1,10)
      WRITE(20,6000) IYNAME,EM4Y(I),(CY(I,J),J=1,10)
 6000 FORMAT (1X,A11,1X,F11.6,1X,10(F11.6,1X))
   30 CONTINUE
      STOP
      END
```

APPENDIX F

Sample Locations

Descriptions of the localities sampled during the course of this study are given below. The geological maps upon which the sampling was based are those included with "The Aeolian Islands an active volcanic arc in the Mediterranean Sea" (Villari, Ed.,1980). Details of sample localities for the Stromboli collection provided by M.Rosi are given in Rosi (1980), the rock units for Stromboli samples referred to below are also taken from Rosi (*op.cit.*).

STROMBOLI

ESTR01 Lava flow 250m east of summit.

ESTR02-ESTR05 Collected along east coast section.

ESTR03 Malpasseddu headland, upper flow unit. (Unit L1).

ESTR02 Flow which cuts beach immediately to the north of Malpasseddu headland. (Unit L2).

ESTR04 Headland at northern end of beach (see ESTR02) (lower unit T3b).

ESTR05 Fallen blocks on track above La Petrazza. (Lower Petrazza tuff formation, T3b).

ESTR06-ESTR09 Collected along north-west coast.

ESTR06 Base of Sciara del Fuoco, northern end. (Unit Ls).

ESTR07 Cliffs where Filo del Fuoco meets coastline. (Unit Lr).

ESTR08 Large sill on coast, 200m south-west of P. Labaronzo. (Unit Ls).

ESTR09 Lava flow on beach 200m west of Pisciata. (Unit L2).

SALINA

ESAL01 Dyke from Vne Martello, 250m south of small road bridge.

ESAL02 S. Marina-Lingua road, thick lava flow with house built on top.

ESAL03 Valley to north-west of the end of the road at P. Brigantino. (200m elevation).

ESAL04 As ESAL03 (100m elevation).

ESAL05 Western end of beach at P. Brigantino.

ESAL06 Serro Spinnato, uppermost unit. (300m elevation).

ESAL07 Crags to west of Serro Spinnato.

ESAL08 Coastal section south-east of Rinella, headland to north-west of Erbe Bianche.

ESAL09 50m above ESAL08 on mountainside.

ESAL11 Rinella-Leni roadside, 50m west of first bridge, (Vallonazzo).
ESAL12 North-west extreme of M. Rivi dyke complex.

ESAL13 M. Rivi lavas, along new track above Valdichiesa.
ESAL14

ESAL15 East of Ospizio, close to path at 500m elevation.

ESAL16 Valdichiesa-Malfa roadside outcrop, 300m west of the east-facing hairpin bend in road.

ESAL17 South of Pollara, contact between M. dei Porri scoria and P. di Corvo
ESAL18 dyke complex.

ESAL19 P. di Perciato, cliff top.

ESAL20 Small outcrop of lava 25m to the north-east of track from Pollara to P. di Perciato.

ESAL21- ESAL24 Capo to Gramignazzo road.

ESAL21 Near Capo, first valley to the south after road turns to the west.

ESAL22 Valley to south of first road bridge. (Dyke)

ESAL23 End of track from Capo to beach, in cliff section.

ESAL24 Upper lava unit, north of Scogliazzo, west of Vne. d'Oliastro, close to footpath.

ESAL25- ESAL27 Path along south slope of M. dei Porri. (east-west).

ESAL25 West of Vne Borrello.

ESAL26 Wide flow, east of Olivio Grande.

ESAL27 First flow after track becomes footpath.

CRUSTAL XENOLITHS

85/SAL/01-08 Pollara pumice unit along Malfa-Pollara road

85/SAL/09-12 Small cliffs on Rinella beach (M.dei Porri pyroclastics).

VULCANO

EVUL01 Roadside outcrops, C. Amendola, near Gelso. N.B. This road is not
EVUL02 indicated on the 1980 map (Keller, 1980b).

EVUL03 Roadside, near La Portella.

EVUL04 Path to Fossa summit, where it crosses obsidian flow.

EVUL05 Breadcrust bombs, western flank of Fossa.
EVUL06

EVUL07 Obsidian flow to the south of Fossa, (Grotta dei Palizzi).

EVUL08 Bomb (Grotta dei Palizzi).

EVUL09 Flow along track at Grotta dei Palizzi, south of Fossa.

EVUL10 Pte. Nere headland.

EVUL11 Vulcanello, beach facing Porto di Ponente, near cafe.
EVUL12

EVUL13- EVUL19 South-north traverse of path to west of M.Rosso and M. Molineddu. Samples taken at *c.* 150m intervals.

EVUL20 Small flow near first hairpin bend in road to Piano. (250m elevation).

EVUL21 South Vulcano lava, western flank of M. Saraceno.

EVUL22 Small quarry into obsidian flow, close to road at P. di Levante, (western
EVUL23 flank of Fossa).

EVUL24 Isolated outcrop of trachyte lava near road from P. di Ponente to Piano.

EVUL25 South M. Lentia.

EVUL26 East M. Lentia.

EVUL27 Cala di Mastro Minico (Onshore side of crags).

EVUL29 South Vulcano, T. del Corvo trachyte.

EVUL30 South Vulcano, cliffs above Scogliazzo.

85/VUL/01 Base of Lentia formation, above villas at P. di Ponente.

85/VUL/02 Sc^{o} di Capo Secco, scoria of Saraceno-Spaggia Lunga unit (Keller, 1980b) near inferred contact with Lentia formation.

85/VUL/03 Large upstanding dyke at P. del Rosario, south Vulcano.

85/VUL/04 Cliffs at Capo Secco.

85/VUL/05 Western flank of M. Saraceno, where path from Sc^{o} di Capo Secco (not shown on Keller, 1980b map), crosses lava flow.

85/VUL/06 Extreme south east of Porto di Levante, in dry stream bed.